La borsa di dottorato è stata cofinanziata con risorse del
Programma Operativo Nazionale Ricerca e Innovazione 2014-202 (CCI 2014IT16M2OP005)
Fondo Sociale Europeo, Azione I.1 "Dottorati Innovativi con caratterizzazione Industriale"

UNIVERSITA' DELLA CALABRIA

Dipartimento di Biologia, Ecologia e Scienze della Terra (DiBEST)

Dottorato di Ricerca in

Life Science and Technology

Con il contributo di

Programma Operativo Nazionale Ricerca e Innovazione 2014-202

(CCI2014IT16M2OP005) Fondo Sociale Europeo, Azione I.1 "Dottorati Innovativi con caratterizzazione Industriale"

CICLO XXXVII

Marine diatoms as a source of bioactive compounds: bioprospecting and cryopreservation

Settore Scientifico Disciplinare BIO/01

Coordinatore: Ch.mo Prof. Tommaso Angelone
Firma _____

Supervisore/Tutor: Ch.mo Prof.ssa Radiana Cozza
Firma_____

Supervisore/Tutor: Ch.mo Dott.ssa Giovanna Romano
Firma_____

Dottorando: Dott.ssa Maria Letizia Madeo

Firma

La borsa di dottorato è stata cofinanziata con risorse del
Programma Operativo Nazionale Ricerca e Innovazione 2014-202 (CCI 2014IT16M2OP005)
Fondo Sociale Europeo, Azione I.1 "Dottorati Innovativi con caratterizzazione Industriale"

Index

La borsa di dottorato è stata cofinanziata con risorse del
Programma Operativo Nazionale Ricerca e Innovazione 2014-202 (CCI 2014IT16M2OP005)
Fondo Sociale Europeo, Azione I.1 "Dottorati Innovativi con caratterizzazione Industriale"

La borsa di dottorato è stata cofinanziata con risorse del
Programma Operativo Nazionale Ricerca e Innovazione 2014-202 (CCI 2014IT16M2OP005)
Fondo Sociale Europeo, Azione I.1 "Dottorati Innovativi con caratterizzazione Industriale"

La borsa di dottorato è stata cofinanziata con risorse del
Programma Operativo Nazionale Ricerca e Innovazione 2014-202 (CCI 2014IT16M2OP005)
Fondo Sociale Europeo, Azione I.1 "Dottorati Innovativi con caratterizzazione Industriale"

RIASSUNTO

Le diatomee (Bacillariophyceae) sono una delle più importanti classi di microalghe fotosintetiche eucariotiche di ambiente marino e di acqua dolce responsabili del 20-25% della produzione primaria totale e di circa il 40% della produzione annuale di biomassa marina e responsabili di una larga frazione di sequestro di carbonio atmosferico (Bhattacharjya *et al.*, 2020).

Uno degli aspetti più interessanti è la loro diversità inter- e intraspecifica, sia da un punto di vista morfologico che funzionale. Le diatomee infatti, presentano una parete cellulare (frustulo) costituita da silice amorfa biomineralizzata, con micro- e nano- ornamentazioni (strie, coste, pori, alveoli) di elevata importanza tassonomica e funzionale (De Meo *et al.*, 2014). Negli ultimi anni questa classe di microalghe è diventata un'attraente risorsa per la produzione di fitocomposti, essendo capaci di sintetizzare varie sostanze biologicamente attive (proteine, lipidi, acidi grassi polinsaturi, vitamine, pigmenti) ed anche di aumentare rapidamente la loro biomassa e adattarsi fisiologicamente a diverse condizioni di crescita (Lauritano *et al.*, 2018; de Jesús-Campos *et al.*, 2020; Cutignano *et al.*, 2022).

In tale contesto, il mio progetto di dottorato ha esplorato la possibilità di usare alcune specie/ceppi di diatomee per la produzione di composti di interesse, quali la fucoxantina, per una eventuale applicabilità a livello industriale. Sempre a scopo applicativo, ho valutato la possibilità di criopreservare i ceppi di interesse come metodo alternativo per la conservazione a lungo termine.

Nello specifico, oggetto di studio per la produzione di fucoxantina è stata la diatomea marina *Thalassiosira rotula*, specie abbondante del Mar Tirreno già nota per la produzione di diversi bio-composti come prostaglandine, acidi grassi polinsaturi, xantofille (Dimier *et al.*, 2007; Di Dato *et al.*, 2019; Matas *et al.* 2023). Al fine di aumentare la resa in biomassa e il contenuto di fucoxantina in coltura, sono stati valutati due diversi ceppi di *T. rotula* e applicati diversi approcci, quali l'impiego di pre-inoculi con diversi volumi e diverse condizioni di coltura (arricchimento di azoto nel mezzo di coltura e/o bassa intensità luminosa). In seguito ai diversi trattamenti, oltre al contenuto di fucoxantina, sono stati valutate le variazioni morfofisiologiche, il contenuto dei pigmenti fotosintetici e la modulazione dei geni chiave coinvolti nel *pathway* di biosintesi della fucoxantina.

La borsa di dottorato è stata cofinanziata con risorse del
Programma Operativo Nazionale Ricerca e Innovazione 2014-202 (CCI 2014IT16M2OP005)
Fondo Sociale Europeo, Azione I.1 "Dottorati Innovativi con caratterizzazione Industriale"

Considerando le potenziali applicazioni di *T. rotula*, e più in generale delle diatomee, in ambito biotecnologico l'altro focus di questo progetto di dottorato è stato quello di testare metodiche di criopreservazione su diverse specie/ceppi di diatomee. È noto, infatti, come i metodi classici di mantenimento delle colture presentano alcune problematiche legate alla potenziale perdita o alterazione delle caratteristiche della specie nel tempo, eventuali mutazioni genetiche con possibile variazione della fisiologia della specie e perdita dell'eventuale tratto di interesse biotecnologico e, non di secondaria importanza, il verificarsi contaminazioni dovute alle ripetute manipolazioni (Godhe & Rynearson, 2017; Bulankova *et al.*, 2021). In questo contesto, metodi alternativi alle subculture, come la criopreservazione, stanno diventando sempre più diffusi nelle collezioni di colture algali (Stock *et al.*, 2018). Al contempo, sebbene siano sperimentate alcune tecniche di criopreservazione di microalghe, non esiste un protocollo universale (Day, 2007; Tanniou *et al.*, 2012; Buhmann *et al.*, 2013; Kumari *et al.*, 2016). Ciò è strettamente legato alla variabilità inter – intraspecifica di questi organismi ed ai diversi meccanismi di risposta agli stress che si innescano durante la criopreservazione. Durante il periodo di stage svolto presso l'Università di Gent -Laboratorio di Protistologia ed Ecologia Acquatica (PAE) e presso la BCCM Diatom Culture Collection (BCCM/DCG), ho condotto sperimentazioni relative a all'applicabilità di criopreservazione in alcune specie/ceppi di diatomee. Considerando la variabilità nel successo delle tecniche di criopreservazione, ho sperimentato l'applicabilità di criopreservazione in diatomee diverse per taglia, ecologia, potenziale biotecnologico e/o stadio biologico (cellule vegetative vs stadi di resistenza).

La borsa di dottorato è stata cofinanziata con risorse del
Programma Operativo Nazionale Ricerca e Innovazione 2014-202 (CCI 2014IT16M2OP005)
Fondo Sociale Europeo, Azione I.1 "Dottorati Innovativi con caratterizzazione Industriale"

ABSTRACT

Diatoms (*Bacillariophyceae*) are photosynthetic eukaryotic microalgae that play a key role in ecosystems, accounting for 20-25% of global primary production, approximately 40% of annual marine biomass production (Bhattacharjya *et al.*, 2020). One of their most intriguing aspects is their inter- and intraspecific diversity, both morphological and functional.

In recent years, this class of microalgae has emerged as an attractive resource for producing high-value compounds due to their ability to synthesize various bioactive substances (proteins, lipids, polyunsaturated fatty acids, vitamins, pigments, etc.), but also to rapidly increase their biomass, and physiologically adapt to diverse growth conditions (Lauritano *et al.*, 2018; de Jesús-Campos *et al.*, 2020; Cutignano *et al.*, 2022).

In this context, the aim of this Ph. D project was to investigate the use of novel diatom species for the production of industrially high-value compounds, such as fucoxanthin, while also evaluating various conditions and techniques for their long-term cryopreservation.

One of the aims of this work focused on the study for fucoxanthin production in *Thalassiosira rotula*, abundant species in the Tyrrhenian Sea with high levels of bioactive compounds (prostaglandins, polyunsaturated fatty acids, xanthophylls). To enhance biomass yield and fucoxanthin content in cultures, two different strains of *T. rotula* were assessed, and various approaches were applied, including the use of pre-inocula with varying volumes and abiotic treatments (low light intensity and increased nitrate concentration in the culture medium). Furthermore, through an omics approach in collaboration with the Zoological Station "Anton Dohrn" of Naples, several aspects of treated and untreated cultures were analysed, including morphophysiological variations, photosynthetic pigment content, and the modulation of key genes involved in the fucoxanthin biosynthesis pathway.

Considering the potential biotechnological applications of *T. rotula,* and in general of diatoms, another focus of this project was to test cryopreservation methods on different diatom species.

In this context, traditional culture maintenance methods are known to present challenges, such as potential loss or alteration of species characteristics over time, genetic mutations leading to physiological changes and reduced biotechnological relevance, and, importantly, contamination due to repeated handling (Godhe & Rynearson, 2017; Bulankova *et al.*, 2021). In light of this, alternative methods such as cryopreservation are becoming increasingly prevalent in algal culture collections (Stock *et al.*, 2018). However, despite experimental efforts in microalgal cryopreservation, no universal protocol exists (Day, 2007; Tanniou *et al.*, 2012; Buhmann *et al.*, 2013; Kumari *et al.*, 2016). This is closely linked to the inter- and intraspecific variability of these organisms and the diverse stress response mechanisms triggered during cryopreservation, which remain poorly understood.

Given the high specificity required for successful cryopreservation techniques, this work evaluated and optimized several parameters, such as incubation time in the cryoprotective agent and freezing methods (rapid freezing or slow cooling freezing), across five different diatom species characterized by size, environmental adaptation, biotechnological potential, and cell cycle stage. Part of the research activities focused on cryopreservation techniques was conducted at Ghent University, within the Protistology and Aquatic Ecology (PAE) laboratories and the BCCM Diatom Culture Collection (BCCM/DCG).

La borsa di dottorato è stata cofinanziata con risorse del
Programma Operativo Nazionale Ricerca e Innovazione 2014-202 (CCI 2014IT16M2OP005)
Fondo Sociale Europeo, Azione I.1 "Dottorati Innovativi con caratterizzazione Industriale"

Premise

This thesis describes the research work conducted in my Ph. D, structured in four main chapters: the introduction in the Chapter I, followed by two chapters (Chapters II and III) detailing the experimental methodologies and results, and concludes with a final chapter (Chapter IV) summarizing the findings and proposing future directions.

In detail:

- Chapter I: explores the potential biotechnological applications of diatoms, focusing on their key morphological traits, life cycle, ecological roles, and the challenges related to their long-term preservation.
- Chapter II investigates two strains of *Thalassiosira rotula* for fucoxanthin production. This includes developing a simple and efficient method for quantifying fucoxanthin content in this species and analysing the impact of environmental factors on fucoxanthin production. Additionally, it examines the expression of key genes involved in the fucoxanthin biosynthesis pathway under different treatment conditions.
- Chapter III addresses the challenges associated with two cryopreservation techniques—two-step freezing and snap-freezing—across various diatom species and strains. These species/strains differ in ecological traits and growth stages (vegetative cells versus resting stages). The study also evaluates the effects of different exposure times to dimethyl sulfoxide (DMSO), a commonly used cryoprotectant, assessing variations in responses to freezing, thawing, and post-thaw recovery processes.

The findings contribute to identifying and optimizing critical factors that enhance fucoxanthin production in *T. rotula* as a promising resource. Furthermore, they underscore the feasibility and efficacy of cryopreservation techniques for certain diatom species and strains, particularly resting spores, offering an alternative growth stage for species preservation.

La borsa di dottorato è stata cofinanziata con risorse del
Programma Operativo Nazionale Ricerca e Innovazione 2014-202 (CCI 2014IT16M2OP005)
Fondo Sociale Europeo, Azione I.1 "Dottorati Innovativi con caratterizzazione Industriale"

Chapter I

Introduction and thesis outline

1.1 Principal Characteristics of Diatoms

Diatoms are unicellular, photosynthetic microalgae belonging to the class *Bacillariophyceae* within the group Ochrophyta (Stramenopiles). These organisms are ubiquitous, colonizing diverse aquatic environments, including freshwater, marine, and brackish ecosystems, as well as soil and other moist terrestrial habitats (Round *et al.*, 1990).

Diatoms play a pivotal role in global carbon and silica cycles, contributing significantly to primary production and biogeochemical processes (Falkowski *et al.*, 1998; Hockin *et al.*, 2012). Their unique structural and functional characteristics make them essential for research in ecology, palaeontology, and environmental monitoring.

Diatoms exhibit highly distinctive structural and morphological features that set them apart from other microorganisms. The primary characteristic of diatoms is their silica-based cell wall, known as frustule, which is intricately patterned and species-specific. The frustule comprises two overlapping valves, the epitheca (larger, upper half) and the hypotheca (smaller, lower half), fitting together like a petri dish (Round *et al.*, 1990). These valves are held together by a girdle band, which allows for expansion and maintenance of the frustule's integrity (Fig. 1). Moreover, the surface of the frustule is perforated with pores and openings, collectively known as areolae, which facilitate the exchange of gases and nutrients. Species-specific patterns of pores, ridges, and spines give the frustules their remarkable diversity (Hustedt, 1930), and this arrangement and patterning are critical for species identification. In addition, these structures, that protect the cell, play ecological and functional roles such as deterring predators, aiding in buoyancy, enhancing light capture for photosynthesis (Mann & Droop, 1996).

Internally, diatoms possess chloroplasts containing chlorophyll *a*, *c*, and the accessory pigment fucoxanthin, which gives them a golden-brown colour. Their chloroplasts are derived from secondary endosymbiosis, reflecting their evolutionary history.

La borsa di dottorato è stata cofinanziata con risorse del
Programma Operativo Nazionale Ricerca e Innovazione 2014-202 (CCI 2014IT16M2OP005)
Fondo Sociale Europeo, Azione I.1 "Dottorati Innovativi con caratterizzazione Industriale"

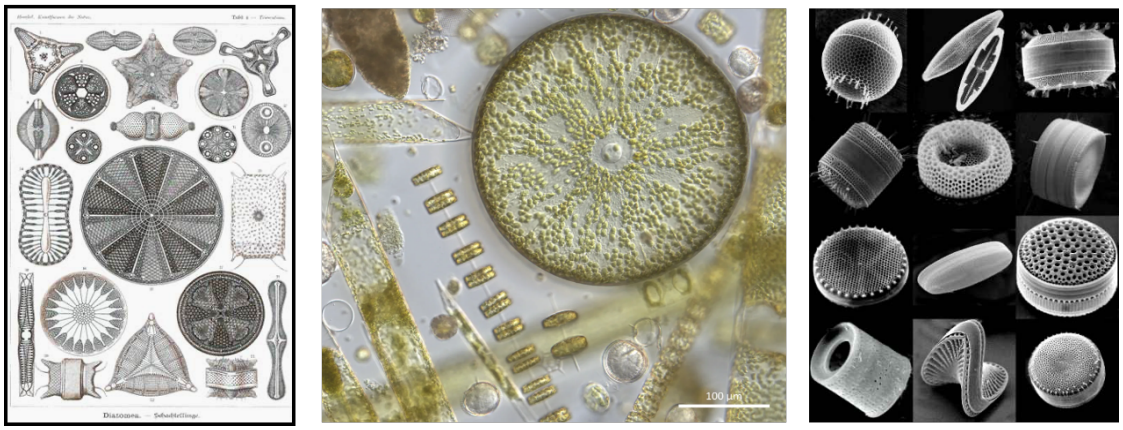

Figure 1. Illustration and microscopic images of diatoms, highlighting their intricate silica-based frustules. Left: Historical artistic representation of diatom diversity (Haeckel, 1904); Center: Light microscopy showing live diatoms in their natural habitat (Western English Channel. Credit Claire Widdicombe, PML); Right: Scanning Electron Microscopy (SEM) revealing the complex and varied architectures of diatom shells, emphasizing their ecological and biological significance (https://nextnature.org/en/magazine/story/2012/nanotech-diatoms).

Life cycle

Diatoms exhibit a diplontic life cycle, with most of their life cycle spent in the vegetative state as diploid cells, primarily reproduce through mitosis. During this process, each daughter cell inherits one of the two valves of the parent cell (epitheca or hypotheca) and constructs a new hypotheca. Over successive generations, this results in a gradual reduction in cell size for one lineage of daughter cells, as each new hypotheca is slightly smaller than the epitheca to which it pairs (Round *et al.*, 1990).

When diatoms reach a critical size threshold (the species-specific minimum size) they undergo sexual reproduction to restore their maximal size. In the centric diatoms sexual reproduction is oogamous, producing non-motile eggs, while the smaller cell produces motile sperm (Mann, 1993); in the pennate diatoms sexual reproduction is typically isogamous, in which gametes of similar size are produced by each cell, and fertilization occurs through direct pairing and fusion of gametes (Mann, 1993).

In addition to this life cycle, diatoms have evolved strategies to survive under unfavourable environmental conditions, such as nutrient depletion, temperature extremes, or salinity changes, forming resting stages and/or resting spores. The spores are morphologically different from vegetative cells, while the resting cells are apparently identical to vegetative cells (McQuoid & Hobson 1996).

These resting stage, characterized by thickened frustules that provide resistance to desiccation and other stressors, are metabolically dormant with high content of storage material, low photosynthetic rates, a high carbon:chlorophyll ratio and a low respiration rate (Hargraves & French, 1983; Ishii *et al.*, 2011, Chamnansinp *et al.*, 2013; Montresor *et al.*, 2013). Spores have been reported in several centric diatoms, but they are extremely rare in pennate species (McQuoid & Hobson 1996). Spores and resting cells play an important role in population dynamics of neritic diatoms. Resting spores settle to the sediment in aquatic environments, where they can remain viable for years and germinate when environmental conditions become favourable, resuming vegetative growth and contributing to seasonal blooms in diatom populations (Hargraves & French, 1983; Härnström *et al.*, 2011; Limoges *et al.*, 2018). This strategy is especially common in marine planktonic diatoms, where nutrient fluctuations are pronounced (Round *et al.*, 1990; Ishi *et al.*, 2011; Montresor *et al.*, 2013).

The diatom life cycle, including both reproduction and resting cells/spore formation, is intricately linked to their ecological success. The ability to alternate between asexual reproduction, sexual reproduction, and spore formation ensures rapid colonization during favourable conditions and resilience during environmental stress. Moreover, sexual reproduction improves the genetic variability, highlighting how in the diatom group, the genetic variability is not only related to the species but also to the level of strains.

Evolutionary history of diatoms

Diatoms (*Bacillariophycae*) are a highly diverse group of microalgae that hold a distinct position within the evolutionary tree of photosynthetic eukaryotes (Fig. 2).

They are part of the Stramenopiles, a broad lineage that includes both photosynthetic organisms (like golden algae and brown algae) and non-photosynthetic protists (such as water moulds).

La borsa di dottorato è stata cofinanziata con risorse del
Programma Operativo Nazionale Ricerca e Innovazione 2014-202 (CCI 2014IT16M2OP005)
Fondo Sociale Europeo, Azione I.1 "Dottorati Innovativi con caratterizzazione Industriale"

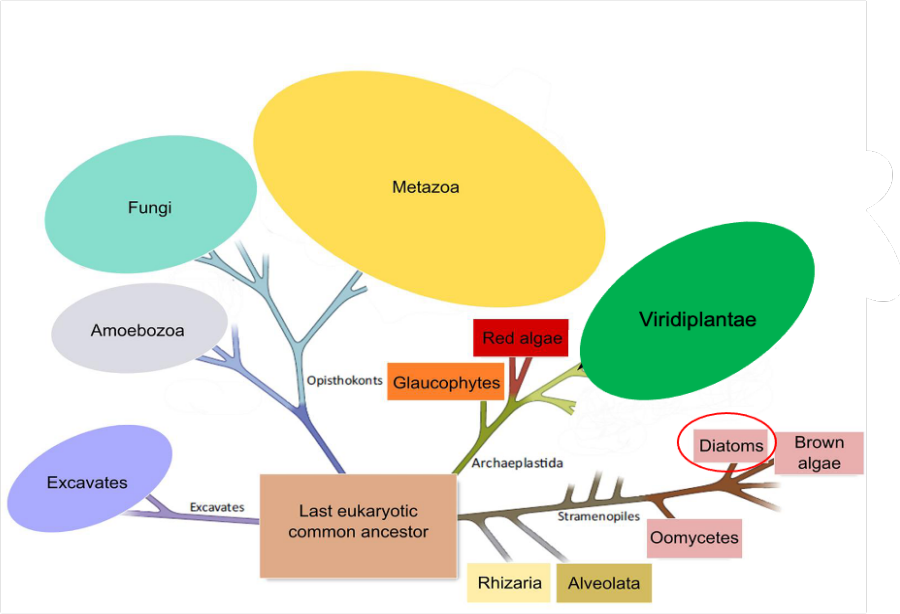

Figure 2. Schematic representation of the eukaryotic tree of life. The red circle highlights the diatom's position on the tree. The image has been taken and adapted by Fernandez et al., 2016.

Their phylogenetic isolation is due to their unique adaptations, diverging from other photosynthetic eukaryotes for unique features such as their silica-based cell walls (frustules), secondary endosymbiotic origin of their chloroplasts, and their specialized life cycles, which have allowed them to dominate marine and freshwater ecosystems for over 200 million years. More in detail, the siliceous cell wall of diatoms is a key evolutionary innovation that sets them apart from all other eukaryotes. The frustule is not unique in structure but is also crucial in protecting cells from predators and helping with buoyancy regulation. This trait underscores the evolutionary distinctiveness of diatoms.

Moreover, the chloroplasts of diatoms are derived from a secondary endosymbiotic event involving a red alga (Fig. 3). This event provided diatoms with pigments such as *fucoxanthin,* which give them their characteristic golden-brown colour and distinct spectral photosynthetic efficiency compared to other phytoplankton groups (Fig. 3) (Falkowski *et al.*, 2004).

La borsa di dottorato è stata cofinanziata con risorse del
Programma Operativo Nazionale Ricerca e Innovazione 2014-202 (CCI 2014IT16M2OP005)
Fondo Sociale Europeo, Azione I.1 "Dottorati Innovativi con caratterizzazione Industriale"

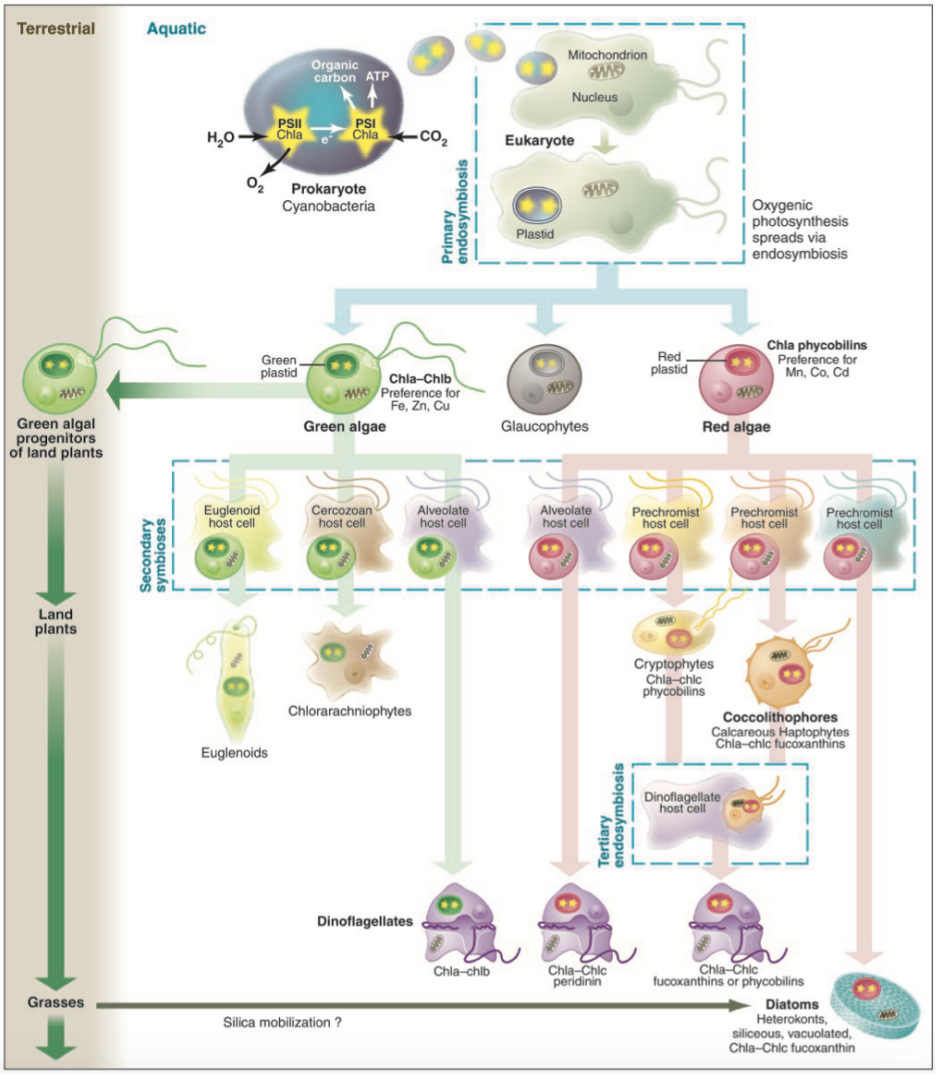

Fig. 3. The picture shows the plastid evolution in eukaryotic phytoplankton: ancestral cyanobacteria became primary symbiotic plastids, leading to three clades: green algae, red algae, and glaucophytes. Secondary symbiosis transferred green plastids to eukaryotic hosts, forming Euglenophytes, Chlorarachnophytes, and "green" dinoflagellates, while red plastids were incorporated into cryptophytes, haptophytes, heterokonts (e.g., diatoms), and peridinin-containing dinoflagellates, the most abundant today. Tertiary symbiosis occurred when heterotrophic dinoflagellates engulfed secondary photosynthetic symbionts like cryptophytes, haptophytes, or diatoms. The image has been taken and adapted by Falkowski et al., 2004.

The first recorded observations of diatoms were made by Antonie van Leeuwenhoek in the late 17th century, describing microorganisms in water, including what are now recognized as diatoms. The systematic study of diatoms began with the pioneering work of Christian Gottfried Ehrenberg in the early 19th century, recognizing the siliceous nature of diatom frustules and their widespread occurrence in both fossil and modern sediments (Khan, 1995).

After this, in the mid-19th century, Kützing described numerous genera and species of diatoms, emphasizing their intricate silica frustules, advancing also in their classification. The development of electron microscopy in the 20th century revolutionized diatom research by revealing previously unseen ultrastructural details of frustules (Sullivan, 1977).

Species identification in diatoms relies on a combination of morphological, molecular, and ecological traits: historically, the primary method of diatom identification has been through the analysis of their silica frustules, including frustule symmetry, ornamentation and raphe system (Medlin *et al.*,1996; Cox & Williams,2006; Cox, 2011). In some cases, the morphology of resting spores and auxospores provides additional clues for species-level identification (Piredda *et al.*, 2017).

With the advent of molecular biology, DNA sequencing has provided new insights into the evolutionary relationships among diatom taxa, challenging traditional morphology-based classifications (Medlin *et al.*, 1996, 2000). Molecular markers, such as ribosomal RNA genes and plastid genes, have been instrumental in resolving ambiguities in diatom phylogeny and in identifying cryptic species (Amato *et al.*, 2007).

Advancements in computational tools and imaging technologies have enhanced the accuracy of diatom identification. Automated image analysis and machine learning algorithms now allow for high-throughput analysis of diatom samples, reducing the reliance on manual microscopy (Finkel *et al.*, 2005). Techniques such as metabarcoding and environmental DNA (eDNA) analysis have further streamlined the detection and monitoring of diatom communities in environmental samples (Zimmermann *et al.*, 2011).

Approximately 200,000 species are identified, showcasing a wide range of sizes and shapes (Round *et al.*, 1990; Drum & Gordon, 2003; Kooistra *et al.*, 2007).

Ecological role

The genetic and phenotypic variability of diatoms play a multifaceted role in ecological systems, making diatoms essential contributors to the health and functioning of aquatic environments. The main roles played by diatoms are listed below.

◊ Primary Production

Diatoms are primary producers in aquatic ecosystems contributing to approximately 20-25% of global photosynthesis and sustaining a vast range of marine and freshwater organisms, from microscopic zooplankton to larger fish and marine mammals (Field *et al.*, 1998; Mann, 1999);

◊ Carbon Sequestration and Climate Regulation

Diatoms are players in the biological pump, fixing atmospheric carbon dioxide, which becomes part of their biomass, and, when they die, their dense silica frustules promote sinking, transporting organic carbon to the ocean floor (Smetacek, 1999);

◊ Silica Cycling

As the primary users of biogenic silica in aquatic ecosystems, diatoms play a central role in the global silica cycle, taking up dissolved silica from water to construct their frustules and influencing the distribution and availability of silica in the environment (Tréguer *et al.*, 1995);

◊ Habitat Formation

Diatoms contribute to the formation of microhabitats within aquatic environments. These biofilms also stabilize sediments, reducing erosion in estuarine and coastal areas (Underwood & Paterson, 2003);

◊ Bioindicators of Environmental Change

Diatoms are widely used as bioindicators due to their sensitivity to environmental conditions, including nutrient availability, pH, temperature, and pollution levels. Specific diatom species thrive in particular ecological niches, making shifts in their community composition indicative of environmental changes (Smol & Stoermer, 2010);

◊ Contribution to Food Web Dynamics

Beyond their role as primary producers, diatoms influence food web dynamics through their high nutritional quality (Goldenberg *et al.*, 2024);

◊ Harmful Algal Blooms

Species can form harmful algal blooms (HABs), producing toxins, such as domoic acid from *Pseudo-nitzschia* species, which accumulate in marine organisms and pose risks to wildlife and human health (Bates *et al.*, 2018).

1.2 Diatoms in the biotechnologies field: challenges and new frontiers

Diatoms have great potential for biotechnological applications due to their biochemical composition, ability to thrive in various water conditions, and high biomass production rates. Their characteristics are valuable for producing bioactive compounds and satisfying the demand for natural, health-promoting products (Fig. 4) (Baldisserotto *et al.*, 2019; Dhaouadi *et al.*, 2020; Marella *et al.*, 2020; Sardo *et al.*, 2021; Sharma *et al.*, 2021).

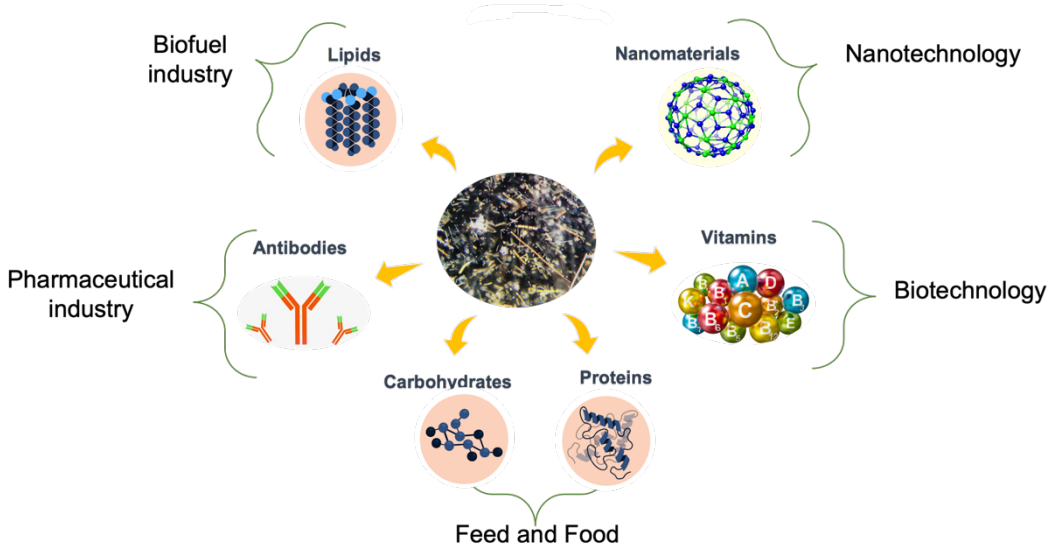

Figure 4. Overview of potential applications of diatoms in different biotechnological fields. Image modified from Dhaouadi et al., 2020.

Moreover, these organisms offer numerous benefits compared to other sources for the production of high-value compounds: they grow quickly, produce a lot of biomass and survive in different environments, adapting themselves to various stresses such as variations in nutrient levels, temperatures, oxygenation, type and intensity of light (Jin and Agustí, 2018; Fu *et al.*, 2022).

As in other organisms, carbohydrates and lipids are vital energy storage metabolites in diatoms, but with changes in the type and the amount. For instance, diatoms are great producers of lipids, including polyunsaturated fatty acids like omega-3, known for their bioactive properties and role in promoting human health, triacylglycerides (TAGs), which are direct precursors for biodiesels, and also steroids and oxylipins (Lauritano *et al.*, 2016; Baldisserotto *et al.*, 2019). Recently, prostaglandins (Pgs), oxygenated natural products derived from the oxidation of PUFAs, similarly to oxylipins, have been identified in some species of marine microalgae, particularly in diatoms (Barbarinaldi *et al.*, 2024; Di Costanzo *et al.*, 2019).

Many studies indicated diatom strains rich in omega fatty acids as an alternative to the dependence on fish, reducing the problems associated with seasonal variations and ocean pollution (Martins *et al.*, 2013). Additionally, species such as *Nitzschia laevis, Nitzschia inconspicua, Navicula saprophila,* and *Phaeodactylum tricornutum* extracts have a noticeable amount of EPA and DHA that can be used as a nutritional feed in human diet and animal feed (Kitano *et al.*, 1997; Wen and Chen, 2001; Wah *et al.*, 2015; Baldisserotto *et al.*, 2019). Environmental stressors have a significant impact on the biosynthesis and production of these compounds. According to Li *et al.* (2014), a deficiency of phosphorus in the growth of *Phaeodactylum tricornutum* causes an increase in TAGs levels in the senescence. Moreover, the growth and accumulation of secondary metabolites in microalgae, such as fatty acids and carotenoids, are influenced by the type and intensity of light, which is considered a crucial environmental factor in the marine ecosystem (Duarte *et al.*, 2021).

Additionally, different types of marine diatoms are being explored for the industrial synthesis of antioxidant pigments like fucoxanthin and other carotenoids (Xia *et al.*, 2013; Kuczynska *et al.*, 2015). Fucoxanthin, in particular, is recognized for its numerous benefits and possible applications in pharmaceuticals, nutraceuticals, as well as the food and cosmetics sectors (Fu *et al.* 2015; Miyashita and Hosokawa 2018).

In this contest, growing diatoms on a large scale for industrial purposes is challenging due to the need to ensure consistent growth conditions, avoid contamination, and optimize the provision of light and nutrients to achieve the highest productivity possible.

However, a significant challenge to their increased use is the maintenance and protection of diatom cultures, especially in large-scale industrial settings.

Keeping diatoms in a continuous culture requires supervision and regulation of their culture's parameters, which can be expensive and impractical for long-term preservation. Hence, the development of effective cryopreservation techniques is a key area of research, offering a possible solution to these problems by enabling diatom strains to be kept for longer periods without compromising their viability and functional integrity. Traditional methods such as serial subculturing may come with high costs, size reduction, sexual reproduction, and genetic mutations over time, leading to changes in their physiology and potentially causing the loss of key characteristics for biotechnological purposes (Godhe & Rynearson, 2017; Bulankova *et al.*, 2021).

Therefore, this led to a demand for alternative methods of subculturing, such as cryopreservation, which are becoming increasingly important in algal culture collections (Stock *et al.*, 2018).

In this view, cryopreservation methods for the long-term storage and the long-lasting health and stability of microalgae are needed, but at the same time, there is no universal protocol (Day, 2007).

Despite these important characteristics of diatoms, many questions remain and need to be investigated.

The objectives of this thesis are aimed at the biotechnological uses of diatoms and for this reason I focused on two aspects: i) enhancing fucoxanthin production; ii) applicability of cryopreservation on some diatom species/strains.

La borsa di dottorato è stata cofinanziata con risorse del
Programma Operativo Nazionale Ricerca e Innovazione 2014-202 (CCI 2014IT16M2OP005)
Fondo Sociale Europeo, Azione I.1 "Dottorati Innovativi con caratterizzazione Industriale"

1.3 Thesis outline

A general overview of the title and the goal of each data chapter is highlighted below.

Chapter 2. Bioprospecting for fucoxanthin from marine diatoms: exploring its improvement and its biosynthetic pathway

In this chapter two different strains of *Thalassiosira rotula,* a centric diatom well described in the Mediterranean Sea, were selected for fucoxanthin production. One of the first aims of this work was to assess an easy and rapid method to evaluate the fucoxanthin content in my species. Based on the spectrophotometric method, edited by Wang *et al.* (2018), and with appropriate modifications, I identify a formula species-specific for *T. rotula*.

After testing the influence of pre-inocula volumes in the growth kinetics and biomass production, the fucoxanthin content was evaluated by spectrophotometric method in *T. rotula Na90A1* strain. I experimented with the influence of environmental factors, such as light intensity and nutrient availability (nitrate) on biomass and fucoxanthin production, linked with morphophysiological analysis. In addition, to validate the spectrophotometric method and to confirm the applicability of this quick method at an industrial scale, I quantify the content of photosynthetic pigments of *T. rotula,* grown in all conditions tested, through HPLC analysis.

The goal was, from one side, to identify the optimal combination of culture conditions for maximizing fucoxanthin yields and on the other side the applicability of the spectrophotometric method.

Furthermore, I investigated the expression levels of the key genes involved in the fucoxanthin biosynthesis pathway and their changes in the expression level in response to the different growth phases and culture conditions.

Altogether, the results obtained contributed to: i) support an alternative low-cost and fast method such as spectrophotometry for the fucoxanthin quantification; ii) identify and optimize key factors that can significantly enhance fucoxanthin productivity in a potential source as *T. rotula*; iii) define the expression level of key genes involved in fucoxanthin

biosynthesis pathway which could contribute to potentially apply bioengineering methods for increasing the sustainable and cost-effective use of diatoms in commercial carotenoid production.

Chapter 3. Improving cryopreservation techniques for diatoms: overcoming the challenges of viability and recovery in marine diatoms species

A recurring problem in the use of diatoms in biotechnological fields is the long-term availability and stability of the high-performing strains. In chapter 3, I aimed to address the significant challenges associated with the cryopreservation of some diatom species/strains, which could exhibit variability in their response to freezing, thawing, post-thawing processes. I assessed the recovery of the cultures after thawing and the physiological health of the cells. I compared two freezing techniques -two-step freezing and snap-freezing- as cryopreservation method on some species/strains of diatoms differing in ecological traits and in different growth stages (vegetative cells vs resting stages) and considering different exposure times to dimethyl sulfoxide, DMSO (the most common cryoprotective agents used).

The results show the applicability and success of cryopreservation techniques for some diatom species and strains of the resting spores as an alternative growth stage for the species preservation. The successful cryopreservation of these life stages could support the sustainable storage and accessibility of high-performing diatom strains for ongoing and future biotechnological applications.

1.4 References

Amato, A., Kooistra, W. H., Ghiron, J. H., Mann, D. G., Proschold, T., & Montresor, M. 2007. Reproductive isolation among sympatric cryptic species in marine diatoms. Protist, 158(2), 193–207;

Baldisserotto, C., Sabia, A., Ferroni, L., Pancaldi, S. 2019. Biological aspects and biotechnological potential of marine diatoms in relation to different light regimens. World J Microbiol Biotechnol 35, 35. https://doi.org/10.1007/s11274-019-2607-z;

Bates, S. S., Hubbard, K. A., Lundholm, N., Montresor, M., & Leaw, C. P. 2018. *Pseudo-nitzschia, Nitzschia,* and domoic acid: new research since 2011. Harmful Algae, 79, 3–43. https://doi.org/10.1016/j.hal.2018.06.001;

Bulankova, P., Sekulić, M., Jallet, D., Nef, C., Van Oosterhout, C., Delmont, T. O., ... & De Veylder, L. 2021. Mitotic recombination between homologous chromosomes drives genomic diversity in diatoms. Current Biology, 31(15), 3221-3232. https://doi.org/10.1016/j.cub.2021.05.013;

Chamnansinp, A., Li, Y., Lundholm, N., & Moestrup, Ø. 2013. Global diversity of two widespread, colony-forming diatoms of the marine plankton, *Chaetoceros socialis* (syn. *C. radians*) and *Chaetoceros gelidus* sp. nov. Journal of Phycology, 49(6), 1128-1141.

Cox, E. J. 2011. Morphology, cell wall, cytology, ultrastructure and morphogenetic studies: overview and specific observations. The diatom world, 21-45;

Cox, E. J., & Williams, D. M. 2006. Systematics of naviculoid diatoms (Bacillariophyta): a preliminary analysis of protoplast and frustule characters for family and order level classification. Systematics and Biodiversity, 4(4), 385-399. https://doi.org/10.1017/S1477200006001940;

Day, J. G. 2007. Cryopreservation of microalgae and cyanobacteria. Cryopreservation and freeze-drying protocols, 141-151. https://doi.org/10.1007/978-1-59745-362-2_10;

Dhaouadi, F., Awwad, F., Diamond, A., & Desgagné-Penix, I. 2020. Diatoms' breakthroughs in biotechnology: *Phaeodactylum tricornutum* as a model for producing high-added value molecules. American Journal of Plant Sciences, 11(10), 1632. doi:10.1007/978-94-007-1327-7_2.;

Drum, R. W., & Gordon, R. 2003. Star Trek replicators and diatom nanotechnology. Trends in Biotechnology, 21(8), 325-328. https://doi.org/10.1016/S0167-7799(03)00169-0;

Duarte, B., Feijão, E., Goessling, J. W., Caçador, I., & Matos, A. R. 2021. Pigment and fatty acid production under different light qualities in the diatom *Phaeodactylum tricornutum*. Applied Sciences, 11(6), 2550. https://doi.org/10.3390/app11062550;

Falkowski, P. G., Barber, R. T., & Smetacek, V. 1998. Biogeochemical controls and feedbacks on ocean primary production. Science, 281(5374), 200–206. https://doi.org/10.1126/science.281.5374.200;

Falkowski, P. G., Katz, M. E., Knoll, A. H., Quigg, A., Raven, J. A., Schofield, O., & Taylor, F. J. R. 2004. The evolution of modern eukaryotic phytoplankton. Science, 305(5682), 354-360. https://doi.org/10.1126/science.1095964;

Fernández, M. B., Tossi, V., Lamattina, L., & Cassia, R. 2016. A Comprehensive Phylogeny Reveals Functional Conservation of the UV-B Photoreceptor UVR8 from Green Algae to Higher Plants. Frontiers in plant science, 7, 1698. https://doi.org/10.3389/fpls.2016.01698;

Field, C. B., Behrenfeld, M. J., Randerson, J. T., & Falkowski, P. 1998. Primary production of the biosphere: integrating terrestrial and oceanic components. Science, 281(5374), 237–240. https://doi.org/10.1126/science.281.5374.237;

Finkel, Z. V., Irwin, A. J., & Schofield, O. 2005. Resource limitation alters the 3/4 size scaling of metabolic rates in phytoplankton. Marine Ecology Progress Series, 273, 269–279. https://doi.org/10.1016/j.jtbi.2009.04.018;

Fu W, Wichuk K, Brynjólfsson S. 2015. Developing diatoms for value-added products: challenges and opportunities. New Biotechnol 32:547–551;

Fu, W., Shu, Y., Yi, Z., Su, Y., Pan, Y., Zhang, F., & Brynjolfsson, S. 2022. Diatom morphology and adaptation: Current progress and potentials for sustainable development. Sustainable Horizons, 2, 100015. https://doi.org/10.1016/j.horiz.2022.100015;

Godhe, A., & Rynearson, T. 2017. The role of intraspecific variation in the ecological and evolutionary success of diatoms in changing environments. Philosophical Transactions of the Royal Society B: Biological Sciences, 372(1728), 20160399. https://doi.org/10.1098/rstb.2016.0399;

Goldenberg, S.U., Spisla, C., Sánchez, N. *et al.* 2024. Diatom-mediated food web functioning under ocean artificial upwelling. Sci Rep 14, 3955. https://doi.org/10.1038/s41598-024-54345-w;

Hargraves, P. E., & French, F. W. 1983. Diatom resting spores: significance and strategies for survival. Marine Biology Letters, 4(1), 49–58. https://doi.org/10.1002/ajb2.1780;

Härnström, K., Ellegaard, M., Andersen, T. J., & Godhe, A. 2011. Hundred years of genetic structure in a sediment revived diatom population. Proceedings of the National Academy of Sciences, 108(10), 4252-425. https://doi.org/10.1073/pnas.1013528108;

Hockin, N. L., Mock, T., Mulholland, F., Kopriva, S., & Malin, G. 2012. The response of diatom central carbon metabolism to nitrogen starvation is different from that of green

algae and higher plants. Plant physiology, 158(1), 299-312. https://doi.org/10.1104/pp.111.184333;

Hustedt, F. 1933. Die Kieselalgen Deutschlands, Osterreichs und der Schweiz. Kryptogamenflora von Deutschland, Osterreich und Schweiz, 7(2), 321-576;

Ishii, K. I., Iwataki, M., Matsuoka, K., & Imai, I. 2011. Proposal of identification criteria for resting spores of *Chaetoceros* species (Bacillariophyceae) from a temperate coastal sea. Phycologia, 50(4), 351-362. https://doi.org/10.2216/10-36.1;

Jin, P., & Agustí, S. 2018. Fast adaptation of tropical diatoms to increased warming with trade-offs. Scientific Reports, 8(1), 17771. https://doi.org/10.1038/s41598-018-36091-y

Kahn, R. 1995. CG Ehrenberg's concept of the diatoms. Archiv für Protistenkunde, 146(2), 109-116;

Kitano, M., Matsukawa, R., & Karube, I. 1997. Changes in eicosapentaenoic acid content of *Navicula saprophila*, *Rhodomonas salina* and *Nitzschia* sp. under mixotrophic conditions. Journal of Applied Phycology, 9, 559-563. https://doi.org/10.1023/A:1007908618017;

Kooistra, W. H., Gersonde, R., Medlin, L. K., & Mann, D. G. 2007. The origin and evolution of the diatoms: their adaptation to a planktonic existence. Evolution of Primary producers in the sea, 207-249. https://doi.org/10.1016/B978-012370518-1/50012-6;

Kuczynska, P., Jemiola-Rzeminska, M., & Strzalka, K. 2015. Photosynthetic pigments in diatoms. Marine Drugs, 13(9), 5847-5881. https://doi.org/10.1007/978-981-19-5920-2_1;

Lamers, P. P., van de Laak, C. C., Kaasenbrood, P. S., Lorier, J., Janssen, M., De Vos, R. C., ... & Wijffels, R. H. 2010. Carotenoid and fatty acid metabolism in light-stressed

Dunaliella salina. Biotechnology and Bioengineering, 106(4), 638-648. https://doi.org/10.1002/bit.22725;

Lauritano, C., Romano, G., Roncalli, V., Amoresano, A., Fontanarosa, C., Bastianini, M., ... & Ianora, A. 2016. New oxylipins produced at the end of a diatom bloom and their effects on copepod reproductive success and gene expression levels. Harmful Algae, 55, 221-229. https://doi.org/10.1016/j.hal.2016.03.015;

Li, S., Xu, J., Chen, J., Chen, J., Zhou, C., & Yan, X. 2014. Characterization of the triacylglycerol profile in marine diatoms by ultra performance liquid chromatography coupled with electrospray ionization–quadrupole time-of-flight mass spectrometry. Journal of Applied Phycology, 26, 1389-1398. https://doi.org/10.1007/s10811-013-0159-4;

Limoges, A., Masse, G., Weckström, K., Poulin, M., Ellegaard, M., Heikkilä, M., ... & Ribeiro, S. 2018. Spring succession and vertical export of diatoms and IP25 in a seasonally ice-covered high Arctic fjord. Frontiers in Earth Science, 6, 226. https://doi.org/10.3389/feart.2018.00226;

Mann, D. G. 1993. Patterns of sexual reproduction in diatoms. Hydrobiologia, 269(270), 11–20;

Mann, D. G. 1999. The species concept in diatoms. Phycologia, 38(6), 437–495;

Mann, D. G., & Droop, S. J. M. 1996. Biodiversity, biogeography and conservation of diatoms. Hydrobiologia, 336(1-3), 19–32;

Marella, T. K., López-Pacheco, I. Y., Parra-Saldívar, R., Dixit, S., & Tiwari, A. 2020. Wealth from waste: Diatoms as tools for phycoremediation of wastewater and for obtaining value from the biomass. Science of the Total Environment, 724, 137960. https://doi.org/10.1016/j.scitotenv.2020.137960;

Martins, D. A., Custódio, L., Barreira, L., Pereira, H., Ben-Hamadou, R., Varela, J., & Abu-Salah, K. M. 2013. Alternative sources of n-3 long-chain polyunsaturated fatty acids in marine microalgae. Marine Drugs, 11(7), 2259-2281. https://doi.org/10.3390/md11072259;

McQuoid, M. R., & Hobson, L. A. 1996. Diatom resting stages. Journal of Phycology, 32(6), 889–902;

Medlin, L. K., Elwood, H. J., Stickel, S., & Sogin, M. L. 2000. Molecular evolution of diatoms. Protist, 151(4), 237–248. https://doi.org/10.3390/ijms23020618;

Medlin, L. K., Kooistra, W. H. C. F., Gersonde, R., Wellbrock, U., 1996. Evolution of the diatoms (Bacillariophyta).2. Nuclear-encoded small-subunit rRNA sequence comparisons confirm a paraphyletic origin for the centric diatoms. Mol. Biol.Evol.13,67–75;

Miyashita K, Hosokawa M. 2018. Health impact of marine carotenoids. J Food Bioact 1:31–40.https://doi.org/10.31665/JFB.2018.1125;

Montresor, M., Di Prisco, C., Sarno, D., Margiotta, F., & Zingone, A. 2013. Diversity and germination patterns of diatom resting stages at a coastal Mediterranean site. Marine Ecology Progress Series, 484, 79-95. https://doi.org/10.3354/meps10236;

Piredda, R., Sarno, D., Lange, C. B., Tomasino, M. P., Zingone, A., & Montresor, M. 2017. Diatom resting stages in surface sediments: A pilot study comparing Next Generation Sequencing and Serial Dilution Cultures. Cryptogamie, Algologie, 38(1), 31-46. https://doi.org/10.7872/crya/v38.iss1.2017.31;

Round, F. E., Crawford, R. M., & Mann, D. G. 1990. The Diatoms: Biology and Morphology of the Genera. Cambridge University Press;

Sardo, A., Orefice, I., Balzano, S., Barra, L., & Romano, G. 2021. Mini-review: potential of diatom-derived silica for biomedical applications. Applied Sciences, 11(10), 4533. https://doi.org/10.3390/app11104533;

Sharma, N., Simon, D. P., Diaz-Garza, A. M., Fantino, E., Messaabi, A., Meddeb-Mouelhi, F., ... & Desgagné-Penix, I. 2021. Diatoms biotechnology: various industrial applications for a greener tomorrow. Frontiers in Marine Science, 8, 636613. https://doi.org/10.3389/fmars.2021.636613;

Smetacek, V. 1999. Diatoms and the ocean carbon cycle. Protist, 150(1), 25–32;

Smol, J. P., & Stoermer, E. F. 2010. The Diatoms: Applications for the Environmental and Earth Sciences. Cambridge University Press;

Stock, W., Pinseel, E., De Decker, S., Sefbom, J., Blommaert, L., Chepurnova, O., ... & Vyverman, W. 2018. Expanding the toolbox for cryopreservation of marine and freshwater diatoms. Scientific Reports, 8(1), 4279. https://doi.org/10.1038/s41598-018-22460-0;

Sullivan, C. W. 1977. Diatom mineralization of silica. Marine Biology Letters, 1(1), 51–54;

Tréguer, P., Nelson, D. M., van Bennekom, A. J., Demaster, D. J., Leynaert, A., & Quéguiner, B. 1995. The silica balance in the world ocean: a reestimate. Science, 268(5209), 375–379;

Underwood, G. J. C., & Paterson, D. M. 2003. The importance of extracellular carbohydrate production by marine epipelic diatoms. Advances in Botanical Research, 40, 184–240. https://doi.org/10.1016/S0065-2296(05)40005-1;

Wah NB, Ahmad AL, Chieh DC and Hwai AT. 2015. Changes in Lipid Profiles of a Tropical Benthic Diatom in different Cultivation Temperature Asian Journal of Applied Science and Engineering, 4, 91-101;

Wang, L. J., Fan, Y., Parsons, R. L., Hu, G. R., Zhang, P. Y., & Li, F. L. 2018. A rapid method for the determination of fucoxanthin in diatom. Marine Drugs, 16(1), 33 https://doi.org/10.3390/md16010033;

Wen, Z. Y., & Chen, F. 2001. Application of statistically-based experimental designs for the optimization of eicosapentaenoic acid production by the diatom *Nitzschia laevis*. Biotechnology and Bioengineering, 75(2), 159-169. https://doi.org/10.1002/bit.1175;

Xia, S., Wang, K., Wan, L., Li, A., Hu, Q., & Zhang, C. 2013. Production, characterization, and antioxidant activity of fucoxanthin from the marine diatom *Odontella aurita*. Marine Drugs, 11(7), 2667-2681. https://doi.org/10.3390/md11072667

Zimmermann, J., Abarca, N., Enke, N., & Jahn, R. 2011. Taxonomic reference libraries for environmental barcoding: a best practice example from diatom research. PLoS ONE, 6(6), e20675.https://doi.org/10.1371/journal.pone.0108793

La borsa di dottorato è stata cofinanziata con risorse del
Programma Operativo Nazionale Ricerca e Innovazione 2014-202 (CCI 2014IT16M2OP005)
Fondo Sociale Europeo, Azione I.1 "Dottorati Innovativi con caratterizzazione Industriale"

Chapter II

Bioprospecting for fucoxanthin from marine diatoms: exploring its improvement and its biosynthetic pathway

Abstract

Diatoms showed a distinctive pigment profile that is crucial for both efficient light capture and photoprotection, contributing to the ecological success of these microalgae in different environments.

Among these pigments, including chlorophylls and various carotenoids, fucoxanthin stands out due to its unique chemical structure, which plays a key role in light absorption. Additionally, fucoxanthin shows significant application in the biotechnology field, especially in the nutraceutical, pharmaceutical, and cosmetic sectors, due to its strong antioxidant, anti-cancer, and anti-inflammatory properties.

This chapter aims to find the optimal conditions for enhancing fucoxanthin production in the diatom *Thalassiosira rotula*, a promising species for biorefinery products.

Two selected treatments' conditions (low-intensity light and nutrient enrichment) were applied to improve fucoxanthin production. Under these treatments also biomass, morphophysiological characters and lipid content were evaluated.

Moreover, another key point was to apply a rapid and efficient method for quantifying fucoxanthin content. A spectrophotometric approach tuned on *T. rotula* was carried out and the results compared with the HPLC methodology.

Lastly, an important aspect of this research was also to explore the role of specific key genes of the fucoxanthin biosynthetic pathway, linking their expression level to different growth stages and culture conditions.

La borsa di dottorato è stata cofinanziata con risorse del
Programma Operativo Nazionale Ricerca e Innovazione 2014-202 (CCI 2014IT16M2OP005)
Fondo Sociale Europeo, Azione I.1 "Dottorati Innovativi con caratterizzazione Industriale"

2.1 Introduction

2.1.1 Chlorophylls and carotenoids in diatoms: key pigments for photosynthesis and photoprotection

Diatoms are well adapted to their habitats through efficient photon accumulation and CO_2 uptake, as well as a fast response to strong light. However, the pigment composition of diatoms differs significantly from that observed in plants and certain algae.

The first group of pigments are chlorophylls that capture light energy to use in the process of photosynthesis (Jeffrey *et al.*, 2005; Kuczynska *et al.*, 2015; da Silva & Lombardi, 2020). Chlorophylls have a mostly unchanging structure in terms of chemistry, except for chlorophyll c (Chl c) found in diatoms, where the phytyl chain is missing in most Chl c pigments. Moreover, Chl c presents mostly in two distinct forms, Chl c_1 and c_2, within diatoms among diverse types (Kuczynska *et al.*, 2015; da Silva & Lombardi, 2020) (Fig. 1). Generally, chls' absorption spectra include two bands: one in the blue range (Soret band) and the other in the red range (Qx and Qy bands), corresponding to S0-S2 and S0-S1 transitions, respectively (Björn *et al.*, 2009; Chen, 2014). Chlorophylls also play a role in electron transfer, with Chl c acting as an antenna pigment, like chlorophyll b in higher plants.

La borsa di dottorato è stata cofinanziata con risorse del
Programma Operativo Nazionale Ricerca e Innovazione 2014-202 (CCI 2014IT16M2OP005)
Fondo Sociale Europeo, Azione I.1 "Dottorati Innovativi con caratterizzazione Industriale"

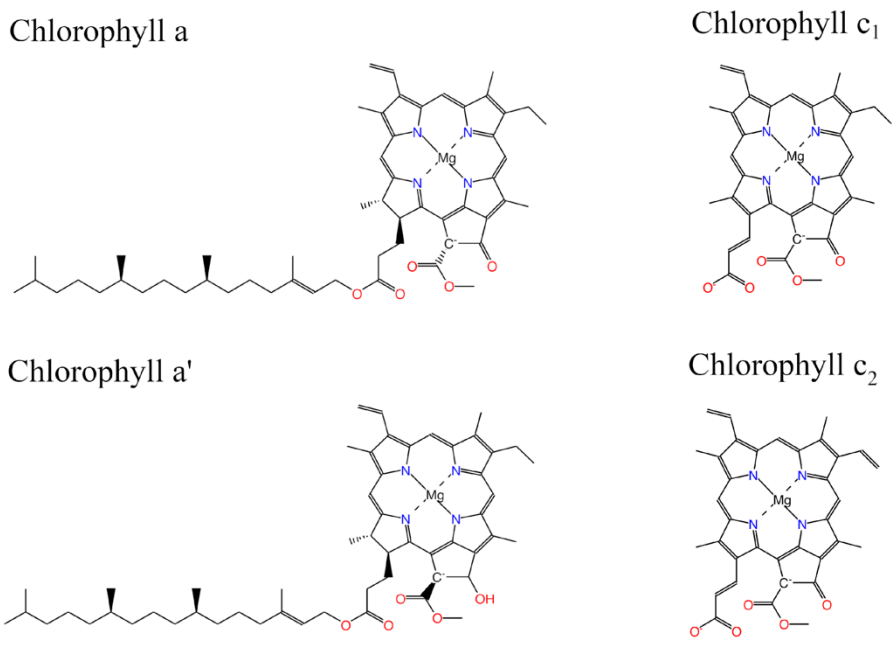

Figure 1. Chemical structure of chlorophyll in diatoms. Image adapted from MetaCYC

The second group of pigments, the carotenoids, are primarily involved in photoprotection. Around 700 types of carotenoids were identified and classically divided in carotenes (hydrocarbons) and xanthophylls, their oxygenated derivatives (Britton *et al.*, 2004). Inside these groups, among the most known pigments are β-carotene (β-car) as carotene, and fucoxanthin (Fx) diadinoxanthin (Ddx), and diatoxanthin (Dtx), violaxanthin (Vx), antheraxanthin (Ax), and zeaxanthin (Zx), as examples of xanthophylls (Fig. 2). This pigment profile is responsible for the ecological success of diatoms by aiding in effective light harvesting.

In addition, the Chl a and Chl c together with Fx are arranged in the fucoxanthin-chlorophyll protein (FCP) complexes, similar to light-harvesting complexes (LHC) in plants, to perform the light-harvesting function (Premvardhan *et al.*, 2009; Gelzinis *et al.*, 2015; Zhou *et al.*, 2024). Furthermore, β-car, Ddx, and Dtx play a crucial part in photoprotection, as Vx, Ax, and Zx may also contribute due to their prevalent all-trans-isomers.

La borsa di dottorato è stata cofinanziata con risorse del
Programma Operativo Nazionale Ricerca e Innovazione 2014-202 (CCI 2014IT16M2OP005)
Fondo Sociale Europeo, Azione I.1 "Dottorati Innovativi con caratterizzazione Industriale"

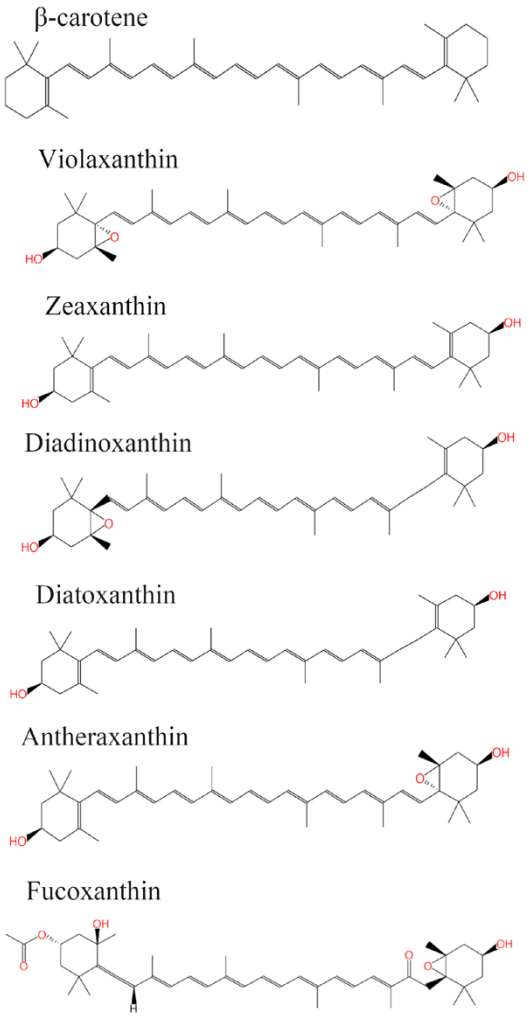

Figure 2. Chemical structure of principal carotenoids in diatom. Image adapted from MetaCYc

2.1.2 Carotenoids in diatoms: biosynthetic pathway and photoprotective mechanisms in xanthophyll cycles

In plants, extensive research has been conducted on the biosynthetic pathways of chlorophylls and carotenoids, providing most of the information about these processes. This knowledge gives numerous possibilities for research on genetic modification and for *in vitro* methods with recombinant proteins.

However, in microalgae, including diatoms, many steps involved in this biosynthetic pathway are still unknown. Most of the genes encoding for enzymes involved in this pathway were studied through genome alignment, yet they remain unidentified.

In this view, the complete genetic sequences of two diatom species, *Phaeodactylum tricornutum* (Bowler *et al.*, 2008) and *Thalassiosira pseudonana* (Armbrust *et al.*, 2004) were analysed and few analogues found in plants were also found in diatoms. It's known that both the two main pathways, methylerythritol phosphate (MEP) and mevalonate (MEV), are involved in the initial steps for the carotenoid biosynthesis and some studies indicate that its regulation is correlated with the taxon or growth rate (Seth *et al.*, 2021). Nevertheless, the results of each pathway are dimethylallyl diphosphate (DMAPP) and its isomer, isopentenyl pyrophosphate (IPP) (Frommholt *et al.*, 2008): DMAPP is converted into geranylgeranyl pyrophosphate (GGPP) using *GGPP synthase* and transformed it into phytoene with *phytoene synthase* (*PSY*). After that, desaturation and isomerization of phytoene form the linear all-trans lycopene in a multistep reaction, is catalyzed by different enzymes: phytoene desaturases (PDS), 15-cis-ζ-carotene isomerase (ZISO), ζ-carotene desaturases (ZDS), and carotenoid isomerase (CRTISO) (Sandmann 2002; Breitenbach and Sandmann 2005; Li *et al.* 2007; Coesel *et al.*, 2008). The last steps determine cyclization by lycopene-β-cyclase (LcyB) to obtain β-carotene (Seth *et al.*, 2021) (Fig. 3).

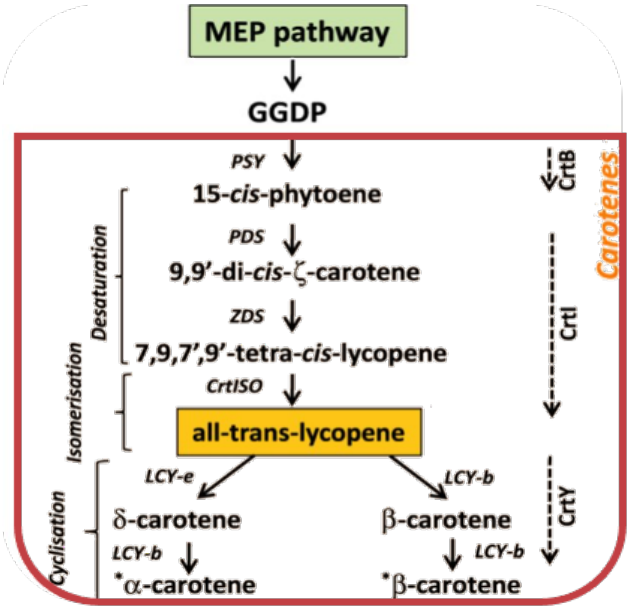

Figure 3. The carotenoid biosynthesis pathway found in almost all plants. GGDP, Geranylgeranyl diphosphate is derived from the plastidial MEP (methylerythritol phosphate) pathway; Abbreviation: PSY, Phytoene synthase; PDS, Phytoene desaturase; ZDS, zeta carotene desaturase; CRITSO, Carotenoid isomerase; LCY-b, Lycopene b-cyclase; Image adapted from Badejo, 2018.

Other steps are classified in the xanthophyll cycle, the diadinoxanthin (Ddx) and the violaxanthin (Vaz) cycles, which play an important photo-protective mechanism preventing high irradiance of light that may lead to photo-inhibition, photo-damage by ROS, and deactivation of photosystems. The xanthophyll cycle involves the transformation of epoxidized carotenoids to de-epoxidized carotenoids and is strongly regulated by light type and intensity (Fig. 4) (Seth *et al.*, 2021). Concerning the Vaz cycle, recent studies proposed that zeaxanthin, via antheraxanthin, was converted into violaxanthin, a reaction regulated by stromal zeaxanthin epoxidase (ZEP) and activated under low light or in the dark (Eilers *et al.*, 2016; Seth *et al.*, 2021). On the contrary, under high light intensity and in the presence of ascorbate and mild acidic conditions in the thylakoid lumen, violaxanthin de-epoxidase (VDE) converts the violaxanthin to zeaxanthin (Eilers *et al.*, 2016). In the model organisms, *T. pseudonana* and *P. tricornutum*, different forms of VDEs and ZEPs were identified: two isoforms in *T. pseudonana*, while three isoforms in *P. tricornutum*, respectively (Frommholt *et al.* 2008).

Moreover, the Ddx cycle is identified as the most important short-term photoprotective mechanism in diatoms; otherwise, it's observed to have a relation with the Vaz cycle. Most probably, Vx is converted in trans-neoxanthin, a precursor of Ddx. Based on the type and intensity of light, mono-epoxy diadinoxanthin is changed to epoxy-free diatoxanthin by the enzyme diadinoxanthin de-epoxidase (DDE), and the back response is catalysed by a diatoxanthin epoxidase (DEP). Indeed, many studies showed that increasing light intensity induces the conversion of Ddx in Dtx for self-protection, reducing fucoxanthin biosynthesis (Fig. 4).

La borsa di dottorato è stata cofinanziata con risorse del
Programma Operativo Nazionale Ricerca e Innovazione 2014-202 (CCI 2014IT16M2OP005)
Fondo Sociale Europeo, Azione I.1 "Dottorati Innovativi con caratterizzazione Industriale"

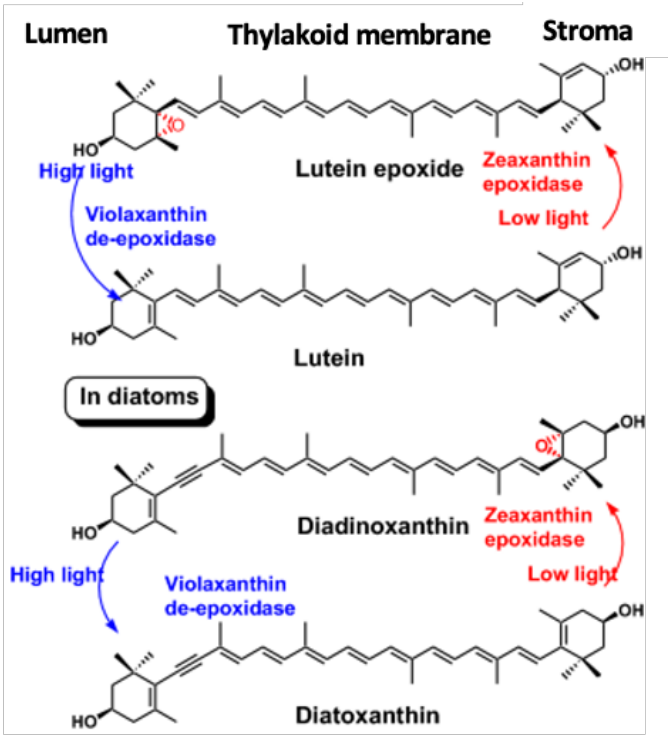

Figure 4. Violaxanthin and diadinoxanthin cycle in diatoms in response to intensity of light. Image adapted from Maoka et al., 2019.

Moreover, the last steps of Fx biosynthesis are still unclear. Lohr and Wilhelm (2001) proposed a via in which Vx is converted in Ddx and then in Fx. The other model proposed the synthesis of neoxanthin (Nx), considered the most likely precursor, from catalyzation of Vx by violaxanthin de-epoxidase–like (VDL) (Dambek *et al.*, 2012; Dautermann *et al.*, 2020). Nonetheless, the synthesis of Fx involves two changes: the ketolation of Nx and the acetylation of an intermediate, fucoxanthinol (Fig. 5) (Bai *et al.*, 2022).

Until now, it's still unknown the enzymes involved in these steps, considering that not all plants and seawater organisms showed this pathway.

Identifying the entire xanthophyll biosynthetic pathway is crucial due to the numerous research possibilities it offers, as well as the potential to develop transgenic organisms with elevated xanthophyll levels (Bai *et al.*, 2022).

La borsa di dottorato è stata cofinanziata con risorse del
Programma Operativo Nazionale Ricerca e Innovazione 2014-202 (CCI 2014IT16M2OP005)
Fondo Sociale Europeo, Azione I.1 "Dottorati Innovativi con caratterizzazione Industriale"

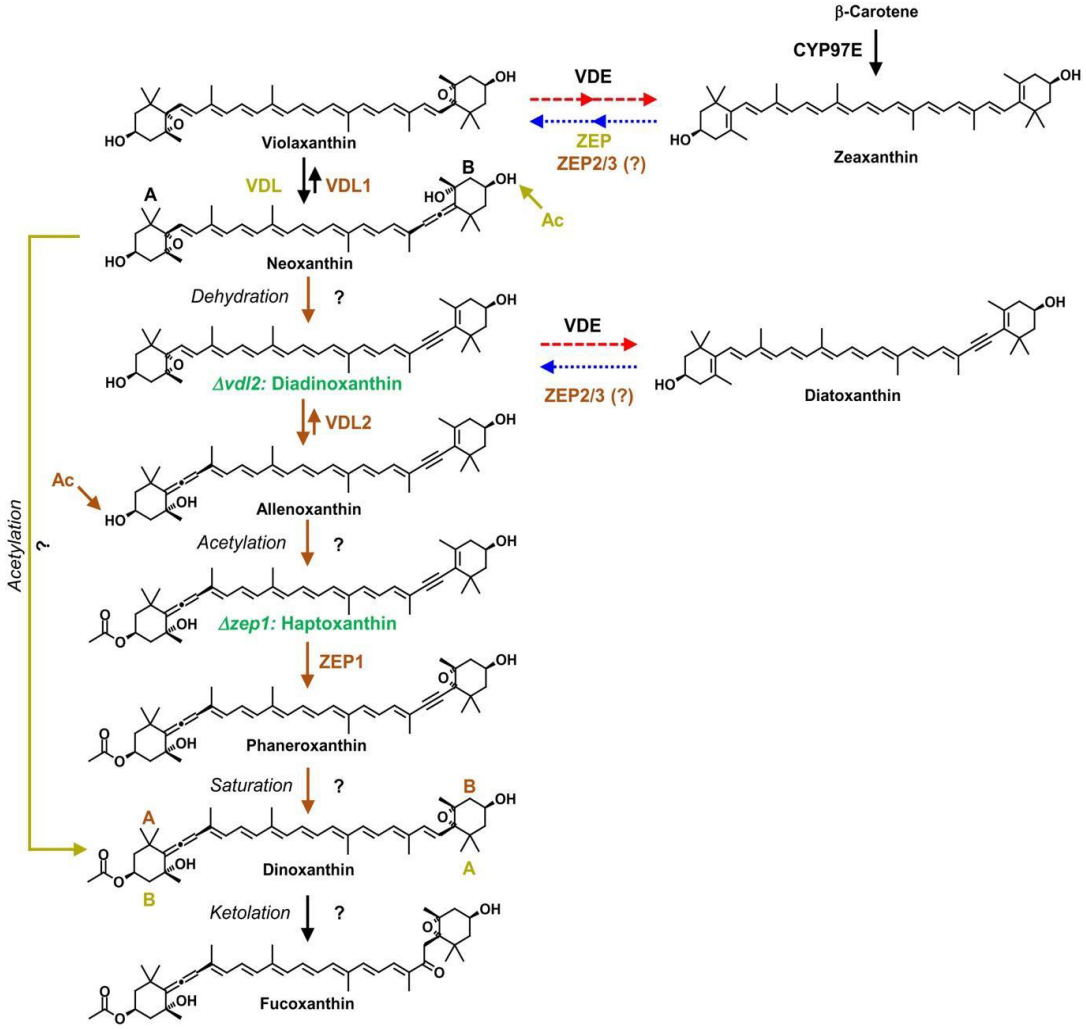

Figure 5. Proposed pathways of fucoxanthin biosynthesis in diatoms. Red arrows with dashes indicate high activity of the xanthophyll cycle induced by light, while blue arrows with dots indicate reverse reactions catalyzed in low light. Abbreviations: VDE, violaxanthin de-epoxidase; VDL, violaxanthin de-epoxidase-like; ZEP, zeaxanthin epoxidase. Image modified from Bai et al., 2022.

2.1.3 Fucoxanthin: a sustainable resource in the biotechnological field and strategies to enhance their biosynthesis

The high attention to fucoxanthin biosynthesis is also correlated with its structure and role: the molecular structure of this pigment gives diatoms special characteristics in absorbing light across a wide range, from blue to green/yellow lights, between 460 and 570 nm, and is involved in crucial biological function for the growth (Wilhelm *et al.*, 2006; Lavaud *et al.*, 2012).

In the photosynthesis process, Fx plays a key role in enhancing light capture efficiency by chlorophylls and protecting against oxidative damage from intense light (Rochaix, 2014). However, different studies showed the highest biotechnological potential as a significant market player in nutraceutical, medicine, and cosmetic fields due to its various health benefits and properties such as being anti-oxidant, anti-cancer, and anti-diabetes (Lee & Nam, 2020; Miyashita *et al.*, 2020; Chen *et al.*, 2021; Pajot *et al.*, 2022). Despite its unique chemical structure, fucoxanthin cannot be chemically synthesized, making it an eco-friendly natural alternative as bio-compound.

The global Fucoxanthin market was valued at US$ 34.6 million in 2023 and is anticipated to reach US$ 44.8 million by 2030, witnessing a CAGR of 3.8% during the forecast period 2024-2030 (Global Fucoxanthin market, 2023, https://reports.valuates.com/market-reports/QYRE-Auto-27O9355/global-fucoxanthin).

Currently, the main sources of fucoxanthin for food are macro-algae like *Laminaria* sp., *Sargassum* sp., *Fucus* sp., *Undaria pinnatifida* and *Hijka fusiformis*, but their low concentration makes extraction expensive and supply restricted (Xia *et al.*, 2013; Bayu *et al.*, 2020). Nevertheless, the marine diatom *Phaeodactylum tricornutum* showed more than 100 times the amount of Fx found in brown algae, making it a potential valuable commercial source (Fig. 6).

Other microalgae showed high concentrations of fucoxanthin ranging from 0.2 to 2.08 mg/g in fresh samples and 2.24 to 59.2 mg/g in dried samples (McClure *et al.*, 2018) (Fig. 6). For example, *Isochrysis* aff. *galbana* has significant levels of Fx 18.23 mg/g DW) and could represent a highly promising source for commercial applications (Kim *et al.*, 2012).

However, the amount of fucoxanthin in microalgae is correlated with the laboratory setting and changes in seasons in the field. In general, microalgae have the potential to be a cheaper and more plentiful source of fucoxanthin than brown macroalgae (Fung *et al.*, 2013; Nomura *et al.*, 2013; Fernandes *et al.*, 2016). Globally, diatoms are easy to cultivate, producing a high biomass in a short time.

The most notable diatoms like *P. tricornutum* and *Thalassosira weissflogii* can reach, for instance, in different types of photobioreactors, a biomass productivity of 1500 $mg \cdot L^{-1} \cdot day^{-1}$ and 538 $mg \cdot L^{-1} \cdot day^{-1,}$ respectively (Gómez-Loredo *et al.*, 2016; Marella & Tiwari, 2020).

La borsa di dottorato è stata cofinanziata con risorse del
Programma Operativo Nazionale Ricerca e Innovazione 2014-202 (CCI 2014IT16M2OP005)
Fondo Sociale Europeo, Azione I.1 "Dottorati Innovativi con caratterizzazione Industriale"

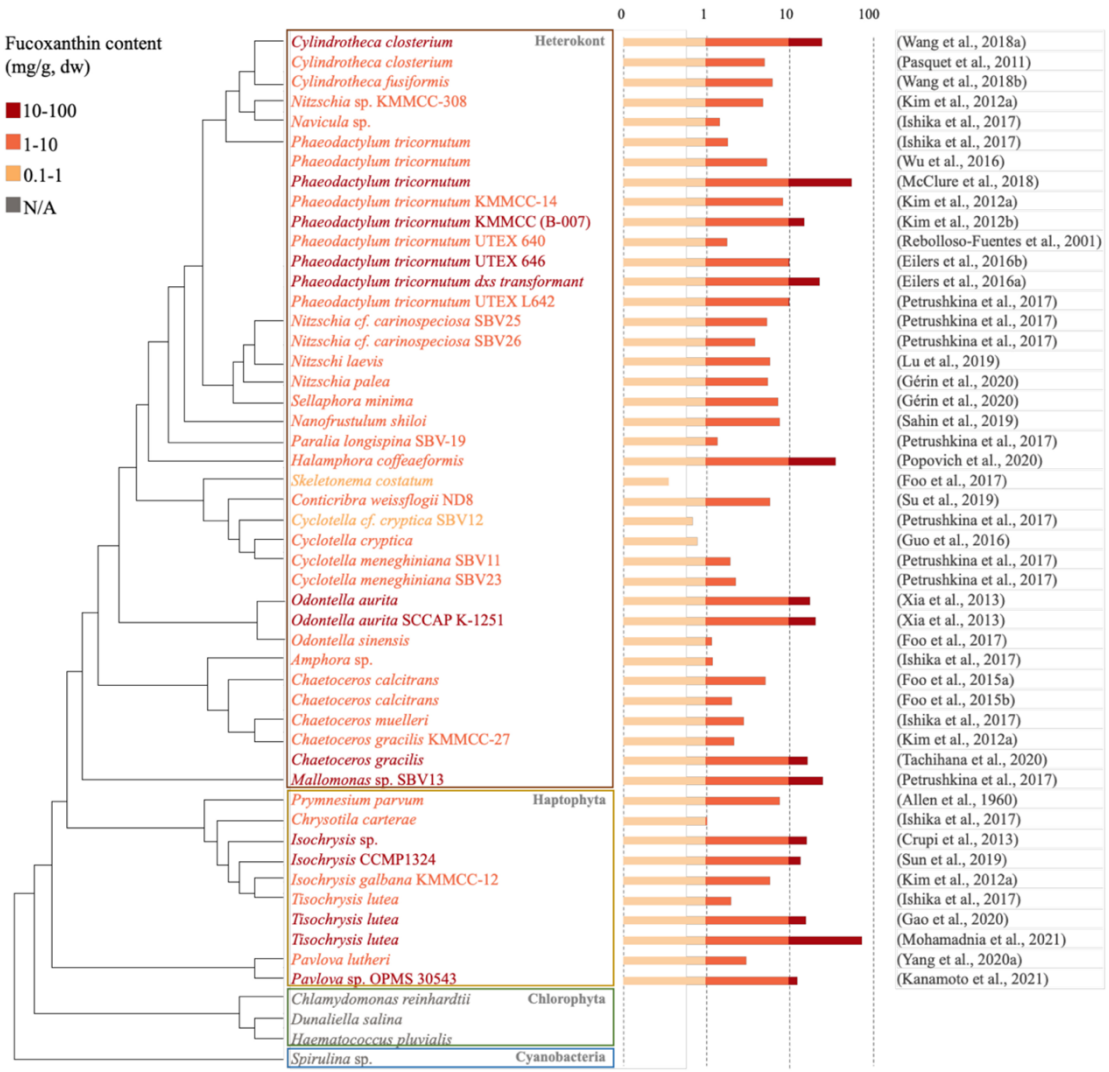

Figure 6. Fucoxanthin content in microalgal cell factories. Microalgae are listed in a phylogenetic tree based on 18S rDNA gene sequences of the representative (image modified from Wang et al., 2021).

Different studies were conducted to identify the best abiotic conditions to improve the production of Fx in various species. It's known that light conditions regulate pigment levels, leading to rapid conversions without changes in gene expression, although long-term acclimation can alter gene transcript levels. Recent studies showed that blue light has a significant impact on diatoms, increasing cell growth and Fx content and eicosapentaenoic acid (EPA) production (Marella and Tiwari, 2020), whereas red light (RL) was more suitable for cell growth and Fx accumulation than blue light (BL) and white light (Zhang *et al.*, 2022).

In addition to light, nitrogen is an important factor in Fx production. It is a crucial nutrient for the growth and development of microalgae due to its presence in nucleic acids and proteins and affects pigment content because porphyrins, including chlorophylls, contain nitrogen (Zarrinmehr *et al.*, 2020).

Various studies have used various methods, such as different nitrogen sources and concentrations, to enhance Fx production from cultivating microalgae (Wang *et al.*, 2018), demonstrating a strong correlation between nitrate concentration and the reliance on fucoxanthin in different types of microalgae (Gao *et al.*, 2017; Xia *et al.*, 2018).
Another interesting aspect to consider is that, although microalgae, like diatoms and Haptophytes, can produce fucoxanthin in large quantities, a standardized extraction method has not yet been established. Obtaining fucoxanthin economically, requires simple, fast, and low-cost technology methods, which has become a significant challenge.

This chapter explores the diatom *Thalassiosira rotula* as a promising candidate for producing fucoxanthin.

The primary focus was on finding the optimal conditions for enhancing both biomass and fucoxanthin biosynthesis. At this aim, low light intensity and the addition of nitrate in the culture medium were tested to stimulate an over-production of Fx in laboratory conditions. Another key focus of this study involves *T. rotula* and a quick, low-cost extraction technique to measure the amount of Fx present, on the basis of previous research by Wang *et al.* (2018) who explored the possible use of a spectrophotometric technique to determine the Fx content comparing the values with those form HPLC analysis.

Moreover, the expression analysis of some key genes of the Fx biosynthetic pathway was conducted. This aspect provides insight in the perspective of biotechnological applications as engineering some steps of the biosynthesis pathway that should result in a high-yield production strain for fucoxanthin.

La borsa di dottorato è stata cofinanziata con risorse del
Programma Operativo Nazionale Ricerca e Innovazione 2014-202 (CCI 2014IT16M2OP005)
Fondo Sociale Europeo, Azione I.1 "Dottorati Innovativi con caratterizzazione Industriale"

2.2 Material and methods

2.2.1 Sample Collection and Strains Culturing

Two different strains of the centric diatom *Thalassiosira rotula, Dirca1* and *Na90A1,* were provided by Culture Collection of Zoological Station "Anton Dorn" (Naples-Italy). *Dirca1* was isolated from resting cells germinated from sediments collected in the frame of the project "EMOBON"; *Na90A1* was isolated from a phytoplankton sample collected at the LTER-MC site in the Gulf of Naples (Tyrrhenian Sea, Mediterranean Sea).

The genotype of the strains was identified and classified as *T. rotula* species by sequencing the D1-D3 region of the nuclear-encoded large subunit ribosomal DNA (partial 28S rDNA) (Gaonkar *et al.*, 2017). Cultures were maintained in sterile filtered oligotrophic seawater at 36 ppt supplemented with f/2 nutrients (Guillard, 1975). The cultures were grown in a 50 ml Erlenmeyer flask with a constant temperature of 19 °C under fluorescent lamp illumination (80 μmol $m^{-2} \cdot s^{-1}$) with light: dark cycles of 12 h:12. Preliminary, in order to improve cell growth, two different pre-inocula volumes (Vi) were tested (Tab.1). A cell density of $1*10^3$ cell/ml was inoculated in pre-inocula #1 (15 ml) and #2 (250 ml) volume in the basal medium (f/2) respectively (Tab. 1) and the growth was monitored.

Table 1. Culture condition to optimize the growth of the two strains of T. rotula

Culture parameter		
Stock	Vi	Cells Density Inoculated
Pre-inoculum #1	15 ml	1 x 10^3 cell/ml
Pre-inoculum #2	250 ml	1 x 10^3 cell/ml

At the exponential phase, the best pre-inoculum was transferred into an Erlenmeyer flask of 2L (Vf 1.5 L), provided by mixing and aeration by bubbling air.

2.2.2 Growth dynamic and morphometric features

Every two days, culture subsamples were fixed in Lugol's iodine solution. Cell density was obtained by counting the cells in 1 ml of samples using the Sedgewick Rafter chamber under a Leica DMi microscope (Leica, Milan, Italy) at 100x magnification. The specific growth rate was determined as:

$$\mu = (\ln N1) - \ln (N0) / (t1 - t0)$$

where N1 and N0 represent the cell densities (cells/ml) at t0 and t1 the time points considered (day). The maximum growth rate (μ_{max}) was calculated from t0 as the beginning of the exponential phase to the end of the exponential phase (t1) when ln(N) versus time was linear.

For morphometric features images of the two strains, at exponential (Exp) and late exponential (Late exp) phases, were taken under a Leica DMRB microscope equipped with a digital camera Leica DFC320 (Leica, Milan, Italy) at 400x magnification.

As morphometric parameters, the pervalvar and apical axes were measured using Fiji software (https://imagej.net/software/fiji/) and biovolume was calculated as reported by Sun and Liu (2003):

$$V = \frac{\pi}{4} \cdot b^2 \cdot a$$

where *a* and *b* represent the height and the radius, respectively.

2.2.3 Spectrophotometry assay

For detecting the concentration of fucoxanthin in *T. rotula* using spectrophotometry, I referred to the work of Wang *et al.* (2018) with some modifications. Specifically, 50 ml of cultures at the exponential phase were collected and centrifuged at 4700 × g for 15 min. The pellet was resuspended in a basal medium (defined as Algal Suspension Culture - ASC) and the absorbance was measured at 750 nm, after dilution with basal medium (the absorbance value at 750 nm needed to be between 0.1 to 0.8). In parallel, the process was repeated, but the pellet was resuspended in an equal volume of

ethanol (Algal Suspension Ethanol- ASE) and the absorbance was measured at 445 nm e 663 nm, after dilution with ethanol (the absorbance value at 445 nm and 663 nm needed to be between 0.2 to 1).

Three biological replicates and three independent readings were carried out within 5 minutes. The concentration of fucoxanthin (Fx) was initially calculated by applying Equation (1) (Wang *et al.*, 2018):

$$[Fx]\ (\text{mg/L}) = 6.39 \times (A445 - n_1) - 5.18 \times (A663 - n_2) \qquad \text{(eq. 1)}$$

where [*Fx*] is the concentration of fucoxanthin in mg/L and n_1 and n_2 represent the correction for interference from other pigments and /or cell debris, calculated by a regression line obtained with the absorbance values of the residue pigment mixture (ASE) and cell debris (ASC) measured at 445 nm and 663 nm, vs absorption data at 750 nm as ordinate, respectively.

$$[Fx]\ (\text{mg/L}) = 6.39 \times A445 - 5.18 \times A663 + 0.312 \times A750 - 5.27 \qquad \text{(eq. 2)}$$

In my culture system, I re-calculated n_1 and n_2 and I used the eq. 1 modified for *T. rotula* (eq. 3)

$$[Fx]'\ (\text{mg/L}) = 6.39 \text{ x } A445 - 5.18 \text{ x } A663 - 3.56 \text{ x } A750 - 0.068 \qquad \text{(eq. 3)}$$

2.2.4 Improvement of Fx production

Growth condition

To improve cell growth/and or Fx production, different culture conditions were tested: i) high nitrate supplementation in the medium (HN, High Nitrate, 882 µM $NaNO_3$) (Afonso *et al.*, 2022); ii) low light intensity treatment (LL, Low Light, 30 µmol photons m^{-2} s^{-1}) (Wang *et al.*, 2018); iii) low light intensity and high nitrate supplementation (LL HN).

As control, the culture was grown in standard condition (Ctrl in f/2 medium at 80 µmol m^{-2} s^{-1}). The experimental set-up is detailed in Tab. 2.

Table 2. Growth condition of T. rotula Na90A1

Culture parameter				
	Cells Density Inoculated (cells/ml)	Final volume (L)	Light intensity	Medium
Ctrl	2 x 10^3 cells/ml	1.5 L	80 µmol photons m^{-2} s^{-1}	f/2
HN	2 x 10^3 cells/ml	1.5 L	80 µmol photons m^{-2} s^{-1}	f/2 modified (882 µM $NaNO_3$)
LL	2 x 10^3 cells/ml	1.5 L	30 µmol photons m^{-2} s^{-1}	f/2
LL HN	2 x 10^3 cells/ml	1.5 L	30 µmol photons m^{-2} s^{-1}	f/2 modified (882 µM $NaNO_3$)

Morphophysiological analyses

Total biomass as dry weight (DW) was determined at the exponential (Exp) and late exponential (Late exp) phases, for all the cultures. Briefly, 100 ml of cultures were filtered using the Whatman GF/C filter and dried at 80°C for 24 h. The biomass was expressed as dry weight per milliliter (DW mg/ml).

Furthermore, at Exp and Late exp phases, the morphometric features of all samples were detected as above reported (sec. 2.2.2). Further, an *in vivo* analysis to detect the intracellular neutral-lipids was conducted by staining the samples with Nile Red (NR, 9-diethylamino-5Hbenzo[α]phenoxazine-5-one) (Sigma-Aldrich) (Alemán-Nava *et al.*,2016). Preliminarily, various concentrations of NR were tested to determine the efficiency of staining in *T. rotula* and finally a working solution of 50 µg/ml diluted in DMSO was used. NL fluorescence was measured by a Confocal Scanning Laser Microscope (Leica TCS SP8 inverted) equipped with a 20x dry objective and using excitation and emission wavelengths of 485-530 nm and 575-580 nm respectively. The

autofluorescence of chlorophylls (Ex: 405 nm; Em: 650-750 nm) and NR signal intensities were detected and their content correlated to the pixel cell fluorescence intensity measured using Fiji software.

Determination of Photosynthetic Pigment Contents: spectrophotometric assay and HPLC profile

The Fx content of all samples was quantified by the spectrophotometric method as reported above. Further, the chlorophylls a and c contents were estimate by spectrophotometric according to the following Ritchie's equations (2008), with absorbance values recorded at wavelengths of 665 nm and 632 nm:

$$Chl\ a\ (\mu g/ml) = 13.2654 \times A665nm - 2.6839 \times A632nm$$
$$Chl\ c\ (\mu g/ml) = 28.8191 \times A632nm - 6.0138 \times A665nm$$

For pigment content using HPLC, *T. rotula* cultures at exponential (Exp) and late exponential (Late exp) phases, were filtered on Glass Fiber Filter (G/FF) and frozen in liquid nitrogen. For pigment extraction, 3 mL methanol 100% were added to freeze-dried filters. The pigment solution was filtered through a 0.22 µm nylon syringe filter (VWR, Radnor, PA, USA). Samples were protected from light exposure. The collected pigment solutions were analysed at 440 nm using a Hewlett Packard photodiode array detector model DAD series 1100 (HPLC - DAD) which gives the 400-700 nm spectrum for each detected pigment. A fluorometer (Hewlett Packard standard FLD cell series 1100) with excitation at 407 nm and emission at 665 nm allowed the detection of fluorescent molecules (chlorophylls and their degraded products). The reversed-phase column corresponded to an apolar stationary phase composed of silica beads possessing aliphatic chains of 8 carbon atoms (2.6 mm diameter C8 Kinetex column; 50 mm × 4.6 mm; Phenomenex®, USA). The mobile phase was composed of two solvents mixture: A, methanol: aqueous ammonium acetate (1M) (70:30, v/v) and B, absolute methanol. During the 12-minute elution, the gradient between the solvents was programmed: 75% A (0 min), 50% A (1 min), 0% A (8 min), 0% A (11 min), and 75% A (12 min).

The samples were analysed to identify pigments based on retention time, absorption spectra, and co-chromatography through the pigment standards purchased from DHI (Hørsholm, Denmark).
The content of pigments in all samples was calculated using the following formula:

$$\mu g/\mu l = (Area * Coeff. * V. Extr.)/(V.Iniet. * V.Filtr. * 0.5/0.75) * 1000$$

In which:

Area= area of picks (DAD);

Coeff. = coefficient of pigment;

V. extr., iniet., filtr. = volume of samples extracted, injected and filtered respectively.

2.2.5 RNA isolation and quantitative Real-time PCR (RT-qPCR)

For RNA extraction, culture pellets at exponential and late exponential phase of growth were collected using a centrifuge 14000 rpm x 30 min. Total RNA was extracted following the RNA Isolation Mini Kit (Agilent Technologies, Santa Clara, CA, USA) protocol. Additional steps, after the addition of extraction buffer and vortexing, were introduced to remove proteins: supernatant obtained after a centrifugation at full speed (13,000 rpm x 5 min), were transferred to a clean Eppendorf and an equal volume of chloroform: isoamyl alcohol (24:1) was added, vortexing vigorously again, and then finally centrifuged at full speed (13,000 rpm x 15 min). Each RNA sample was treated with RNAse- free DNAse (Qiagen, Hilden, Germany), to further purify the solution. The RNA extracted was assessed for purity and concentration using a NanoDrop (ND-1000 UV-VIS spectrophotometer; NanoDrop Technologies, Wilmington, DE, USA). RNA samples were converted into cDNA through reverse transcription using the SuperScript III First-Strand Synthesis System for RT-PCR (Invitrogen), following the manufacturer's guidelines.

Quantitative Real-time PCR (RT-qPCR)

Gene expression analyses were performed using specific primer pairs for selected genes designed using Primer3 (Koressaar and Remm 2007; Untergasser *et al.* 2012; Koressaar *et al.* 2018) (Tab. 3). PCR and gel electrophoresis were utilized to find primer pairs that specifically amplified the target without forming dimers. The efficiency of the primers was determined by analysing a standard curve, where the -1/slope efficiency was substituted with newly designed primers and subsequently re-evaluated.
GADPH and TUBα were chosen as endogenous controls, as stated by Di Dato *et al.* (2019) (Tab. 3). Gene expression was relatively quantified using the ΔCT method as described by Schmittgen and Livak (2008).

Table 3. Sequence of primers used for RT-qPCR

List of primers tested	**SEQUENCE 5'-3' Forward**	**SEQUENCE 5'-3' Reverse**	**Amplification**
Phytoene Synthase (PSY1)	ATTGTAAGGTGAAGTATCCCGC	GGTCCCAGCCACACGATAAC	166 bp
Phytoene Synthase (PSY2)	TGAAGAGCAGCCAATCGGAC	ACATCATCCGTTATTTCGTCCA	185 bp
Phytoene Desaturase (PDS1)	GTGTGTTCCAGTCCCGTGATG	CTGGGTTGGTATGAGGCGTTTG	150 bp
Phytoene Desaturase (PDS2)	GATGCTTACGCTGGGTGAGAAA	CACCTCCTCGTTGATTCTCTCG	151 bp
Zeta Carotene Desaturase (ZDS)	GGCGTGACCGTGAATCTCTC	GGCAGCACCTTCTTGATTCCG	170 bp
Zeta Carotene Isomerase (ZCIS)	CCGTTCCAGGCTATTTGAGGC	CCACCAGCATTCAACCCCGA	166 bp
Lycopene Beta Cyclase (LCYB)	CTGGATTCTTGGCGGGATGGA	GTATCAGGCTCTCCCAACAATG	205 bp
Lycopene Beta Cyclase (LCYB)	GCCTCCTGCTCCCTCGCC	GTATCGGACCAATGCGTATCG	200 bp
Zeaxanthin Epoxidase (ZEP1)	CCCGTAGCATTGTGTGGCGA	CGAATGACACGAACACGGGAA	170 bp

Zeaxanthin Epoxidase (ZEP2)	CGTGAAGCGGCGGGACCTAT	GAACTCCCTCCAACTCTCGTC	170 bp
Zeaxanthin Epoxidase (ZEP3)	GTCTCCTCCTTCTCGCCATCA	AAGCGTTTGTTCGGATGATTGTG	213 bp
Violaxanthin De-Epoxidase like (VDL1)	GGCTAAGGCAGGGTTGGACT	ATACTCGCCACGCCATCCTG	181 bp
Violaxanthin De-Epoxidase like (VDL2)	GCGGACTGGTGGATGAAGCG	TCCCCTCCCAGCGATTCCC	155 bp
Violaxanthin De-Epoxidase like (VDL3)	CAATGGTGGTGTTGGGGAGAA	CTTGTCCTGGGTCATTCTCGC	205 bp
Diadinoxanthin De-Epoxidase (DDE)	GATACGGAGGTGCGGTGGTC	AATCGCCATCTTCCCCGCAAA	194 bp
Carotenoid isomerase (CRTISO1)	GAGCGGCAAGGCAGTGGGA	GCCTTGACCCCGAGATGCA	237 bp
Carotenoid isomerase (CRTISO 2)	GATTGCGGGATGGCGTCGTC	CATTCCCGCAGTCAACGCCAC	158 bp
Carotenoid isomerase (CRTISO 3)	GCTCGCCTTTGACCCACGC	CTCCACTCAACGCCACAGCA	165 bp
Tubulina alfa (TUBa)	GTATCGCCAGCTCTACCATCC	GTGGCGTGGAAGATGAGGAATC	176 bp
Glyceraldehyde-3-phosphate dehydrogenase (GAPDH)	CTGCGAAGGTCCATCCACCGTC	CCACAAGGAGTACGAGAACAGC	172 bp

* in red primers that didn't give any amplification

Identification of Violaxanthin de-epoxidase like and phylogenetic analysis

The three isoforms of predicted *Violaxanthin de-epoxidase like* were identified using Unipro UGENE 51.0 software (http://ugene.net) and the NCBI BLAST database tool (https://blast.ncbi.nlm.nih.gov/Blast.cgi).

These 3 genes were also analysed with the most similar *VDL* of different diatoms using for the alignments using the MUSCLE algorithm inbuilt in Unipro UGENE 51.0 software (http://ugene.net). The aligned sequences were used to construct a Maximum likelihood tree with the Bootstrap method (1000 bootstrap) through MEGA11 (Molecular Evolutionary Genetics Analysis).

2.2.6 Two-phase culturing system in a short time

In a later experiment, a two-phase culture approach was investigated to promote biomass and Fx production by light shift for a short time. My two-phase system was applied using in the first phase the optimal wavelength (80 µm m^{-2} s^{-1}), and after three days of grown, the cultures (T0) were transferred to low light condition (LL 30 µm m^{-2} s^{-1}) for two days (T1). For these treatments, the cell's biovolume and the total biomass as dry weight (DW mg/ml) were determined. To evaluate the pigment content, spectrophotometry and HPLC analysis were performed as above reported. The expression of the key genes of the Fx biosynthetic pathway was also assessed.

2.2.7 Statistical analysis

For each condition, three Erlenmeyer flasks were employed as biological replicates, and for morphometric analysis, a minimum of 70 cells were measured. All data are expressed as mean ± standard error of biological replicates. Statistical analyses, including one-way and two-way analysis of variance (ANOVA), followed by Tukey's test, were performed using the statistical software GraphPad PRISM 9 (GraphPad Software Inc., San Diego, CA, USA). Statistical significance differences were considered at $p < 0.05$ or $p < 0.01$.

La borsa di dottorato è stata cofinanziata con risorse del
Programma Operativo Nazionale Ricerca e Innovazione 2014-202 (CCI 2014IT16M2OP005)
Fondo Sociale Europeo, Azione I.1 "Dottorati Innovativi con caratterizzazione Industriale"

2.3 Results

2.3.1 Growth dynamics of *Thalassiosira rotula* strains

To improve the growth kinetic and the biomass of the cultures I tested for the two strains of *Thalassiosira rotula*, *Dirca1* and *Na90A1*, two different volumes as pre-inocula in basal medium (f/2), namely pre-inocula #1 (15 ml) and #2 (250 ml). As shown in Fig. 1, the pre-inocula growth curves were different in both the two strains. *Dirca1* pre-inocula #1 showed a longer lag phase (Fig. 7 A), while in pre-inocula #2, the exponential phase peaked around 6 days (Fig. 7 B). In contrast, *Na90A1* pre-inocula #1 grew quickly in the first 3 days (Fig. 7 C), while the pre-inoculum #2 showed a slow exponential growth with a trend similar to *Dirca1* (Fig. 7 D).

According to the growth curves, the maximum growth rate (μ_{max}) showed relevant differences between both the strains as well as the pre-inocula: the pre-inocula #2 showed higher values respect to pre-inocula#1 with the highest value for *Dirca1* (Fig. 7 B). As for biomass, *Dirca1* pre-inocula#2 reached a maximum cell density of 7×10^4 cell/ml at a late exponential phase respect to *Na90A1* that reached 1.2×10^4 cell/ml (Fig. 7 B, D).

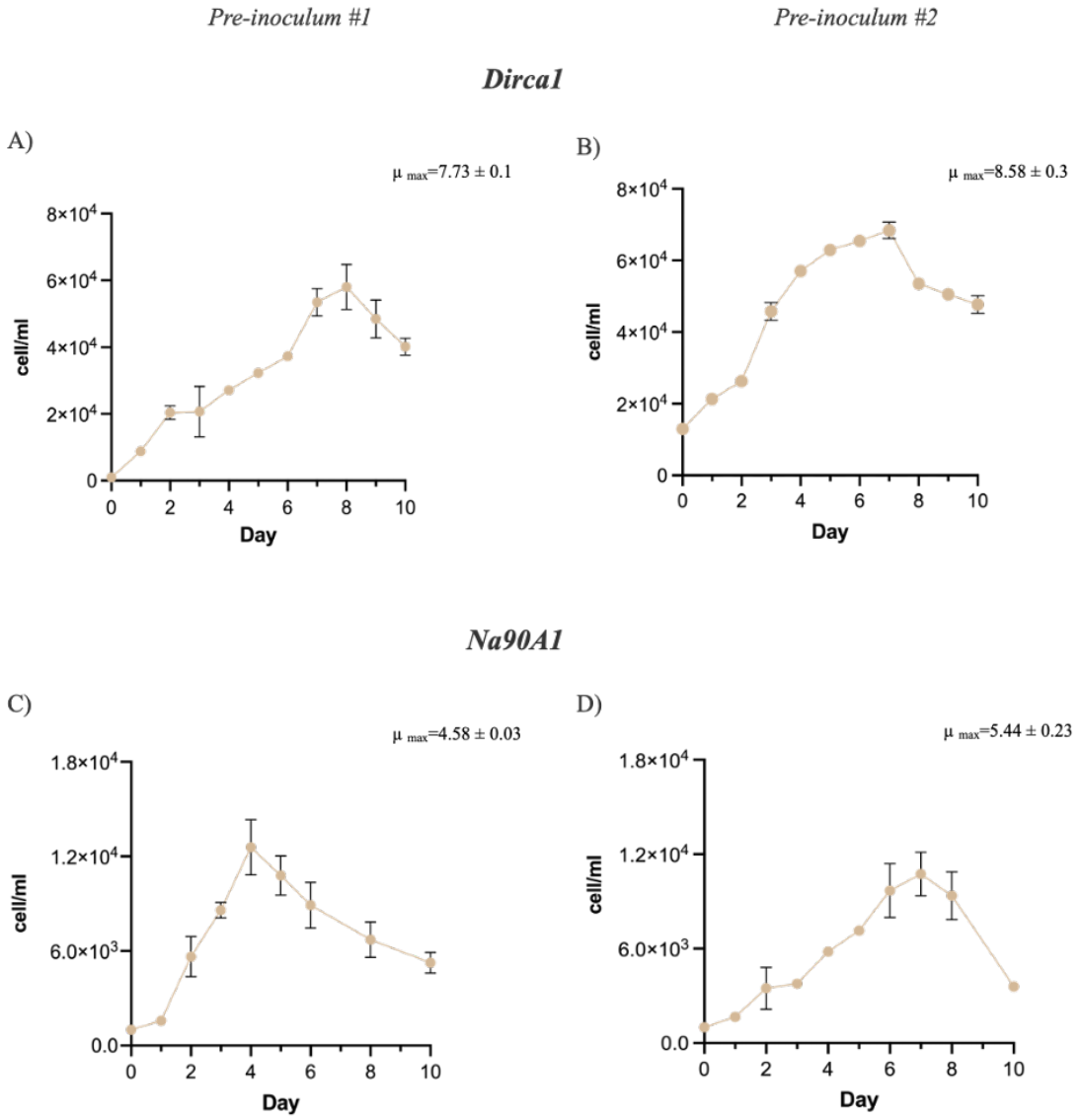

Figure 7. Growth curves of the two strains of Thalassiosira rotula *grown in the basal medium in two different pre-inocula volumes.* Dirca1 *pre-inocula #1 (A) and #2 (B);* Na90A1 *pre-inocula #1 (C) and #2 (D), respectively. For each strain and inocula, the values of maximum growth rate (μmax) were reported on the graph.*

By evidence that pre-inocula #2 showed a higher μmax, as well as a higher cell density, the pre-inocula #2, at the exponential phase, were transferred to a final volume of 1.5 L in a fresh f/2 medium and the growth curves were monitored for both strains (Fig. 8).

The growth curve showed that *Dirca1* reached the pick of exponential growth at 7 days (Fig. 8 A), while *Na90A1* grew faster with the peak of exponential phase at 5 days (Fig. 8 B); despite that, no significant differences in μmax between the two strains were observed, showing values of about 9.0.

La borsa di dottorato è stata cofinanziata con risorse del
Programma Operativo Nazionale Ricerca e Innovazione 2014-202 (CCI 2014IT16M2OP005)
Fondo Sociale Europeo, Azione I.1 "Dottorati Innovativi con caratterizzazione Industriale"

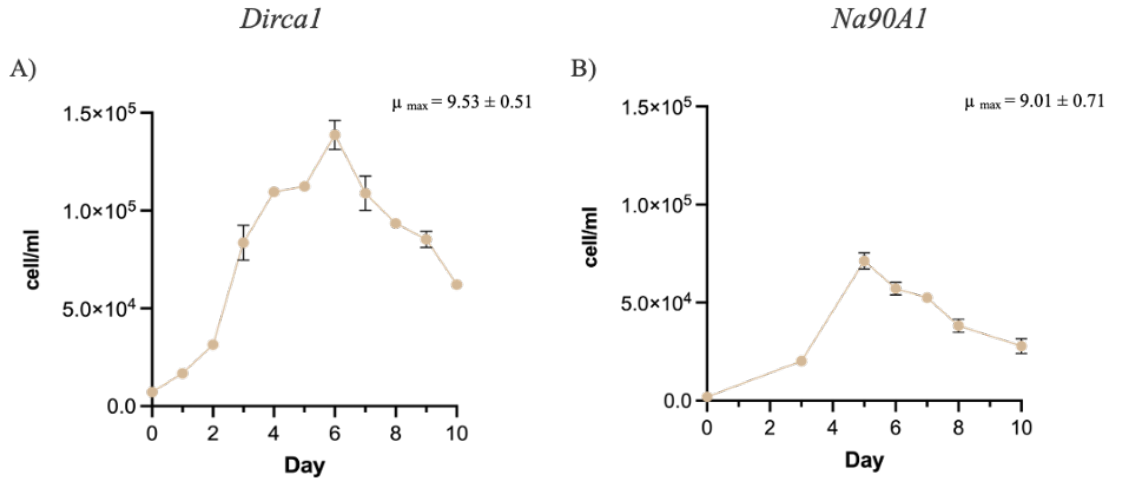

Figure 8. Growth curve and maximum growth rate (μmax) of Thalassiosira rotula Dirca1 *(A) and* Na90A1 *(B) strains after transferring pre-inocula #2 in a final volume of 1.5 L of fresh basal medium. The value of the maximum growth rate (μmax) was marked on the graph. Values are the means ± standard error.*

Furthermore, the *Dirca1* strain reached, at the peak of the exponential phase, a higher cell density than *Na90A1* (2.3 x 10^5 cell/ml vs 6 x 10^4 cell/ml); nonetheless, as highlighted also in the Fig. 9, *Na90A1* showed a higher size and biovolume more than 5 times than *Dirca1* (Tab.4).

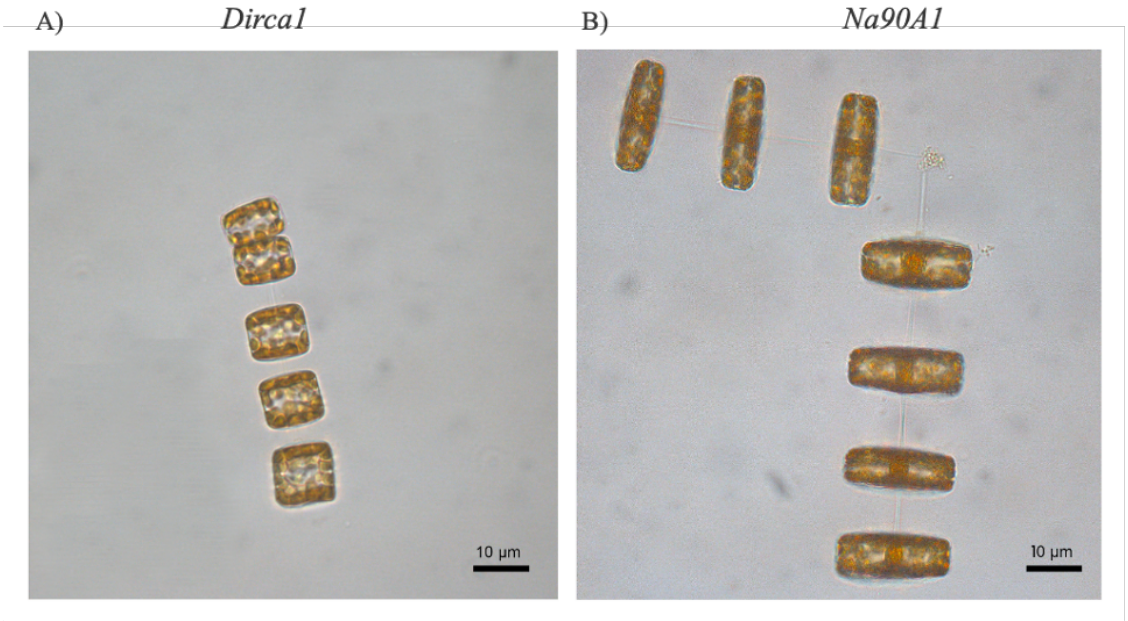

Fig. 9. Representative images of cells of Thalassiosira rotula Dirca1 *(A) and* Na90A1 *(B). Scale bar 10 μm.*

Table 4. Apical and perivalvar axes and biovolume of Thalassiosira rotula Dirca1 *and* Na90A1 *strains measured at late exponential phase. Values are the means ± standard error.*

	Dirca1	*Na90A1*
Apical axis (µm)	14.05 ± 0.8	45.12 ± 1.2
Pervalval axis (µm)	20.97 ± 1.1	8.33 ± 0.7
Biovolume (μm^3)	3078.18 ± 211	21579.40 ± 255

2.3.2 Rapid spectrophotometric assay to determine Fx content in the two strains of *Thalassiosira rotula*

The preliminary evaluation of Fx content in both two *T. rotula* strains grown in basal medium was carried out by a spectrophotometric rapid test. I chose the late exponential phase (Late exp) for these experiments considering the peak of cell density and biomass at this stage (Fig. 8) (Tab. 4).
Based on Wang *et al.* (2018), eq. 1 was usable for different species of diatoms, including one species in the genus *Thalassiosira* (i.e. *T. pseudonana*).

$$[Fx]\ (mg/L) = 6.39 \times (A445 - n_1) - 5.18 \times (A663 - n_2) \qquad (eq.1)$$

where [Fx] is the concentration of fucoxanthin expressed as mg/L and n_1 and n_2 represent the correction for interference from other pigments and /or cell debris, determined by a regression line obtained with the absorbance value of the residue pigment mixture (ASE) measured at 445 nm and 663 nm as abscissa, vs absorption data of cell debris (ASC) at 750 nm as ordinate.
Replacing n_1 and n_2 with the value reported by Wang *et al.* (2018), eq. 1 results in eq. 2

$$[Fx]\ (mg/L) = 6.39 \times A445 - 5.18 \times A663 + 0.312 \times A750 - 5.27 \qquad (eq.\ 2)$$

Using eq. 2, the content of Fx both in *Dirca1* and *Na90A1* resulted in negative values (Tab. 5).

La borsa di dottorato è stata cofinanziata con risorse del
Programma Operativo Nazionale Ricerca e Innovazione 2014-202 (CCI 2014IT16M2OP005)
Fondo Sociale Europeo, Azione I.1 "Dottorati Innovativi con caratterizzazione Industriale"

Table 5. Fx content, expressed both as mg/L and µg/mg, in the two strains of Thalassiosira rotula*,* Dirca1 *and* Na90A1*, using the spectrophotometric equation reported by Wang et al., 2018. Values are the averages ± standard error.*

[Fx]	mg/L	µg/mg
Dirca1	- 6.7 ± 0.8	-3.3 ± 1.2
Na90A1	-6.9 7 ± 1.1	- 3.5 ± 0.7

These results suggested that the equation used by Wang *et al.* (2018) cannot accurately predict the level of Fx in *T. rotula*. Considering that the "background noise" is a function of the number and the type of cells used to make the measurements, I thought it was appropriate to recalculate n_1 and n_2 in eq. 1. As reported by Wang *et al.*, (2018), the correlation between the density of cells (ASC) and other pigments (Chl c, and carotenoids) was demonstrated by the coefficients n_1 and n_2, excluding Chl a and Fx. So, I measured different culture dilutions in triplicate at A750 nm (ASC) and then extracted other pigments in absolute ethanol (ASE) (see Mat & Met section) and measured at 445 nm and 663 nm. By plotting the absorption values of ASE at 445 nm and 663 nm as the x-axis, and ASC measured at 750 nm represented on the y-axis, I obtained the regression lines (Fig. 10).

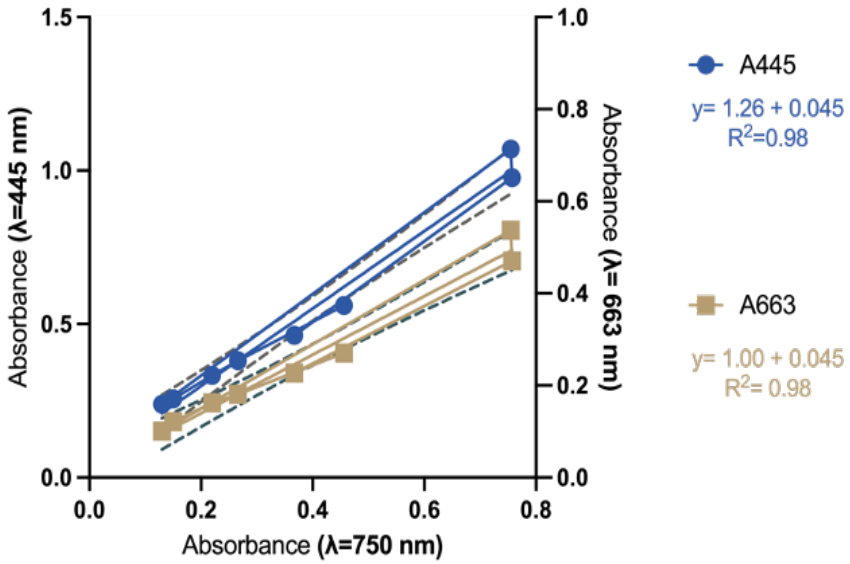

Figure 10. The absorbance value of the residue pigment mixture and cell debris at 445 nm and 663 nm. The abscissa displayed the absorbance of cell culture at 750 nm. The blue circle represents A445 in the mixture; the brown square represents A663. The fit curve of the data was shown in blue and brown lines at different wavelengths.

The equations for the regression lines, shown in Fig. 10, represented the "background noise" interfering at 445 nm (y =1.26+0.045) and 663 nm (y=1+0.01), respectively.
As reported in Wang *et al.*, (2018), n_1 and n_2 correspond to the equation of the regression line. So, for *T. rotula*, n_1 and n_2 were as follows:

n_1 (A445') = 1.26 x A750 + 0.045
n_2 (A663') = 1.00 x A750 + 0.01

At last, n_1 and n_2 were substituted in the previous eq. 1,

$$[Fx](mg/L) = 6.39 \times (A445 - n_1) - 5.18 \times (A663 - n_2) \quad \text{(eq. 1)}$$

resulting in the final eq. 3 suitable for estimation of Fx in *T. rotula*:

$$[Fx]' (mg/L) = 6.39 \text{ x } A445 - 5.18 \text{ x } A663 - 2.87 \text{ x } A750 - 0.24 \quad \text{(eq. 3)}$$

Applying eq. 3 the amounts of Fx calculated in the two *T. rotula* strains and expressed as µg/mg DW, were shown in table 6. The results showed that the Fx content was significantly higher in *Na90A1* with respect to *Dirca1* (3.3 ± 0.3 µg/mg vs 0.8 ± 0.3 µg/mg). Table 6 also resumes the other parameters relating to cell density, biomass and biovolume, from which *Na90A1* appears more suitable than *Dirca1*, overall, for Fx content, so *Na90A1* strain was chosen for the successive experiments.

Table 6. Summary of the parameters measured in the two strains of Thalassiosira rotula.

	Dirca1	*Na90A1*
Cell density (cells/ml)	$2.3*10^5$	$6*10^4$
Biomass DW (mg/ml)	0.19 ± 0.06	0.2 ± 0.06
Biovolume (μm^3)	3078.18 ± 211	21579.40 ± 255
Fx content (µg/mg)	0.8 ± 0.3	3.3 ± 0.3

La borsa di dottorato è stata cofinanziata con risorse del
Programma Operativo Nazionale Ricerca e Innovazione 2014-202 (CCI 2014IT16M2OP005)
Fondo Sociale Europeo, Azione I.1 "Dottorati Innovativi con caratterizzazione Industriale"

2.3.3. Improvement of Fx content in *T. rotula Na90A1*

Growth kinetics and morphophysiological analyses

In order to enhance Fx content in my strain, was experimented the effect of High Nitrate supplementation in the medium (HN) and Low Light conditions (LL) and also the combined condition (LL HN).

T. rotula Na90A1, grown in these different culture conditions for 7 days, reached the peak of the exponential phase (Late exp) at day 5, in all the culture conditions (Fig. 11). The HN supplementation significantly enhanced the cell density respect with the control as with the other LL and LL HN treatments (Fig. 11). In addition, the highest µmax resulted for HN treatment (Fig. 11).

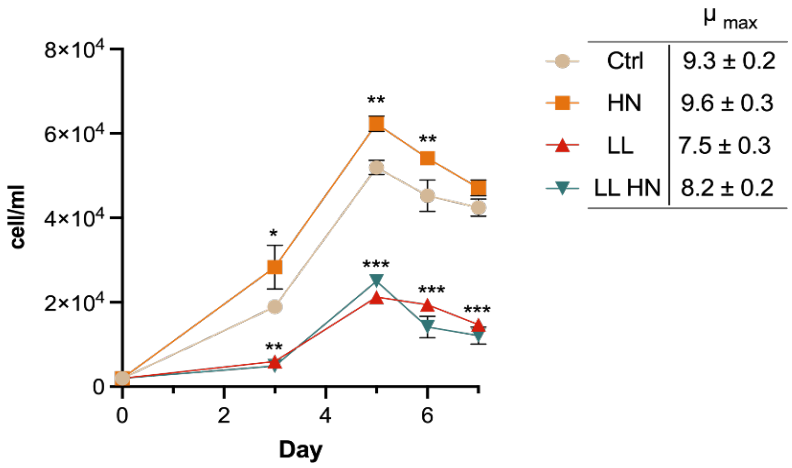

Figure 11. Growth curves of Thalassiosira rotula Na90A1 *in the control condition (Ctrl), in nitrate enrichment of the medium (HN), in low light condition (LL), and in a combination of both (LL HN); µmax was also reported on the graph.*

In line with this result, the biomass concentration (DW mg/ml) was significantly increased in HN condition compared to the Ctrl, both in Exponential (Exp) as Late exponential (Late exp); on the other hand, LL and LL HN treatment induced a rise of biomass in the in Exp phase (Fig. 12 A, B), notwithstanding the cell densities were low (Fig. 12).

La borsa di dottorato è stata cofinanziata con risorse del
Programma Operativo Nazionale Ricerca e Innovazione 2014-202 (CCI 2014IT16M2OP005)
Fondo Sociale Europeo, Azione I.1 "Dottorati Innovativi con caratterizzazione Industriale"

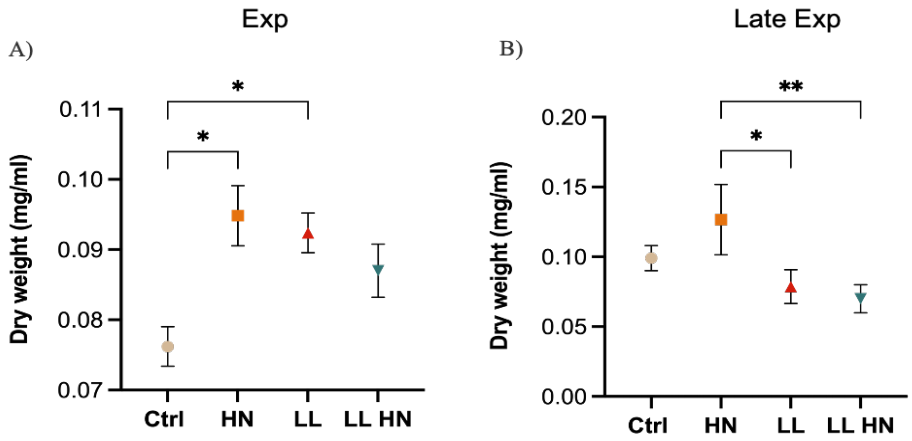

Figure 12. Dry weight (DW mg/ml) of Thalassiosira rotula Na90A1 *in the control condition (Ctrl), nitrate enrichment of the medium (HN), low light condition (LL), and combination of both (LL HN). (A) at Exp and (B) Late exp phases. Averages ± standard error were represented. Statistical analyses were performed using one-way ANOVA and Tukey's range test. "*" ($p < 0.05$); "**" ($p < 0.01$).*

Both at Exp as Late exp phases, morphometric analyses were carried out to assess related changes. As shown in Fig. 13, at the Exp phase, all the treatments enhanced the cell biovolume: in particular, LL and LL HN improved cell size and biovolume (Fig. 13 A, C). At the Late exp, HN also induced an increase of biovolume with values comparable to the LL and LL HN treatments (Fig. 13 B, D).

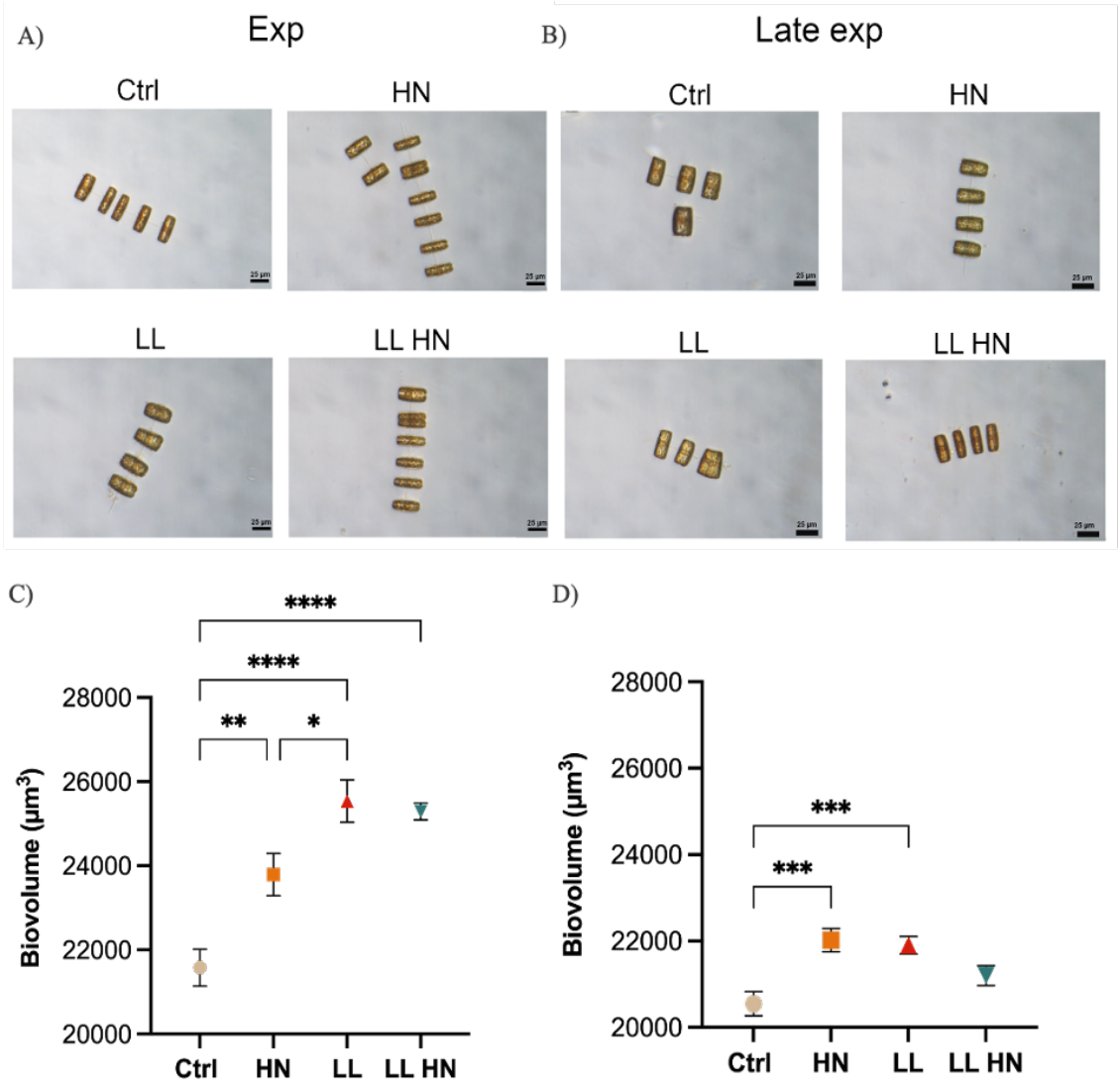

Figure 13. Representative images of cells of Thalassiosira rotula Na90A1*in Exp (A) and Late exp (B) phases, in control (Ctrl) condition, high nitrate (HN) medium, low light condition (LL), and in a combination of both conditions (HN LL). Scale bar 25 µm. Cell biovolume (µm3) at Exp (C), and Late Exp (D) under the same treatments. Averages ± standard error were represented. Statistical analyses were performed using one-way ANOVA and Tukey's range test. "*" ($p \leq 0.05$); "**" ($p \leq 0.01$); "***" ($p \leq 0.001$); "****" ($p \leq 0.0001$).*

Moreover, to assess some physiological variations, an in vivo analysis was performed estimating the neutral lipids content using the Nile Red (NR) staining.

By confocal laser scanning microscope, the NR fluorescence was used to assess in situ neutral lipid amounts; an *in situ* evaluation of chlorophyll content was also performed by estimating the chlorophyll autofluorescence. As shown in Fig. 14 (A - H) no neutral lipids were observed in Exp and Late Exp phases, whereas the cells appeared red in colour due to the Chls autofluorescence (Fig. 14 A - H).

The estimation of Chls content by measuring fluorescence intensity showed a high content in the Late exp phase overall in the Ctrl condition and LL condition (Fig. 14 M, N). Otherwise, at senescence phase (Sen) several lipid droplets as yellow colour, both in the Ctrl as HN cultures were detected, but few in LL and HN LL treatments (Fig. 14 I - L). According to these observations, the NR fluorescence intensity indicated the highest content of both neutral lipids in Ctrl medium followed by HN treatment (Fig. 14 O).

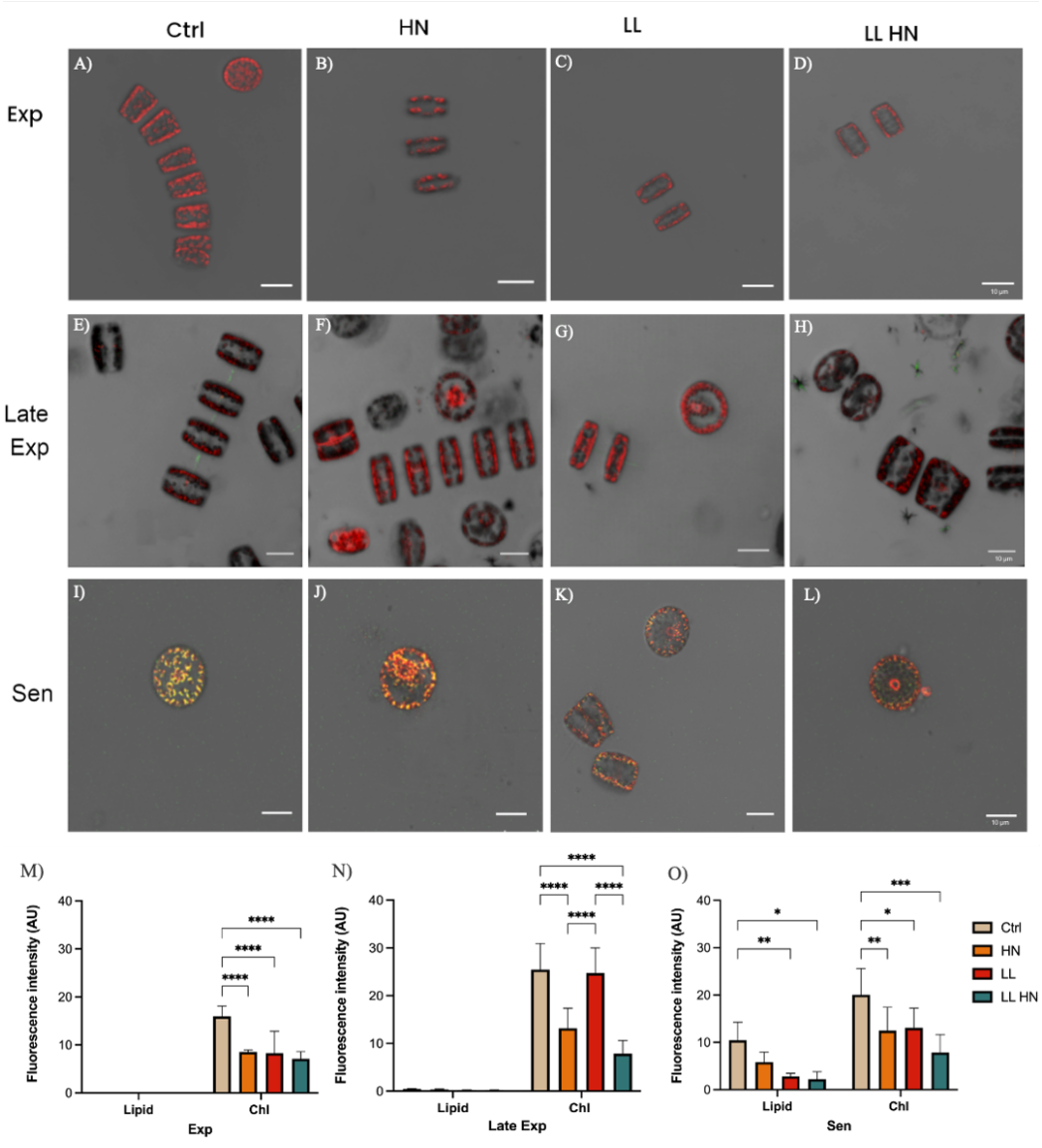

Figure 14. Confocal laser images of Thalassiosira rotula Na90A1 *stained with Nile Red in control condition (Ctrl), high nitrate (HN) medium, low light condition (LL), and in a combination of both conditions (LL HN) at Exp (A, B, C, D), Late exp (E,F,G,H) and Sen (I,J,K,L) phases. Scale bar 10 µm. M), N), O): fluorescence intensity, expressed as arbitrary units (AU) of Nile Red and Chlorophylls at the same growth phases and upon the same treatments. The vertical bars represent averages ± standard error. Statistical analyses were performed using two-way ANOVA and Tukey's range test. "*" ($p \leq 0.05$); "**" ($p \leq 0.01$); "***" ($p \leq 0.001$); "****" ($p \leq 0.0001$).*

Photosynthetic Pigment Contents by spectrophotometric method and HPLC profile: effect of nitrate supplementation and low light condition

The visible spectrum scan of the total extracted pigments in *T. rotula Na90A1* strain at late exponential (Late exp) phase after culturing in control (Ctrl) condition, high nitrate concentrations (HN), low light condition (LL) and both (LL HN) showed a broad peak centred at 445 nm and a sharper peak centred at 663 nm (Fig. 15). It was noted that HN and LL treatments induced an increase not only in the height but also in the width of the peaks (Fig. 15).

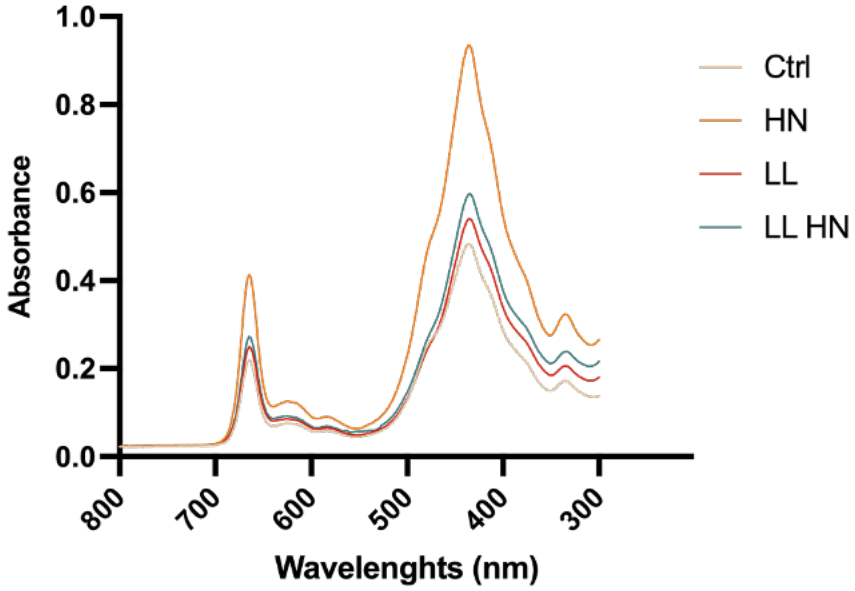

Figure 15. The visible spectrum scan of pigments in Thalassiosira rotula Na90A1 *grown in Ctrl condition and treated with high nitrate concentrated medium (HN), low light (LL), and in combination of both conditions (LL HN).*

On the same samples, Fx content was determined using the equation from Wang *et al.* (2018) as modified specifically for *T. rotula* in this work (see section 2.3.2). Chlorophylls concentrations were also calculated using the equation from Ritchie *et al.* (2006).

The results showed that Fx content increased under the LL treatment reaching a value of 10.8 ± 0.9 µg/mg, about twice the amount of Ctrl (Fig. 16 A).

In addition, the chlorophyll a (Chl a) content is shown to increase in response to HN and LL treatment, while under LL treatment a significant rise of Chlorophyll c (Chl c) content vs Ctrl was found (Fig. 16 B, C).

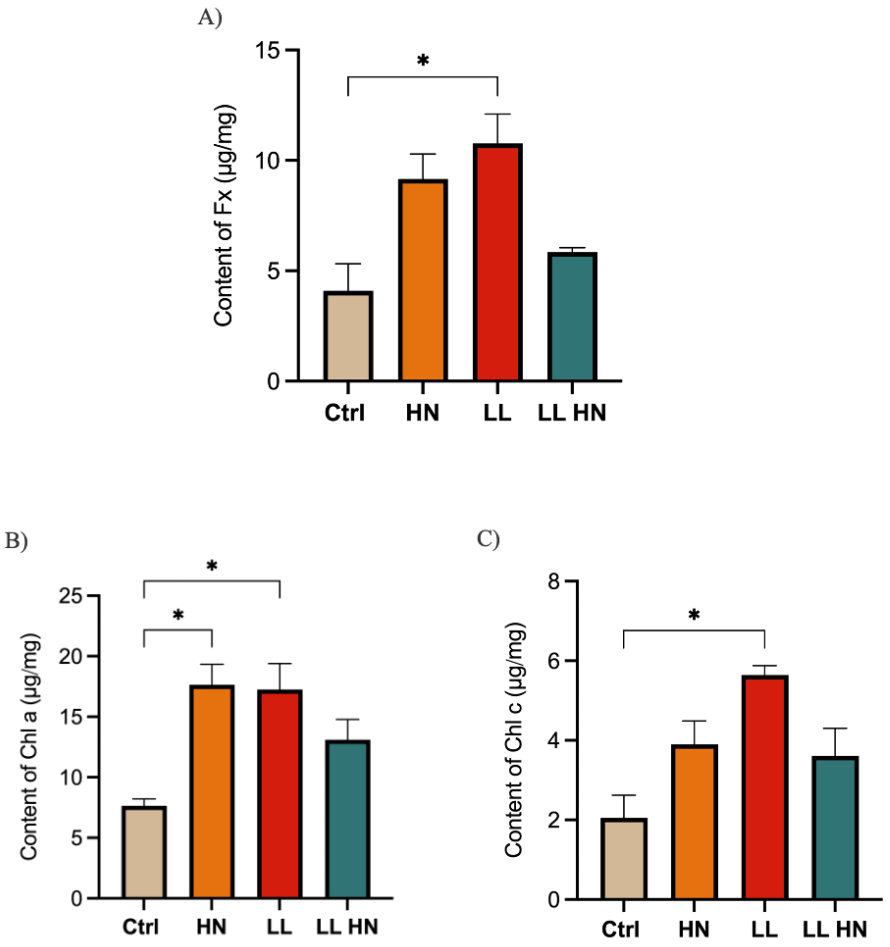

Figure 16. Fucoxanthin (A), Chlorophyll a (B), and Chlorophyll c (C) content measured through the spectrophotometric method in Thalassiosira rotula Na90A1 *grown in Ctrl condition and treated with high nitrate concentrated medium (HN), low light (LL) and combining these two conditions (LL HN). The vertical bars represent averages ± standard error. Statistical analyses were performed using one-way ANOVA and Tukey's range test. "*" ($p < 0.05$); "**" ($p < 0.01$).*

To validate the spectrophotometric measures and to profile the different pigments and their variation under the different culture conditions, HPLC analyses were performed both at the Exp and Late exp phases. As shown in Fig. 17 A, in the Exp phase the treatments induced a decrease in Chl a content, while in the Late exp a significant rise was seen in the LL condition compared to the others (Fig. 17 B).

On the other hand, in the Exp phase a higher content of Chl c was observed in the Ctrl and HN conditions compared to LL conditions; Chl c content was instead stable in the Late exp across all the treatments (Fig. 17 D).

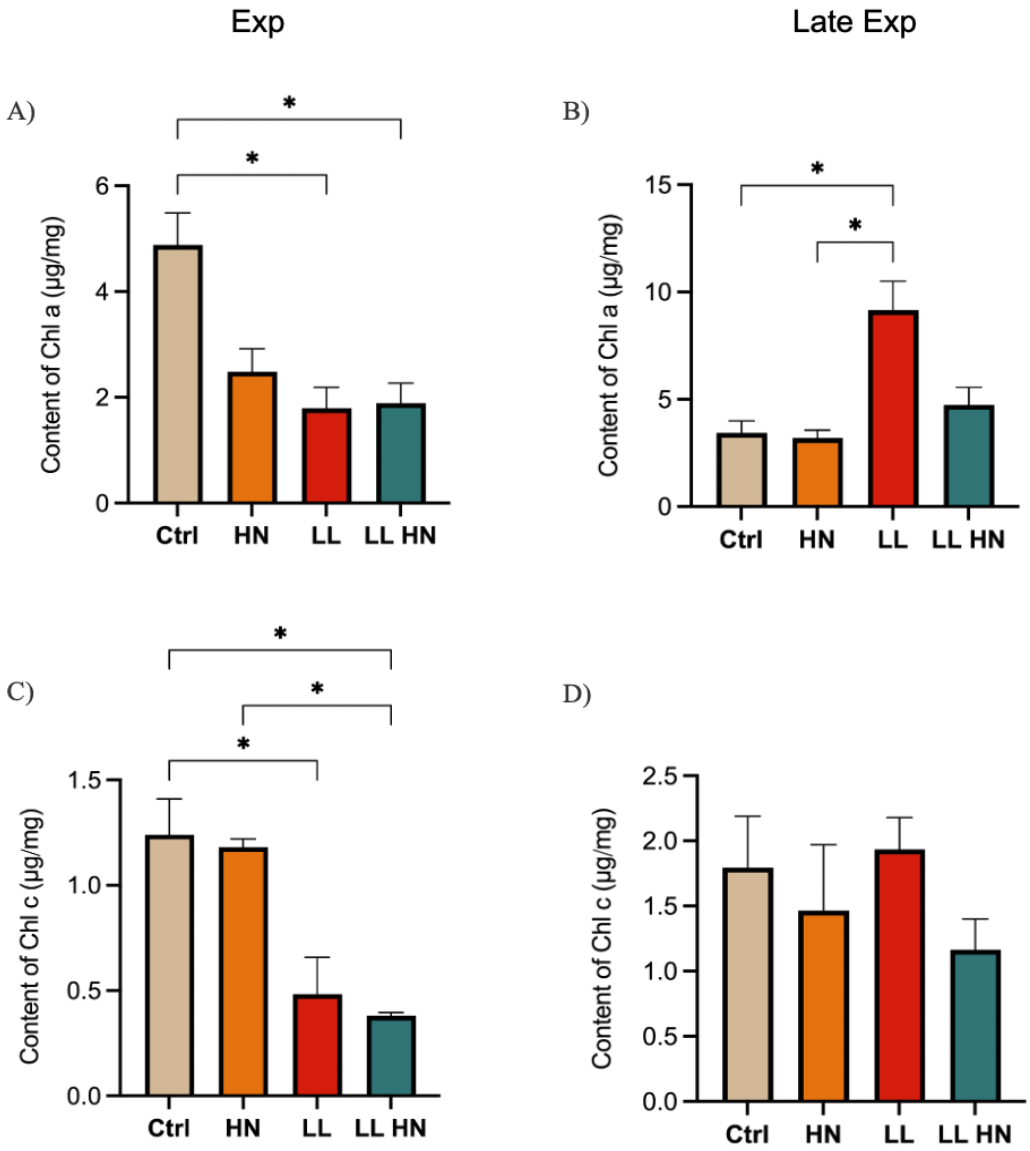

Figure 17. Chlorophylls content(µg/mg) of Thalassiosira rotula Na90A1 *strain measured by HPLC method in exponential (Exp A, C) and in late exponential (Late exp B, D) under basal medium (Ctrl), high nitrate medium (HN), low light condition (LL) and in a combination of both conditions (LL HN). The vertical bars represent averages ± standard error. Statistical analyses were performed using one-way ANOVA and Tukey's range test. "*" ($p < 0.05$); "**" ($p < 0.01$).*

Significant variations were also observed in the carotenoid content, from ß-carotene to fucoxanthin and intermediates of its biosynthesis (Fig. 18, 19).

La borsa di dottorato è stata cofinanziata con risorse del
Programma Operativo Nazionale Ricerca e Innovazione 2014-202 (CCI 2014IT16M2OP005)
Fondo Sociale Europeo, Azione I.1 "Dottorati Innovativi con caratterizzazione Industriale"

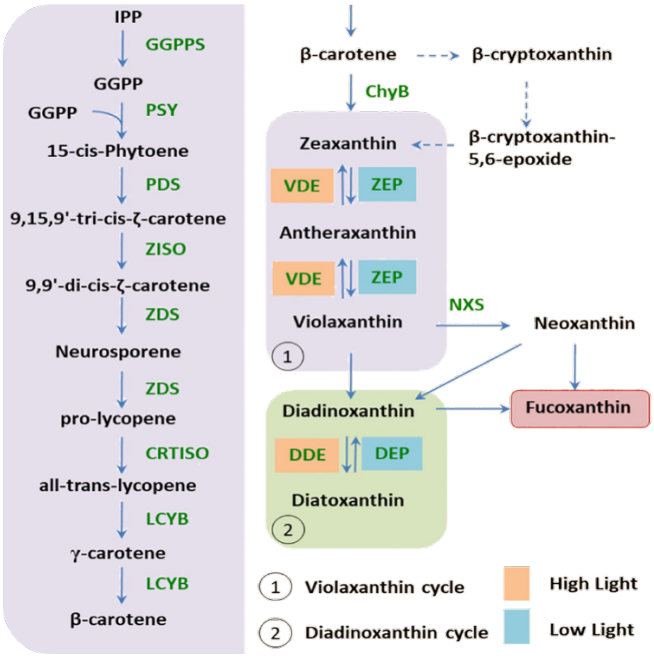

Figure 18. Schematic representation of fucoxanthin biosynthetic pathways and precursors

As seen in Fig. 19, Ctrl condition showed the highest in ß-carotene (ßcar) content, while in the Late exp phase LL condition induced a significant enhancement of this pigment (0.12 ± 0.09 µg/mg).

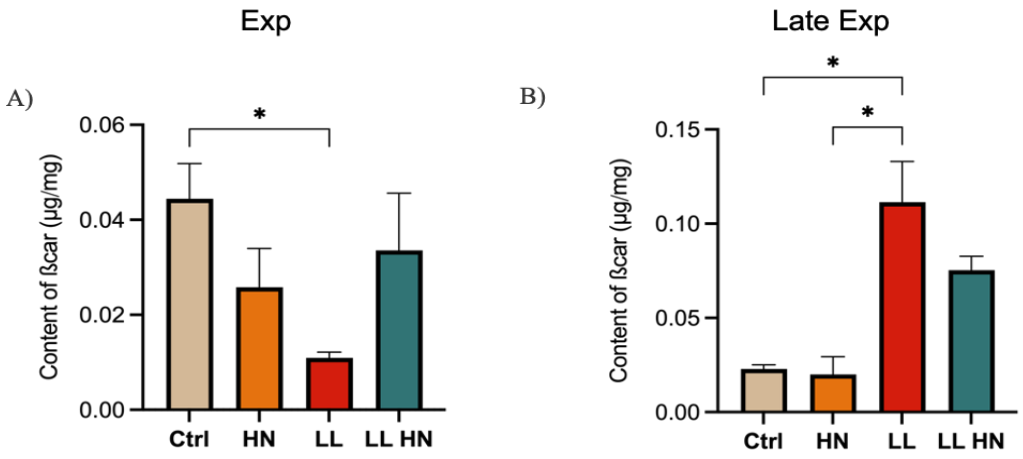

Figure 19. ß-carotene (ßcar) content of Thalassiosira rotula Na90A1 *measured using HPLC method in Exp (A) and Late exp (B) phases. Cultures were grown under standard medium (Ctrl), high nitrate medium (HN), low light condition (LL), and in a combination of both conditions (LL HN). The vertical bars represent averages ± standard error. Statistical analyses were performed using two-way ANOVA and Tukey's range test. "*" (p≤ 0.05); "**" (p ≤ 0.01); "***" (p ≤ 0.001); "****" (p ≤ 0.0001).*

Moreover, important variations were observed in the Violaxanthin (Vx) and Diadinoxanthin (Ddx) cycles (Fig. 18).

Regarding the Vx content, the Ctrl condition at the Exp phase exhibited the highest level (0.025 ± 0.01µg/mg) followed by HN, which in the Late Exp showed a noteworthy increase (Fig. 20 A, B). Additionally, the Ddx content showed the highest level both in Ctrl and HN conditions (both in Exp as Late exp phase) (Fig. 20 C, D). On the other hand, I have seen a most variable trend of Diatoxanthin (Dtx) content: in the Exp phase, the highest content was observed in the LL condition, while at the Late exp phase, Ctrl and HN conditions showed a significant rise (Fig. 20 E, F).

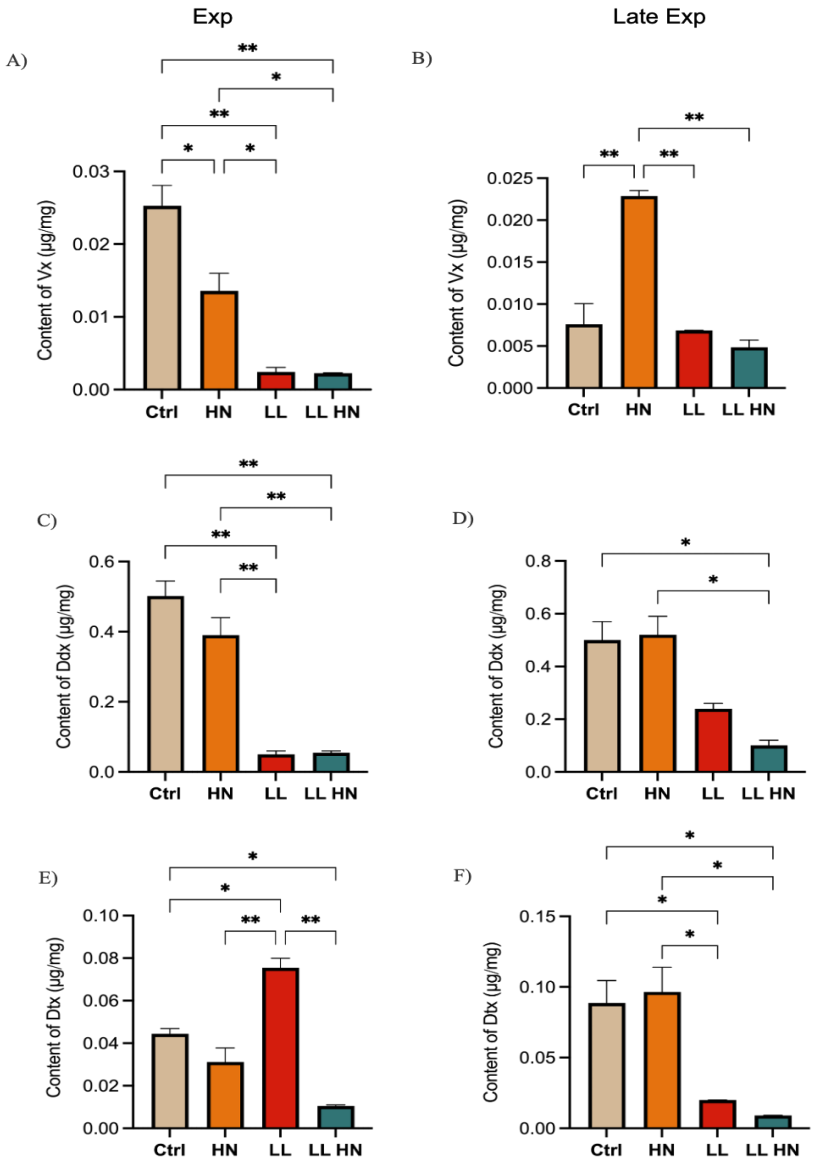

Figure 20. Violaxanthin (Vx), Diadinoxanthin (Ddx), and Diatoxanthin (Dtx) content (µg/mg) of Thalassiosira rotula Na90A1 *strain measured using the HPLC method in Exp (A, C, E) and Late exp (B, D, F) phases. Cultures were grown under standard medium (Ctrl), high nitrate medium (HN), low light condition (LL), and in a combination of both conditions (LL HN). The vertical bars represent averages ± standard error. Statistical analyses were performed using one-way ANOVA and Tukey's range test. "*" (p≤ 0.05); "**" (p ≤ 0.01).*

Regarding fucoxanthin (Fx) content, in the Exp phase, the highest value was in Ctrl condition (4.7 ± 0.4 µg/mg); in the Late exp phase, the Fx amount rise to 5.2 ± 0.8 µg/mg in LL condition (Fig. 21); otherwise, HN treatment maintained stable the Fx content (3.4 ± 0.3 µg/mg) in both the growth phases (Fig. 21).

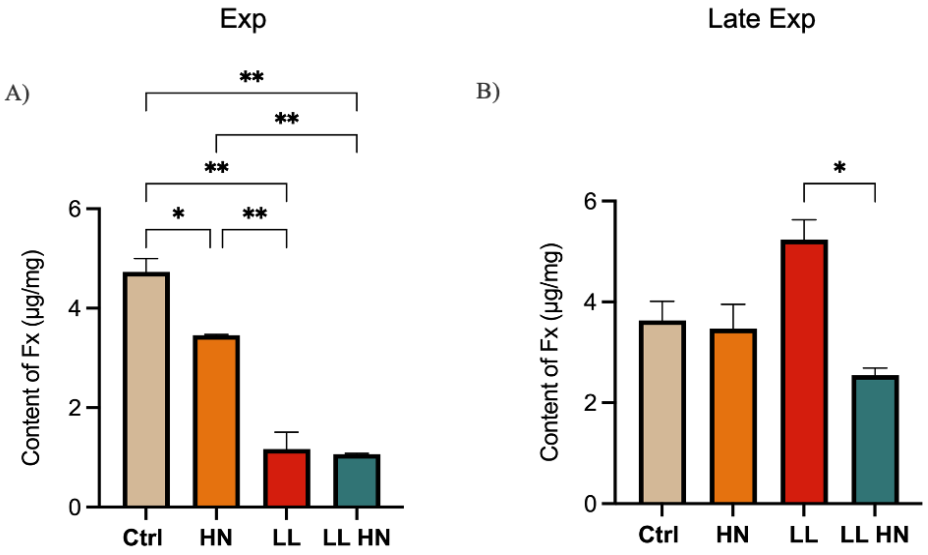

Figure 21. Fucoxanthin (Fx) content (µg/mg) in Thalassiosira rotula Na90A1 *strain measured using HPLC method in Exp (A) and Late exp (B) phases. Cultures were grown under standard medium (Ctrl), high nitrate medium (HN), low light condition (LL), and in a combination of both conditions (LL HN). The vertical bars represent averages ± standard error. Statistical analyses were performed using one-way ANOVA and Tukey's range test. "*" (p≤ 0.05); "**" (p ≤ 0.01); "***" (p ≤ 0.001); "****" (p ≤ 0.0001).*

Content of Fucoxanthin and Chlorophylls under different culture conditions: comparison of spectrophotometric vs HPLC method

In this work, I used a rapid and easy method to evaluate the content of Fx in *Na90A1*. To verify the correctness of eq. 3 (see Materials and Methods section), I compared the spectrophotometric values with those HPLC ones. Globally, the values resulting from the two different methods showed significant differences in the treated samples (HN, LL, LL HN). The spectrophotometric method overestimates both Fx as well as Chl a and Chl c content when compared with HPLC ones (Fig. 22).

La borsa di dottorato è stata cofinanziata con risorse del
Programma Operativo Nazionale Ricerca e Innovazione 2014-202 (CCI 2014IT16M2OP005)
Fondo Sociale Europeo, Azione I.1 "Dottorati Innovativi con caratterizzazione Industriale"

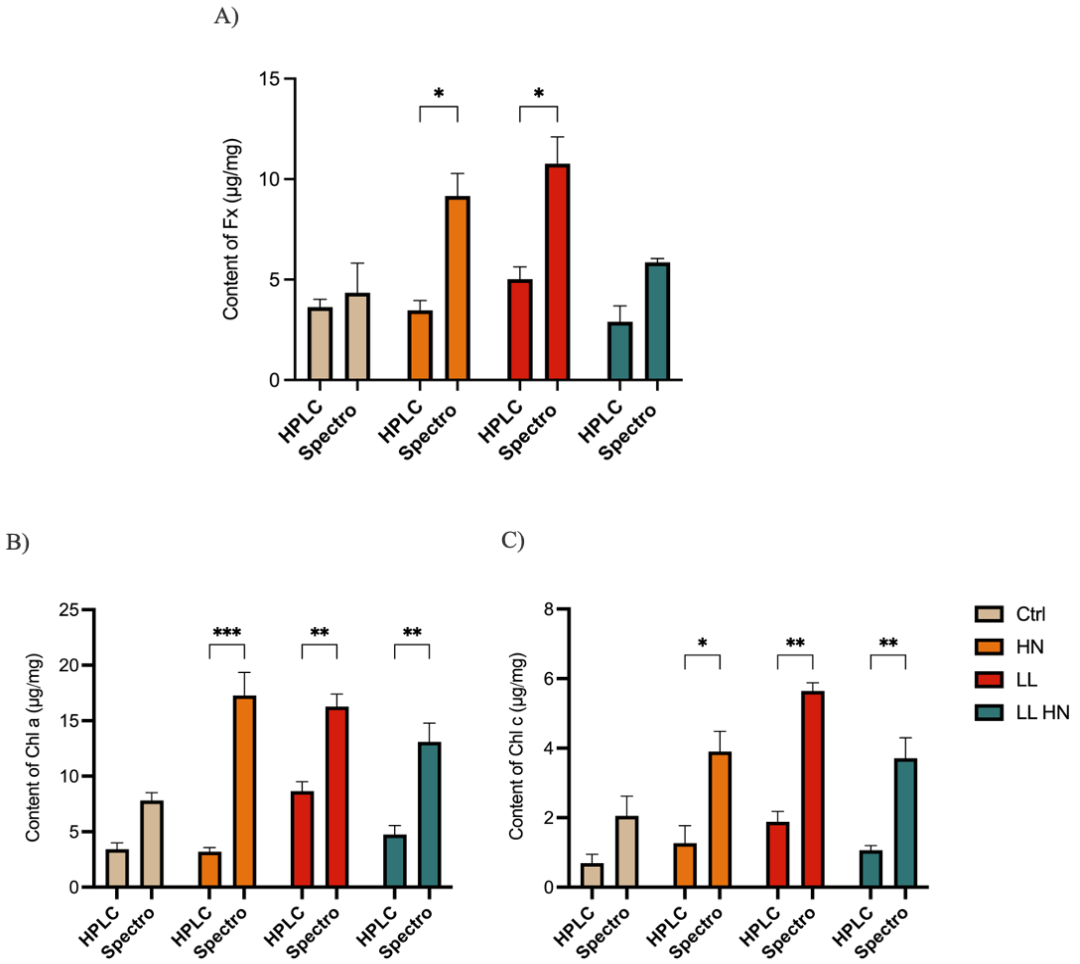

Figure 22. Comparison of spectrophotometric (spectro) vs HPLC method. Content of Fx (A) Chl a (B), Chl c (C), in Thalassiosira rotula Na90A1 *grown in Ctrl condition and treated with high nitrate concentrated medium (HN), low light (LL), and combining these two conditions (LL HN). The vertical bars represent averages ± standard error. Statistical analyses were performed using two-way ANOVA and Tukey's range test. "*" (p≤ 0.05); "**" (p ≤ 0.01); "***" (p ≤ 0.001).*

2.3.4 Fucoxanthin biosynthesis pathway: identification of key genes and modulation of their expression

Considering the variation of the most photosynthetic pigments under different culture conditions, I performed the RT-qPCR analysis of some key genes involved in the carotenoid pathway.

In particular, about the final biosynthetic step, although the biosynthesis pathway of Fx has not been fully elucidated yet, several enzymes involved in steps from violaxanthin to Fx have been identified in *Phaeodactylum tricornutum* (Fig. 23).

La borsa di dottorato è stata cofinanziata con risorse del
Programma Operativo Nazionale Ricerca e Innovazione 2014-202 (CCI 2014IT16M2OP005)
Fondo Sociale Europeo, Azione I.1 "Dottorati Innovativi con caratterizzazione Industriale"

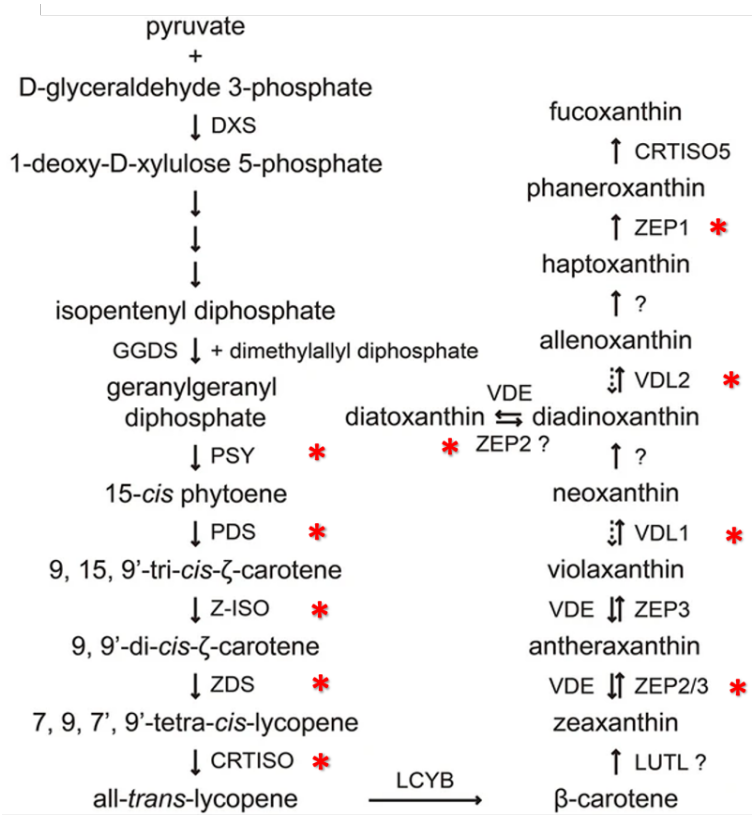

Figure 23. Genes involved in fucoxanthin biosynthesis in Phaeodactylum tricornutum *(from Li et al., 2024). The red asterisks mark the genes investigated in this work.*

The genes investigated in this work are marked in Fig. 23.

Globally, my results showed that the key investigated genes have remarkable varying degrees of level expression (Fig. 24- 29). More in detail, the expression of the two *PSY* isoforms (*PSY1* and *PYS2*) involved in the synthesis of phytoene in the first step of the biosynthesis of carotenoid pathway, showed for *PSY1* a high expression level in the Ctrl and HN condition with a significant increase in Late exp phase in HN and LL conditions (Fig. 24 A, B); while *PYS2* level increased only in Late exp in HN condition (Fig. 24 C, D). The *PDS1* (codifying for a phytoene desaturase) showed the highest expression in Late exp LL condition (Fig. 24 F) as the other isoform *PDS2* (Fig. 24 H); on the other hand, in Exp phase, *PDS2* level was higher in HN than other treatments (Fig. 24 G).

La borsa di dottorato è stata cofinanziata con risorse del
Programma Operativo Nazionale Ricerca e Innovazione 2014-202 (CCI 2014IT16M2OP005)
Fondo Sociale Europeo, Azione I.1 "Dottorati Innovativi con caratterizzazione Industriale"

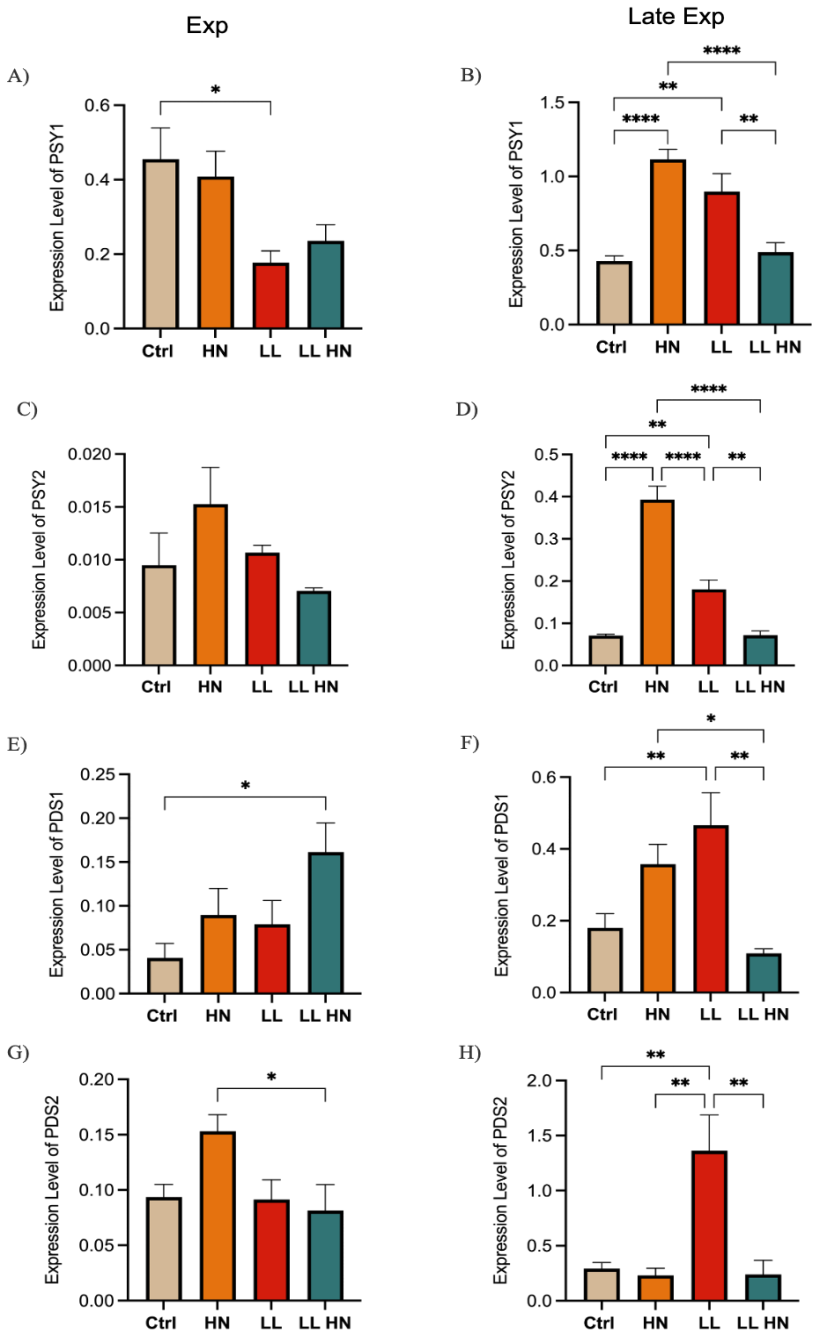

Figure 24. Relative mRNA expression level of key genes involved in the carotenoid biosynthesis pathway in Thalassiosira rotula Na90A1 *in Exp (A, C, E, G) and Late exp (B, D, F, H) phases. Cultures were grown under standard medium (Ctrl), high nitrate medium (HN), low light condition (LL), and in a combination of both conditions (LL HN). Abbreviations: PSY, phytoene synthase; PDS, phytoene desaturase. The vertical bars represent averages ± standard error. Statistical analyses were performed using two-way ANOVA and Tukey's range test. "*" (p≤ 0.05); "**" (p ≤ 0.01); "***" (p ≤ 0.001); "****" (p ≤ 0.0001).*

In the next step of the biosynthetic pathway, the expression levels of *ZCIS* gene (codifying for a 15-cis-ζ-carotene isomerase desaturases) showed a high expression in the Exp phase in HN condition, while in the Late exp it was globally low expressed except in LL HN condition (Fig. 25 A, B). In contrast, *ZDS* (*ζ-carotene desaturases*) were mostly expressed in LL condition (Fig. 25 C, D). Moreover, two isoforms of *CRTISO* genes (codifying for the carotenoid isomerase) were investigated. *CRTISO1* showed a relative high expression in the Exp phase in all culture conditions except for the LL, while in Late Exp, the HN treatment induced a significant rise (Fig. 25 E, F); on the other hand, *CRTISO3* showed a peak of level expression in HN treatment in both the growth phases (Fig. 25 G, H).

La borsa di dottorato è stata cofinanziata con risorse del
Programma Operativo Nazionale Ricerca e Innovazione 2014-202 (CCI 2014IT16M2OP005)
Fondo Sociale Europeo, Azione I.1 "Dottorati Innovativi con caratterizzazione Industriale"

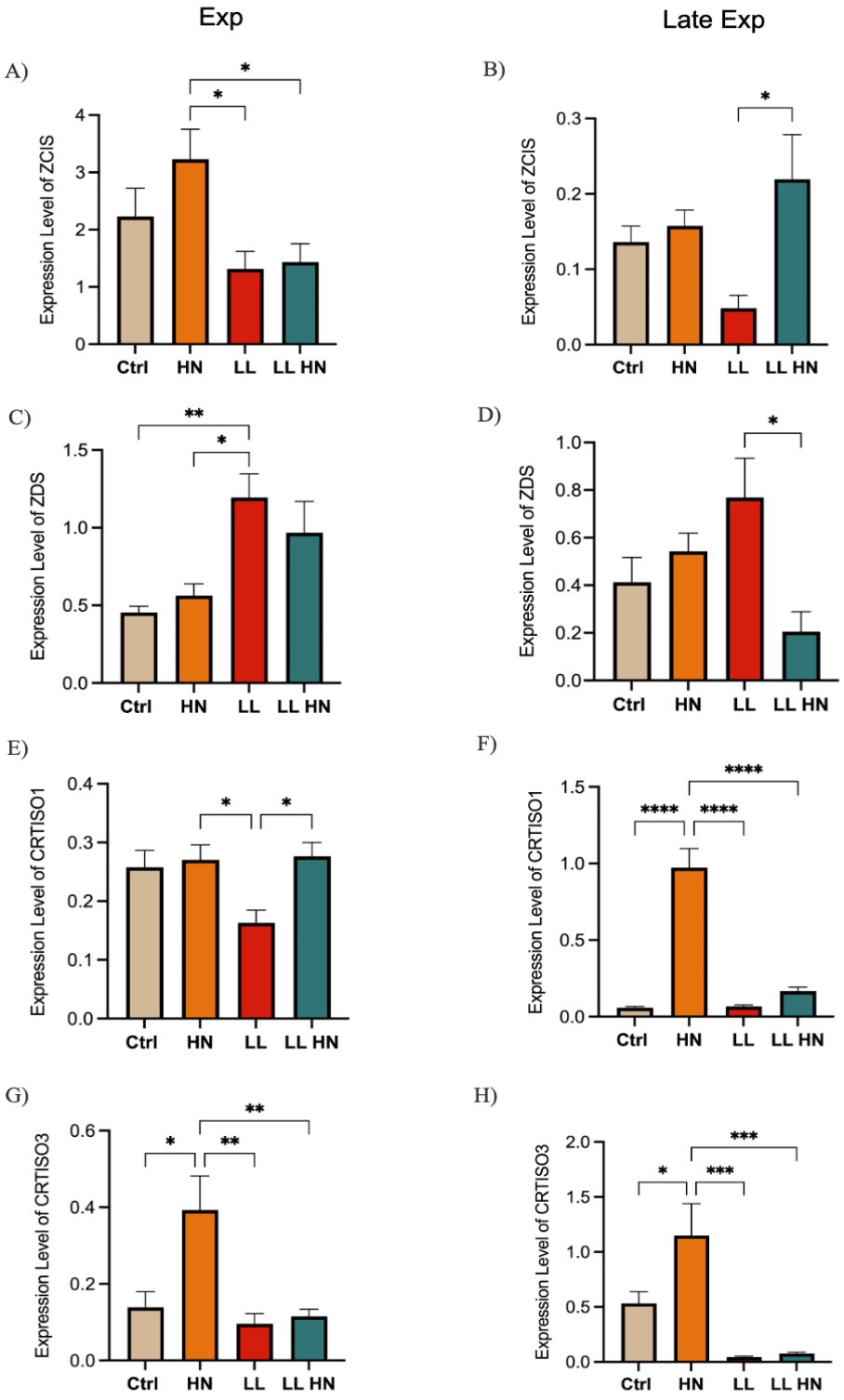

Figure 25. Relative expression level of key genes involved in the carotenoid biosynthesis pathway in Thalassiosira rotula Na90A1 *in Exp (A, C, E, G) and Late exp (B, D, F, H) phases. Cultures were grown under standard medium (Ctrl), high nitrate medium (HN), low light condition (LL), and in a combination of both conditions (LL HN). Abbreviations: ZCIS, 15-cis-ζ-carotene isomerase desaturases; ZDS, ζ-carotene desaturases; CRTISO, carotenoid isomerase. The vertical bars represent averages ± standard error. Statistical analyses were performed using two-way ANOVA and Tukey's range test. "*" (p≤ 0.05); "**" (p ≤ 0.01); "***" (p ≤ 0.001); "****" (p ≤ 0.0001).*

I focused the attention on the genes involved in the xanthophyll cycle, *ZEP* (*zeaxanthin epoxidase*) and *VDL* (*violaxanthin de-epoxidase-like*) respectively. The expression level of an isoforms of *ZEP* found in *T. rotula, ZEP1,* showed a high expression level in HN and LL HN treatments in both growth phase (Fig. 26 A, B); *ZEP2* level in Exp phase, was high in all conditions, except for HN; in Late Exp phase, the highest expression of this gene was noted in LL treatment (Fig. 26 C, D).

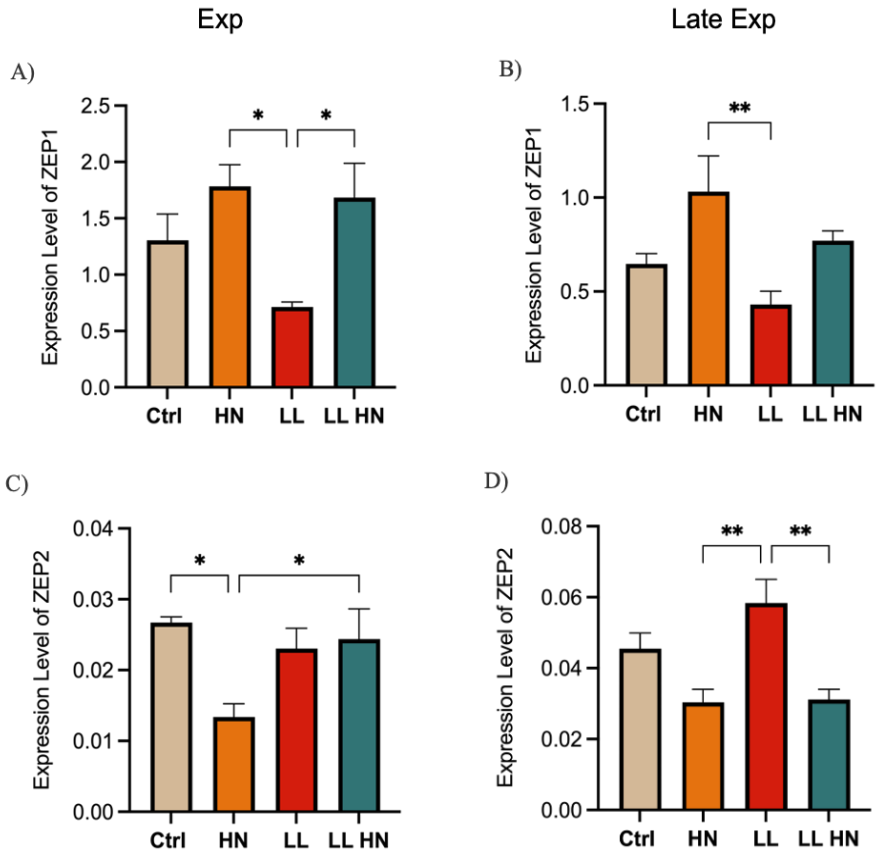

Figure 26. Relative expression level of key genes involved in the xanthophyll cycle in Thalassiosira rotula Na90A1 *in Exp (A, C) and Late exp (B, D) phases. Cultures were grown under standard medium (Ctrl), high nitrate medium (HN), low light condition (LL), and in a combination of both conditions (LL HN). Abbreviations: ZEP, zeaxanthin epoxidase. The vertical bars represent averages ± standard error. Statistical analyses were performed using two-way ANOVA and Tukey's range test. "*" (p≤ 0.05); "**" (p ≤ 0.01); "***" (p ≤ 0.001); "****" (p ≤ 0.0001).*

As far as the *violaxanthin de-epoxidase* (*VDE*) genes, I investigated three different isoforms. The comparative analysis of these sequences with the recent annotation of the genes involved in the final steps of Fx biosynthesis, reveal that my genes are *VDL*, genes catalysing for the final steps (Fig. 27).

La borsa di dottorato è stata cofinanziata con risorse del
Programma Operativo Nazionale Ricerca e Innovazione 2014-202 (CCI 2014IT16M2OP005)
Fondo Sociale Europeo, Azione I.1 "Dottorati Innovativi con caratterizzazione Industriale"

The phylogenetic tree showed that *VDL1* of *T. rotula* was close to *VDL1* of *T. pseudonana* and *P. tricorunutum*; *VDL2* and *VDL3* were both close to *VDL2* of *T. pseudonana* and *P. tricornutum* (Fig. 27).

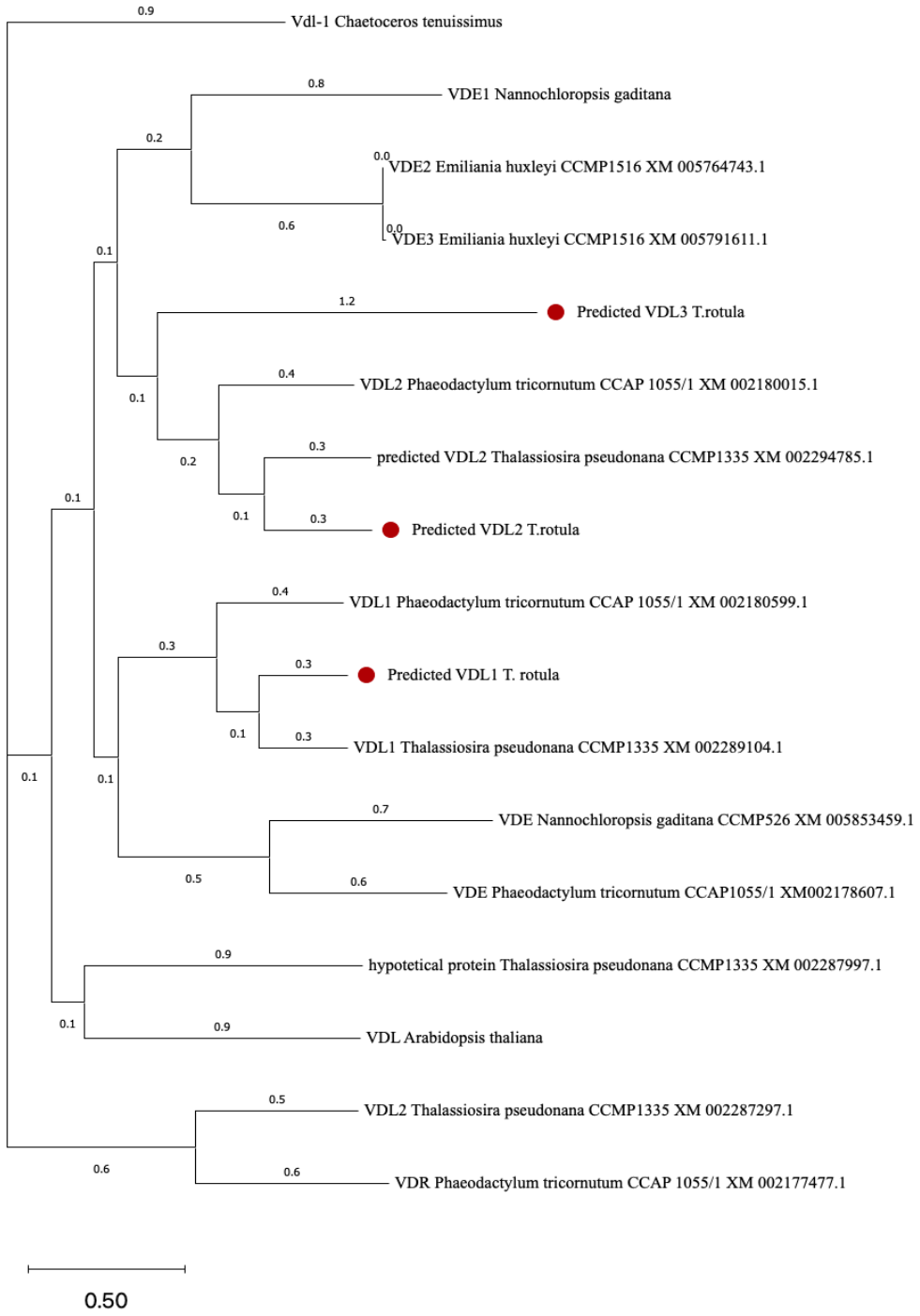

Figure 27. Phylogenetic tree of Violaxanthin de-epoxidase like genes (VDL). The tree was created by Muscle multiple alignment packages and maximum likelihood method. The predicted VDLs of Thalassiosira rotula *were highlighted with a red circle.*

La borsa di dottorato è stata cofinanziata con risorse del
Programma Operativo Nazionale Ricerca e Innovazione 2014-202 (CCI 2014IT16M2OP005)
Fondo Sociale Europeo, Azione I.1 "Dottorati Innovativi con caratterizzazione Industriale"

The expression analysis showed that *VDL1* had a high expression in the Exp phase both in HN as LL HN treatments whereas in Late exp only in HN condition (Fig. 28 A, B). *VDL2* level significantly increased in Late exp both in HN as LL condition (Fig. 28 C, D) whereas *VDL3* showed the highest level in the Late exp phase in HN condition (Fig. 28 E, F).

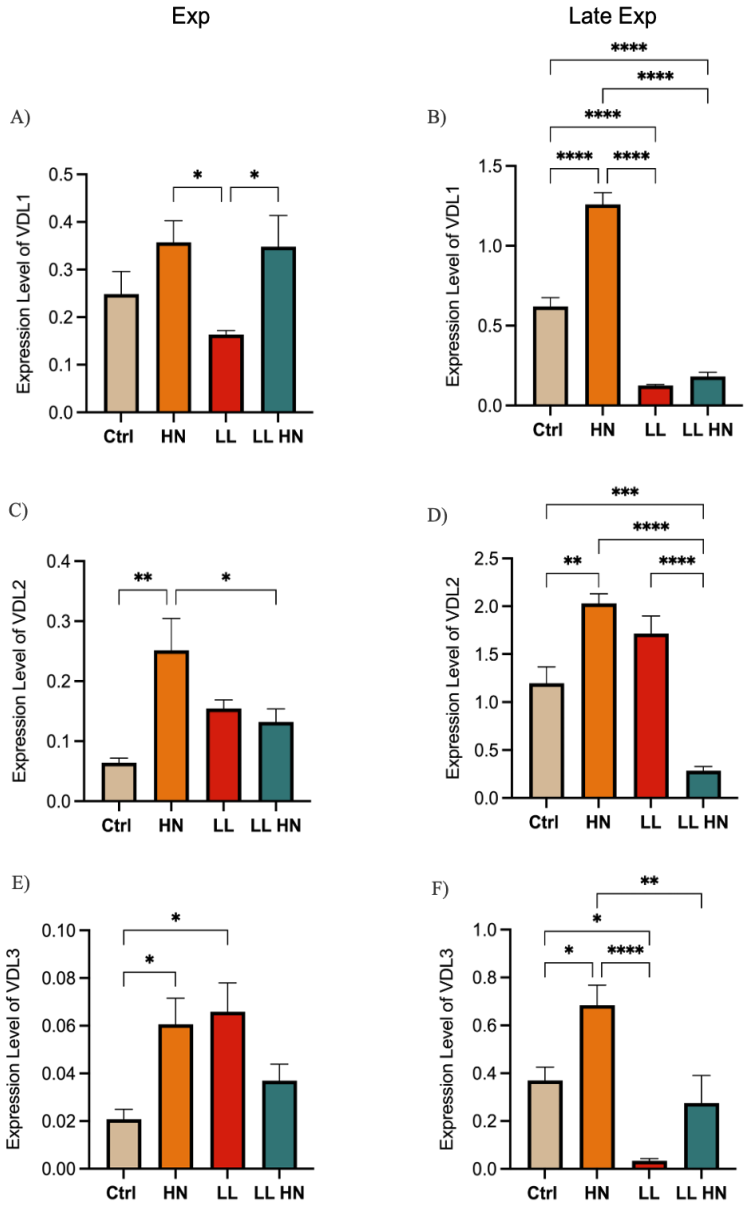

Figure 28. Relative expression level of key genes involved in the xanthophyll cycle in Thalassiosira rotula Na90A1 *in Exp (A, C, E) and Late exp (B, D, F) phases. Cultures were grown under standard medium (Ctrl), high nitrate medium (HN), low light condition (LL), and in a combination of both conditions (LL HN). Abbreviation: VDL, violaxanthin de-epoxidase like. The vertical bars represent averages ± standard error. Statistical analyses were performed using two-way ANOVA and Tukey's range test. "*" (p≤ 0.05); "**" (p ≤ 0.01); "***" (p ≤ 0.001); "****" (p ≤ 0.0001).*

Finally, in *T. rotula* only one isoform was found for *DDE* (*diadinoxanthin de-epoxidase*), a gene involved in the Diadinoxanthin (Ddx) cycle (Fig 29). This gene showed the highest expression in Ctrl condition at Exp phase, whereas in the Late exp, LL and LL HN treatments induced an increase (Fig. 29).

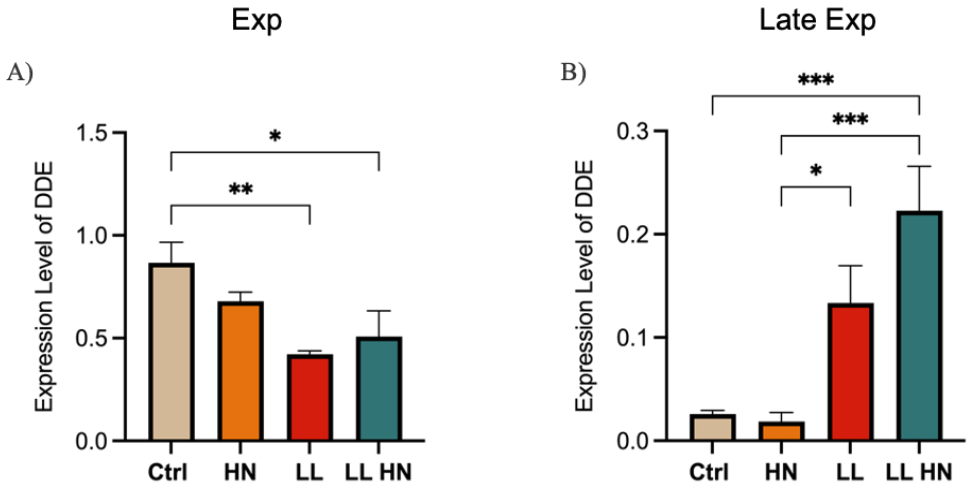

Figure 28. Relative expression level of key genes involved in the diadinoxanthin cycle in Thalassiosira rotula Na90A1 *in Exp (A) and Late exp (B) phases. Abbreviation: DDE, diadinoxanthin de-epoxidase. Cultures were grown under standard medium (Ctrl), high nitrate medium (HN), low light condition (LL), and in a combination of both conditions (LL HN). The vertical bars represent averages ± standard error. Statistical analyses were performed using two-way ANOVA and Tukey's range test. "*" (p≤ 0.05); "**" (p ≤ 0.01); "***" (p ≤ 0.001); "****" (p ≤ 0.0001).*

La borsa di dottorato è stata cofinanziata con risorse del
Programma Operativo Nazionale Ricerca e Innovazione 2014-202 (CCI 2014IT16M2OP005)
Fondo Sociale Europeo, Azione I.1 "Dottorati Innovativi con caratterizzazione Industriale"

2.3.5 Two-phase culturing system in short time

Based on my results, the LL condition seems to improve Fx content in *T. rotula Na90A1*. However, the LL condition induced a reduction of cell density (Tab. 7).

Table 7. Cellular parameters and Fx content of Thalassiosira rotula Na90A1 *grown in standard medium (Ctrl), high nitrate medium (HN), low light condition (LL), and in a combination of both conditions (LL HN).*

	Cell density (cells/ml)	Biomass (DW mg/ml)	Biovolume (μm^3)	Fx content spectro assay (µg/mg)	Fx content HPLC (µg/mg)
Ctrl	5.8 x10^4 cells/ml	0.1 ± 0.05	20547.8 ± 280	4.8 ± 0.5	3.6 ± 0.2
HN	6.2 x10^4 cells/ml	0.13 ± 0.05	22021.6 ± 270	9.4 ± 0.6	3.0 ± 0.3
LL	1.8 x10^4 cells/ml	0.05 ± 0.02	21905.5 ± 205	10.7 ± 0.5	5.02 ± 0.4
LL HN	2.3 x10^4 cells/ml	0.06 ± 0.02	21201.7± 230	5.8 ± 0.6	2.9 ± 0.3

In a wider application perspective, to obtain a good increase of cell density in combination with the LL condition, I experimented with a two-phase short time culturing system. I applied the optimal light intensity (80 µm m^{-2} s^{-1}) for first 3 day to obtain a high cell density and then transferring the cultures to low light intensity (LL 30 µm m^{-2} s^{-1}) condition for only 2 days, to improve the Fx synthesis. The results showed that the growth curve revealed a constant increase also after the transfer to LL condition (Fig. 30).

La borsa di dottorato è stata cofinanziata con risorse del
Programma Operativo Nazionale Ricerca e Innovazione 2014-202 (CCI 2014IT16M2OP005)
Fondo Sociale Europeo, Azione I.1 "Dottorati Innovativi con caratterizzazione Industriale"

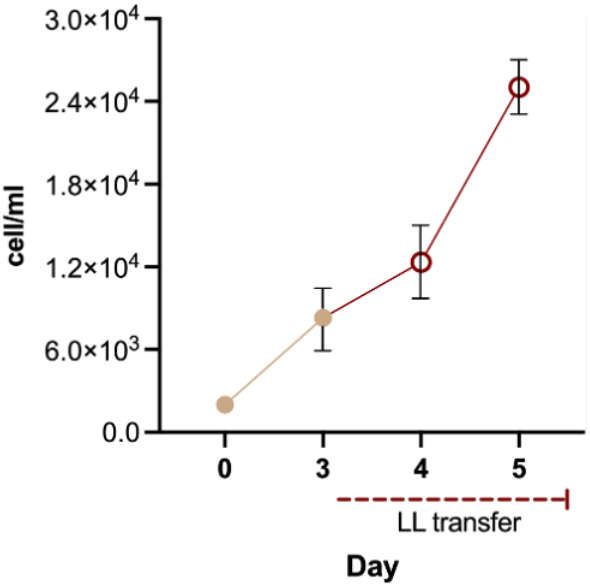

Figure 30. Thalassiosira rotula Na90A1 *grown in the two-phase short culturing system and transferred in low light (LL) condition. Brown circles indicate the culture growth until three days, while red circles indicate the growth after transfer. Averages ± standard errors were represented.*

.

In addition, a significant increase of the cell biovolume was observed after the transfer to LL (T1) (Fig. 31 A), while no significant differences were reported in the biomass (Fig. 31 B).

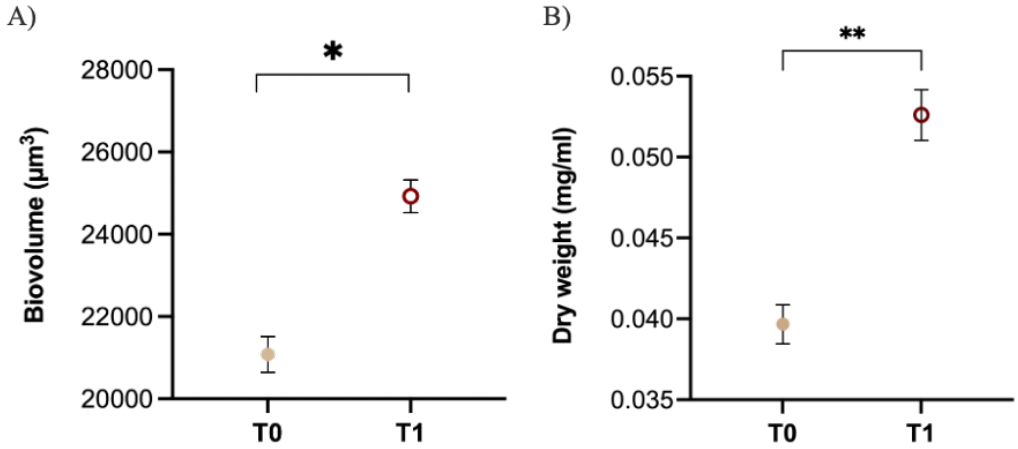

Figure 31. Biovolume (A) and dry weight (DW mg/ml) (B). T0, three days in optimal light intensity; T1, two days after transfer to low light intensity (LL) Averages ± standard errors were represented. Statistical analyses were performed using one-way ANOVA and Tukey's range test. "" ($p < 0.05$); "**" ($p < 0.01$).*

The pigment content assessed by the rapid spectrophotometric method resulted in a significant increase in Fx content as Chl a and Chl c (Fig. 32).

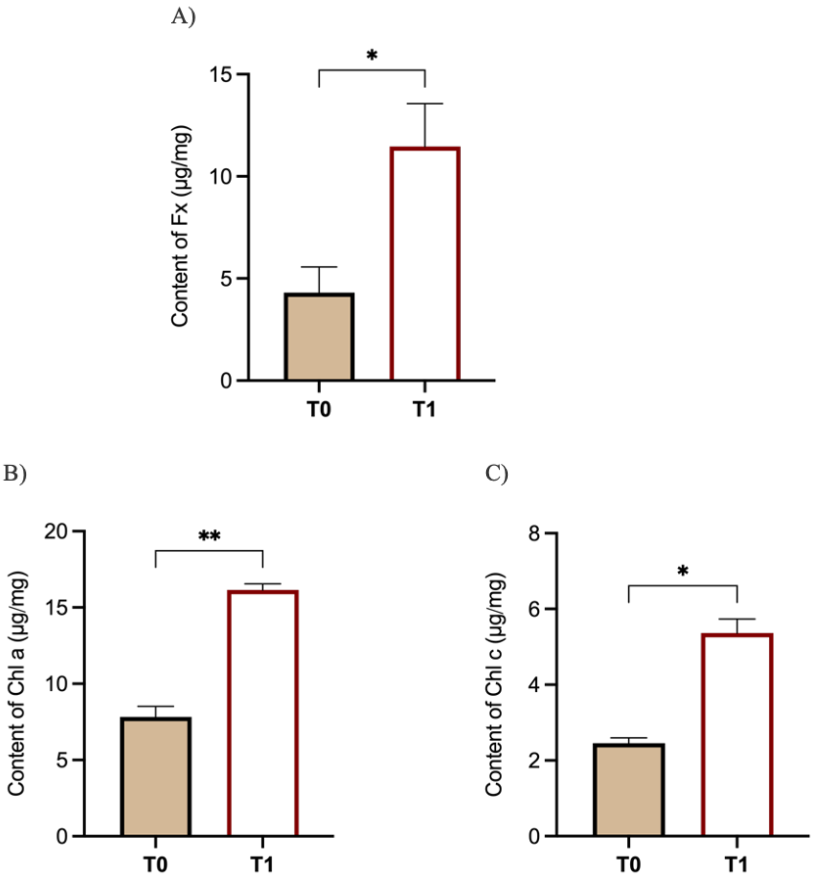

Figure 32. Pigments content (µg/mg) in Thalassiosira rotula Na90A1 *cultures grown in a two-phase short system. T0, three days in optimal light intensity; T1, two days after transfer to low light intensity (LL). The vertical bars represent averages ± standard error. Statistical analyses were performed using one-way ANOVA and Tukey's range test. "*" ($p < 0.05$); "**" ($p < 0.01$).*

The HPLC results of the same samples showed no significant differences in the levels of Chl a and Chl c (Fig. 33 A, B). Regarding carotenoids amount, ßcar was not affected by the treatments (Fig. 33 C), while a significant decrease was shown in Vx and Ddx contents after the transferring in LL condition (Fig. 33 D, E), otherwise, Fx levels remained stable (Fig. 33 G).

La borsa di dottorato è stata cofinanziata con risorse del
Programma Operativo Nazionale Ricerca e Innovazione 2014-202 (CCI 2014IT16M2OP005)
Fondo Sociale Europeo, Azione I.1 "Dottorati Innovativi con caratterizzazione Industriale"

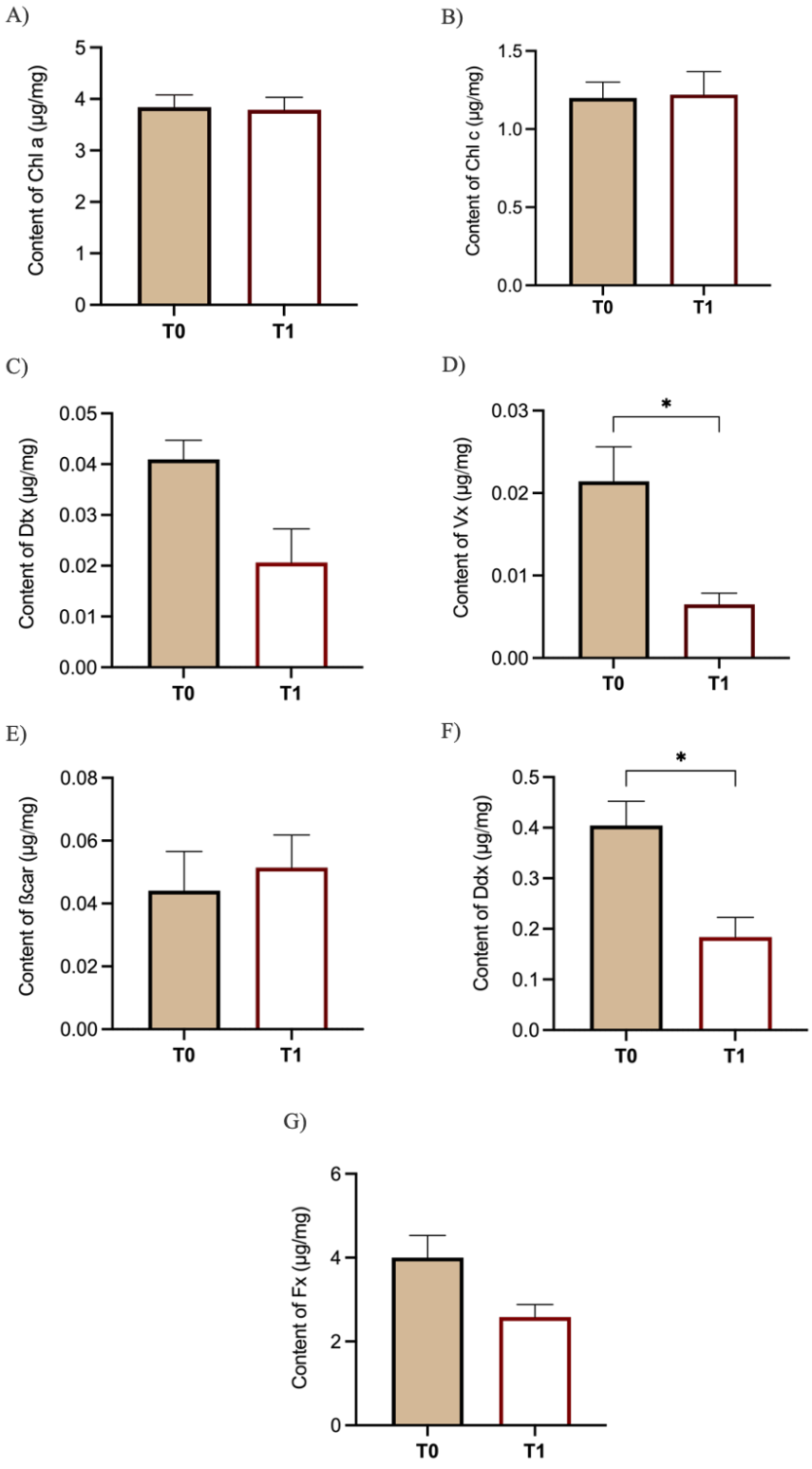

Figure 33. The content of chlorophylls and carotenoids in Thalassiosira rotula Na90A1 *cultures grown in a short time two-phase system. T0, three days in optimal light intensity; T1, two days after transfer to low light intensity (LL). The vertical bars represent averages ± standard error. Statistical analyses were performed using one-way ANOVA and Tukey's range test. "*" ($p \leq 0.05$); "**" ($p \leq 0.01$).*

Finally, by comparing spectrophotometric values with HPLC ones, the spectrophotometric method overestimates also in this two-phase short system, the content of all the pigments in LL condition, whereas the values at T0 (optimal light intensity) resulted comparable (Fig. 34 A-C).

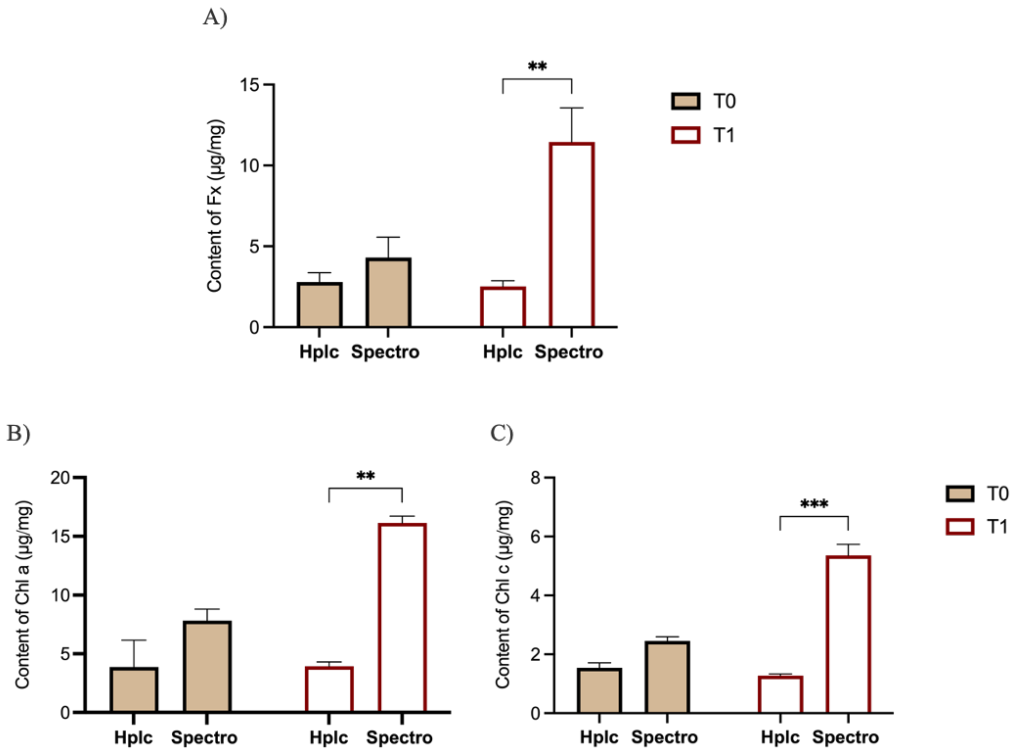

Figure 34. Comparison of spectrophotometric method (spectro) vs HPLC method. Content of Fx (A) Chl a (B), Chl c (C), in Thalassiosira rotula Na90A1 *grown in a short time two-phase system. T0, three days in optimal light intensity; T1, two days after transfer to low light intensity (LL). The vertical bars represent averages ± standard error. Statistical analyses were performed using two-way ANOVA and Tukey's range test. "*" ($p \leq 0.05$); "**" ($p \leq 0.01$).*

Concerning the expression levels of key genes of the Fx biosynthesis, significant differences were observed in expression levels between T0 and T1. Globally, all the analysed genes showed an increase in their expression level in T1 (after transferring for 2 days in LL condition) (Fig. 35).

La borsa di dottorato è stata cofinanziata con risorse del
Programma Operativo Nazionale Ricerca e Innovazione 2014-202 (CCI 2014IT16M2OP005)
Fondo Sociale Europeo, Azione I.1 "Dottorati Innovativi con caratterizzazione Industriale"

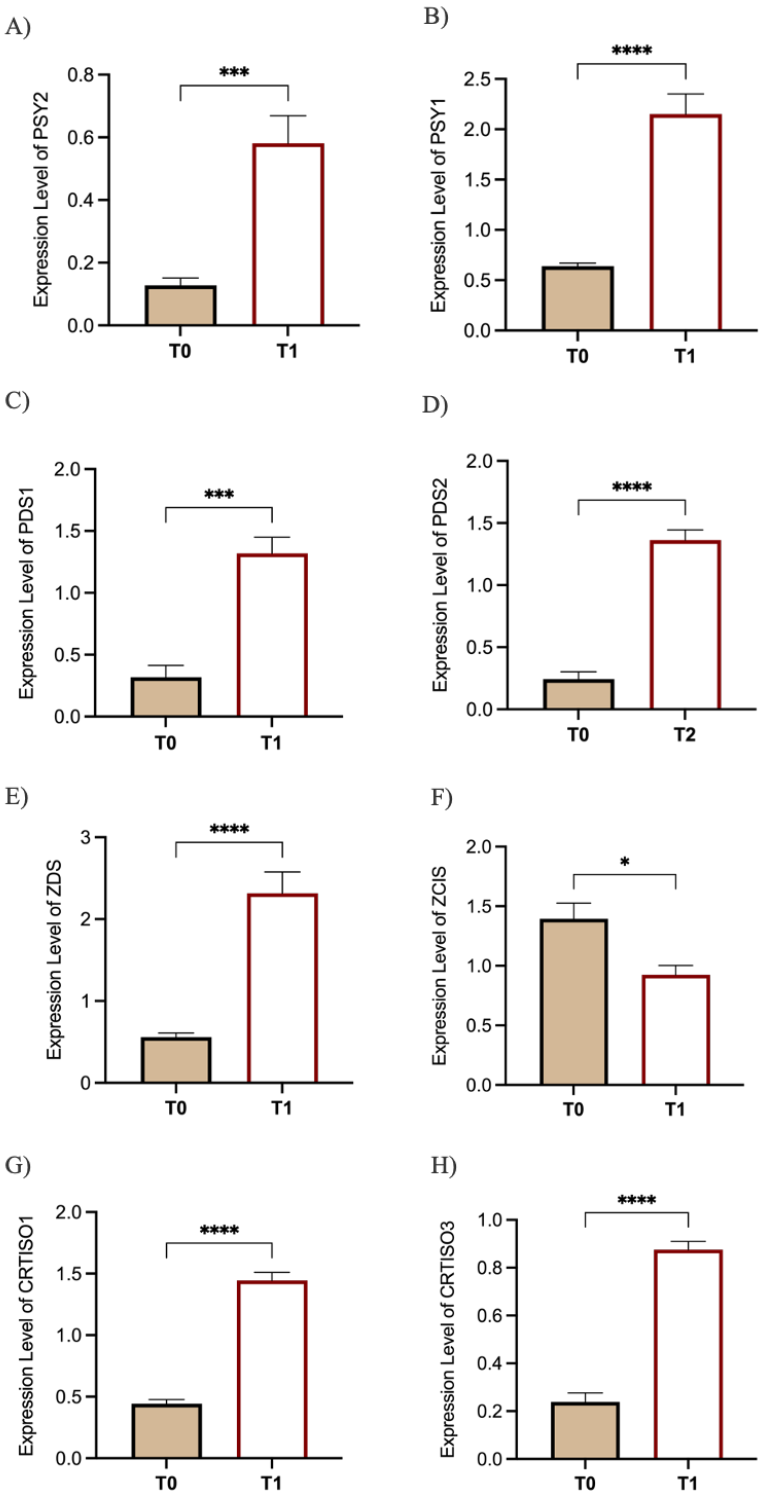

Figure 35. Relative expression level of key genes involved in the carotenoid biosynthesis pathway in Thalassiosira rotula Na90A1 *grown in a short time two-phase system. T0, three days in optimal light intensity; T1, two days after transfer to low light intensity (LL). Abbreviations: PSY, phytoene synthase; PDS, phytoene desaturase; ZCIS, 15-cis-ζ-carotene isomerase desaturases, ZDS, ζ-carotene desaturases; CRTISO, carotenoid isomerase. The vertical bars represent averages ± standard error. Statistical analyses were performed using two-way ANOVA and Tukey's range test. "*" ($p \leq 0.05$); "**" ($p \leq 0.01$); "***" ($p \leq 0.001$); "****" ($p \leq 0.0001$).*

In particular, the expression level of the genes involved in the Violaxanthin and Diadinoxanthin cycle (*ZEP1, ZEP2* and *VDL1, VDL2, VDL3* and *DDE*) showed a higher level after the transfer to LL condition (Fig. 36).

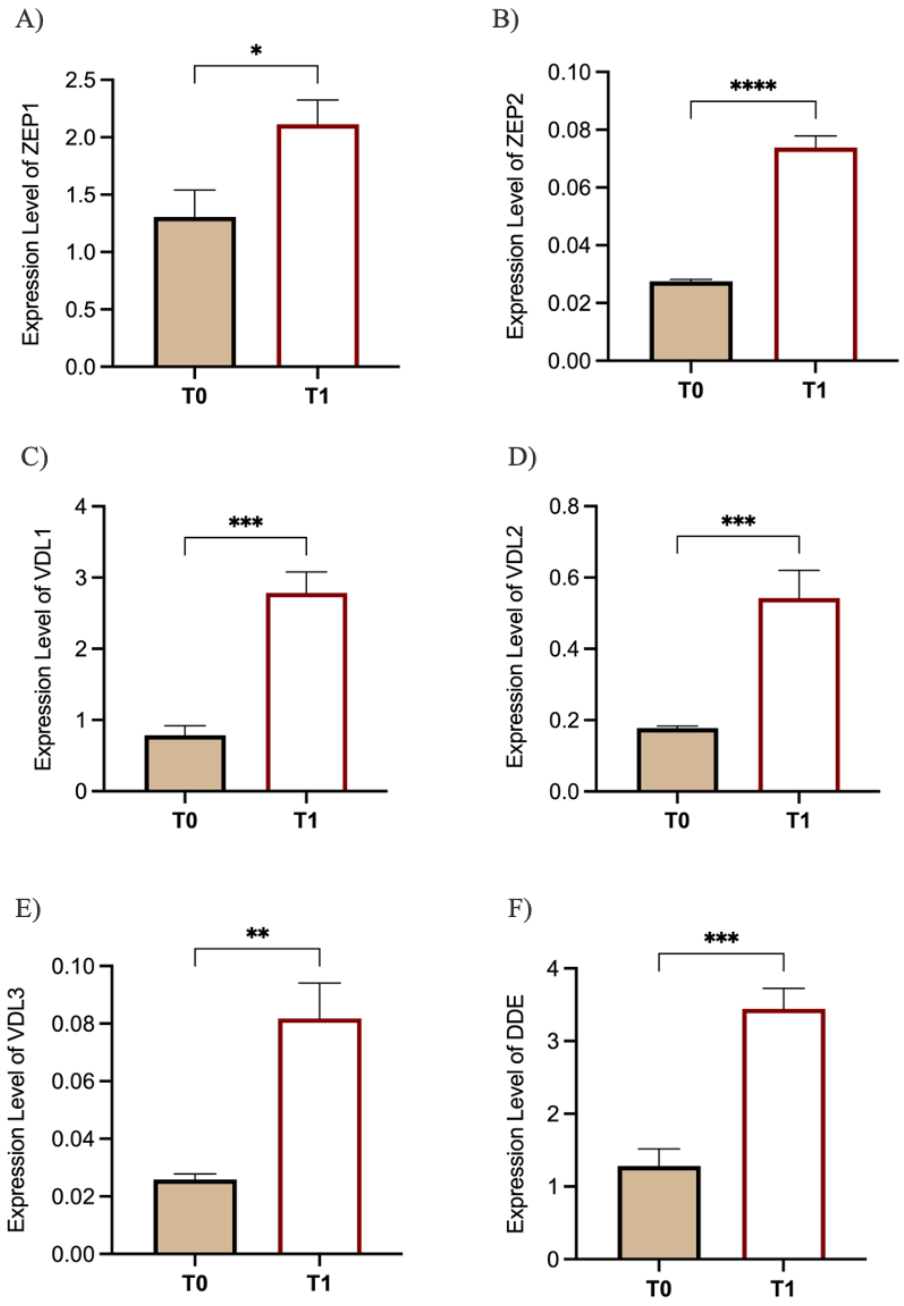

Figure 36. Relative expression level of key genes involved in xanthophyll cycle in Thalassiosira rotula Na90A1 *grown in a short time two-phase system. T0, three days in optimal light intensity; T1, two days after transfer to low light intensity (LL). Abbreviations: ZEP, zeaxanthin epoxidase; VDL, violaxanthin de-epoxidase like, DDE, diadinoxanthin de-epoxidase. The vertical bars represent averages ± standard error. Statistical analyses were performed using two-way ANOVA and Tukey's range test. "*" (p≤ 0.05); "**" (p ≤ 0.01); "***" (p ≤ 0.001); "****" (p ≤ 0.0001).*

2.4 Discussion

This PhD project was focused on the characterization of *Thalassiosira rotula* as a potential producer of fucoxanthin (Fx), a carotenoid known for its significant ecological role and health benefits.

In this study, two strains of *T. rotula*, *Dirca1* and *Na90A1*, isolated respectively from sediments and phytoplankton sampled in the Tyrrhenian Sea, were evaluated.

These were cultivated in laboratory conditions and in a specific climate cell set to guarantee good growth. Considering that growth and biomass are critical steps in biotechnological applications, to optimize growth kinetics and biomass yield I examined the impact of pre-inoculum volumes as it is known that the optimal initial size of inoculum depends on the strains and it could play a key role in the growth (Minggat *et al.*, 2021; Bastos *et al.*, 2022).

In my study, among the two different pre-inoculum volumes used, 15 mL (#1) and 250 mL (#2) respectively, at the same cell density of $1x10^3$ cell/ml, the pre-inocula #2 resulted in a shortening of the lag phase and an increase of cell density. These data align with Wang and Seibert (2017) who affirm that increased pre-inoculum volumes can result in a quick and high biomass establishment, which improves nutrient uptake and increases competition for resources among the cells. On the other hand, I noticed slow growth, especially in *Dirca1* pre-inocula #1, showing that a smaller inoculum can lead to a delay in the growth since cells need time to adjust to the culture medium before growing rapidly (Matsumoto *et al.*, 2017; Syed *et al.*, 2018). Likewise, studies on the diatoms *Skeletonema costatum* and *Chaetoceros calcitrans* have shown different growth responses depending on inoculum volume, with optimal growth observed at specific volumes that balance nutrient availability and light penetration (Minggat *et al.*, 2021; Bastos *et al.*, 2022).

Based on the best performance of the pre-inocula #2, it was chosen to be scaled up to a larger volume of 1.5 L.

Despite the rapid growth observed in both strains, significant differences were noted in cell density between the two strains: *Dirca1* reached a higher cell density than *Na90A1*, although no significant differences were observed in their maximum growth rates.

This difference in cell density can be attributed to the cell size and biovolume, measured during the exponential phase; according to this, I observed that *Na90A1* showed a higher

biovolume than *Dirca1*, which influenced the growth and density of the cultures. As Passy (2008) reported, cell density is inversely related to biovolume and body size, and my results reflect this trend, with larger cell sizes corresponding to lower cell densities in my strains.

Following the successful growth and biomass production of the two *T. rotula* strains, I initially evaluated the fucoxanthin (Fx) content in both cultures grown in basal medium (f/2), using a spectrophotometric method as a rapid screening for Fx estimation. The Fx is a carotenoid that showed a very wide absorption spectrum, including, overall, in the range of 400-500 nm, where absorption peaks of other pigments, as chlorophyll a and c, ß-carotene and diadinoxanthin, are overlapping (Fig. 37).

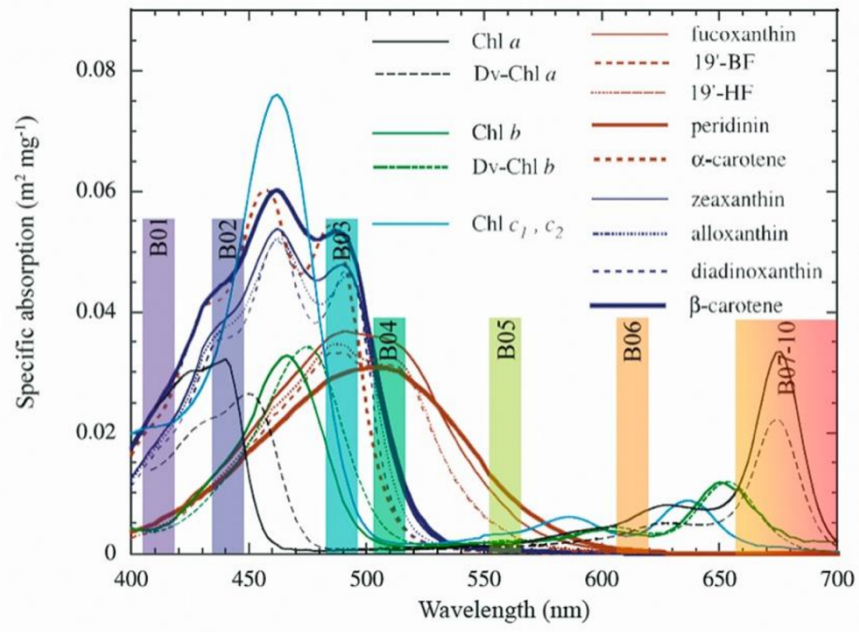

Figure 37. The absorption spectrum of photosynthetic pigment (from Bricaud et al. 2004 and modified by Kraus et al. 2021). The thick brown line showed the wide flat absorption spectra of fucoxanthin, with a peak around 500 nm.

Considering the challenges involved in extracting, isolating, and specifically identifying Fx, establishing a rapid and simple method to estimate the Fx content in cultures is crucial for every biotechnological application.

In this context, the recent study conducted by Wang *et al.* (2018) developed a spectrophotometric method to measure Fx levels that has been applied to several diatom species, including *Phaeodactylum tricornutum*, *Thalassiosira pseudonana*, and more

recently to *Craspedostauros ineffabilis* and *Craspedostauros zucchellii* (Afonso *et al.*, 2022; Li *et al.*, 2024; Trentin *et al.*, 2024).

The work of Wang *et al.* (2018) outlined a method involving several critical steps: extraction of the pigment from diatom biomass, measurement of absorbance at specific wavelengths and the application of some corrections for the interference from other pigments and/or cell debris, representing the "background noise". However, applying the equation reported in Wang *et al.* (2018) to my strains of *T. rotula*, the values of Fx content resulted negative (Tab. 5), suggesting that it was necessary to improve the formula. Since the "background noise", defined by Wang *et al.* (2018) as correction factors n_1 and n_2, depends on the type of cells as well as their density and other pigments (Chl c, and carotenoids), it was essential to recalculate n_1 and n_2 specifically for *T. rotula*. Thus, in this work, I modified the formula of Wang *et al.* (2018) for *T. rotula* resulting in a new equation that works well for both the strains, despite variations in cell density and biovolume.

My results showed a higher Fx content in *Na90A1* strain compared to *Dirca1*. These different Fx contents in different strains within the same species, have been also shown in other species of diatoms, like *P. tricornutum*, and also of green microalgae like *Chlorella vulgaris* (Wu *et al.*, 2015; Derwenskus *et al.*, 2018), as well as in Haptophytes as *Isochrysis* sp. and *Pavlova* sp. (Kim *et al.*, 2012; Crupi *et al.*, 2013; Kanamoto *et al.*, 2021), where strains from different geographic regions exhibited significant variation in fucoxanthin concentrations, suggesting that both local environmental conditions and genetic diversity contribute to these differences.

Considering that *Na90A1* strain exhibited a faster growth, a greater biovolume and a higher Fx content compared to *Dirca1*, I selected *Na90A1* strain as a promising candidate for fucoxanthin production.

In general, many studies have investigated different growth conditions in diatoms to increase Fx production, showing that the regime of light and the amount of nutrients, particularly nitrogen, are key factors in Fx biosynthesis (Wu *et al.*, 2015; Gómez-Loredo *et al.*, 2015; Guo *et al.*, 2016; Lu *et al.*, 2018; McClure *et al.*, 2018).

Several studies showed that in *Nitzschia* spp. (from 12 to 32.8 mg/g), *P. tricornutum* (Fx content ranges from 8.5 to 59.2 mg/g), but also in microalgae belonging to the Haptophyta group, like *Isochrysis* spp. (Fx content ranges from 7.5 to 23.3 mg/g), *Tisochrysis lutea*

(Fx content ranges from 2.1 to 9.4 mg/g), have increased their growth rate and Fx content under various culture conditions, as intensity and type of light, but also nutrient concentration (Gómez-Loredo *et al.*, 2015; Guo *et al.*, 2016; Lu *et al.*, 2018; McClure *et al.* 2018; Lu *et al.*, 2019; Gao *et al.*, 2021; Mohamadnia *et al.*, 2022; Erdoğan *et al.*, 2023).
It's well known that nitrogen supplementation in diatoms is a key factor in enhancing Fx biosynthesis. Research has shown that nitrogen supports growth, metabolic activities and the synthesis of chlorophyll and other carotenoids (Guo *et al.*, 2016; Nur *et al.*, 2018; Rui *et al.*, 2023; Truong *et al.*, 2024). Moreover, studies have shown that also low light treatment increase Fx levels in different species, such as *Phaeodactylum tricornutum*, *Cyclotella cryptica*, and *Nitzschia laevis* (Frick, 2023; Guo *et al.*, 2016; Erdoğan *et al.*, 2023). This enhancement is closely related to the presence of a Light-Harvesting Complexes, specifically Fucoxanthin-Chlorophyll a/c binding Proteins (FCPs), to improve the photosynthetic efficacy (Yang & Dong, 2020; Duarte *et al.*, 2021; Truong *et al.*, 2023). This adaptive mechanism leads to the upregulation of genes associated with FCPs, further increasing Fx production under low light conditions (Yang & Dong, 2020; Truong *et al.*, 2024; Chinnappan *et al.*, 2024).
Based on this evidence, I also examined how the interaction between nitrogen availability and low light conditions affected the production of fucoxanthin. Many studies have shown that nitrate supplementation in low light environments increased fucoxanthin production (Guo *et al.*, 2016; Nur *et al.*, 2018; Wang *et al.*, 2018; Truong, 2024). For instance, as reported by Yang and Dong (2020) it was shown that combining nitrogen supplementation with appropriate light intensity can significantly enhance fucoxanthin production in *P. tricornutum*, leading to yields of 16.28 mg/g.
In agreement with other studies, my results showed that the HN treatment significantly enhanced the growth and biomass of my strain, while in the LL condition a low cell density was noted, as reported in literature (Guo *et al.*, 2016; Lu *et al.*, 2018; Derwenskus *et al.*, 2020; Afonso *et al.*, 2022). Conversely, whereas I expected a positive effect combining these two conditions, LL HN resulted similarly to LL in cell density and biomass.
The impact of these different culture condition on the size and biovolume (at exponential and late exponential phases) showed that HN improved the cell biovolume of *T. rotula*, as also reported for *P. tricornutum* grown in nitrogen-enriched media (Zhang *et al.*, 2012).

Furthermore, also the LL treatment showed a rise in cell biovolume, despite the low density, explaining also the high biomass noted in these culture conditions.
In order to consider if the increase of the size would be correlated with the increase of other metabolites of potential biotechnological use besides Fx, I estimated, by a fluorescent in vivo analysis by Nile Red (NR) staining, the neutral lipids content.
In *T. rotula* the treatments did not induce an increase in lipid content but lipid droplets were only observed at the final stage of the growth curve (senescence phase). It's known that rather than nitrogen supplementation it is the nitrogen starvation that triggers enhanced lipid accumulation (Longworth *et al.*, 2016; Curcuraci *et al.*, 2022; Murison *et al.*, 2023). In my case, the beneficial impact of high-nitrogen treatment is overall on the growth and biomass increase rather than lipid biosynthesis, which instead seem to increase with senescence overall in the control conditions.

The application of the quick and simple spectrophotometric method that I optimized for *T. rotula* for Fx measurements, using could represent a potential benefit for companies to reduce costs with respect to other methods and also to obtain fast results. So, the pigments extracted from the cells at late exponential phases were analysed by spectrophotometric as well as by HPLC method in order to compare the Fx content and finally validate the spectrophotometric rapid method. Clearly, HPLC analyses also allowed to profile the other pigments and Fx precursors.
Spectrophotometric results showed an increase of Fx as well as chlorophyll a and c content in response to HN and LL conditions. Several studies reported that high nitrate supplementation and low light induced an improvement of the Fx production in *P. tricornutum* (Cvjetinovic *et al.* 2020; Afonso *et al.* 2022; Truong *et al.* 2023). As reported by Kuczynska *et al.* (2015), diatoms can adapt their pigment composition in response to varying nutrient conditions; in addition, Cvjetinovic *et al.* (2020) highlighted that chlorophyll a and c, along with carotenoids, are crucial for the light-harvesting processes in diatoms, which are particularly efficient in nutrient-rich environments.
The pigments content estimated through HPLC analysis confirm that the treatments impact on their concentration. Firstly, a significant increase was observed in chlorophyll a and c content in LL treatment, according to their crucial role for capturing energy during light-harvesting and may be linked to the energy transfer pathways of the fucoxanthin–chlorophyll protein (FCP) complex in *T. rotula* (Yi *et al.*, 2019; Chinnappan *et al.*, 2024).

Inside the carotenoids, β-carotene also plays a key role in photosynthesis under low light conditions (Chinnappan *et al.*, 2024), explaining why its levels increased in LL and LL HN (Fig. 19). Regarding the other carotenoids, the regulation of the xanthophyll cycle with nitrate addition is a significant research topic. Various studies have highlighted the importance of nitrogen in carotenoid synthesis, such as Jauffrais *et al.* (2016) which showed that nitrate supplementation can enhance pigment production, while the absence of these nutrients can trigger a different adaptive response. My results, in line with Guo *et al.* (2016) and Xia *et al.* (2018), which reported a rise of biomass and carotenoids production in *C. cryptica* and *O. aurita* under nitrogen supplementation, have shown a wide improvement of carotenoid content in response to HN, with the highest value, excluding β-car, observed for Diadinoxanthin (Fig. 20). This trend is in agreement with other studies that reported a strong correlation of Ddx with the last step of fucoxanthin biosynthesis (Lavaud *et al.*, 2003; Xia *et al.*, 2018; Yi *et al.*, 2019).

Concerning my pigment of interest, the Fx, my results showed a high concentration yet in the Ctrl in the Exp phase (4.7 μg/mg DW).

Based on the data of Fx content in microalgae reported in the other works, I found that the amount in *T. rotula* is higher than other microalgae as *Skeletonema costatum* (0.36 μg/mg), *Odontella sinesis* (1.18 μg/mg), *Nitzschia laevis* (1.68 μg/mg), *Chaetoceros gracilis* and *C. calcitrans* (2.24 and 2.33 μg/mg respectively); however, the Fx content detected in my *T. rotula* is relative lower than commercially used microalgae as *Cylindrotheca closterium* (5.24 μg/mg), *Isochrysis galbana* (6.04 μg/mg), *P. tricornutum* (8.55 μg/mg) and *O. aurita* (9.41 μg/mg) (Pasquet *et al.*, 2011; Goiris *et al.*, 2012; Kim *et al.*, 2012; Song *et al.*, 2013; Foo *et al.*, 2017; Sun *et al.*, 2019; Zhang *et al.*, 2022). As it's well known, several parameters are involved and influence the pigment content, so it's need to highlight that most of these higher concentrations were obtained by culturing in photobioreactors and modifying the abiotic conditions to improve the production of Fx.

Considering also this aspect, my results obtained in the laboratory conditions, showed a significant rise in the LL condition, in line with Gómez-Loredo *et al.* (2015), McClure *et al.* (2018), and Chinnappan *et al.* (2024) who reported an enhancement of this pigment in *P. tricornutum* and *Cyclotella meneghiniana*.

Nevertheless, in my system, the Fx level achieved through the HN treatment was not the highest. Although it was reported that increasing nutrient levels of nitrogen there was a graded enhancement of fucoxanthin % DW in the culture of *P. tricornutum*, and *T. weissflogii* (McClure *et al.*, 2018; Marella and Tiwari, 2020), in *T. rotula* probably the nitrate enrichment only helped my culture to maintain a high content of Fx during the time.

About the HPLC findings, the comparison with the spectrophotometric analysis revealed a comparable Fx quantification in the Ctrl condition, but significant differences were noted in the Fx amount especially in the HN and LL conditions. Indeed, the spectrophotometer overestimates the Fx contents in the cells after the treatments. To explain this, I have to consider the visible absorption spectrum scan of the total extracted pigments which showed an increase not only in the height but also in the width of the peaks after HN and LL treatments. Thus, I might hypothesize that the Fx absorption spectrum ranging from 400 to 500 nm, overlaps with the total pigments and also with Fx precursors; furthermore, I can hypothesize that my treatments, which actually influence total pigments, could influence Fx biosynthesis pathways and so its precursor, leading a total Fx overestimation by spectrophotometric methods.

These results show that enhancing Fx production is a complex and fine-tuned process influenced by various factors such as precursor formation and its impact on gene expression.

Due to the health benefits and economic importance of Fx, its biosynthetic pathway has been extensively studied, particularly in diatoms (Seth *et al.*, 2021; Truong *et al.*, 2023; Seo *et al.*, 2024), but not entirely explained yet and many key enzymes remain to be isolate and identify.

Since the Fx biosynthesis pathway is still unknown, I investigated the main genes involved. Dambek *et al.* (2012) firstly described this process in *P. tricornutum*: the first step in the Fx biosynthesis is the condensation of Geranylgeranyl diphosphate (GGPP) catalysed by phytoene synthase (PSY), followed by the activity of phytoene desaturases (*PDS*), carotenoid isomerase (CRTISO), ζ-carotene desaturases (ZDS), lycopene β-cyclase (LYCb). Furthermore, the roles of genes *PSY*, *PDS* and *ZDS* in carotenoid and Fx accumulation have been revealed (Dambek *et al.*, 2012; Kadono *et al.*, 2015; Cen *et al.*, 2022; Li *et al.*, 2024).

In my work, I studied the expression levels of these key genes during both the Exp and Late Exp phases in all culture conditions.

Firstly, the expression of key regulatory genes as *PSY* (*PSY1* and *PSY2*) and *PDS* (*PDS1* and *PDS2*) has shown high levels in response to HN and LL conditions compared to the control. My results suggested that globally in the Exp phase, *PSY* and *PDS2* were up-regulated in the HN condition. In the Late Exp all *PSY* isoforms showed high expression level in response to HN, while *PDS* showed high levels in LL condition (Fig. 24). Among the genes regulated under nitrate supplementation, it's described the upregulation of *PSY* and *PDS*, highlighting that this modulation is essential for diatoms to enhance their carotenoid production (Kadono *et al.*, 2015; Hao *et al.*, 2021; Truong *et al.*, 2023 and 2024). For instance, studies conducted to silence *PDS* resulted in the downregulation of genes involved in subsequent steps of carotenogenesis and significantly decreased carotenoid content (Kadono *et al.*, 2015; Velmurugan and Muthukaliannan, 2022). Also, the effect of nitrogen availability on carotenogenesis could have a regulatory mechanism of Fx biosynthesis (Truong *et al.*, 2024). Specifically, the overexpression of *PSY* increased the FX content up to 1.8 folds in *P. tricornutum* (Eilers *et al.*, 2016).

Although the last steps of Fx synthesis are not completely clear, it's well-known that a key role is mediated by the violaxanthin cycle, starting with the formation of zeaxanthin from ß-car (Fig. 23). The zeaxanthin epoxidase (ZEP) converts zeaxanthin in violaxanthin through the intermediate antheraxanthin and this regulation is mediated by light intensity, functioning as a light protection strategy not only in diatoms but also in green algae and plants (Coesel *et al.*, 2008; Wang *et al.*, 2021). In addition, the violaxanthin produced is converted to neoxanthin and the last studies proposed that violaxanthin de-epoxidase-like (VDL) protein 1 (VDL1) catalyses this reaction, while VDL2 catalyses the conversion of diadinoxanthin (Ddx) to allenoxanthin.

In my study, I identified in *T. rotula* two isoforms of *ZEP (ZEP1* and *ZEP2*), similarly as reported in *T. pseduonana*, whereas three isoforms were found in *P. tricornutum* (Seth *et al.*, 2021). In addition, multiple *violaxanthin de-epoxidase-like* (*VDL*) genes were identified in *T. rotula* (Fig. 27). The results of the expression level of the different isoforms have shown that *ZEP1* was up-regulated by HN and LL HN in both phases, confirming an interesting role of this gene in the regulation of the final biosynthesis pigments; on the other hand, *ZEP2* showed high levels in response to the LL condition,

although the values of gene expression are much lower than *ZEP1*. The role of these different isoforms is not completely clear, but a recent study has recently found that in *P. tricornutum ZEP1* encodes an enzyme essential for the synthesis of Fx, whereas *ZEP2* and/or *ZEP3* are candidate genes for encoding the epoxidase converting Dtx to Ddx (Coesel *et al.*, 2008; Eilers *et al.*, 2016; Bai *et al.*, 2022).

Moreover, whereas genes involved in the last steps of the Fx biosynthetic pathway are not completely identified, many studies validate the role of *VDE*, *VDL*, and *ZEP* using their overexpression in *P. tricornutum*, revealing their ability to enhance the FX accumulation (Kadono *et al.* 2015; Eilers *et al.* 2016; Manfellotto *et al.*, 2020).

In my study, the *VDL* isoforms showed a different expression related to the growth conditions: in Exp phase, the *VDL* isoforms showed the highest expression level in response to the different treatments vs Ctrl (HN, LL and LL HN); nonetheless, in the Late exp the highest expression levels were observed only in HN, except for *VDL2* for which a high level was also present in LL condition. This different expression could be related with the different role of the isoforms: as reported by Seo *et al.*, (2024), *VDL1* catalyses the conversion of violaxanthin to neoxanthin, the early product of Fx biosynthesis, while *VDL2* converts diadinoxanthin to allenoxanthin (Seo *et al.*, 2024). This modulated expression highlights the key role that interplays these genes and the growth condition as nitrate supplementation and the low light, also shown in the studies performed on *P. tricornutum* by Truong *et al.* (2024) and Chinnappan *et al.* (2024).

Based on the previous results, the LL condition has been shown to induce the greatest enhancement of Fx, modulating also the biosynthetic pathway. However, this condition led to a significantly reduced biomass, marking a critical step for the biotechnological yield. To overcome this, I evaluated a short time two-phase culturing system over a brief period of five days. Lu *et al.* (2018) have noted that cultivation techniques as two-stage method, can significantly enhance fucoxanthin production in diatoms such as *Nitzschia laevis*. This approach is successful in reaching high growth rates and promoting pigment accumulation.

During my experiment, the first stage of growth occurred under optimal medium and light conditions, followed by a shift to low light conditions. Firstly, the estimate of Fx content in the cells cultured in this short time two-phase culturing system, confirmed the discrepancy between the two methods in the treated sample (in this case LL).

As reported in my previous experiment, spectrophotometric measurements tended to overestimate fucoxanthin levels in the treated samples. In contrast, HPLC analysis showed no significant difference in the chlorophylls and primary carotenoid, except for Vx and Ddx. Interestingly, gene expression analysis showed a significant increase in the expression levels of all genes investigated, except for *ZCIS*, following the transition to low-light conditions. These results suggest an early modulation of the biosynthetic pathway due to the treatment: the genes involved in the violaxanthin and diadinoxanthin cycle showed the highest expression levels after the shift in LL condition. These support that in the short time two-phase culturing systems, the treatment induced changes in the biosynthetic pathway but probably a longer period might be needed to enhance fucoxanthin production effectively.

La borsa di dottorato è stata cofinanziata con risorse del
Programma Operativo Nazionale Ricerca e Innovazione 2014-202 (CCI 2014IT16M2OP005)
Fondo Sociale Europeo, Azione I.1 "Dottorati Innovativi con caratterizzazione Industriale"

2.5 Conclusions

The results from this PhD research underscore the potential of *Thalassiosira rotula* as a promising candidate for scaling up in bioreactors and industrial settings applications. This species shows noteworthy capacity for fucoxanthin (Fx) production, even without any special treatment under typical laboratory conditions. Compared with other species such as *Skeletonema costatum*, *Odontella sinesis*, *Nitzschia laevis*, *Chaetoceros gracilis* and *C. calcitrans*, my strain of *T. rotula,* growth in a relative small culture system (1.5 L), showed the highest content of Fx, suggesting her potential use in commercially field. Moreover, my results show that high nitrogen (HN) treatment led to an enhancement in both biomass and morphophysiological characteristics of *T. rotula*, with its primary benefit being the stabilization of Fx content throughout the growth period. This stability in fucoxanthin levels is crucial for industrial applications where consistent product quality is essential. Additionally, the study also examined how low light (LL) impacts the production of Fx, finding that it increases significantly, although this comes at the expense of reduced cell density and biomass. This balance between challenges and opportunities in optimizing production processes emphasizes the importance of carefully managing growth conditions to enhance pigment yields without compromising overall biomass. Moreover, this research highlights the critical role of key genes involved in the biosynthetic pathway for fucoxanthin. The identification and analysis of these genes opens the door for potential genetic engineering of *T. rotula*, which could enhance its efficiency as a biofactory for producing this valuable carotenoid. By targeting these genes for manipulation, future research could reveal their specific functions and how they adapt to varying environmental conditions, leading to improved strategies for enhancing Fx production.

In conclusion, the results from this research illustrate the potential for *T. rotula* in biotechnological applications. Eventually the application of an "omics" approach and/or genome manipulation could give significant opportunities for advancing my understanding of gene functions and improving fucoxanthin yields under diverse conditions. So, this work provides knowledge advancement in the field of microalgal biotechnology and also sets the stage for future investigations that could maximize the productivity of *T. rotula* as a bioresource.

2.6 References

Afonso, C., Bragança, A. R., Rebelo, B. A., Serra, T. S., & Abranches, R. 2022. Optimal nitrate supplementation in *Phaeodactylum tricornutum* culture medium increases biomass and fucoxanthin production. Foods, 11(4), 568M. https://doi.org/10.3390/foods11040568;

Alemán-Nava, G. S., Cuellar-Bermudez, S. P., Cuaresma, M., Bosma, R., Muylaert, K., Ritmann, B. E., & Parra, R. 2016. How to use Nile Red, a selective fluorescent stain for microalgal neutral lipids. Journal of Microbiological Methods, 128, 74-79;

Armbrust, E. V., Berges, J. A., Bowler, C., Green, B. R., Martinez, D., Putnam, N. H., ... & Rokhsar, D. S. 2004. The genome of the diatom *Thalassiosira pseudonana*: ecology, evolution, and metabolism. Science, 306(5693), 79-86. https://doi.org/10.1126/science.1101156;

Bai, Y., Cao, T., Dautermann, O., Buschbeck, P., Cantrell, M. B., Chen, Y., ... & Lohr, M. 2022. Green diatom mutants reveal an intricate biosynthetic pathway of fucoxanthin. Proceedings of the National Academy of Sciences, 119(38), e2203708119. https://doi.org/10.1073/pnas.2203708119

Bastos, C., Maia, I., Pereira, H., Navalho, J., & Varela, J. 2022. Optimisation of biomass production and nutritional value of two marine diatoms (Bacillariophyceae), *Skeletonema costatum* and *Chaetoceros calcitrans*. Biology, 11(4), 594. https://doi.org/10.3390/biology11040594;

Bayu, A., Rachman, A., Noerdjito, D. R., Putra, M. Y., & Widayatno, W. B. 2020. High-value chemicals from marine diatoms: A biorefinery approach. In IOP Conference Series: Earth and Environmental Science (Vol. 460, No. 1, p. 012012). IOP Publishing. DOI 10.1088/1755-1315/460/1/012012;

Badejo, A. A. 2018. Elevated carotenoids in staple crops: The biosynthesis, challenges and measures for target delivery. Journal of Genetic Engineering and Biotechnology, 16(2), 553-562. https://doi.org/10.1016/j.jgeb.2018.02.010;

Björn, L. O., Papageorgiou, G. C., Blankenship, R. E., & Govindjee. 2009. A viewpoint: why chlorophyll a?. Photosynthesis Research, 99, 85-98. https://doi.org/10.1007/s11120-008-9395-x;

Bowler, C., Allen, A., Badger, J. *et al.* 2008. The *Phaeodactylum* genome reveals the evolutionary history of diatom genomes. Nature 456, 239–244. https://doi.org/10.1038/nature07410;

Breitenbach, J., & Sandmann, G. 2005. ζ-Carotene cis isomers as products and substrates in the plant poly-cis carotenoid biosynthetic pathway to lycopene. Planta, 220, 785-793. https://doi.org/10.1007/s00425-004-1395-2;

Bricaud, A., Claustre, H., Ras, J., & Oubelkheir, K. 2004. Natural variability of phytoplanktonic absorption in oceanic waters: Influence of the size structure of algal populations. Journal of Geophysical Research: Oceans, 109(C11). https://doi.org/10.1029/2004JC002419;

Britton, G.; Liaaen-Jensen, S.; Pfander, H. 2004. Carotenoids, 1st ed.; Britton, G., Liaaen-Jensen, S., Pfander, H., Eds.; Birkhäuser Verlag: Basel, Switzerland;

Cen S-Y, Li D-W, Huang X-L, Huang D, Balamurugan S, Liu W-J, Zheng J-W, Yang W-D, Li H-Y. 2022. Crucial carotenogenic genes elevate hyperaccumulation of both fucoxanthin and β-carotene in *Phaeodactylum tricornutum*. Algal Res. 64: 102691. https://doi.org/10.1016/j.algal.2022.102691;

Chen, M. 2014. Chlorophyll modifications and their spectral extension in oxygenic photosynthesis. Annual review of biochemistry, 83(1), 317-340. https://doi.org/10.1146/annurev-biochem-072711-162943;

Chen, S. J., Lin, T. B., Peng, H. Y., Liu, H. J., Lee, A. S., Lin, C. H., & Tseng, K. W. 2021. Cytoprotective potential of fucoxanthin in oxidative stress-induced age-related macular degeneration and retinal pigment epithelial cell senescence *in vivo* and *in vitro*. Marine Drugs, 19(2), 114. https://doi.org/10.3390/md19020114;

Chinnappan, S., Cai, J., Li, Y., Yang, Z., Sheng, Y., Cheng, K., ... & Li, P. 2024. Light and nutrient conditions influence fucoxanthin production of the microalgae *Cyclotella meneghiniana*. Applied Sciences, 14(13), 5504.https://doi.org/10.3390/app14135504;

Coesel S., Obornik M., Varela J., Falciatore A., Bowler C. 2008. Evolutionary Origins and Functions of the Carotenoid Biosynthetic Pathway in Marine Diatoms. PLoS ONE.;3:e2896. doi: 10.1371/journal.pone.0002896.

Crupi, P., Toci, A. T., Mangini, S., Wrubl, F., Rodolfi, L., Tredici, M. R., ... & Antonacci, D. 2013. Determination of fucoxanthin isomers in microalgae (*Isochrysis* sp.) by high-performance liquid chromatography coupled with diode-array detector multistage mass spectrometry coupled with positive electrospray ionization. Rapid Communications in Mass Spectrometry, 27(9), 1027-1035.https://doi.org/10.1002/rcm.6531

Curcuraci, E., Manuguerra, S., Messina, C., Arena, R., Renda, G., Ioannou, T., … & Santulli, A. 2022. Culture conditions affect antioxidant production, metabolism and related biomarkers of the microalgae *Phaeodactylum tricornutum*. Antioxidants, 11(2), 411. https://doi.org/10.3390/antiox11020411

Cvjetinovic, J., Salimon, A. I., Novoselova, M. V., Sapozhnikov, P. V., Shirshin, E. A., Yashchenok, A. M., ... & Gorin, D. A. 2020. Photoacoustic and fluorescence lifetime imaging of diatoms. Photoacoustics, 18, 100171. https://doi.org/10.1016/j.pacs.2020.100171;

da Silva, J. C., & Lombardi, A. T. 2020. Chlorophylls in microalgae: Occurrence, distribution, and biosynthesis. Pigments from microalgae handbook, 1-18; https://doi.org/10.1007/978-3-030-50971-2_1;

Dambek, M., Eilers, U., Breitenbach, J., Steiger, S., Büchel, C., & Sandmann, G. 2012. Biosynthesis of fucoxanthin and diadinoxanthin and function of initial pathway genes in *Phaeodactylum tricornutum.* Journal of Experimental Botany, 63(15), 5607-5612. https://doi.org/10.1093/jxb/ers211;

Dautermann, O., Lyska, D., Andersen-Ranberg, J., Becker, M., Fröhlich-Nowoisky, J., Gartmann, H., Krämer, L. C., Mayr, K., Pieper, D., Rij, L. M., Wipf, H. M., Niyogi, K. K., & Lohr, M. 2020. An algal enzyme required for biosynthesis of the most abundant marine carotenoids. Science Advances, 6(10), eaaw9183. https://doi.org/10.1126/sciadv.aaw9183;

Derwenskus, F., Metz, F., Gille, A., Schmid-Staiger, U., Briviba, K., Schließmann, U., … & Hirth, T. 2018. Pressurized extraction of unsaturated fatty acids and carotenoids from wet *Chlorella vulgaris* and *Phaeodactylum tricornutum* biomass using subcritical liquids. GCB Bioenergy, 11(1), 335-344. https://doi.org/10.1111/gcbb.12563;

Di Dato, V., Di Costanzo, F., Barbarinaldi, R., Perna, A., Ianora, A., & Romano, G. 2019. Unveiling the presence of biosynthetic pathways for bioactive compounds in the *Thalassiosira rotula* transcriptome. Scientific Reports, 9(1), 9893. https://doi.org/10.1038/s41598-019-46276-8;

Duarte, B., Feijão, E., Goessling, J., Caçador, I., & Matos, A. 2021. Pigment and fatty acid production under different light qualities in the diatom *Phaeodactylum tricornutum*. Applied Sciences, 11(6), 2550. https://doi.org/10.3390/app11062550;

Eilers U., Dietzel L., Breitenbach J., Büchel C., Sandmann G. 2016. Identification of Genes Coding for Functional Zeaxanthin Epoxidases in the Diatom *Phaeodactylum Tricornutum*. J. Plant Physiol.;192:64–70. doi: 10.1016/j.jplph.2016.01.006;

Erdoğan, A., Karataş, A., Demir, D., Demirel, Z., Aktürk, M., Çopur, Ö., … & Dalay, M. 2023. Manipulation in culture conditions of *Nanofrustulum shiloi* for enhanced fucoxanthin production and isolation by preparative chromatography. Molecules, 28(4), 1988. https://doi.org/10.3390/molecules28041988;

Fernandes, F., Barbosa, M., Oliveira, A. P., Azevedo, I. C., Sousa-Pinto, I., Valentão, P., & Andrade, P. B. 2016. The pigments of kelps (Ochrophyta) as part of the flexible response to highly variable marine environments. Journal of Applied Phycology, 28, 3689-3696. https://doi.org/10.1007/s10811-016-0883-7;

Frick, K. 2023. Influence of light conditions on the production of chrysolaminarin using *Phaeodactylum tricornutum* in artificially illuminated photobioreactors. Microbiologyopen, 12(5). https://doi.org/10.1002/mbo3.1378;

Frommholt R., Werner S., Paulsen H., Goss R., Wilhelm C., Zauner S., Maier UG., Grossman AR., Bhattacharya D., Lohr M. 2008. Ancient recruitment by chromists of green algal genes encoding enzymes for carotenoid biosynthesis. Mol Biol Evol 25:2653–2667. https://doi.org/10.1093/molbev/msn206;

Fung, A., Hamid, N., & Lu, J. 2013. Fucoxanthin content and antioxidant properties of *Undaria pinnatifida*. Food chemistry, 136(2), 1055-1062. https://doi.org/10.1016/j.foodchem.2012.09.024;

Gao, B., Chen, A., Zhang, W., Li, A., & Zhang, C. 2017. Co-production of lipids, eicosapentaenoic acid, fucoxanthin, and chrysolaminarin by *Phaeodactylum tricornutum* cultured in a flat-plate photobioreactor under varying nitrogen conditions. Journal of Ocean University of China, 16, 916-924. https://doi.org/10.1007/s11802-017-3174-2;

Gao, F., Sá, M., Cabanelas, I. T. D., Wijffels, R. H., & Barbosa, M. J. 2021. Improved fucoxanthin and docosahexaenoic acid productivities of a sorted self-settling *Tisochrysis*

lutea phenotype at pilot scale. Bioresource Technology, *325*, 124725. https://doi.org/10.1016/j.biortech.2021.124725;

Gelzinis, A., Butkus, V., Songaila, E., Augulis, R., Gall, A., Büchel, C., ... & Valkunas, L. 2015. Mapping energy transfer channels in fucoxanthin–chlorophyll protein complex. Biochimica et Biophysica Acta (BBA)-Bioenergetics, 1847(2), 241-247. https://doi.org/10.1016/j.bbabio.2014.11.004;

Goiris, K., Muylaert, K., Fraeye, I., Foubert, I., De Brabanter, J., & De Cooman, L. 2012. Antioxidant potential of microalgae in relation to their phenolic and carotenoid content. Journal of Applied Phycology, 24, 1477-1486. https://dx.doi.org/10.1007/s10811-012-9804-6;

Gómez-Loredo, A., Benavides, J., & Rito-Palomares, M. 2015. Growth kinetics and fucoxanthin production of *Phaeodactylum tricornutum* and *Isochrysis galbana* cultures at different light and agitation conditions. Journal of Applied Phycology, 28(2), 849-860. https://doi.org/10.1007/s10811-015-0635-0;

Guo, B., Liu, B., Yang, B., Sun, P., Lu, X., Liu, J., … & Chen, F. 2016. Screening of diatom strains and characterization of *Cyclotella cryptica* as a potential fucoxanthin producer. Marine Drugs, 14(7), 125. https://doi.org/10.3390/md14070125;

Hao, T. B., Lu, Y., Zhang, Z. H., Liu, S. F., Wang, X., Yang, W. D., ... & Li, H. Y. 2021. Hyperaccumulation of fucoxanthin by enhancing methylerythritol phosphate pathway in *Phaeodactylum tricornutum.* Applied Microbiology and Biotechnology, 105(23), 8783-8793. https://doi.org/10.1007/s00253-021-11660-w;

Jauffrais, T., Jesus, B., Méléder, V., Turpin, V., Russo, A. D. P., Raimbault, P., & Jézéquel, V. M. 2016. Physiological and photophysiological responses of the benthic diatom *Entomoneis paludosa* (Bacillariophyceae) to dissolved inorganic and organic nitrogen in culture. Marine Biology, 163, 1-14. https://doi.org/10.1007/s00227-016-2888-9;

Jeffrey, S. W., Mantoura, R. F. C., & Wright, S. W. 2005. Phytoplankton pigments in oceanography: guidelines to modern methods;

Kadono, T., Kira, N., Suzuki, K., Iwata, O., Ohama, T., Okada, S., Nishimura, T., Akakabe, M., Tsuda, M., & Adachi, M. 2015. Effect of an Introduced Phytoene Synthase Gene Expression on Carotenoid Biosynthesis in the Marine Diatom *Phaeodactylum tricornutum*. Marine Drugs, 13(8), 5334–5357. https://doi.org/10.3390/md13085334;

Kanamoto, A., Kato, Y., Yoshida, E., Hasunuma, T., & Kondo, A. 2021. Development of a method for fucoxanthin production using the haptophyte marine microalga *Pavlova* sp. Marine Biotechnology, 23(2), 331-341. https://doi.org/10.1007/s10126-021-10028-5;

Kim, S. M., Kang, S., Kwon, O., Chung, D., & Pan, C. 2012. Fucoxanthin as a major carotenoid in *Isochrysis* aff. *galbana*: characterization of extraction for commercial application. Journal of the Korean Society for Applied Biological Chemistry, 55(4), 477-483. https://doi.org/10.1007/s13765-012-2108-3;

Koressaar, T., & Remm, M. 2007. Enhancements and modifications of primer design program Primer3. Bioinformatics (Oxford, England), 23(10), 1289–1291. https://doi.org/10.1093/bioinformatics/btm091;

Kraus, C. N., Maciel, D. A., Bonnet, M. P., & Novo, E. M. L. D. M. 2021. Phytoplankton genera structure revealed from the multispectral vertical diffuse attenuation coefficient. Remote Sensing, 13(20), 4114. https://doi.org/10.3390/rs13204114;

Kuczynska, P., Jemiola-Rzeminska, M., & Strzalka, K. 2015. Photosynthetic Pigments in Diatoms. Marine Drugs, 13(9), 5847–5881. https://doi.org/10.3390/md13095847;

Lavaud, J., Materna, A. C., Sturm, S., Vugrinec, S., & Kroth, P. G. 2012. Silencing of the violaxanthin de-epoxidase gene in the diatom *Phaeodactylum tricornutum* reduces

diatoxanthin synthesis and non-photochemical quenching. PLoS One, 7(5), e36806. https://doi.org/10.1371/journal.pone.0036806;

Lee, Y. J., & Nam, G. W. 2020. Sunscreen boosting effect by solid lipid nanoparticles-loaded fucoxanthin formulation. Cosmetics, 7(1), 14. https://doi.org/10.3390/cosmetics7010014;

Li, C., Pan, Y., Yin, W., Liu, J., & Hu, H. 2024. A key gene, violaxanthin de-epoxidase-like 1, enhances fucoxanthin accumulation in *Phaeodactylum tricornutum*. Biotechnology for Biofuels and Bioproducts, 17(1), 49. https://doi.org/10.1186/s13068-024-02496-3;

Li, F., Murillo, C., & Wurtzel, E. T. 2007. Maize Y9 encodes a product essential for 15-cis-ζ-carotene isomerization. Plant Physiology, 144(2), 1181-1189. https://doi.org/10.1104/pp.107.098996;

Li, F., Rui, X., Amenorfenyo, D. K., Pan, Y., Huang, X., & Li, C. 2023. Effects of temperature, light and salt on the production of fucoxanthin from *Conticribra weissflogii*. Marine Drugs, 21(9), 495. https://doi.org/10.3390/md21090495;

Lohr, M., & Wilhelm, C. 2001. Xanthophyll synthesis in diatoms: quantification of putative intermediates and comparison of pigment conversion kinetics with rate constants derived from a model. Planta, 212(3), 382-391. https://doi.org/10.1007/s004250000403;

Longworth, J., Wu, D., Huete-Ortega, M., Wright, P., & Vaidyanathan, S. 2016. Proteome response of *Phaeodactylum tricornutum*, during lipid accumulation induced by nitrogen depletion. Algal Research, 18, 213-224. https://doi.org/10.1016/j.algal.2016.06.015;

Lu, X., Sun, H., Zhao, W., Cheng, K., Chen, F., & Liu, B. 2018. A hetero-photoautotrophic two-stage cultivation process for production of fucoxanthin by the

marine diatom *Nitzschia laevis*. Marine Drugs, 16(7), 219. https://doi.org/10.3390/md16070219;

Manfellotto, F., Stella, G. R., Falciatore, A., Brunet, C., & Ferrante, M. I. 2020. Engineering the unicellular alga *Phaeodactylum tricornutum* for enhancing carotenoid production. Antioxidants, 9(8), 757. https://doi.org/10.3390/antiox9080757;

Maoka, T. 2020. Carotenoids as natural functional pigments. J Nat Med 74, 1–16. https://doi.org/10.1007/s11418-019-01364-x;

Marella, T. K., & Tiwari, A. 2020. Marine diatom *Thalassiosira weissflogii* based biorefinery for co-production of eicosapentaenoic acid and fucoxanthin. Bioresource Technology, 307, 123245. https://doi.org/10.1016/j.biortech.2020.123245;

Market Reports World Global Fucoxanthin Market. 2023. Available online: https://reports.valuates.com/market-reports/QYRE-Auto-27O9355/global-fucoxanthin;

Matsumoto, M., Nojima, D., Nonoyama, T., Ikeda, K., Maeda, Y., Yoshino, T., … & Tanaka, T. 2017. Outdoor cultivation of marine diatoms for year-round production of biofuels. Marine Drugs, 15(4), 94. https://doi.org/10.3390/md15040094;

McClure, D. D., Luiz, A., Gerber, B., Barton, G. W., & Kavanagh, J. M. 2018. An investigation into the effect of culture conditions on fucoxanthin production using the marine microalgae *Phaeodactylum tricornutum*. Algal Research, 29, 41-48. https://doi.org/10.1016/j.algal.2017.11.015;

Minggat, E., Roseli, W., & Tanaka, Y. 2021. Nutrient absorption and biomass production by the marine diatom *Chaetoceros muelleri*: effects of temperature, salinity, photoperiod, and light intensity. Journal of Ecological Engineering, 22(1), 231-240, https://doi.org/10.12911/22998993/129253;

Miyashita, K., Beppu, F., Hosokawa, M., Liu, X., & Wang, S. 2020. Nutraceutical characteristics of the brown seaweed carotenoid fucoxanthin. Archives of Biochemistry and Biophysics, 686, 108364. https://doi.org/10.1016/j.abb.2020.108364;

Mohamadnia, S., Tavakoli, O., & Faramarzi, M. A. 2022. Optimization of metabolic intermediates to enhance the production of fucoxanthin from *Tisochrysis lutea*. Journal of Applied Phycology, 34(3), 1269-1279. https://doi.org/10.1007/s10811-022-02717-y;

Murison, V., Hérault, J., Schoefs, B., Marchand, J., & Ulmann, L. 2023. Bioinformatics-based screening approach for the identification and characterization of lipolytic enzymes from the marine diatom *Phaeodactylum tricornutum*. Marine Drugs, 21(2), 125. https://doi.org/10.3390/md21020125;

Nomura, M., Kamogawa, H., Susanto, E., Kawagoe, C., Yasui, H., Saga, N., ... & Miyashita, K. 2013. Seasonal variations of total lipids, fatty acid composition, and fucoxanthin contents of *Sargassum horneri* (Turner) and *Cystoseira hakodatensis* (Yendo) from the northern seashore of Japan. Journal of Applied Phycology, 25, 1159-1169. https://doi.org/10.1007/s10811-012-9934-x;

Nur, M., Muizelaar, W., Boelen, P., & Buma, A. 2018. Environmental and nutrient conditions influence fucoxanthin productivity of the marine diatom *Phaeodactylum tricornutum* grown on palm oil mill effluent. Journal of Applied Phycology, 31(1), 111-122. https://doi.org/10.1007/s10811-018-1563-6;

Pajot, A., Hao Huynh, G., Picot, L., Marchal, L., & Nicolau, E. 2022. Fucoxanthin from Algae to Human, an Extraordinary Bioresource: Insights and Advances in up and Downstream Processes. Marine Drugs, 20(4), 222. https://doi.org/10.3390/md20040222;

Pasquet, V., Chérouvrier, J. R., Farhat, F., Thiéry, V., Piot, J. M., Bérard, J. B., ... & Picot, L. 2011. Study on the microalgal pigments extraction process: Performance of microwave assisted extraction. Process Biochemistry, 46(1), 59-67. https://doi.org/10.1016/j.procbio.2010.07.009;

Passy, S. I. 2008. Species size and distribution jointly and differentially determine diatom densities in u.s. streams. Ecology, 89(2), 475-484. https://doi.org/10.1890/07-0405.1;

Premvardhan, L., Bordes, L., Beer, A., Büchel, C., & Robert, B. 2009. Carotenoid structures and environments in trimeric and oligomeric fucoxanthin chlorophyll a/c2 proteins from resonance Raman spectroscopy. The Journal of Physical Chemistry B, 113(37), 12565-12574. https://doi.org/10.1021/jp903029g;

Ritchie, R.J. 2008. Universal chlorophyll equations for estimating chlorophylls *a, b, c*, and *d* and total chlorophylls in natural assemblages of photosynthetic organisms using acetone, methanol, or ethanol solvents. Photosynthetica 46, 115–126. https://doi.org/10.1007/s11099-008-0019-7;

Rochaix, J. D. 2014. Regulation and dynamics of the light-harvesting system. Annual Review of Plant Biology, 65(1), 287-309. https://doi.org/10.1146/annurev-arplant-050213-040226;

Rui, X., Amenorfenyo, D., Peng, K., Li, H., Wang, L., Huang, X., … & Feng, L. 2023. Effects of different nitrogen concentrations on co-production of fucoxanthin and fatty acids in *Conticribra weissflogii.* Marine Drugs, 21(2), 106. https://doi.org/10.3390/md21020106;

Sandmann, G. 2002. Molecular evolution of carotenoid biosynthesis from bacteria to plants. Physiologia Plantarum, 116(4), 431-440. https://doi.org/10.1034/j.1399-3054.2002.1160401.x;

Schmittgen, T. D., & Livak, K. J. 2008. Analyzing real-time PCR data by the comparative CT method. Nature protocols, 3(6), 1101-1108. https://doi.org/10.1038/nprot.2008.73;

Seo, S., Chang, K. S., Choi, M. S., & Jin, E. 2024. Overexpression of PtVDL1 in *Phaeodactylum tricornutum* increases Fucoxanthin content under Red Light. Journal of Microbiology and Biotechnology, 34(1), 198. https://doi.org/10.4014/jmb.2309.09018;

Seth, K., Kumar, A., Rastogi, R. P., Meena, M., & Vinayak, V. 2021. Bioprospecting of fucoxanthin from diatoms—Challenges and perspectives. Algal Research, 60, 102475. https://doi.org/10.1016/j.algal.2021.102475;

Song, X., Wang, K., Wan, L., Li, A., Hu, Q., & Zhang, C. 2013. Production, characterization, and antioxidant activity of fucoxanthin from the marine diatom *Odontella aurita*. Marine Drugs, 11(7), 2667-2681. https://doi.org/10.3390/md11072667;

Sun, P., Wong, C. C., Li, Y., He, Y., Mao, X., Wu, T., ... & Chen, F. 2019. A novel strategy for isolation and purification of fucoxanthinol and fucoxanthin from the diatom *Nitzschia laevis.* Food Chemistry, 277, 566-572. https://doi.org/10.1016/j.foodchem.2018.10.133;

Syed, M., Rafeie, M., Vandamme, D., Asadnia, M., Henderson, R., Taylor, R., … & Warkiani, M. 2018. Selective separation of microalgae cells using inertial microfluidics. Bioresource Technology, 252, 91-99. https://doi.org/10.1016/j.biortech.2017.12.065;

Trentin, R., Moschin, E., Custódio, L., & Moro, I. 2024. Bioprospection of the Antarctic Diatoms *Craspedostauros ineffabilis* IMA082A and *Craspedostauros zucchelli* IMA088A. Marine Drugs, 22(1), 35. https://doi.org/10.3390/md22010035;

Truong, T. Q., Park, Y. J., Winarto, J., Huynh, P. K., Moon, J., Choi, Y. B., ... & Kim, S. M. 2024. Understanding the Impact of Nitrogen Availability: A Limiting Factor for Enhancing Fucoxanthin Productivity in Microalgae Cultivation. Marine Drugs, 22(2), 93. https://doi.org/10.3390/md22020093;

Truong, T.Q., Park, Y.J., Koo, S.Y. 2023. Interdependence of fucoxanthin biosynthesis and fucoxanthin-chlorophyll *a*/*c* binding proteins in *Phaeodactylum tricornutum* under different light intensities. J Appl Phycol 35, 25–42. https://doi.org/10.1007/s10811-022-02856-2;

Untergasser, A., Cutcutache, I., Koressaar, T., Ye, J., Faircloth, B. C., Remm, M., *et al.* 2012. Primer3–new capabilities and interfaces. Nucleic Acids Res. 40, e115– e115. doi: 10.1093/nar/gks596;

Velmurugan, A., & Muthukaliannan, G. K. 2022. Genetic manipulation for carotenoid production in microalgae an overview. Current Research in Biotechnology, 4, 221-228. https://doi.org/10.1016/j.crbiot.2022.03.005;

Wang, H., Zhang, Y., Chen, L., Cheng, W., & Liu, T. 2018. Combined production of fucoxanthin and EPA from two diatom strains *Phaeodactylum tricornutum* and *Cylindrotheca fusiformis* cultures. Bioprocess and Biosystems Engineering, 41, 1061-1071. https://doi.org/10.1007/s00449-018-1935-y;

Wang, J. and Seibert, M. 2017. Prospects for commercial production of diatoms. Biotechnology for Biofuels, 10(1). https://doi.org/10.1186/s13068-017-0699-y;

Wang, L. J., Fan, Y., Parsons, R. L., Hu, G. R., Zhang, P. Y., & Li, F. L. 2018. A rapid method for the determination of fucoxanthin in diatom. Marine Drugs, 16(1), 33 https://doi.org/10.3390/md16010033;

Wang, S., Verma, S., Said, I., Thomsen, L., Ullrich, M., & Kuhnert, N. 2018. Changes in the fucoxanthin production and protein profiles in *Cylindrotheca closterium* in response to blue light-emitting diode light. Microbial Cell Factories, 17(1). https://doi.org/10.1186/s12934-018-0957-0;

Wang, S., Wu, S., Yang, G., Pan, K., Wang, L., & Hu, Z. 2021. A review on the progress, challenges and prospects in commercializing microalgal fucoxanthin. Biotechnology Advances, 53, 107865. https://doi.org/10.1016/j.biotechadv.2021.107865;

Wilhelm, C., Büchel, C., Fisahn, J., Goss, R., Jakob, T., LaRoche, J., ... & Kroth, P. G. 2006. The regulation of carbon and nutrient assimilation in diatoms is significantly

different from green algae. Protist, 157(2), 91-124. https://doi.org/10.1016/j.protis.2006.02.003

Wu, H., Li, T., Wang, G., Dai, S., He, H., & Xiang, W. 2015. A comparative analysis of fatty acid composition and fucoxanthin content in six *Phaeodactylum tricornutum* strains from different origins. Chinese Journal of Oceanology and Limnology, 34(2), 391-398. https://doi.org/10.1007/s00343-015-4325-1;

Wu, Z., Qiu, S., Abbew, A. W., Chen, Z., Liu, Y., Zuo, J., & Ge, S. 2022. Evaluation of nitrogen source, concentration and feeding mode for co-production of fucoxanthin and fatty acids in *Phaeodactylum tricornutum*. Algal Research, 63, 102655. https://doi.org/10.1016/j.algal.2022.102655;

Xia, S., Gao, B., Fu, J., Xiong, J., & Zhang, C. 2018. Production of fucoxanthin, chrysolaminarin, and eicosapentaenoic acid by *Odontella aurita* under different nitrogen supply regimes. Journal of Bioscience and Bioengineering, 126(6), 723-729. https://doi.org/10.1016/j.jbiosc.2018.06.002;

Yang, R. and Dong, W. 2020. Improving fucoxanthin production in mixotrophic culture of marine diatom *Phaeodactylum tricornutum* by led light shift and nitrogen supplementation. Frontiers in Bioengineering and Biotechnology, 8. https://doi.org/10.3389/fbioe.2020.00820**;**

Yi, Z., Magnusdottir, M., Xu, M., Brynjólfsson, S., & Fu, W. 2015. Photo-oxidative stress-driven mutagenesis and adaptive evolution on the marine diatom *Phaeodactylum tricornutum* for enhanced carotenoid accumulation. Marine Drugs, 13(10), 6138-6151. https://doi.org/10.3390/md13106138;

Yi, Z., Su, Y., Cherek, P., Nelson, D., Lin, J., Rolfsson, Ó., … & Fu, W. 2019. Combined artificial high-silicate medium and led illumination promote carotenoid accumulation in the marine diatom *Phaeodactylum tricornutum*. Microbial Cell Factories, 18(1). https://doi.org/10.1186/s12934-019-1263-1;

Zarrinmehr, M. J., Farhadian, O., Heyrati, F. P., Keramat, J., Koutra, E., Kornaros, M., & Daneshvar, E. 2020. Effect of nitrogen concentration on the growth rate and biochemical composition of the microalga, *Isochrysis galbana*. The Egyptian Journal of Aquatic Research, 46(2), 153-158. https://doi.org/10.1016/j.ejar.2019.11.003;

Zhang, J. Y., Ni, W., Zhu, Y., & Pan, Y. 2012. Effects of different nitrogen species on sensitivity and photosynthetic stress of three common freshwater diatoms. Aquatic Ecology, 47(1), 25-35. https://doi.org/10.1007/s10452-012-9422-z;

Zhang, H., Gong, P., Cai, Q., Zhang, C., & Gao, B. 2022. Maximizing fucoxanthin production in *Odontella aurita* by optimizing the ratio of red and blue light-emitting diodes in an auto-controlled internally illuminated photobioreactor. Bioresource Technology, 344, 126260. https://doi.org/10.1016/j.biortech.2021.126260;

Zhou, C., Feng, Y., Li, Z., Shen, L., Li, X., Wang, Y., ... & Wang, W. 2024. Structural and spectroscopic insights into fucoxanthin chlorophyll a/c-binding proteins of diatoms in diverse oligomeric states. Plant Communications. https://doi.org/10.1016/j.xplc.2024.101041

La borsa di dottorato è stata cofinanziata con risorse del
Programma Operativo Nazionale Ricerca e Innovazione 2014-202 (CCI 2014IT16M2OP005)
Fondo Sociale Europeo, Azione I.1 "Dottorati Innovativi con caratterizzazione Industriale"

Chapter III

Improving cryopreservation techniques for diatoms: overcoming the challenges of viability and recovery in marine diatoms species

Abstract

This chapter investigates the applicability and success of cryopreservation techniques for some diatom species and strains, focusing on the potential of the resting spores as an alternative growth stage for the species preservation. Resting spores and resting cells, essential for species resilience and biogeochemical cycles, exhibit diverse physiological and morphological adaptations to stress.

Even today, cryopreservation showed limits in the successful and long-term storage of different diatoms due to their high morphological and genetic variability. In this study, I examined two freezing techniques - *two-step freezing* and *snap-freezing* - as cryopreservation methods on some species/strains of diatoms differing in ecological traits and in different growth stages (vegetative cells vs resting stages). In particular, the preservation of resting stages represents a new and valid strategy reducing the limits of cryopreservation techniques.

To verify the applicability and success of the cryopreservation, post-thaw viability, growth recovery and cryoinjury effects were evaluated.

My results emphasize that the successful cryopreservation methods are species/strain-dependent, and strains belonging to the same genus can have different requirements. Moreover, I experimented for the first time the cryopreservation of the resting stage as spores and their possible application in scientific and/or industrial fields.

La borsa di dottorato è stata cofinanziata con risorse del
Programma Operativo Nazionale Ricerca e Innovazione 2014-202 (CCI 2014IT16M2OP005)
Fondo Sociale Europeo, Azione I.1 "Dottorati Innovativi con caratterizzazione Industriale"

3.1 Introduction

3.1.1 Importance of Diatoms and their long-term preservation

Diatoms, considered one of the most diverse and ecologically important phytoplanktonic groups, contribute around 20% of global primary productivity (Field *et al.*, 1998; Falkowski *et al.*, 1998) and are believed to be of great importance in the functioning of aquatic food webs as in biogeochemical cycles (Falkowski, 2002).

Diatoms are objects of interest across several research fields such as ecology, climate science, aquatic biology, and biotechnology, providing an ongoing source of genetic material and physiological diversity for various applications. Preserving diatom biodiversity is not only vital for maintaining ecosystem balance but also for understanding and mitigating the impacts of climate change.

Research on diatom physiology, genetics, and responses to environmental stressors can inform conservation strategies, reveal adaptation mechanisms, and improve resilience (Falkowski and Oliver, 2007; Bowler *et al.*, 2010; Falciatore *et al.*, 2020; Litchman, E. 2022; Morozov *et al.*, 2024).

As a natural mechanism to survive for long periods and in unfavourable conditions, diatoms present a stage in their life cycle as producing a resting stage (Ellegaard and Ribeiro, 2018). In several species, resting stage has been reported at the end of the bloom period: as nutrients become exhausted, the vegetative cells convert into resting stage, which facilitates rapid sinking and contributes to the vertical export of organic material in marine ecosystems (Romero *et al.*, 2015). This process not only aids in the survival of the species but also plays a significant role in biogeochemical cycles, particularly in carbon export to deeper ocean layers (Romero *et al.*, 2015; Rembauville *et al.*, 2016).

Diatom resting stages can be divided into two different types: resting spores and resting cells. The resting spores exhibit a morphology that is markedly distinct from typical vegetative cells, characterized by highly specialized, dense, and heavily silicified walls (Fig. 1). The thickened silica walls serve as a robust protective barrier, shielding the cell's internal components from physical damage, microbial decay, and various environmental stressors, including fluctuations in pressure and temperature (Hargraves & French, 1983; McQuoid & Hobson, 1996). In contrast, the resting cells are morphologically similar to

the vegetative cells; however, they show physiological and cytoplasmic differences relative to vegetative cells, i.e. a higher lipid content as an internal energy reserve, enabling them to survive prolonged periods of nutrient scarcity (Sicko-Goad *et al.*, 1986; McQuoid & Hobson, 1996).

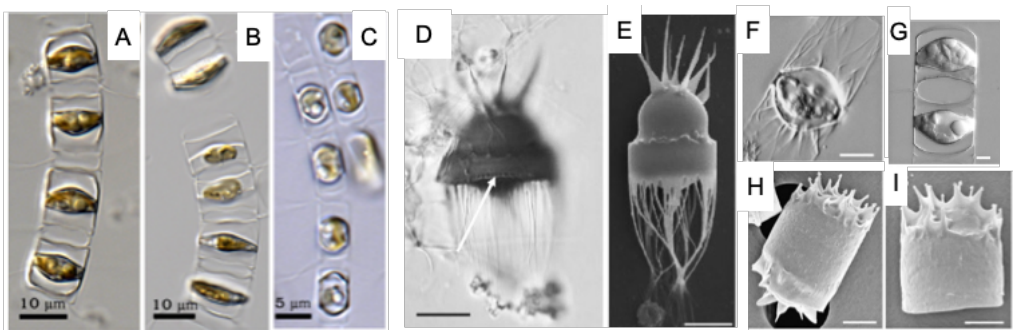

Figure 1. Resting spores of different Chaetoceros spp: Chaetoceros socialis *(A, B, C),* C. lauderi *(D, E, F),* C. curvisetus *(G), and* C. costatus *(H, I). Pictures from Ishii et al. 2011, Chamnansinp et al. 2013.*

In some diatom species, both spores and resting cells store carbohydrates as an additional energy reserve, representing a key adaptation for long-term survival under challenging conditions (French & Hargraves, 1980). Moreover, in this resting stage, diatoms reduce oxidative stress and cellular repair needs, by slowing or stopping their metabolism and conserving essential resources (Oku & Kamatani, 1995; Sugie & Kuma, 2008). The decrease of cellular metabolism is crucial for cells surviving in stress conditions such as in low-light, nutrient-deprived, and oxygen-free conditions, where there is minimal energy production from photosynthesis or respiration. Furthermore, the accumulation of antioxidants and stress-protective proteins helps maintain cellular integrity by reducing oxidative damage while dormant and promoting recovery during favourable conditions (Kuwata *et al.*, 1993).

However, the development of resting spores in diatoms serves not only as a survival strategy but also as a response to environmental signals indicating unfavourable growth conditions.

Studies conducted on wild populations have shown that the formation of spores and resting cells is frequently linked to nutrient depletion, particularly nitrogen, which plays a key role in triggering this transition.

Studies on *Chaetoceros socialis* and *Thalassiosira nordenskioeldii,* have shown that a low nitrogen availability triggers the formation of spores (Oku & Kamatani, 1995; Kuwata & Takahashi, 1999; Pelusi *et al.*, 2019).
Moreover, recent studies highlight that both abiotic and biotic factors can induce spore formation. In the case of the *Chaetoceros* genus, viral infections have been shown to stimulate the transformation of vegetative cells into spores, acting as a defence mechanism to prevent viral propagation (Pelusi *et al.*, 2020).
The stage of spores and/or resting cells have the ability to remain dormant on the ocean sediments reactivating and resuming vegetative growth in response to environmental changes such as nutrient influx, temperature variations, or light exposure (McQuoid & Hobson, 1996; Sugie & Kuma, 2008; Montresor *et al.*, 2013).
The ability of diatom spores and resting cells to persist in sediments for extended periods has profound ecological implications. These stages in the diatom life cycle constitute a "seed bank" in marine sediments, preserving genetic diversity and enhancing the resilience of diatom populations (Sanyal *et al.*, 2021). This seed bank supports ecosystem stability and ensures the continuity of diatom blooms across seasons and in the face of environmental disturbances (Hargraves & French, 1983).

Hence, the diatom's resting stages have great ecological importance as defensive mechanisms enable it to survive in stressful environments and allow it to preserve the species. Also, in the context of a conservation strategy such as Culture Collections technique (that satisfies a multitude of purposes as a service in support of biodiversity and a tool for commercial sustainable species/strain exploitation as well), the conservation of these resting stages would be very useful.
With this object, in this work I was interested in applying for the first time, techniques of long-term preservation, such as cryopreservation, not only to diatom vegetative cells but also to resting stages such as the spores. Therefore, cryopreservation may offer a long-term method for conserving algal cultures and diatom's genetic diversity, and it also allows the conservation of species/strains of biotechnological interest.

3.1.2 Cryopreservation techniques

Traditional approaches to maintaining diatom cultures, such as continuous subculturing and preserving live culture collections, include many risks as genetic drift and contamination, as well as the considerable amount of resources needed for their long-term maintenance (Godhe & Rynearson, 2017; Bulankova *et al.*, 2021).

In contrast to natural environments, where selection pressures promote a wide variety of traits and genotypes, in diatom collections, repeated subculturing, can reduce genetic diversity within the population. Another substantial challenge in maintaining live diatom cultures is the risk of contamination by other microorganisms, such as bacteria, fungi, or other algal species. In some cases, contamination can result in the loss of rare or sensitive diatom strains, thereby reducing the genetic and phenotypic diversity within culture collections (Taylor & Fletcher, 1998). This evidence highlights the need for alternative long-term culture maintenance to preservation methods.

Given these challenges, cryopreservation has emerged as a promising alternative for preserving diatom cultures, offering a way to maintain genetic and phenotypic stability over extended periods (Day, 2007; Hipkin *et al.*, 2014; Day *et al.*, 2017; Stock *et al.*, 2018). Cryopreservation is a technique used to preserve biological material at ultra-low temperatures, typically around -196°C, often in liquid nitrogen and specialized containers. At these temperatures, cellular metabolic processes are completely arrested, suspending all biological activities such as growth, reproduction, and cellular degradation. This method has been successfully applied to preserve various organisms, including animals, plants, microorganisms, and some diatoms (Tsuru, 1973; Day *et al.*, 2005; Rhodes *et al.*, 2006; Matsumura *et al.*, 2013; Stock *et al.*, 2018).

In the case of diatoms, cryopreservation offers an opportunity to store strains that have unique characteristics, whether for ecological research or biotechnological applications such as biofuel production, nanotechnology, and pharmaceuticals.

Despite its significant potential, cryopreservation shows notable challenges: the success varies among diatom species, as it depends on factors such as cell structure, membrane composition, cell size, and freezing tolerance, considering cell vulnerability to physical damage from ice crystal formation during the freezing process (Taylor & Fletcher, 1999).

Several studies identified key parameters as fundamental to the success of cryopreservation techniques. First of all, the addition of cryoprotectants is necessary to prevent the formation of ice crystals. The cryoprotectant agents (CPA), such as dimethyl sulfoxide (DMSO) and glycerol, help to permeate the cells and reduce the freezing point of the solution, thereby preventing ice formation within the cells (McLellan, 1989; Canavate *et al.*, 1995; Zhang *et al.*, 2009; Elliot *et al.*, 2017).

Dimethyl sulfoxide (DMSO) is widely recognized as a potent CPA, minimizing the ice crystal formation during the freezing process, a crucial step for maintaining cell viability post-thaw. Additionally, research indicates that concentrations in the range of 10%-15% of DMSO are optimal for the cryopreservation of diatoms, such as *Skeletonema marinoi*, leading to improved survival rates compared to other CPAs (Day *et al.*, 2017). However, DMSO can induce cellular toxicity, particularly if cells are exposed for prolonged periods and/or at high concentrations (Zhou *et al.*, 2014; Yi *et al.*, 2017). Therefore, optimization of incubation times and concentrations is essential to mitigate these toxic effects while maximizing cryoprotection (Whaley *et al.*, 2021).

Based on these, the equilibration time, indicating the incubation time of cells in cryoprotectants before freezing, is a critical factor influencing diatom cryopreservation.

Lastly, another key parameter to minimize cellular damage during the cryopreservation process is the freezing rate. In this context, different methods are employed but the two currently used protocols are the *two-step freezing* and the direct freezing or *snap-freezing* (Morris, 1978; Bodas *et al.*, 1995; Canavate *et al.*, 1995; Day *et al.*, 1997). The two-step freezing method uses a controlled and gradual cooling process, until - 40 °C before the storage, which can help cells to adapt to the low temperatures, reducing the risk of mechanical damage from ice crystals; in the snap-freezing, the sample is plunged directly in liquid nitrogen, and this it is known to increase the risks of cellular injuries due to intracellular ice formation (Morris, 1978; Canavate *et al.*, 1995; Day *et al.*, 2017).

Nevertheless, these different techniques assess how to cryopreserve microalgae and diatoms, it's known that showed a species-specific response, with some diatoms surviving cryopreservation with near-perfect recovery rates, while others fail to recover completely or show diminished growth post-thaw.

Overall, some studies showed that strains particularly adapted to extreme environments, such as cold water or high-salinity conditions, may have cellular adaptations that confer increased resistance to cryopreservation stress; in contrast, strains from temperate or warm aquatic environments might be more vulnerable to the damage caused by freezing and thawing. For instance, species such as *Opephora guenter-grassii* and *Pinnularia borealis,* like have been reported to exhibit relatively high survival rates after cryopreservation (Souffreau *et al.*, 2013; Hejduková *et al.*, 2017; Stock *et al.*, 2018), while others, such as *Skeletonema marinoi*, show reduced viability (Day *et al.*, 2017). This highlights that individualized protocols may be necessary to achieve optimal preservation outcomes for different strains.

This chapter will explore the challenges of cryopreservation of different species/strains of diatoms, characterized by different sizes, ecological features, and tolerance to various stresses. Despite significant advancements in cryopreservation techniques, challenges remain in improving the post-thaw viability of diatoms. For this reason, I tested two different cryopreservation approaches (*two-step freezing* vs *snap-freezing)* on vegetative cells and spores, after inducing the culture to produce them. The post-thaw viability was evaluated and the resume of the growth was monitored. Moreover, further morphophysiological parameters were detected, with the aim to investigate the mechanisms of cryoinjury and their effect on post-thaw recovery.

La borsa di dottorato è stata cofinanziata con risorse del
Programma Operativo Nazionale Ricerca e Innovazione 2014-202 (CCI 2014IT16M2OP005)
Fondo Sociale Europeo, Azione I.1 "Dottorati Innovativi con caratterizzazione Industriale"

3.2 Material and Methods

3.2.1 Species Studied

The diatom species/strains and the stage used for cryopreservation experiments are reported in Table 1. All the cultures were established from spore germination during incubation of sediments collected at station LTER-MC in the Gulf of Naples (Tyrrhenian Sea, Mediterranean Sea) except for *Chaetoceros socialis ZU1B1* and *Thalassiosira rotula FE80,* isolated from phytoplankton sample collected respectively in the North Sea and LTER-MC station. Genotyping of all strains was performed by sequencing the D1–D3 region of the nuclear-encoded large subunit ribosomal DNA (partial 28S rDNA) as the methodology outlined in Gaonkar *et al.* (2017).

All cultures were maintained in sterile filtered oligotrophic seawater at 36 ppt supplemented with f/2 nutrients (Guillard, 1975), and incubated at a constant temperature of 19 °C under a 12:12 h light: dark cycle, with a photon flux of 100 µmol $m^{2\cdot}$ s^{-1} (Pelusi *et al.*, 2019).

In the case of *C. costatus*, during the standard maintenance protocol, a conspicuous vegetative enlargement (VE) (Kaczmarska *et al.*, 2022) was observed and the large cell size (from 35 to 45 µm) made it unsuitable for cryopreservation, for this reason, I tested only the cryopreservation of spores.

Table 1. Species and strains used for the cryopreservation experiments

Species/strains	Stage used for cryopreservation
Chaetoceros socialis APC12	Vegetative cells and spores
Chaetoceros socialis ZU1B1	Vegetative cells and spores
Chaetoceros costatus	Spores

Chaetoceros lauderi	Spores
Chaetoceros didymus	Vegetative cells
Thalassiosira rotula FE80	Vegetative cells

3.2.2 Induction of Spore Formation

To induce spore formation, a modified f/2 medium, precisely a nitrogen-depleted medium (N-depleted), with a low nitrate concentration (23 µM) but with a high silicon concentration (300 µM) to prevent silicon limitation, were experimented (Pelusi *et al.*, 2020). I used, together with the N-depleted medium, a low cell density inocula (500 cells/ml). Each species was inoculated into culture flasks containing 150 ml of culture medium and the growth was monitored over 8 days for *C. socialis* and up to 35 days for the other species. Every two days, culture subsamples were fixed in Lugol's iodine solution. Cell density was obtained by counting the cells in 1 ml of samples using the Sedgewick Rafter chamber under a Leica DMi microscope (Leica, Milan, Italy) at 100x magnification.

3.2.3 Cryopreservation methodology

Cryopreservation experiments were conducted within the facilities of the BCCM/DCG diatom culture collection at Ghent University. A solution of 10% dimethyl sulfoxide (DMSO) (Sigma-Aldrich) was used as the cryoprotective agent (CPA) according to Stock *et al.* (2018).

At this CPA concentration, I selected three equilibration times (ET) precisely 15 min, 30 min, and 45 min respectively.

The chloroplast integrity was chosen as a marker of cell viability (Anchordoguy *et al.*, 1992) and I evaluated the DMSO toxicity by monitoring chloroplast integrity every 15 minutes for 2 hours, by an inverted light microscopy Zeiss Axiovert 40 C (Göttingen, Germany).

For the cryopreservation technique, the cultures in the late exponential growth phase (Late exp) were initially placed in darkness overnight; for all the species I selected the same cell density of $5*10^4$ cell/ml. Subsequently, cell suspensions were treated with 10% (v/v) DMSO as a cryoprotective agent (CPA) and divided into three cryovials (3 ml) for each ETs, resulting in three technical replicates per treatment. Two different cryopreservation methods were assessed: i) a "two-step freezing" (T-F), involving initial storage at −80 °C for 2 hours followed by transfer to liquid nitrogen; ii) a "snap freezing" (S-F), a procedure that bypassed the initial −80 °C storage step.
All procedures were conducted under subdued light conditions (± 2 μmol $m^{-2}\cdot s^{-1}$). After 15 days in cryostorage, the samples were reactivated as follows.

Thawing and reinoculation

For the two different freezing protocols (T-F vs S-F), the same thawing procedure was employed as follows. Cryovials containing the frozen cell samples were removed from cryotanks and placed in a 37 °C water bath until all ice crystals had dissolved (approximately 2 minutes); then, equal aliquots of thawed cultures were added to 50 ml of fresh growth medium in culture flasks without CPA. To acclimatize the cells to standard culture conditions, flasks were incubated in darkness for 24 hours, followed by incubation under low-intensity light at 19°C for 7 days. Then, the cultures were transferred to standard growth conditions (at 19°C under a 12:12 h light: dark cycle, with a photon flux of 100 μmol $m^{-2}\cdot s^{-1}$) and the samples were analyzed for post-thaw viability assessment and growth monitoring.

3.2.4 Post-thaw assessments: Recovery – Viability – Re-growth

Post-thaw assessment was monitored for 35 days. Subsamples were fixed every 7 days in 1% glutaraldehyde (v/v%), Sigma-Aldrich, Saint-Louis, Missouri, USA). Preliminarily, cell morphology and bacterial growth as potential contaminants were evaluated.

The microscopic observation of cultures was performed by a Zeiss Axiovert 40 C inverted light microscope (Göttingen, Germany).

Meanwhile, after staining with SYBR Green I (1X) (Thermo Fisher Scientific) to bind DNA, the subsamples were analysed by Imaging Flow Cytometry (Amnis ® ImagestreamX Mark II, iFCM) (Luminex Corporation, Austin, Texas, USA) and the images, at a 40×magnification (0.5 µm/pixel), were acquired in channel 01 (brightfield, LED; collecting filter 457/45 nm), channel 02 (SYBR Green I (1X) signal of DNA, 494 nm laser; collecting filter 480/560 nm), channel 09 (brightfield, LED; collecting filter 582/25 nm), and channel 11 (autofluorescence of pigments, 642 nm; collecting filter 702/85 nm). The images for at least 10,000 events, gated for an intensity of min. 2500, max. 10,000,000 in channel 02 and an intensity in channel 11 of min. 1500 and max. 10,000,000, were acquired using the INSPIRE software (Luminex Corporation, Austin, Texas, USA) (Fig. 2). Next, the obtained Raw Image Files (*.rif files) were analysed using IDEAS software version 6.2.187.0 (Luminex Corporation, Austin, TX, USA).

Following the time point, the data of iFCM has been correlated to autofluorescence of chlorophyll and the DNA staining and, showing a different distribution of the cells in the plot (Adler *et al.*, 2007; Hildebrand *et al.*, 2016).

La borsa di dottorato è stata cofinanziata con risorse del
Programma Operativo Nazionale Ricerca e Innovazione 2014-202 (CCI 2014IT16M2OP005)
Fondo Sociale Europeo, Azione I.1 "Dottorati Innovativi con caratterizzazione Industriale"

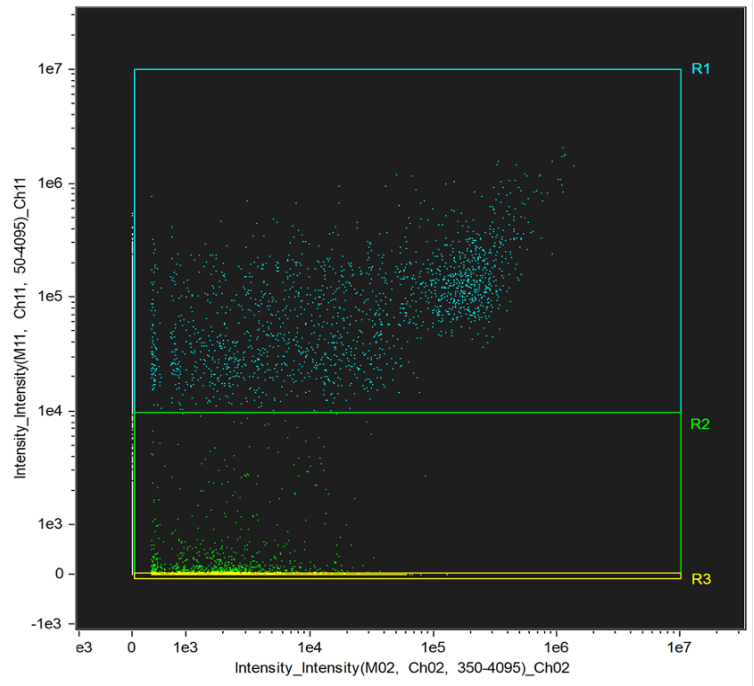

Figure 2. The distribution of plotted cells, correlating the intensity of Channel 02 (SYBR Green I staining) and Channel 11 (autofluorescence of pigments) using the Imaging Flow Cytometry.

In order to compare the two different cryopreservation methods and/or the three different ETs, the following post-thaw parameters were analysed.

Cell recovery (%), calculated at 7 days after thawing, as the ratio of healthy cells (R1) to the number of cells before cryopreservation (Garrido-Cardenas *et al.*, 2019; Murray and Gibson, 2020).

$$\text{Recovery}\,(\%) = (\text{cells}_{\text{healthy}} * \text{cells}_{\text{before cryopreservation}}) \times 100$$

Cell viability (%), calculated as the ratio of healthy cells to the number of cells inactive/dying in the earlier growth phase. In my work, I used to count the dot-plot on R1 (active/healthy cells) out of the total number of cells (R1+R2) and express the results as a percentage.

$$\text{Cell viability}\,(\%) = \text{cells}_{(R1)} * \text{cells}_{(R1+R2)} \times 100$$

The re-growth curves were assessed until 35 days and the growth rate (μ) was calculated until the exponential phase, as followed reported:

$$\mu = (\ln N1) - \ln (N0) / (t1 - t0)$$

in which N1 and N0 were the cell density (cells/ml) at time t0 and t1, respectively (day). The maximum growth rate (μmax) was calculated from t0 as the beginning of the exponential phase to the end of the exponential phase (t1) when ln(N) versus time was linear.

Finally, the recovery time (RT) was taken as the time required by the culture to reach half of the exponential growth phase and the maximum growth rate (μ_{max}) (Stock *et al.*, 2018).

3.2.5 Morphophysiological analyses after post-cryopreservation

Morphophysiological analyses, before and after post-cryopreservation, were performed based on the iFCM data. The organization of cells in solitary form and/or colonies was identified by analysing the active cells plotted in the R1 region by iFCM; in addition, also the size of cells and/or colonies was detected.

Moreover, the correlation of channel 11 (autofluorescence of pigments) with the cell surface of active cells were used to measure the relative Chlorophyll content intensity and expressed as Chl/area ratio.

3.2.6 Statistical Analysis

All experiments were conducted in triplicate. All data are expressed as mean ± standard error of biological replicates. Statistical analyses, including one-way and two-way analysis of variance (ANOVA), followed by Tukey's test, and the heatmaps were performed using the statistical software GraphPad PRISM 9 (GraphPad Software Inc., San Diego, CA, USA). Statistical significance differences were considered at $p < 0.05$ or $p < 0.01$.

La borsa di dottorato è stata cofinanziata con risorse del
Programma Operativo Nazionale Ricerca e Innovazione 2014-202 (CCI 2014IT16M2OP005)
Fondo Sociale Europeo, Azione I.1 "Dottorati Innovativi con caratterizzazione Industriale"

3.3 Results

3.3.1 Induction of spore formation

Cultures of *Chaetoceros socialis*, *C. costatus,* and *C. lauderi,* growing until the exponential phase, were inoculated in a nitrogen-depletion medium (N-depletion) and an induction of spore formation was seen (Fig. 3).

C. socialis showed a fast spore formation both in Ctrl as N-depleted medium, although the highest percentage of spores (97%) was obtained in the N-depletion medium after 8 days of growth curve (Fig. 3 A).

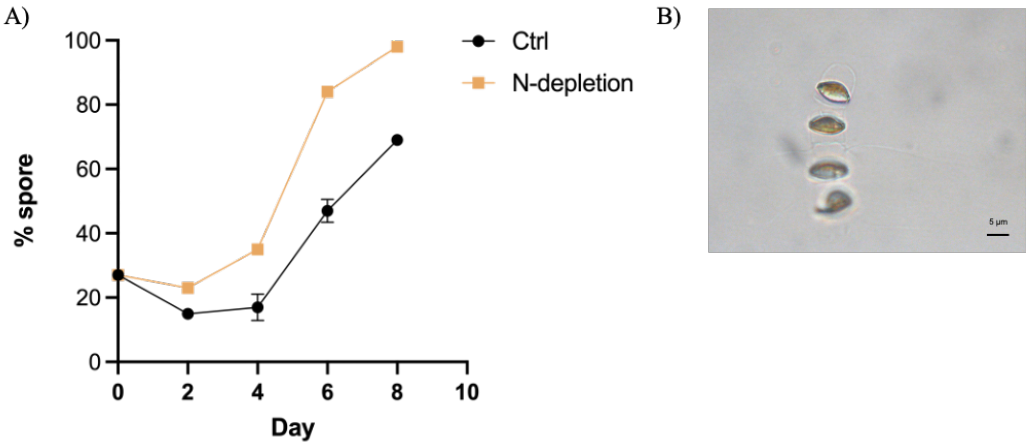

Figure 3. Dynamic of spore formation in Chaetoceros socialis *in control condition (Ctrl) and in nitrogen-depleted medium (N-depletion) (A). Data shown as mean ± SD. Pictures of spores of C. socialis in colonial form taken in light microscopy (B).* Scale b*ar 5 µm.*

On the other side, in *C. costatus* and *C. lauderi,* I observed a delay in the formation of the spores that started after 20 days of growth in the N-depletion medium and reached the highest spore percentage at 35 days, with values of 97% and 98%, respectively (Fig. 4 A, C).

La borsa di dottorato è stata cofinanziata con risorse del
Programma Operativo Nazionale Ricerca e Innovazione 2014-202 (CCI 2014IT16M2OP005)
Fondo Sociale Europeo, Azione I.1 "Dottorati Innovativi con caratterizzazione Industriale"

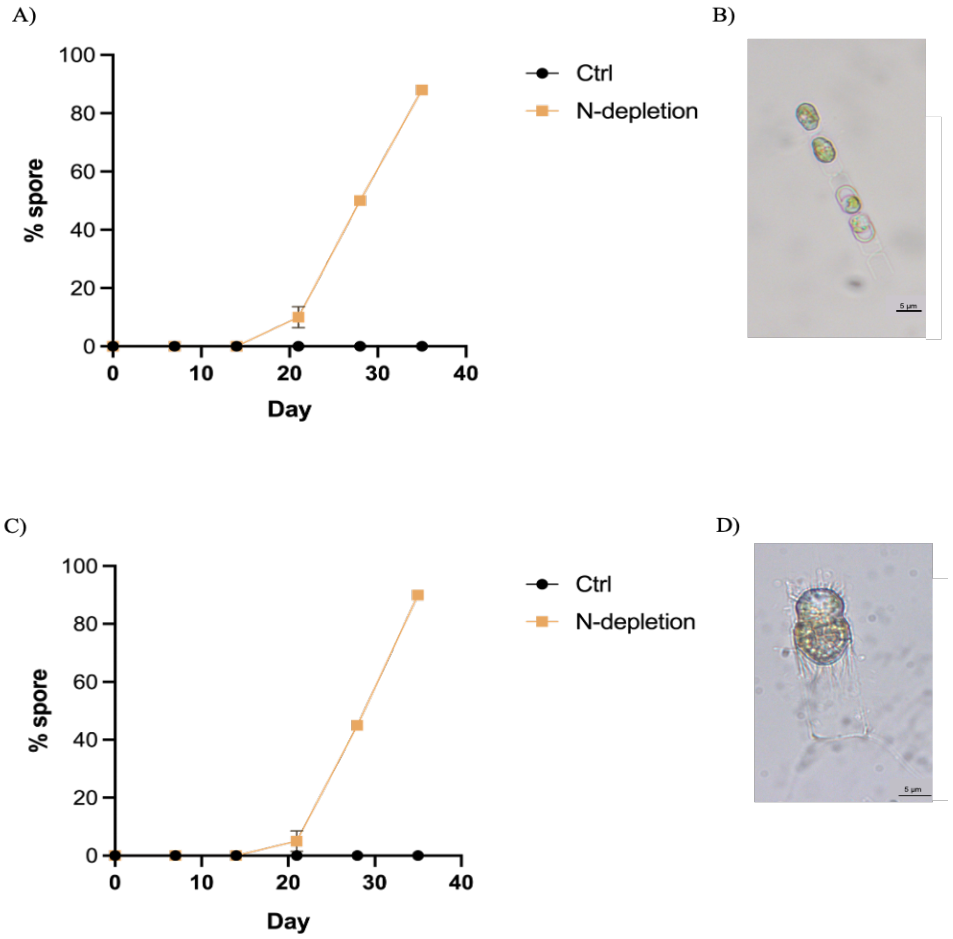

Figure 4. Dynamics of spore formation in Chaetoceros costatus *(A) and* Chaetoceros lauderi *(C) in control condition (Ctrl) and in nitrogen-depleted medium (N-depletion) (A). Data shown as mean ± SD. Pictures of spores of C. costatus (B) and C. lauderi (D) taken in the light microscopy. Scale bar 5 µm.*

The N-depletion condition was also tested to induce spore formation in *C. didymus* and resting cells in *T. rotula*. These culture conditions did not induce the resting stage for both these species so, for successive cryopreservation experiments, only the vegetative cells were used.

3.3.2 Post-thaw Assessments: Recovery, Viability and Re-growth

The cryopreservation processes and thawing were described in section 3.2.3. Briefly, the DMSO was selected as a cryoprotective agent (CPA) and three equilibration times (ET) were tested (15, 30', and 45' respectively); to cryopreserve spores and/or vegetative cells two methods were tested: two-step freezing (T-F) and snap-freezing (S-F).

La borsa di dottorato è stata cofinanziata con risorse del
Programma Operativo Nazionale Ricerca e Innovazione 2014-202 (CCI 2014IT16M2OP005)
Fondo Sociale Europeo, Azione I.1 "Dottorati Innovativi con caratterizzazione Industriale"

To evaluate the status of cultures after thawing, the subsamples were analysed by Imaging Flow Cytometry, dividing the cells into different regions: in region R1 the active/healthy cells were plotted (Fig. 5 A), in R2 the inactive/dying cells (Fig. 5 B) and lastly in the region R3, bacteria were plotted (Fig. 5 C).

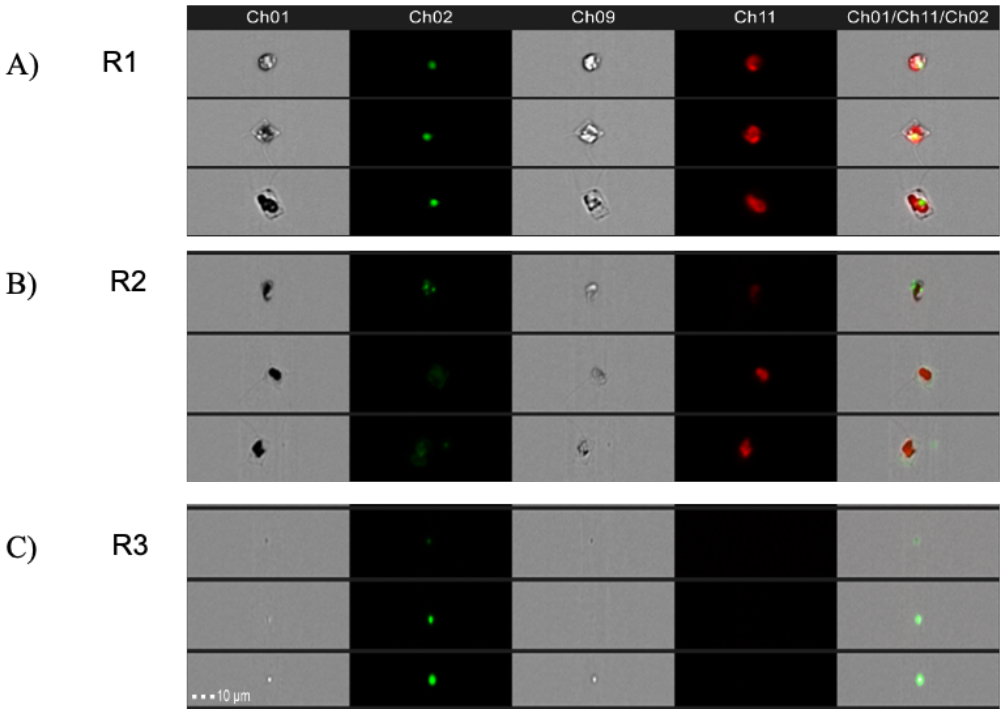

Figure 5. Pictures show cells detected in the different channels and plotted in different regions: Channell 01, brightfield; Channel 02, SYBR Green I staining; Channel 09, brightfield; Channel 11, autofluorescence of pigments, and images of merged channels. R1, active/healthy cells (A); R2, inactive/ dormant cells (B); R3, bacteria (C). Scale bar 10 µm.

Globally, the results of post-thaw assessments, summarized in Tab 2, showed a clear success in cryogenic storage for *C. socialis* and *C. costatus* (Tab. 2). In particular, for *C. socialis,* both the strain *APC12* and *ZU1B1* showed a good performance in most cryopreservation conditions used, in which the spores showed the best success (Tab. 2). In addition, good results were observed also for the spore of *C. costatus* but when cryopreserved at ET 45' and using the snap-freezing method (S-F) (Tab. 2). For the other species tested in this work, the cryopreservation techniques showed variable results.

La borsa di dottorato è stata cofinanziata con risorse del
Programma Operativo Nazionale Ricerca e Innovazione 2014-202 (CCI 2014IT16M2OP005)
Fondo Sociale Europeo, Azione I.1 "Dottorati Innovativi con caratterizzazione Industriale"

Table 2. Experimental results of diatom species/strains cryopreserved. Post-thaw assessment: "+" indicates moderate success; "++" indicates high success; "-" indicates unsuccess; Freezing techniques: T-F: two-step; S-F: snap-freezing; "" indicates bacteria growth.*

Species/Strain	Stage	Equilibration Times (ETs)	Post-thaw assessments
C. socialis APC12	Vegetative	15 min	+ (S-F)
		30 min	+ (S-F)
		45 min	-
	Spore	15 min	++ (S-F)
		30 min	++ (S-F)
		45 min	++ (S-F)
C. socialis ZU1B1	Vegetative	15 min	+ (S-F)
		30 min	-
		45 min	-
	Spore	15 min	+ (S-F)
		30 min	-
		45 min	-
C. costatus	Spore	15 min	-
		30 min	-
		45 min	++ (S-F)
C. lauderi	Spore	15 min	-*
		30 min	-*
		45 min	-*
C. didymus	Vegetative	15 min	-
		30 min	-
		45 min	-
T. rotula	Vegetative	15 min	-
		30 min	-
		45 min	-

La borsa di dottorato è stata cofinanziata con risorse del
Programma Operativo Nazionale Ricerca e Innovazione 2014-202 (CCI 2014IT16M2OP005)
Fondo Sociale Europeo, Azione I.1 "Dottorati Innovativi con caratterizzazione Industriale"

Recovery

To investigate the effects of cryopreservation and the ability of cells to survive, the recovery percentage (ratio of healthy cells after thawing to the number of cells before cryopreservation) at the different equilibration times (ETs) and cryopreservation methods (T-F vs S-F) were calculated at 7 days post thawing for the different species/strains (Tab. 3 - 5). For *C. socialis APC12*, only the cryopreservation through the snap-freezing method (S-F) showed good results, both for spores as vegetative cells (Tab. 3). The best recovery value was seen for the spores cryopreserved by the S-F method with an ET 45', showing a recovery of 47% (Tab. 3), whereas the vegetative cells showed low recovery with the highest value through the S-F method too, but at ET 30' (9%) (Tab.3).

Table 3. Recovery percentage of Chaetoceros socialis APC12 *at 7 days post-thawing. ET, equilibration time (minutes); T-F, two-step freezing; S-F, snap-freezing.*

	Vegetative cells		Spores	
ET	T-F	S-F	T-F	S-F
15'	0%	3%	0%	17%
30'	0%	9%	0%	29%
45'	0%	2%	0%	47%

C. socialis ZU1B1 showed a different response to the cryopreservation process. As shown in Tab. 3, the recovery values were very low, with a maximum of 2% for the spores using the S-F protocols at ET 30' (Tab.4).

Table 4. Recovery percentage of Chaetoceros socialis ZU1B1 *at 7 days post-thawing. ET, equilibration time (minutes); T-F, two-step freezing; S-F, snap-freezing.*

	Vegetative cells		Spores	
ET	T-F	S-F	T-F	S-F
15'	0%	1%	1%	1%
30'	0%	0%	0%	2%
45'	0%	0%	0%	1%

Otherwise, after cryopreservation, *C. costatus* spores showed a recovery of 31% in the S-F method at ET 45' (Tab. 5).

Table 5. The recovery percentage of Chaetoceros costatus *at 7 days post-thawing. ET, equilibration time (minutes); T-F, two-step freezing; S-F, snap-freezing.*

	Spores	
ET	T-F	S-F
15'	0%	0%
30'	0%	0%
45'	0%	31%

The spores of *C. lauderi* after thawing showed no recovery. The monitoring for the successive three weeks revealed an overgrowth of bacteria which covered and killed all spores, causing a colour change of the culture from transparent to purple colour (Fig. 6). The presence of bacteria was confirmed by their autofluorescence (Fig. 6 B).

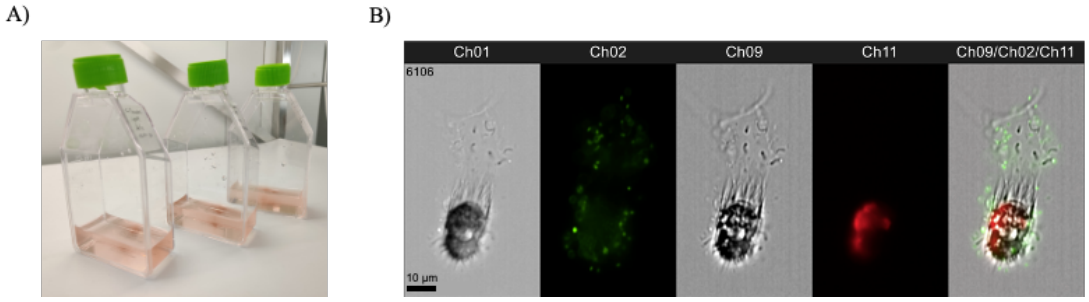

Figure 6. Chaetoceros lauderi *spore culture at 7 days post-thawing* (A). *Picture of spores and cyanobacteria analysed under Imaging Flow Cytometry: Channell 01, brightfield; Channel 02, SYBR Green I staining; Channel 09, brightfield; Channel 11, autofluorescence of pigments* (*B). Scale bar 10 µm.*

Finally, the vegetative cells of both *C. didymus* as well as *T. rotula* exhibit no recovery after thawing.

La borsa di dottorato è stata cofinanziata con risorse del
Programma Operativo Nazionale Ricerca e Innovazione 2014-202 (CCI 2014IT16M2OP005)
Fondo Sociale Europeo, Azione I.1 "Dottorati Innovativi con caratterizzazione Industriale"

Viability

Cell viability (%) was calculated as the ratio of active cells to the number of cells inactive/dormant in the earlier growth phase, by using Imaging Flow Cytometry (see Mat & Met section). I calculated the viability at 7 days (T1) and 14 days (T2) after post-thawing.

The viability of *C. socialis APC12* was globally low at T1 with the highest value (5%) for the spores in S-F related to the ETs of 30' and 45'; whereas at T2 a clear increase, for the spores, was noted (Tab 6). In particular, the spores cryopreserved through the S-F method exhibited the highest percentage of viability in all ETs, reaching a viability of 96 % both in ET 30' and 45'.

On the other hand, a rise of viability was observed also in vegetative cells in S-F condition at ET of 15' and 30' (from 15% to 20%), while, for the same vegetative cryopreserved cells, low values in the T-F method were reported (Tab. 6).

Table 6. Viability percentage of Chaetoceros socialis APC12 *vegetative cells and spores at T1 (7 days post-thawing) and T2 (14 days post-thawing). ET, equilibration time (minutes); T-F, two-step freezing; S-F, snap freezing.*

	T1				T2			
	Vegetative cells		Spore		Vegetative cells		Spore	
ET	T-F	S-F	T-F	S-F	T-F	S-F	T-F	S-F
15'	0%	0%	0%	5%	0%	15%	27%	90%
30'	0%	2%	0%	0%	3%	20%	33%	96%
45'	4%	0%	2%	5%	4%	2%	35%	96%

Concerning *C. socialis ZU1B1*, at 7 days after thawing, the vegetative cells showed very low viability only at ET 15' using S-F method, whereas the spores showed a little better value in S-F methods (range from 1% to 5 %) (Tab. 7).
At T2, the viability values remained globally constant with a slight increase in the vegetative cells in S-F method at ET 15', while the values were low (Tab. 7).

Table 7. Viability percentage of Chaetoceros socialis ZU1B1 *vegetative cells and spores at T1 (7 days post-thawing) and T2 (14 days post-thawing). ET, equilibration time (minutes); T-F, two-step freezing; S-F, snap-freezing.*

	T1				T2			
	Vegetative cells		Spore		Vegetative cells		Spore	
ET	T-F	S-F	T-F	S-F	T-F	S-F	T-F	S-F
15'	0%	1%	1%	3%	0%	3%	1%	1%
30'	0%	0%	0%	5%	0%	1%	0%	2%
45'	0%	0%	0%	1%	0%	0%	0%	1%

Lastly, *C. costatus* spore showed viable cells only at ET 30' using the S-F method at T1 (Tab. 8); however, at T2, the same cultures showed a decrease of viability in ET 30' and a significant rise in ET 45' (Tab. 8).

Table 8. Viability percentage of Chaetoceros costatus *spores at T1 (7 days post-thawing) and T2 (14 days post-thawing). ET, equilibration time (minutes); T-F, two-step freezing; S-F, snap freezing.*

	T1		T2	
ET	T-F	S-F	T-F	S-F
15'	0%	0%	0%	0%
30'	0%	6%	0%	1%
45'	0%	0%	0%	66%

La borsa di dottorato è stata cofinanziata con risorse del
Programma Operativo Nazionale Ricerca e Innovazione 2014-202 (CCI 2014IT16M2OP005)
Fondo Sociale Europeo, Azione I.1 "Dottorati Innovativi con caratterizzazione Industriale"

Re-growth

The viable cells (both vegetative cells and that derived from germination of spores) were grown (re-growth) and monitored until 35 days. The growth curves and the maximum growth rate (μ_{max}) were reported in Fig. 7 - 9.

The re-growth of vegetative cells of *C. socialis APC12* cryopreserved using the T-F method, showed no growth (Fig. 7 A); on the other hand, the vegetative cells cryopreserved using the S-F method, exhibited a clear resume growth after 21 days for all ETs used (Fig. 7 B). The highest cell density was obtained at ET 30', reaching a peak at 35 days with the highest μ_{max} (10.5 ± 0.4) followed by ET 15' (Fig. 7 B).

The cryopreserved spores of the same strain showed a different trend.

Applying the T-F technique, a good growth rate was seen in all ETs, although the cell density was low, with the peak at 14 days for ET 15' as 45', and at 21 days for ET 30' (Fig. 7 C). Instead, in the S-F method a quick recovery was detected in all ETs when the exponential phase started from 7 days (Fig. 7 D). In particular ETs 15' and 30' exhibited comparable patterns of growth with a long exponential phase, from 7 to 21 days, but ET 15' reached the highest cell density ($1.8 \times 10^6 \pm 0.5$ cell/ml), while in ET 30' the cells density was $1.2 \times 10^6 \pm 0.5$ cell/ml and with the highest μ_{max} (13.2 ± 0.5) (Fig. 7 D). On the other hand, ET 45' reached the pick of exponential phase after 18 days with a cell density of $8.5 \times 10^5 \pm 0.4$ cell/ml and a maximum growth rate of 12.2 ± 0.5 (Fig. 7 D).

La borsa di dottorato è stata cofinanziata con risorse del
Programma Operativo Nazionale Ricerca e Innovazione 2014-202 (CCI 2014IT16M2OP005)
Fondo Sociale Europeo, Azione I.1 "Dottorati Innovativi con caratterizzazione Industriale"

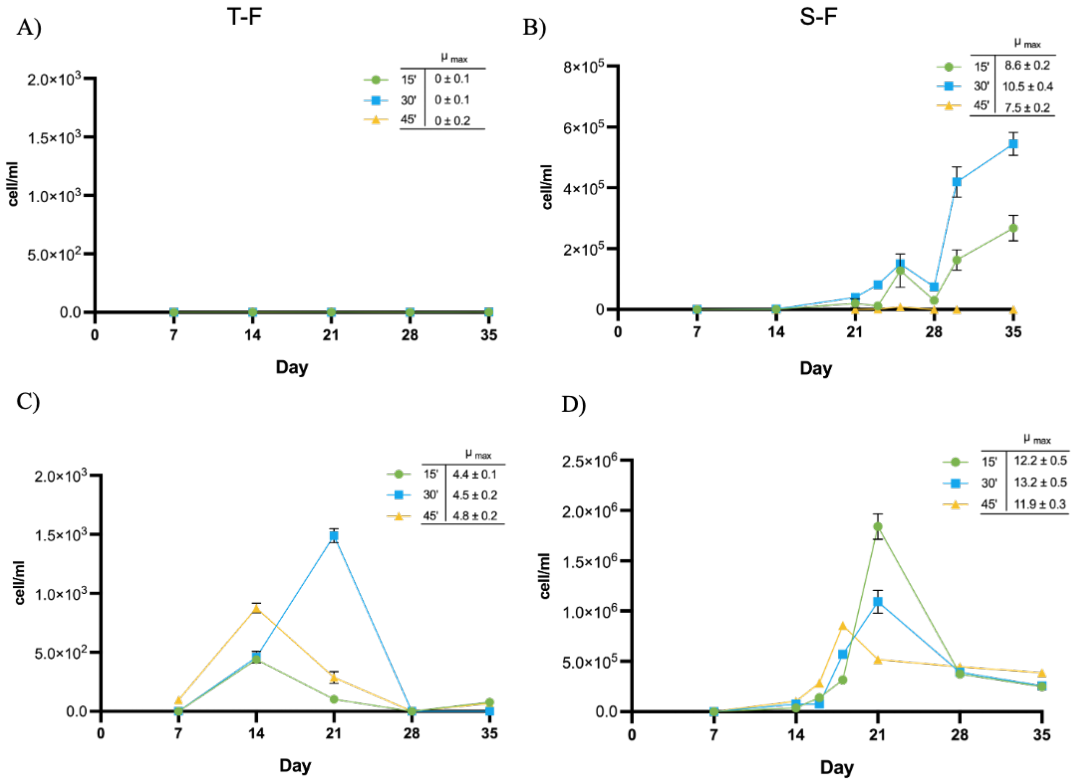

Figure 7. Growth curve of vegetative cells (A, B) and spores (C, D) of Chaetoceros socialis APC12 *cryopreserved through two-step method (A, C) and snap-freezing method (B, D); different symbols indicate different equilibration time (ET minutes); Data shown as mean ± SD and the maximum growth rate was reported in the graph.*

Concerning the cryopreserved vegetative cells of *C. socialis ZU1B1*, in line with the recovery and viability data, they showed very low growth after both T-F and S-F methods (Fig. 8 A, B).

A similar trend was noted also in the culture of *ZU1B1* spores where a very low growth was reported in the cultures cryopreserved through the T-F method (Fig. 8 C). Despite this, a good result was obtained using the S-F approach. As shown in Fig. 8 D, despite the low cell density in all ETs, the growth curve showed the peak of the exponential phase at 14 days for ET 30', while ET 15' showed a long lag phase and the peak of the exponential phase at 21 days (Fig. 8 D).

La borsa di dottorato è stata cofinanziata con risorse del
Programma Operativo Nazionale Ricerca e Innovazione 2014-202 (CCI 2014IT16M2OP005)
Fondo Sociale Europeo, Azione I.1 "Dottorati Innovativi con caratterizzazione Industriale"

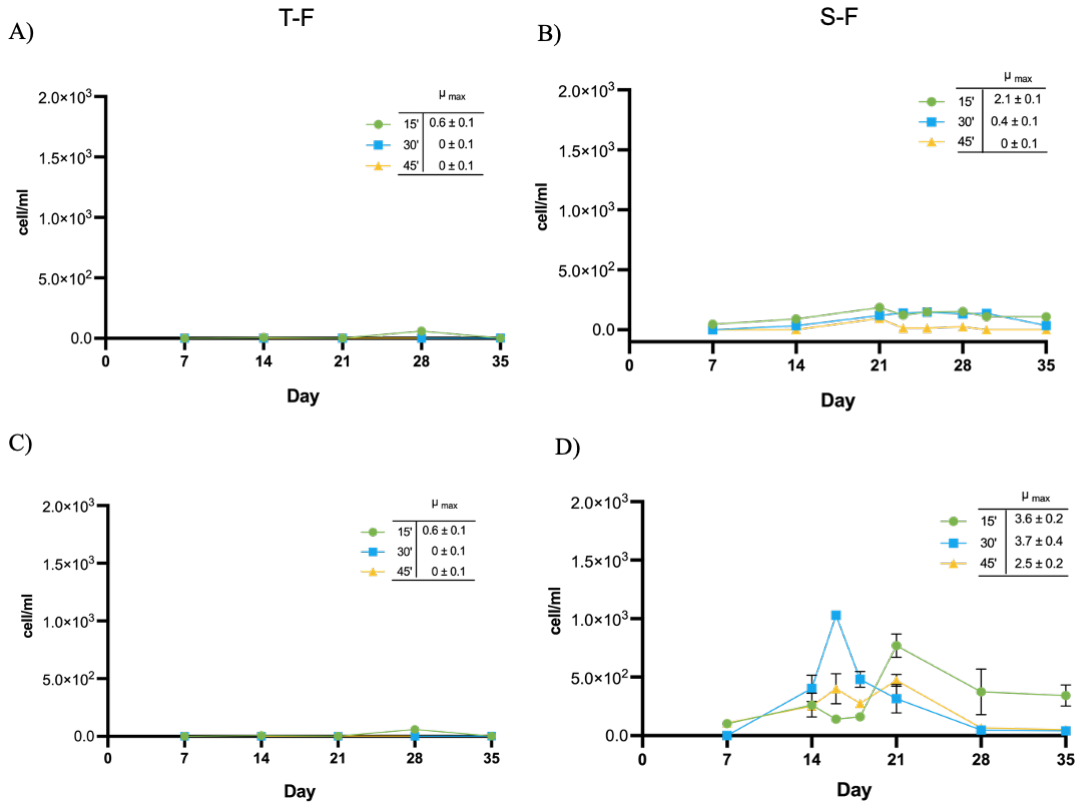

Figure 8. Growth curve of vegetative cells (A, B) and spores (C, D) of Chaetoceros socialis ZU1B1 *cryopreserved through two-step and snap-freezing method. Different symbols indicate different equilibration times (ET, minutes). Data shown as mean ± SD and the maximum growth rate was reported in the graph.*

Lastly, for the cryopreserved *C. costatus* spores, using the T-F method, they didn't exhibit a regrowth after the thawing in all conditions (Fig. 9 A); the best result was obtained after the S-F method at ET 45' when the growth curve showed an exponential phase starting from 14 days with a first peak at 21 days (Fig. 9 B). Then, there was a decrease in cellular vitality with a minimum of density at 28 days, after that a renewed growth appeared, reaching a cell density of 9 x 10^5 ± 0.3 cell/ml (Fig. 9 B).

La borsa di dottorato è stata cofinanziata con risorse del
Programma Operativo Nazionale Ricerca e Innovazione 2014-202 (CCI 2014IT16M2OP005)
Fondo Sociale Europeo, Azione I.1 "Dottorati Innovativi con caratterizzazione Industriale"

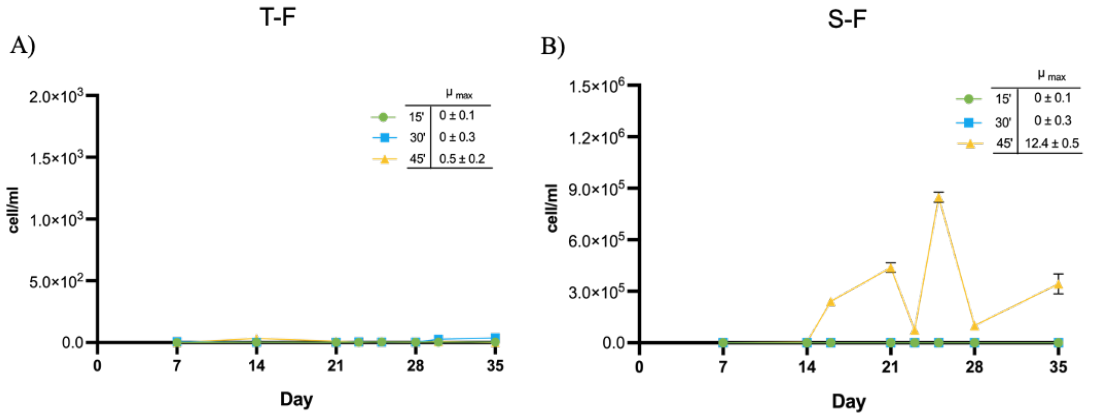

Figure 9. The growth curve of cells germinated from Chaetoceros costatus *spores cryopreserved through two-step (A) and snap-freezing method (B). Different symbols indicate different equilibration times (ET, minutes). Data shown as mean ± SD and the maximum growth rate was reported in the graph.*

Finally, considering the differences in the recovery and re-growth of cultures, I compared the recovery time (RT) calculated as the time needed to reach the mid-exponential phase (Fig. 10). As shown in Fig. 10, spores need less time to recover compared with the vegetative cells in both strains of *C. socialis*, while, as seen also in the growth curve, *C. costatus* showed a recovery only at ET 45' using S-F method.

La borsa di dottorato è stata cofinanziata con risorse del
Programma Operativo Nazionale Ricerca e Innovazione 2014-202 (CCI 2014IT16M2OP005)
Fondo Sociale Europeo, Azione I.1 "Dottorati Innovativi con caratterizzazione Industriale"

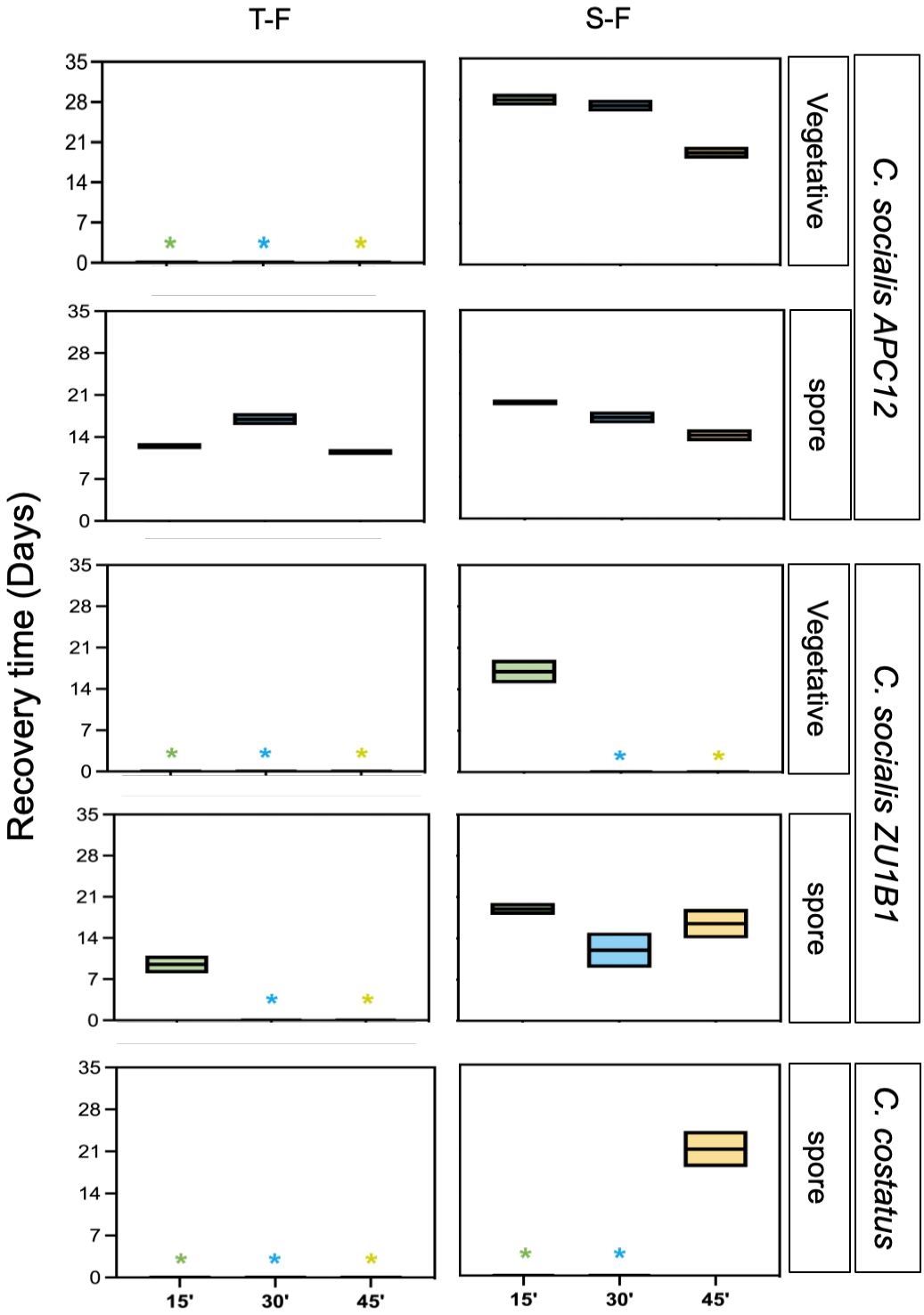

Figure 10. Recovery time of the diatoms cryopreserved through two-step and snap-freezing methods. Boxplots showing the time until the culture reaches mid exponential phase after cryopreservation for the different species. The different colours indicate different equilibration times (minutes). Cultures not recovered are indicated with an asterisk.

3.3.3 Post-cryopreservation culture viability and morphophysiological changes

To evaluate in detail the post-cryopreservation viability and the morphophysiological changes of the cultures after post-thawing due to the freezing events, I assessed, by Imaging Flow Cytometry (iFCM), the following parameters:
i) Percentage of active (healthy) cells vs inactive (not healthy) cells and/or dormant cells;
ii) Morphological organization of active cells (single cells vs colonies) and their size;
iii) Basal fluorescence intensity of chlorophyll.
All the parameters were detected before cryopreservation (b. c) and after cryopreservation (a. c) at 7 days (T1), 14 days (T2), and until the peak of exponential phase (T3).
For each species/strain culture, the results are below reported.

Active cells vs cell inactive and/or dormant cells in cultures of Chaetoceros socialis APC12 deriving from cryopreserved vegetative cells vs cryopreserved spores

The cultures deriving from cryopreserved vegetative cells *C. socialis APC12* showed the highest percentage of active cells (80%) at T3 and ET 15' using the T-F method (Fig. 11 A), while in the S-F method, a gradual rise of active cells was observed from T1 to T3 (Fig. 11 A). At ET 30' a very low percentage of active cells was observed after the T-F method, while in S-F the active cells rose from T2 to T3, reaching 95% (Fig. 11 B). On the other hand, at ET 45' in the T-F method, the total cells were inactive and/or dormant, and only in the S-F method some active cells were detected at T3 (30 %) (Fig. 11 C).

La borsa di dottorato è stata cofinanziata con risorse del
Programma Operativo Nazionale Ricerca e Innovazione 2014-202 (CCI 2014IT16M2OP005)
Fondo Sociale Europeo, Azione I.1 "Dottorati Innovativi con caratterizzazione Industriale"

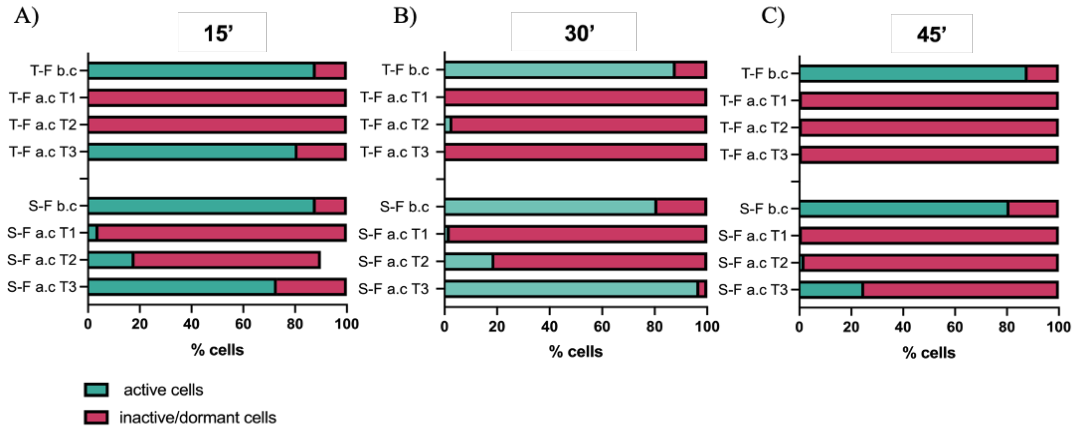

Figure 11. The average proportion of physiological status of Chaetoceros socialis APC12 *cultures derived from cryopreserved vegetative cells. Two-step freezing (T-F), snap-freezing (S-F) before cryopreservation (b. c), after cryopreservation (a. c) at 7 days (T1), 14 days (T2) and 21 days (T3) after thawing. Equilibration time 15' (A), 30' (B) and 45' (C) minutes.*

In the culture deriving from cryopreserved spores, the highest value of active cells was at ET 15' using the T-F method at T2, followed by a decrease of percentage at T3 (Fig. 12 A); also, for the S-F condition I have seen an increase in the active cells in the cultures, with the highest percentage in T2 (96%) (Fig. 12 A). A similar trend was reported for other ETs, 30' and 45' (Fig. 12 B, C).

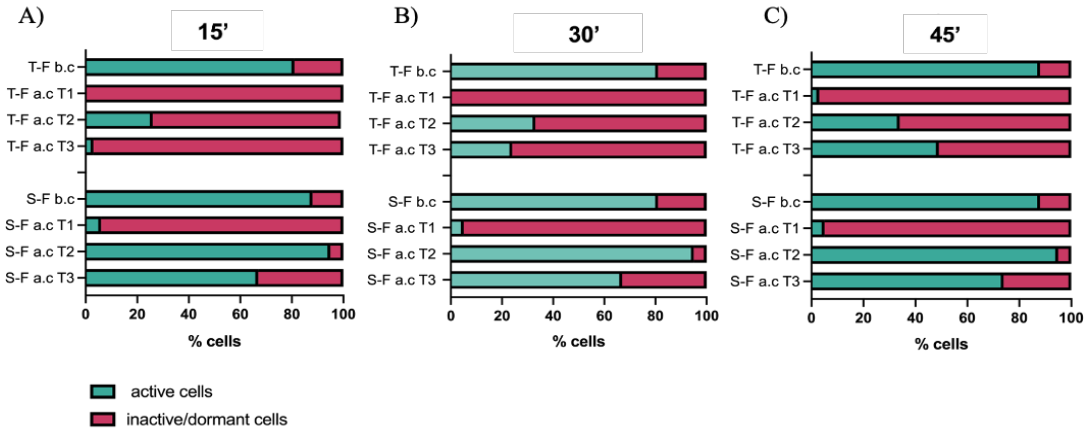

Figure 12. The average proportion of physiological status of Chaetoceros socialis APC12 *cultures derived from cryopreserved spores. Two-step freezing (T-F), snap-freezing (S-F) before cryopreservation (b. c), after cryopreservation (a. c) at 7 days (T1), 14 days (T2) and 21 days (T3) after thawing. Equilibration time 15' (A), 30' (B) and 45' (C) minutes.*

Morphological organization in cultures of Chaetoceros socialis APC12 deriving from cryopreserved vegetative cells vs cryopreserved spores

I evaluated the tendency of the active cells to remain as a single or colonial form post-thawing and re-growth.

In the culture deriving from cryopreserved vegetative cells both the cryopreservation techniques as ETs affected the morphological organization. In particular the cells in the culture ET 15' showed the tendency to stay as a single cell (Fig. 13 A); whereas in ET 30' under the T-F method, all the cells were organized in colonies at T2; in the S-F method, colonies organization were found at T1 while at T2 and T3, a shift to single-cell organization was seen (Fig. 13 B). In ET 45' after the T-F method, a prevalent colony organization at T3 was observed, as in S-F at T2 (Fig. 13 C).

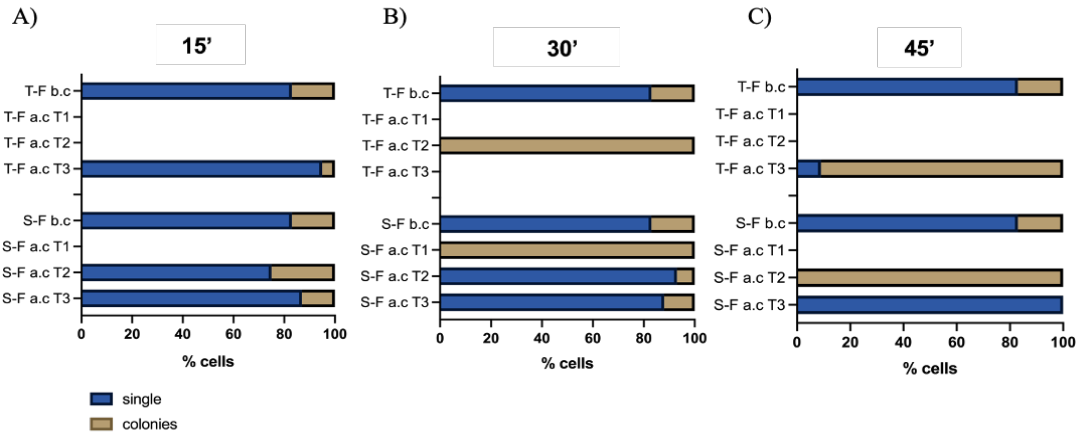

Figure 13. Average proportion of unicellular vs colonial form of active cells of Chaetoceros socialis APC12 *cultures derived from cryopreserved vegetative cells. Two-step freezing (T-F), snap-freezing (S-F) before cryopreservation (b. c), after cryopreservation (a. c) at 7 days (T1), 14 days (T2), and 21 days (T3). Equilibration time 15' (A), 30' (B) and 45' (C) minutes.*

When I considered the size of the single cells, I detected a significant reduction at T3 in the T-F method after cryopreservation with respect to the size before cryopreservation (b. c), while no differences were noted in the S-F condition (Tab. 9).

La borsa di dottorato è stata cofinanziata con risorse del
Programma Operativo Nazionale Ricerca e Innovazione 2014-202 (CCI 2014IT16M2OP005)
Fondo Sociale Europeo, Azione I.1 "Dottorati Innovativi con caratterizzazione Industriale"

Table 9. Size of active single cells of Chaetoceros socialis APC12 *cultures derived from cryopreserved vegetative cells. Two-step freezing (T-F); snap-freezing (S-F); before cryopreservation (b.c); after cryopreservation (a.c) at 7 days (T1), 14 days (T2), and 21 days (T3). Equilibration time 15', 30' and 45' minutes. Data show the average ± S.D. Statistical analyses were performed using one-way ANOVA and Tukey's range test. "*" ($p < 0.05$); "**" ($p < 0.01$).*

Single cell		T-F			S-F		
		15'	30'	45'	15'	30'	45'
Size (µm)	b.c	7.5± 1.2	7.5 ±1.2	7.5 ± 1.2	7.5 ± 1.2	7.5 ± 1.2	7.5 ± 1.2
	T1	0	0	0	0	0	0
	T2	0	0	0	6.8 ± 1.1	6.5 ± 1.3	0
	T3	6.4 ± 1.2 *	0	5.2 ± 0.9 *	6.9 ± 1.1	6.8 ± 0.9	0

On the other hand, the size of the colonies showed a rise in all ETs in the T-F condition, except for the ET 15'; in the S-F method, the size remained stable in T1 and T2, whereas at ET 45' a conspicuous size increase at T2 was observed (Tab. 10).

Table 10. Size of colonies of Chaetoceros socialis APC12 *cultures derived from cryopreserved vegetative cells. Two-step freezing (T-F), snap freezing (S-F) before cryopreservation (b. c) after cryopreservation (a. c) at 7 days (T1), 14 days (T2) and 21 days (T3). Equilibration time 15', 30' and 45' minutes. Data show the average ± S.D. Statistical analyses were performed using one-way ANOVA and Tukey's range test. "*" ($p < 0.05$); "**" ($p < 0.01$).*

Colonies		T-F			S-F		
		15'	30'	45'	15'	30'	45'
Size (µm)	b.c	14.2± 2.4	14.2± 2.4	14.2± 2.4	14.2± 2.4	14.2± 2.4	14.2± 2.4
	T1	0	0	39.5 ± 2.9 **	0	15.9± 2.3	0
	T2	0	23.75 ± 3.4 *	25 ± 3.4 **	15.5 ± 2.1	11.9 ± 1.9	34.5± 3.2**
	T3	11 ± 2.2	0	0	12.4 ± 1.8	13.5 ± 1.7	0

Regarding the cells germinated from *APC12* spores, in ET 15' after the T-F method, in the culture the cells showed the tendency to stay as solitary form until the T2, followed by a shift in colonies organization at T3 (Fig. 14 A); on the other hand, in S-F, mostly single cells were found in all phases of the regrowth (Fig. 14 A).

A different trend was noted in ETs 30' and 45'. More in detail, in ET 30' globally, the single cell was prevalent in all the ETs (Fig. 14 B), otherwise in ET 45' after the T-F method an increase of colonies was seen at T2 while in the S-F method, the cultures showed a prevalent distribution in single-cell (Fig. 14 C).

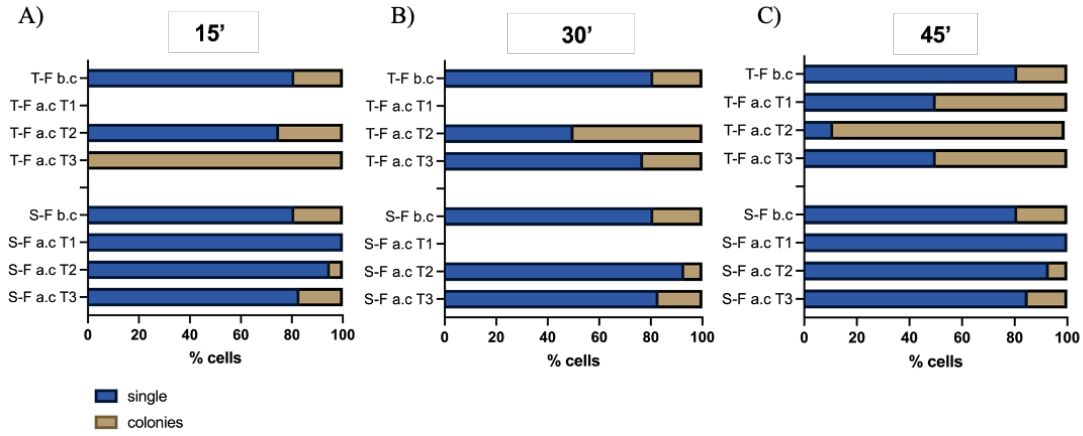

Figure 14. Average proportion of unicellular vs colonial form of active cells of Chaetoceros socialis APC12 *cultures derived from cryopreserved spores. Two-step freezing (T-F); snap-freezing (S-F); before cryopreservation (b. c), after cryopreservation (a. c) at 7 days (T1), 14 days (T2) and 21 days (T3). Equilibration time 15' (A), 30' (B) and 45' (C) minutes.*

La borsa di dottorato è stata cofinanziata con risorse del
Programma Operativo Nazionale Ricerca e Innovazione 2014-202 (CCI 2014IT16M2OP005)
Fondo Sociale Europeo, Azione I.1 "Dottorati Innovativi con caratterizzazione Industriale"

Regarding the cell size, I observed a slight increase in the cell size after spore germination, in all the different protocols, though small values were maintained (Tab. 11).

Table 11. Size of active single cells of Chaetoceros socialis APC12 *cultures derived from cryopreserved spores. Two-step freezing (T-F), snap-freezing (S-F) before cryopreservation (b. c), after cryopreservation (a .c) at 7 days (T1), 14 days (T2) and 21 days (T3). Equilibration time 15', 30' and 45' minutes. Data show the average ± S.D. Statistical analyses were performed using one-way ANOVA and Tukey's range test. "*" ($p < 0.05$); "**" ($p < 0.01$).*

Single cell		T-F			S-F		
		15'	30'	45'	15'	30'	45'
Size (µm)	T1	0	0	7.5 ± 0.3	6.5 ± 0.7	0	8 ± 0.7 *
	T2	6 ± 0.9	6.7 ± 0.5	7 ± 0.3	6. 9 ± 1.1	6.9 ± 0.8	7.2 ± 0.6
	T3	8.4 ± 0.9 *	7.2 ± 1.1	7 ± 0.3	6. 6 ± 1.2	7.3 ± 0.7	7.2 ± 0.6

A similar trend was observed also for the colonies, showing a size rise from T2 to T3 after both cryopreservation methods (Tab. 12).

Table 12. Size of colonies of Chaetoceros socialis APC12 *cultures derived from cryopreserved spores. Two-step freezing (T-F), snap-freezing (S-F) before cryopreservation (b. c), after cryopreservation (a. c) at 7 days (T1), 14 days (T2) and 21 days (T3). Equilibration time 15', 30' and 45' minutes. Data show the average ± S.D. Statistical analyses were performed using one-way ANOVA and Tukey's range test. "*" ($p < 0.05$); "**" ($p < 0.01$).*

Colonies		T-F			S-F		
		15'	30'	45'	15'	30'	45'
Size (µm)	b.c	12.5 ± 2.1	12.5 ± 2.1	12.5 ± 2.1	12.5 ± 2.1	12.5 ± 2.1	12.5 ± 2.1
	T1	0	0	0	0	0	0
	T2	24	25.75 ± 3.4*	23.6 ± 3.4 **	16.4 ± 1.3*	16.2 ± 1.3*	13.6 ± 1.4
	T3	20.5 ± 2.2	15.33 ± 1.4	21.5 ± 2.1 **	17.2 ± 1.4*	18.3 ± 1.4*	16.7 ± 1.4 *

La borsa di dottorato è stata cofinanziata con risorse del
Programma Operativo Nazionale Ricerca e Innovazione 2014-202 (CCI 2014IT16M2OP005)
Fondo Sociale Europeo, Azione I.1 "Dottorati Innovativi con caratterizzazione Industriale"

Basal fluorescence intensity of chlorophyll in cultures of Chaetoceros socialis APC12 deriving from cryopreserved vegetative cells vs cryopreserved spores

By the iFCM method, I correlated chlorophyll intensity with cell surface (Chl/area ratio) as a feature in determining the activity of cells. The results showed that the Chl/area ratio after the T-F method exhibited a recovery exclusively in T3 for all ETs, both for the single cells as colonies (Fig. 15). Otherwise, in the single cells after the S-F method, a rise in Chl/area was observed in T2 and T3 but only for ET 15' and 30', while the colonies showed globally a low Chl/area ratio (Fig. 15).

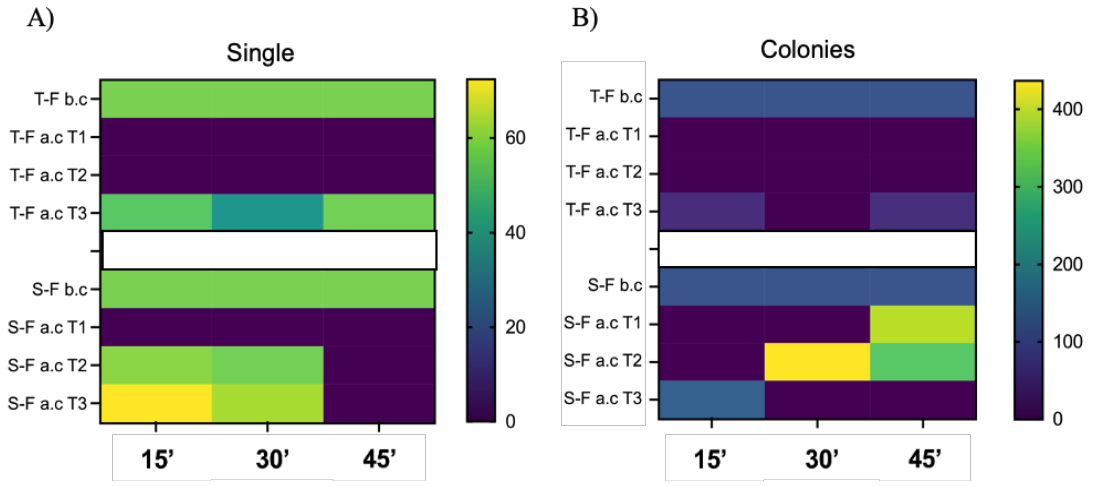

Figure 15. The Heat maps indicate the trend of the intensity of chlorophyll related to the area of cell surface (Chl/area) in Chaetoceros socialis APC12 *cultures derived from cryopreserved vegetative cells. A) single cells, B) colonies. Two-step freezing (T-F); snap-freezing (S-F); before cryopreservation (b. c), after cryopreservation (a. c) at 7 days (T1), (T2), and 21 days (T3). Equilibration time 15', 30', and 45 minutes.*

Regarding the cells germinated from spores, each treatment showed an increase in the Chl/area ratio compared with the status before cryopreservation in the single cells at ET 30' and 45' (Fig. 16 A) and for the colonies after the T-F cryopreservation method (Fig. 16 B). A similar trend was observed in the S-F treatment, whereas, as shown in Fig. 16 (A), the single cells organization rise their Chl/area ratio in all ETs during the growth; in contrast, colonies showed a low intensity correlated also with the low percentage of colonies cells (Fig. 16 B, Fig. 14).

La borsa di dottorato è stata cofinanziata con risorse del
Programma Operativo Nazionale Ricerca e Innovazione 2014-202 (CCI 2014IT16M2OP005)
Fondo Sociale Europeo, Azione I.1 "Dottorati Innovativi con caratterizzazione Industriale"

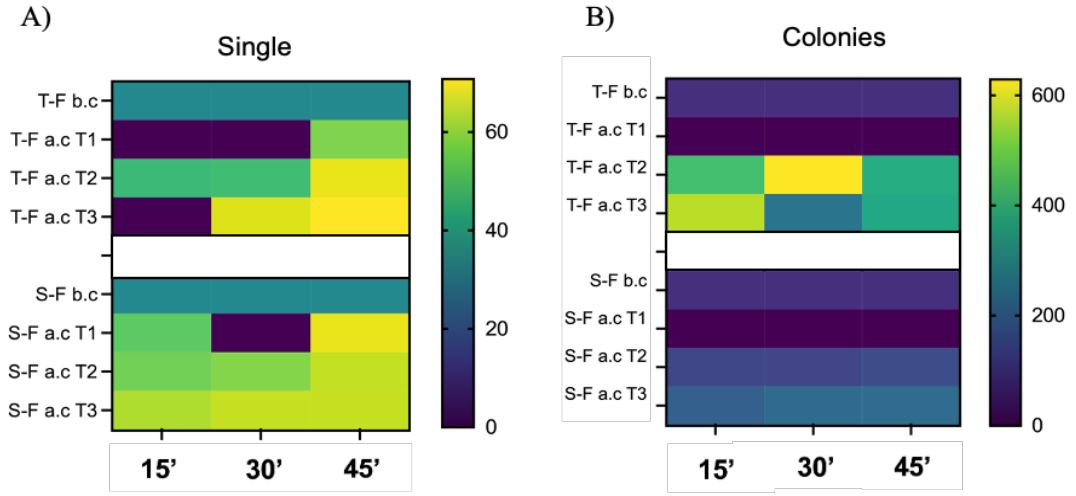

Figure 16. The Heat maps indicate the trend of the intensity of chlorophyll related to the area of cell surface (Chl/area) in Chaetoceros socialis APC12 *cultures derived from cryopreserved spore. A) single cells, B) colonies. Two-step freezing (T-F); snap-freezing (S-F); before cryopreservation (b. c), after cryopreservation (a. c) at 7 days (T1), 14 days (T2), and 21 days (T3). Equilibration time 15', 30', and 45 minutes.*

Active cells vs cell inactive and/or dormant cells in cultures of Chaetoceros socialis ZU1B1 deriving from cryopreserved vegetative cells vs cryopreserved spore

In *C. socialis ZU1B1*, T-F treatment induced a high percentage of inactive/dormant cells in all ETs (Fig. 17). In contrast, the S-F method induced a slight increase in the percentage of active cells at T3 for all ETs (Fig. 17 A) when the active cells in average were about 18% (Fig. 17).

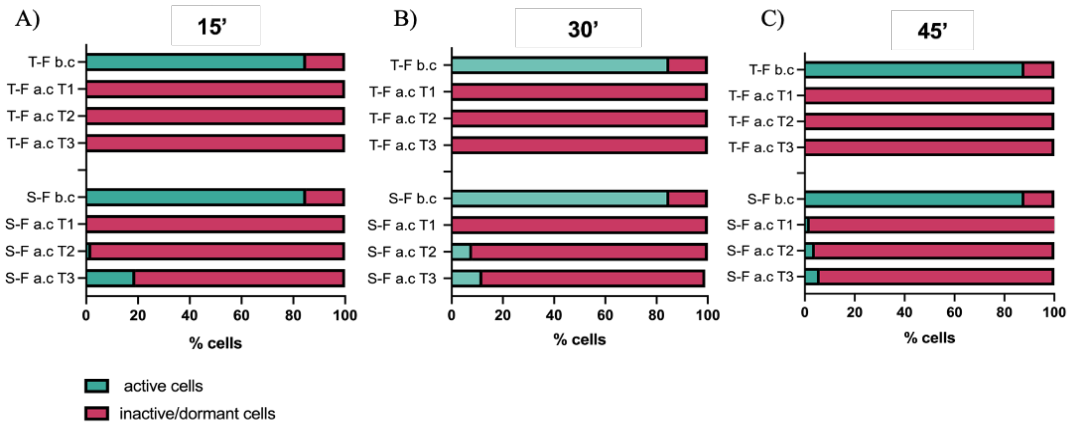

Figure 17. Average proportion of physiological status of Chaetoceros socialis ZU1B1 *cultures derived from cryopreserved vegetative cells. Two-step freezing (T-F); snap freezing (S-F); before cryopreservation (b. c), after cryopreservation (a. c) at 7 days (T1), 14 days (T2), and 21 days (T3). Equilibration time 15' (A), 30' (B) and 45' (C) minutes.*

A relatively better response was observed in the cryopreserved spores than cryopreserved vegetative cells: in ET 15' using the T-F method, a rise of active cells was seen at T2 and T3 (Fig. 18 A) while using the S-F method, an increase of the active cells was shown especially at ET 45' with the highest percentage at T3 (55%) (Fig. 18 C).

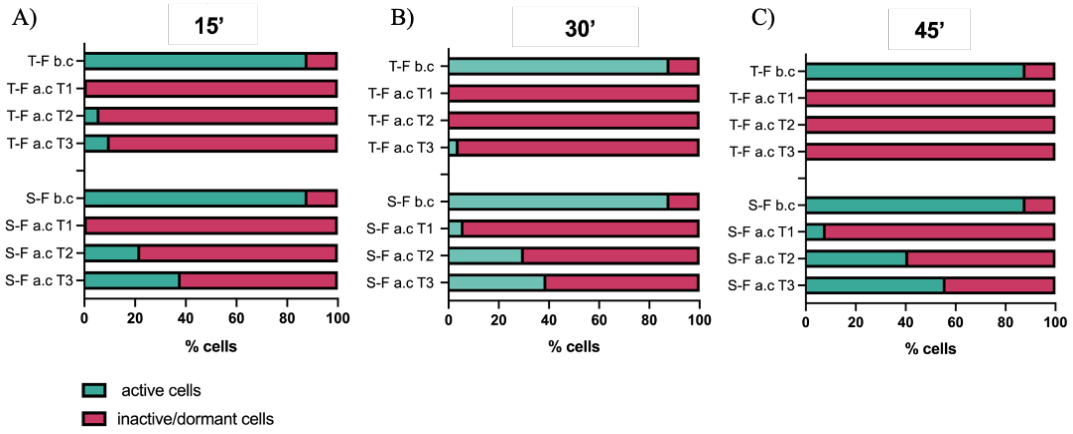

Figure 18. Average proportion of physiological status of Chaetoceros socialis ZU1B1 *cultures derived from cryopreserved spores. Two-step freezing (T-F); snap-freezing (S-F); before cryopreservation (b. c), after cryopreservation (a. c) at 7 days (T1), 14 days (T2) and 21 days (T3) after thawing. Equilibration time 15' (A), 30' (B) and 45' (C) minutes.*

Morphological organization in cultures of Chaetoceros socialis ZU1B1 deriving from cryopreserved vegetative cells vs cryopreserved spore

Considering that only in the S-F treatment I have seen active cells, I observed a high percentage of single/unicellular organization despite the tendency to form colonies before the cryopreservation in all the ETs (Fig. 19).

La borsa di dottorato è stata cofinanziata con risorse del
Programma Operativo Nazionale Ricerca e Innovazione 2014-202 (CCI 2014IT16M2OP005)
Fondo Sociale Europeo, Azione I.1 "Dottorati Innovativi con caratterizzazione Industriale"

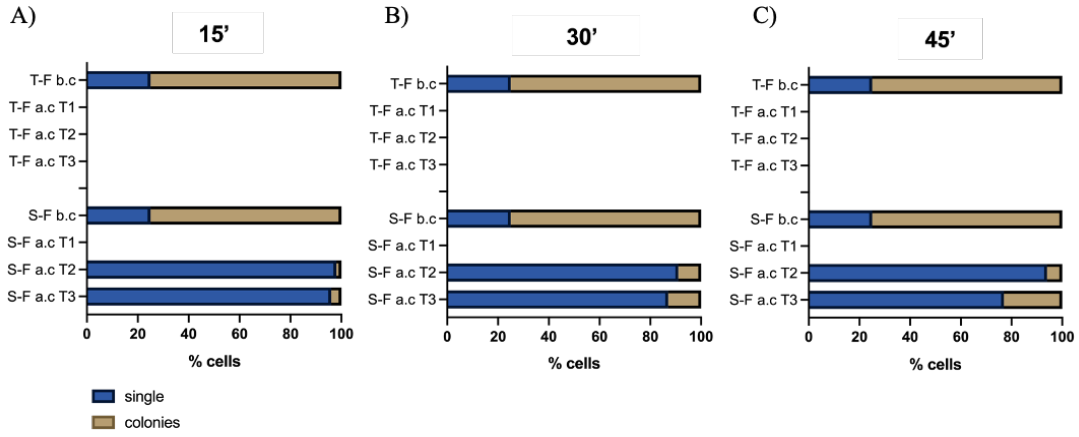

Figure 19. Average proportion of unicellular vs colonial form of active cells of Chaetoceros socialis ZU1B1 *cultures derived from cryopreserved vegetative cells. Two-step freezing (T-F); snap-freezing (S-F); before cryopreservation (b. c), after cryopreservation (a. c) at 7 days (T1), 14 days (T2), and 21 days (T3). Equilibration time 15' (A), 30' (B) and 45' (C) minutes.*

In addition, no significant differences were observed in the size of single cells. (Tab. 13).

Table 13. Size of single cells of Chaetoceros socialis ZU1B1 *cultures derived from cryopreserved vegetative cells. Two-step freezing (T-F), snap-freezing (S-F); before cryopreservation (b. c), after cryopreservation (a. c) at 7 days (T1), 14 days (T2), and 21 days (T3). Equilibration time 15', 30' and 45' minutes. Data show the average ± S.D. Statistical analyses were performed using one-way ANOVA and Tukey's range test. "*" ($p < 0.05$); "**" ($p < 0.01$).*

Single cell		T-F			S-F		
		15'	30'	45'	15'	30'	45'
Size (µm)	b.c	8.4 ± 0.7	8.4 ± 0.7	8.4 ± 0.7	8.4 ± 0.7	8.4 ± 0.7	8.4 ± 0.7
	T1	0	0	0	0	0	0
	T2	0	0	0	7. 4 ± 0.5	6.8 ± 0.9	7.2 ± 0.7
	T3	0	0	0	7.5 ± 0.5	7.2 ± 0.7	7.3 ± 0.6

As is shown in Table 14, a significant decrease was noted in the colony's size in the S-F in all ETs.

Table 14. Size of colony cells of Chaetoceros socialis ZU1B1 *cultures derived from cryopreserved vegetative cells. Two-step freezing (T-F), snap-freezing (S-F); before cryopreservation (b. c), after cryopreservation (a. c) at 7 days (T1), 14 days (T2), and 21 days (T3). Equilibration time 15', 30' and 45' minutes. Data show the average ± S.D. Statistical analyses were performed using one-way ANOVA and Tukey's range test. "*" ($p < 0.05$); "**" ($p < 0.01$).*

Colonies		T-F			S-F		
		15	30	45	15	30	45
Size (µm)	b.c	33.5± 2.1	33.5± 2.1	33.5± 2.1	33.5± 2.1	33.5± 2.1	33.5± 2.1
	T1	0	0	0	0	0	0
	T2	0	0	0	26.4 ± 1.3*	25.4 ± 1.4*	23.2± 1.6*
	T3	0	0	0	27.1 ± 1.2*	26.3 ± 1.5*	27.1± 1.2*

Similarly, during the regrowth of the cryopreserved *ZU1B1* spores, the germinated cells showed the tendency to organize as a single form both in T-F as well as S-F method, while an increase of colonies was observed during the time. In particular, at T3 in all ETs, the percentage of colony organization increased (Fig. 20).

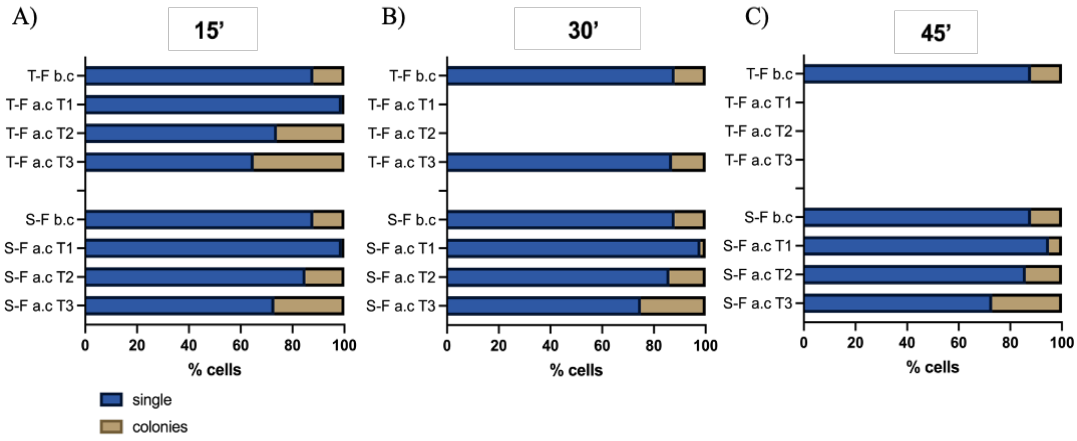

Figure 20. Average proportion of unicellular vs colonial form of active cells of Chaetoceros socialis ZU1B1 *cultures derived from cryopreserved spore. Two-step freezing (T-F); snap-freezing (S-F); before cryopreservation (b. c), after cryopreservation (a. c) at 7 days (T1), 14 days (T2), and 21 days (T3). Equilibration time 15' (A), 30' (B) and 45' (C) minutes.*

Moreover, as reported in Table 15, I have seen that T-F and S-F treatment did not induce any alteration in the size of single cells germinated from the cryopreserved *ZU1B1* spores.

Table 15. Size of single cells of Chaetoceros socialis ZU1B1 *cultures derived from cryopreserved spore. Two-step freezing (T-F), snap-freezing (S-F); before cryopreservation (b. c), after cryopreservation (a. c) at 7 days (T1), 14 days (T2), and 21 days (T3). Equilibration time 15', 30' and 45' minutes. Data show the average ± S.D. Statistical analyses were performed using one-way ANOVA and Tukey's range test. "*" ($p < 0.05$); "**" ($p < 0.01$).*

Single cell		T-F			S-F		
		15'	30'	45'	15'	30'	45'
Size (µm)	b.c	6.7 ± 0.8	6.7 ± 0.8	6.7 ± 0.8	6.7 ± 0.8	6.7 ± 0.8	6.7 ± 0.8
	T1	6.2 ± 0.8	0	0	6.3 ± 0.9	6.4 ± 0.8	6.1 ± 0.7
	T2	6.5 ± 0.8	0	0	6.8 ± 0.6	6.9 ± 0.6	6.5 ± 0.7
	T3	7.2 ± 0.8	7.1 ± 0.7	0	7.5 ± 0.5	7.5 ± 0.6	7.6 ± 0.9

Otherwise, a significant reduction was observed in the size of colonies for all treatments (Tab. 16).

Table 16. Size of colonies of Chaetoceros socialis ZU1B1 *cultures derived from cryopreserved spore. Two-step freezing (T-F), snap-freezing (S-F); before cryopreservation (b. c), after cryopreservation (a. c) at 7 days (T1), 14 days (T2), and 21 days (T3). Equilibration time 15', 30' and 45 minutes. Data show the average ± S.D. Statistical analyses were performed using one-way ANOVA and Tukey's range test. "*" ($p < 0.05$); "**" ($p < 0.01$).*

Colonies		T-F			S-F		
		15'	30'	45'	15'	30'	45'
Size (µm)	b.c	38.5± 1.9	38.5± 1.9	38.5± 1.9	38.5± 1.9	38.5± 1.9	38.5± 1.9
	T1	21.5± 1.1*	0	0	23.5± 1.7*	28.5± 1.8*	22.5± 1.6*
	T2	28.5± 1.9*	0	0	26.4 ± 1.3*	25.4 ± 1.4*	22.2± 1.4*
	T3	33.5± 1.6*	24± 1.8*	0	27.1 ± 1.2*	26.3 ± 1.5*	21.1± 1.7*

Basal fluorescence intensity of chlorophyll in Cultures of Chaetoceros socialis ZU1B1 deriving from cryopreserved vegetative cells vs cryopreserved spores

Similarly to *C. socialis APC12*, the Chl/area ratio of vegetative cells deriving from cryopreserved vegetative cells of *C. socialis ZU1B1* exhibited very low values in T-F, both in single as in colonies organization (Fig. 21). On the contrary, in the S-F method, a rise in intensity was observed in single forms in T2 and T3 in all ETs (Fig. 21 A), while colonies forms showed globally low levels in T2 and T3 in all ETs (Fig. 21 B).

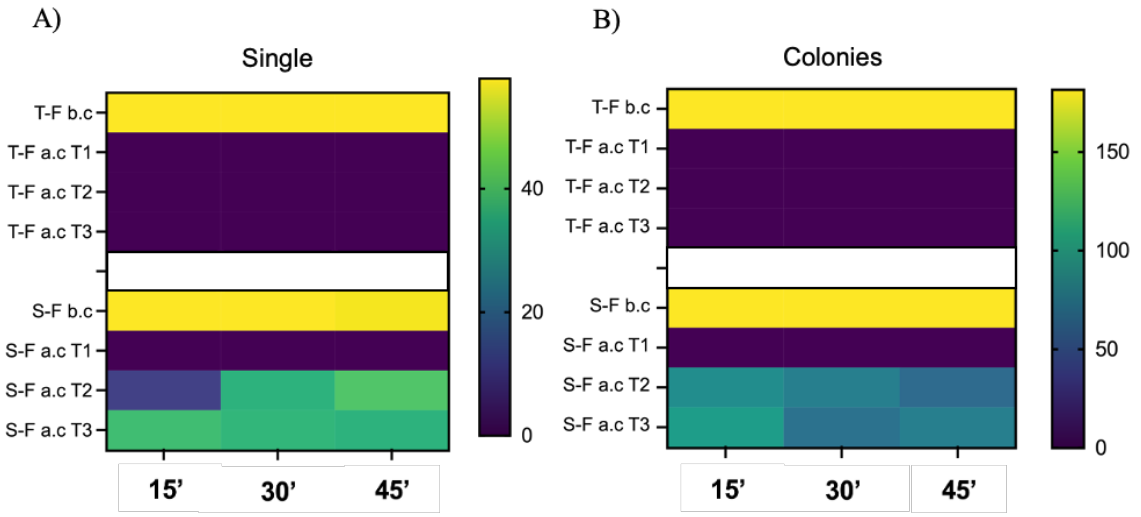

Figure 21. The Heat maps indicate the trend of the intensity of chlorophyll related to the area of cell surface (Chl/area) in Chaetoceros socialis ZU1B1 *cultures derived from cryopreserved vegetative cells. A) single cells, B) colonies. Two-step freezing (T-F); snap-freezing (S-F); before cryopreservation (b. c), after cryopreservation (a. c) at 7 days (T1), 14 days (T2), and 21 days (T3). Equilibration time 15', 30' and 45' minutes.*

Regarding cells germinated from spores, a low increase in Chl/area ratio was reported in the T-F treatment both in singles and colonies at ET 15' (from T1 to T3), while at ET 30' an increase was seen only at T3 (Fig. 22).

On the contrary, after the S-F treatment, both single cells and colonies form showed a rise of the values in all ETs during the growth (from T1 to T3). Globally, Chl/area ratio values remained much higher before cryopreservation compared with after freezing (Fig. 22).

La borsa di dottorato è stata cofinanziata con risorse del
Programma Operativo Nazionale Ricerca e Innovazione 2014-202 (CCI 2014IT16M2OP005)
Fondo Sociale Europeo, Azione I.1 "Dottorati Innovativi con caratterizzazione Industriale"

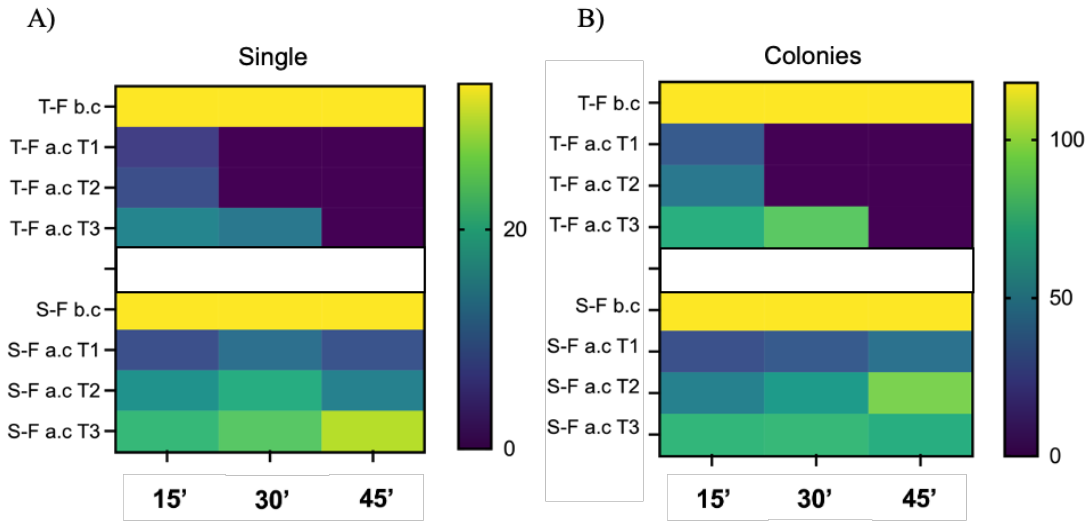

Figure 22. The Heat maps indicate the trend of the intensity of chlorophyll related to the area of the cell surface (Chl/area) in Chaetoceros socialis ZU1B1 *cultures derived from cryopreserved spore. A) single cells, B) colonies. Two-step freezing (T-F); snap-freezing (S-F); before cryopreservation (b. c), after cryopreservation (a. c) at 7 days (T1), 14 days (T2), and 21 days (T3). Equilibration time 15', 30' and 45' minutes.*

Active cells vs cell inactive and/or dormant cells in cultures of Chaetoceros costatus deriving from cryopreserved spores

The growth curve of the cultures derived from cryopreserved spores of *C. costatus* was monitored successfully for up to 35 days (T4 and T5). In *C. costatus*, a very low percentage of active cells was obtained in both cryopreservation methods. Although at ET 30' using the T-F method a very low percentage of active cells were noted at T1 (Fig, 23 B), the best results were obtained at ET 45' using S-F (Fig. 23 C).

La borsa di dottorato è stata cofinanziata con risorse del
Programma Operativo Nazionale Ricerca e Innovazione 2014-202 (CCI 2014IT16M2OP005)
Fondo Sociale Europeo, Azione I.1 "Dottorati Innovativi con caratterizzazione Industriale"

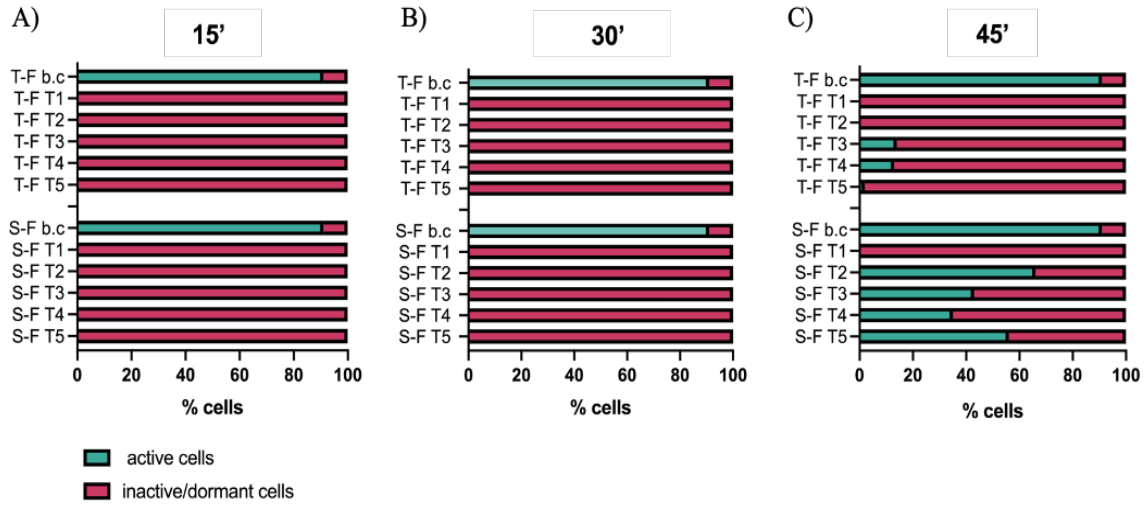

Figure 23. Average proportion of physiological status of Chaetoceros costatus *cultures derived from cryopreserved spores. Two-step freezing (T-F); snap-freezing (S-F); before cryopreservation (b. c), after cryopreservation (a. c) at 7 days (T1), 14 days (T2), 21 days (T3), 28 days (T4) and 35 days (T5) after thawing. Equilibration time 15' (A), 30' (B) and 45' (C) minutes.*

Morphological organization in cultures of Chaetoceros costatus deriving from cryopreserved spores

Considering ET 45' from T3 to T5 in both methods a predominant presence of single cells vs colonies was observed, in contrast with the condition in b. c (Fig. 24 C).

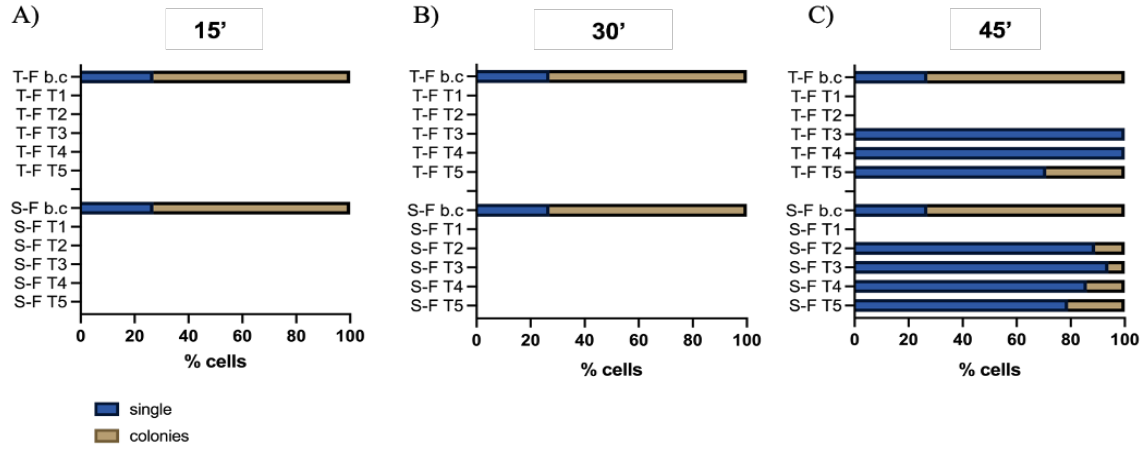

Figure 24. Average proportion of unicellular vs colonial form of active cells of Chaetoceros costatus *cultures derived from cryopreserved spore. Two-step freezing (T-F); snap-freezing (S-F); before cryopreservation (b. c), after cryopreservation (a. c) at 7 days (T1), 14 days (T2), 21 days (T3), 28 days (T4) and 35 days (T5). Equilibration time 15' (A), 30' (B) and 45' (C) minutes.*

Moreover, changes were also observed in cell size as single cells and colonies showed a significant reduction after the cryopreservation from T1 to T3 (Tab. 17).

Table 17. Size of single and colony's form of Chaetoceros costatus *cultures derived from cryopreserved spore using snap-freezing (S-F) at ET 45'. Before cryopreservation (b. c), after cryopreservation (a. c) at 7 days (T1), 14 days (T2), 21 days (T3), 28 days (T4), and 35 days (T5). Data show the average ± S.D. Statistical analyses were performed using one-way ANOVA and Tukey's range test. "*" ($p < 0.05$); "**" ($p < 0.01$).*

	Size (µm)	
	Single	Colonies
b. c.	14.35 ± 2.3	114.6 8 ± 22.4
a. c T1	-	-
a. c T2	12.25 ± 1.3	65.51 ± 12.3**
a. c T3	13.69 ± 1.8	76.51 ± 11.2**
a. c T4	13.59 ± 1.2	49.66 ± 13.6**
a. c T5	17.01 ± 1.5	50.32 ± 16.4 **

Basal fluorescence intensity of chlorophyll in cultures of Chaetoceros costatus deriving from cryopreserved spores

The Chl/area ratio showed a good increase both in single as in colonies organization during the time (Fig. 25).

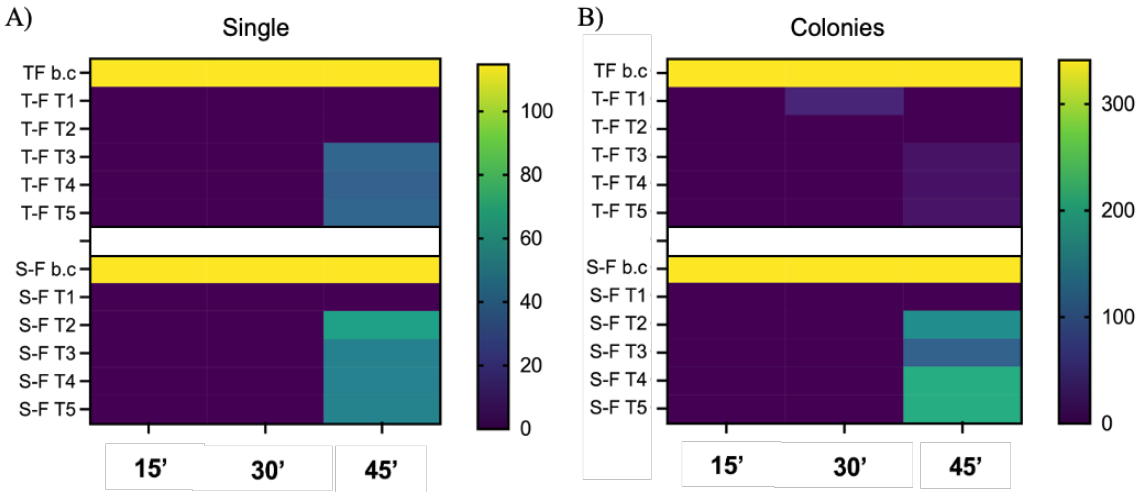

Figure 25. The Heat maps indicate the trend of the intensity of chlorophyll related to the area of the cell surface (Chl/area) in Chaetoceros costatus *cultures derived from cryopreserved spores. A) single cells, B) colonies. Two-step freezing (T-F); snap-freezing (S-F); before cryopreservation (b. c), after cryopreservation (a. c) at 7 days (T1), 14 days (T2), 21 days (T3), 28 days (T4) and 35 days (T5). Equilibration time 15', 30', and 45 minutes.*

Active cells vs cell inactive and/or dormant cells in cultures of Thalassiosira rotula deriving from cryopreserved vegetative cells

Although the *T. rotula* culture after cryopreservation didn't show recovery, considering its biotechnological potential investigated in the first part of this PhD project, a deep analysis of the parameters involved in the unsuccessful cryopreservation became interesting.

As shown in Fig. 26, culture of *T. rotula* globally remains in the inactive/dormant state, and only with the S-F method at 15' ET, a very low percentage of active were seen at T2 (2 - 4%).

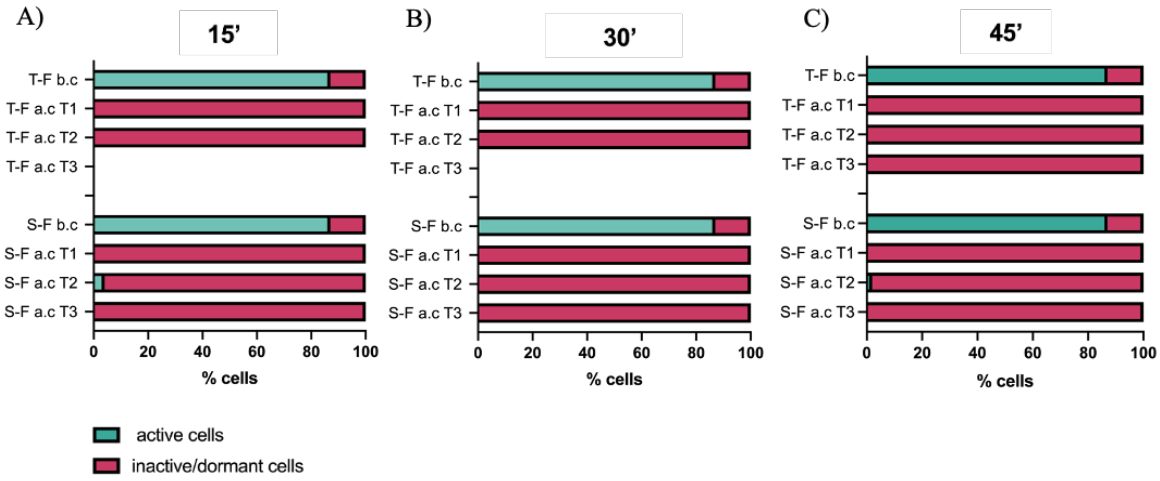

Figure 26. Average proportion of physiological status of Thalassiosira rotula *cultures derived from cryopreserved spores. Two-step freezing (T-F); snap-freezing (S-F); before cryopreservation (b. c), after cryopreservation (a. c) at 7 days (T1), 14 days (T2), 21 days (T3) after thawing. Equilibration time 15' (A), 30' (B) and 45' (C) minutes.*

Morphological organization in cultures of Thalassiosira rotula deriving from cryopreserved vegetative cells

Notwithstanding this very low rate of active cells, after the thawing the single form was prevalent respect with the colonial organization visible before cryopreservation (Fig. 27).

La borsa di dottorato è stata cofinanziata con risorse del
Programma Operativo Nazionale Ricerca e Innovazione 2014-202 (CCI 2014IT16M2OP005)
Fondo Sociale Europeo, Azione I.1 "Dottorati Innovativi con caratterizzazione Industriale"

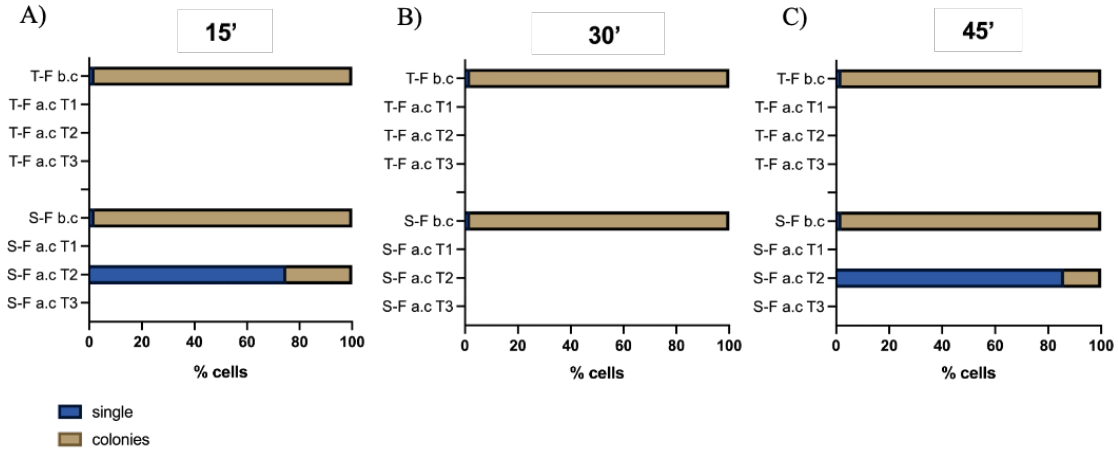

Figure 27. Average proportion of physiological status of Thalassiosira rotula *cultures derived from cryopreserved spores. Two-step freezing (T-F); snap-freezing (S-F); before cryopreservation (b. c), after cryopreservation (a. c) at 7 days (T1), 14 days (T2), 21 days (T3) after thawing. Equilibration time 15' (A), 30' (B) and 45' (C) minutes.*

Considering the size, whereas in the single cells no significant differences were observed after cryopreservation (Tab. 18) on the contrary, the size of colonies, which resulted very high before the cryopreservation, showed a significant reduction after the thawing (Table 19).

Table 18. Size of single cells of Thalassiosira rotula *cultures derived from cryopreserved vegetative cells. Two-step freezing (T-F), snap-freezing (S-F); before cryopreservation (b.c), after cryopreservation (a.c) at 7 days (T1), 14 days (T2), and 21 days (T3). Equilibration time 15', 30'and 45' minutes. Data show the average ± S.D. Statistical analyses were performed using one-way ANOVA and Tukey's range test. "*" ($p < 0.05$); "**" ($p < 0.01$).*

Single cell		T-F			S-F		
		15'	30'	45'	15'	30'	45'
Size (µm)	b.c	15.6 ± 0.6	15.6 ± 0.6	15.6 ± 0.6	15.6 ± 0.6	15.6 ± 0.6	15.6 ± 0.6
	T1	0	0	0	0	0	0
	T2	0	0	0	14.32 ± 0.8	0	15.2 ± 0.8
	T3	0	0	0	0	0	0

La borsa di dottorato è stata cofinanziata con risorse del
Programma Operativo Nazionale Ricerca e Innovazione 2014-202 (CCI 2014IT16M2OP005)
Fondo Sociale Europeo, Azione I.1 "Dottorati Innovativi con caratterizzazione Industriale"

Table 19. Size of colonies of Thalassiosira rotula *cultures derived from cryopreserved vegetative cells. Two-step freezing (T-F), snap-freezing (S-F); before cryopreservation (b. c), after cryopreservation (a. c) at 7 days (T1), 14 days (T2), and 21 days (T3). Equilibration time 15', 30' and 45' minutes. Data show the average ± S.D. Statistical analyses were performed using one-way ANOVA and Tukey's range test. "*" ($p < 0.05$); "**" ($p < 0.01$).*

Colonies		T-F			S-F		
		15'	30'	45'	15'	30'	45'
Size (µm)	b.c	437± 1.9	437± 1.9	437± 1.9	437± 1.9	437± 1.9	437± 1.9
	T1	0	0	0	0	0	0
	T2	0	0	0	146 ± 1.7**	0	141 ± 1.6**
	T3	0	0	0	0	0	0

Basal fluorescence intensity of chlorophyll in cultures of Thalassiosira rotula deriving from cryopreserved vegetative cells

Globally, Chl/area ratio values remained much higher before cryopreservation compared with after freezing (Fig. 28).

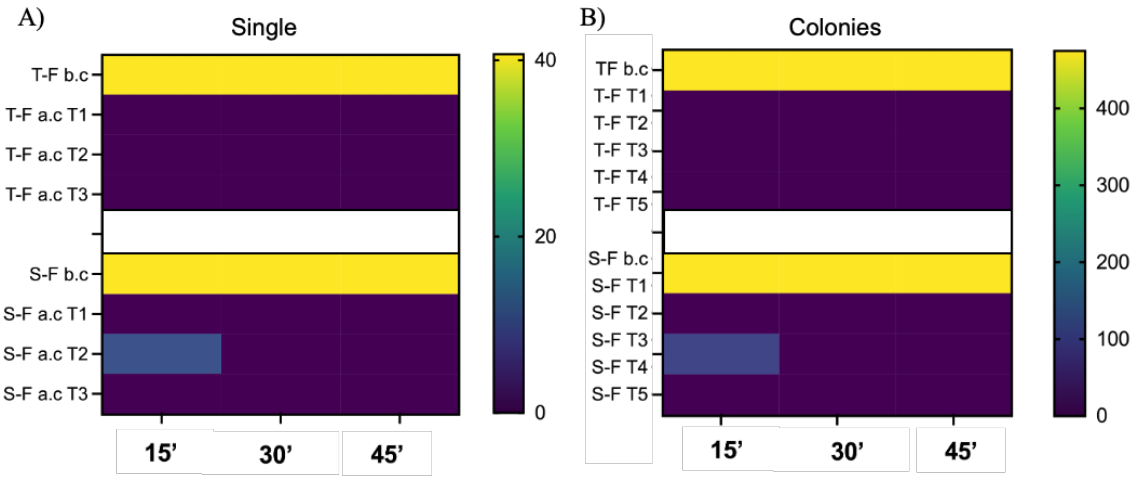

Figure 25. The Heat maps indicate the trend of the intensity of chlorophyll related to the area of the cell surface (Chl/area) in Thalassiosira rotula *cultures derived from cryopreserved vegetative cells. A) single cells, B) colonies. Two-step freezing (T-F); snap-freezing (S-F); before cryopreservation (b. c), after cryopreservation (a. c) at 7 days (T1), 14 days (T2), 21 days (T3), 28 days (T4) and 35 days (T5). Equilibration time 15', 30', and 45 minutes.*

La borsa di dottorato è stata cofinanziata con risorse del
Programma Operativo Nazionale Ricerca e Innovazione 2014-202 (CCI 2014IT16M2OP005)
Fondo Sociale Europeo, Azione I.1 "Dottorati Innovativi con caratterizzazione Industriale"

3.4 Discussion

In this chapter, I discuss the results on the applicability and/or success of the cryopreservation technique for some species/strains of diatoms and in particular for the resting spores. Because of the increasing interest in diatoms, both within fundamental and applied research, it's crucial to improve current cryopreservation protocols (Taylor and Fletcher, 1998; Boroda *et al.*, 2014).

Several parameters have been described as determinants for successful cryopreservation of microalgae, such as species, strain, cell size and form (Day and DeVille, 1995), growth phase and rate (Piasecki *et al.*, 2009) cooling rate, storage temperature, and duration of storage, thawing and post thawing manipulation (McLellan, 1989; Day and McLellan 1995; Day 1998; Tanniou *et al.*, 2012; Buhman *et al.*, 2013; Day *et al.*, 2017; Stock *et al.*, 2018).

Although diatom tolerance to freezing is relatively limited, I tested different protocols and cryopreservation conditions with the aim to maintain the structural and functional integrity of species/strains of diatoms investigated. In particular, I tested the cryopreservation technique on both vegetative cells as well as resting stages (spores or resting cells). Among the diatom species/strains focused on in this study, different features, such as sizes (range from 6.5 to 40 μm) and ecological features (sampling site and/or tolerance to various stresses) have been taken into account. More in detail, *Chaetoceros socialis, Chaetoceros costatus,* and *Chaetoceros lauderi* are abundant species in the Mediterranean Sea, playing a crucial role in the Gulf of Naples' warm temperate coastal ecosystem and noted for the abundant presence of spores in surface sediments (Zingone *et al.*, 1990, 1995, 2010; Montresor *et al.*, 2013; Piredda *et al.*, 2017). In particular, *C. socialis,* a colony-forming centric diatom, showed a significant diversity and global distribution, being present from the frigid Arctic and North Atlantic to the much warmer Mediterranean Sea and Gulf of California, blooming in a temperature range of -2 to 29°C in various oceanic regions (Degerlund *et al.*, 2010; Booth *et al.*, 2022). For these reasons, I tested two strains of *C. socialis,* isolated in different ecological areas: *APC12* strain, derived from spore germination of sediments by the Gulf of Naples, and *ZU1B*1 strain isolated by phytoplankton samples of the North Sea.

The other species, *C. costatus* and *C. didymus,* were investigated especially for their mechanism to tolerance of various stresses: *C. costatus* showed a high antioxidant potential, denoted when cultured were placed in a nitrogen-deprived medium characterized by a high content of loliolide, pheophorbide a, pheophytin b, known with an antioxidant activity (Frleta Matas *et al.*, 2024); while *C. didymus* was defined as a "resistant" species, producing proteases and oxylipins potentially involved in the resistance to lysis by *Kordia algicida*, an algicidal bacterium (Paul and Pohnert, 2011; Meyer *et al.*, 2018). Meanwhile, *C. lauderi* is a species characterized by a very large size (range 28-50 μm), with a global distribution and seasonal occurrence, also noted as producers of endogenous spore, which the morphological aspects are well described (Ishi *et al.*, 2011; Montresor *et al.*, 2013).

Lastly, the centric diatom *Thalassiosira rotula* was tested in my study not only because it is a cosmopolitan species and it is very abundant in the Mediterranean Sea, both in phytoplankton and/or sediment samples, but also for its potential application in the biotechnological field. As reported by several studies, *T. rotula* is a potential sustainable source of lipids, pigments, PUFA, and other bioactive compounds (Di Dato *et al.*, 2019; Matas *et al.*, 2023). For instance, as described in Cutignano *et al.*, (2022), extract of *T. rotula* showed an enrichment in cytotoxic molecules like the phytosterol 24-methylene cholesterol (24-MChol) with an anticancer activity. Moreover, *Thalassiosira* spp. are a potential candidate in biorefinery, nanotechnology, and biomedicine field, not only to naturally produce high-value biomolecules but also to reach high densities even in mass culture (Kusumaningtyas *et al.*, 2017; Marella and Tiwari, 2020; Mishra *et al.*, 2020). For this reason, *T. rotula* was also investigated in the first part of this PhD research project as a potential producer of fucoxanthin. Finally, it has been found that some *Thalassiosira* species, including *T. rotula,* develop resting cells which, unlike the spores, are morphologically similar to vegetative cells (McQuoid and Hobson, 1996) and probably more suitable for cryopreservation.

My main focus was to assess the potential use of spores in cryopreservation and testing for the first time this technique in this growth stage, as well as to allow cryopreservation in species that are typically challenging to preserve.

The induction of spore formation, their cryopreservation, and finally their revival, could represent a valid alternative for the long-term maintenance of species/strains to avoid phenotypic and genotypic modification that may arise in culture conditions.

To this aim, firstly I tried to induce spore formation in my species. The spore formation is largely studied, but the mechanism that induces this stage is not completely clear for many diatoms (McQuoid and Hobson 1996; Sugi and Kuma, 2008; Pelusi *et al.*, 2019). Several studies have shown that, in natural populations, nutrient depletion, particularly nitrogen, is the most effective trigger inducing this life cycle transition (Kuwata *et al.*, 1993; McQuoid and Hobson 1996; Kudo *et al.*, 2000; Michel *et al.*, 2002; Pelusi *et al.*, 2019). Pelusi *et al.* (2019) reported that in *C. socialis,* in laboratory conditions, the cell density also plays a role in inducing spore formation.

Based on this, I conducted experiments to obtain resting spores in my diatom species using low nitrate concentration (N-depletion) together with a low cell density inocula in the basal medium. In my experiments, the treatment of nitrogen depletion induced spores' formation in both *C. socialis* strains as well as in *C. costatus* and *C. lauderi;* on the other hand, the same conditions did not induce resting stages (i.e spore in *C. didymus* and resting cells in *T. rotula*).

As reported by McQuoid and Hobson (1996) and Sugie and Kuma (2008), nitrogen is one of the factors involved in spore formation but not for all the species and other elements, such as silicate availability, temperature fluctuations, darkness, and other environmental stressors could play a role in spore formation. Then, with the perspective of the possible difficulty of producing spores, I compared cryopreservation success on the vegetative cells vs spores for some strains. Interestingly, the spores of *C. lauderi*, as for the small size (range 12-15 μm) resulted particularly suitable for cryopreservation; unfortunately, the cryopreserved spores showed, during the post-thaw monitoring, high growth of cyanobacteria that inhibited further recovery. On the other hand, *C. lauderi* vegetative cells showed a large size (30-45 μm) that negatively influenced the success of cryopreservation.

Indeed, as reported by Whaley *et al.* (2021), smaller diatoms may allow for more efficient penetration of CPA, enhancing the protective effects of the cryoprotectant and leading to improved survival rates post-cryopreservation; in contrast, larger diatoms showed a very low percentage of successful of cryopreservation (Whaley *et al.*, 2021).

In thus study, I evaluated different cryopreservation protocols changing also two key parameters: the equilibration times (ETs), like the incubation time in DMSO, and the freezing techniques (Rhodes *et al.*, 2005; Day *et al.*, 2017; Stock *et al.*, 2018; Yee and Yang, 2023). Preliminary tests using DMSO (10%) allowed us to select three different equilibration times (15, 30, and 45 minutes, respectively). Studies highlight that optimal equilibration times vary across species, with a range from 5 to 30 minutes often effective for small diatom strains, whereas larger species may benefit from slightly extended times (Imelda *et al.*, 2000; Buhmann *et al.*, 2013; Stock *et al.*, 2018).

My results showed that ETs even longer, i.e. up to 45', had good results for the cryopreservation of spores of *C. socialis* (strain *APC12*).

Furthermore, the freezing technique is another important key to the success of cryopreservation for microalgae, and two methods were reported as more successful: the slow controlled cooling rates, commonly defined as the *two-step freezing* method (T-F) and a rapid-freezing technique, as *snap-freezing* (S-F). Variations in these two freezing methods have been explored to further minimize cell damage during cryopreservation (Morris, 1978; Canavate and Lubian, 1997; Mitbavkar and Anil, 2006; Day *et al.*, 2017; Stock *et al.*, 2018).

Overall, my results suggest rapid freezing (S-F) as a successful method for my species and a high tolerance to cryopreservation has been observed in the spores of *C. socialis* and *C. costatus*. Some studies suggest that diatoms have better survival rates with two-step freezing due to reduction of intracellular ice formation. In contrast, snap-freezing (and/or insufficient cryoprotectant exposure) often results in low survival rates, indicating diatoms are sensitive to freezing-induced osmotic stress (Day *et al.*, 1997; Bui *et al.*, 2013; Koh *et al.*, 2014). In this study in the post-thawing monitoring, the highest viability was observed in spores of *C. socialis APC12* (90-96 %) and also of *C. costatus* (66 %) using the snap-freezing method, in line with the study of Morschett *et al.* (2016), in which for *Chlor*ella *vulgaris*, S-F determined high post-thawing viability (63 %). Probably, the small size of my *Chaetoceros* species, could benefit the rapid freezing method as in the cooling of smaller cells (with high surface area: volume ratio) the water is lost more effectively during thawing than larger cells (with low surface area: volume ratio), where the rapid freezing induces ice formation, hence slower cooling rates (T-F) should be selected in order to prevent this (McLellan, 1989).

In the post-thaw re-growth, I have seen different responses strongly correlated not only with the technique but also with the strains and stage of cells cryopreserved.

In particular, in both strains of *C. socialis* I have seen different regrowth curves, including different peaks of cell density, correlated to the ETs used, with the highest value in *C. socialis APC12* spores at ET 15' vs *C. socialis APC12* vegetative cells at ET 30'. Otherwise, the spore cryopreserved with the S-F method in the strain *ZU1B1*, showed a low increase of cell density in ETs 15' and 30'. These results are in line with Day *et al.* (2017) in which 38 strains of *Skeletonema marinoi* were tested with different cryopreservation techniques but approximately 35% of the strains tested survived, highlighting that the cryopreservation is not only species-specific but also strains-specific. Moreover, I noted that ETs influenced not only the health of cells but also their metabolism and physiological function, such as reproduction. These differences are in line with Chong *et al.* (2006) and Stock *et al.* (2018), in which suggested that longer equilibration times can improve the viability of cells after thawing, as they allow for better distribution of the cryoprotectant and minimize osmotic shock during the freezing process (Stock *et al.*, 2018). Besides, Leiva and Dupré (2011) indicated that different exposure times to the cryoprotectant DMSO influenced the viability of *Chaetoceros calcitrans*, with optimal times yielding the highest survival rates.

In line with the results obtained in *C. socialis,* I have seen a similar response also in the spores of *C. costatus* but only related to the ET 45', highlighting the role of equilibration time and the high species-specificity.

Another surprising evidence was that the cells germinated from *C. costatus* spore showed a biphasic re-growth curve, without any change in culture conditions nor adding new medium. This result could suggest a different germination timing of the spores: in the first 21 days the cultures reached a first peak and then a fall as a consequence of senescence and /or a decrease in the light amount; then a second recovery and growth was observed. Therefore, I might suppose an intrinsic spore germination asynchrony, that from a biotechnological view, could be interesting, providing a post-thawing "seed cells" with different germination capability.

Also considering the very low recovery percentage and re-growth of *C. socialis ZU1B1* spores which remain dormant for over 35 days and/or reaching low density, support this

hypothesis: for *C. socialis ZU1B1*, a strain isolated from the North Sea, probably a long storage at low temperature as cryopreservation, could be a well-adapted genotypic trait. Moreover, I expected a similar trend also for the *C. lauderi* cryopreserved spores: unfortunately, an overgrowth of cyanobacteria was assessed after the thawing, although before the cryopreservation, the same cultures didn't show such contamination. Based on my results, these outline multiple factors that are involved in cryopreservation success, such as the role of bacteria and the relation with the CPA. Generally, DMSO is not known to benefit bacterial growth. Stock *et al.* (2018) experimented that adding antibiotics immediately after thawing, can substantially improve post-thaw recovery in some species. The study has shown that in the diatom *Seminavis robusta* the positive effect of antibiotics increased with decreasing CPA concentrations suggesting that, when the initial number of viable cells was low (as a consequence of low CPA concentrations), antibiotics suppressed bacterial growth long enough for the surviving cells to recover and start dividing; while in the absence of antibiotics, fast bacterial growth appears to prevent recovery of the relatively few surviving algal cells. However, the effect of the antibiotic treatment was highly species-specific. The same authors showed that the addition of antibiotics did not have any effect on the recovery of *Thalassiosira weissflogii,* concluding that some species might benefit from bacterially derived compounds thus exhibiting lower growth when bacteria are suppressed.

Lastly, I have seen an unsuccess of my cryopreservation protocols also in the vegetative cultures of *T. rotula* which showed after thawing and over the time, a very high number of dormant/inactive cells. In the case of *T. rotula* the failure may be explained by the different compositions and properties of the algal cell walls that may be a reason for differences in freezing injury; also, the peculiarities in the cell wall composition, i.e. high content of silica and/or the shape/morphology of these cells, could be implicated. Then, the relatively high size of vegetative cells of *T. rotula* and/or their main organization in colonial form before cryopreservation, could have influenced the success of the freezing technique. In fact, large unicellular and colony forming marine microalgal species, especially those containing large vacuoles, have been difficult to cryopreserve (Rhodes *et al.*, 2006, Boroda *et al.*, 2013).

Large vacuole cells have a higher water content than small vacuole cells, and during freezing this may lead to the formation of large intracellular ice crystals that damage the

cell membranes because the cryoprotectants (CPAs) may fail to equilibrate the cells properly. Therefore, the cell size of microalgae can affect their success rate during cryopreservation.

Thus, also my results suggest that for each diatom species, the protocol for cryopreservation needs to be optimized and could be species-specific.

Considering the changes after the cryopreservation technique, the imaging Flow Cytometry (iFCM), allowed us to perform a multiparametric characterization as morphophysiological features. My results have shown that cryopreservation can also change the population organization (% of single cells vs colonies). In fact, I have seen that my cultures showed a different distribution in single cells or forming colonies before and after the cryopreservation. Interestingly, I noted that the culture organized in colonies showed low survival and tended to change their organization in a solitary form during the time. As reported above, *C. socialis* is a colony-forming diatom, whereas I observed a global organization in single form after the cryopreservation both in cultures derived from vegetative cells as that derived from spore. In addition, the high percentage of single cells could be also related to the small size that could be more resilient during the cryopreservation process and facilitate post-thaw recovery (Fleck *et al.*, 2006). As just before reported, *T. rotula* showed an organization in colony before cryopreservation with a large size (437± 1.9 µm), explaining probably the unsuccess of cryopreservation: large diatoms or colonies may show slower metabolic rates, potentially leading to increased susceptibility to cryoinjury (Day *et al.*, 2000; Bui *et al.*, 2013). This suggests that under unfavourable conditions i.e. cryoinjury stress, the solitary forms have an advantage. Despite the low rate of active cells in the post-thawing of *T. rotula*, I observed no alteration in the size of active cells in solitary form, while the colonies showed a consistent size reduction. As reported by Svensson *et al.* (2014), also in the natural environment, abiotic factors such as temperature and light levels, may affect the morphology, namely if solitary or colony-forming species dominate in diatom populations.

All these evidences could be also particularly relevant for diatoms and other microalgae used in biotechnological applications, suggesting that cryopreservation could select specific phenotypic traits that are more resistant to freezing and thawing stresses (Rohdes *et al.*, 2006; Passy, 2007; Stock *et al.*, 2018).

To have additional indicators of the algal functional activity after freezing, I evaluated the intensity of chlorophyll fluorescence related to the cell surface (Chl/area ratio). After cryopreservation, the data highlighted the highest values of Chl/area ratio for single cell respect with colony organization, to support a good photosynthetic performance, especially for the single cells. However, sometime in the first period of re-growth, a low value of Chl/area ratio in the culture was observed, but with a rise during the time. These results are in line with many studies in which was noted that thawed diatom cells may show decreased chlorophyll fluorescence, possibly due to damage in chloroplast membranes or other cellular processes, potentially due to ice formation or osmotic stress during freezing (Buhmann *et al.*, 2013; Stock *et al.*, 2018), where then promptly a recovery of the culture was established; otherwise, algal pigments tend to decrease as the cells adapt to stress and /or changes in pigment content may depend on the cell division cycle, which is connected with the light/dark cycle in algae (Sournia 1974).

Globally, my results help to confirm that cryopreservation success is not only highly specie-specific but also depends on strains and the cells characteristics, like cell wall properties, size, length of colonies, ecological features and physiological state (i.e vegetative cells vs resting stage) (Rhodes *et al.*, 2006; Bui *et al.*, 2013; Stock *et al.*, 2028; Paredes *et al.* 2021). Moreover, my study highlighted that spore showed a higher tolerance to freezing, resulting in a fast resume of growth and also in the recovery of the metabolic activity after thawing. Finally, an important key result is related to the shift of cell diatom organization as cryopreservation seems to select solitary cells vs colonies form that could be more resilient to cryopreservation injuries.

La borsa di dottorato è stata cofinanziata con risorse del
Programma Operativo Nazionale Ricerca e Innovazione 2014-202 (CCI 2014IT16M2OP005)
Fondo Sociale Europeo, Azione I.1 "Dottorati Innovativi con caratterizzazione Industriale"

3.5 Conclusion

This study advances knowledge of diatom cryopreservation, offering critical insights into how structural, physiological, and environmental factors influence post-thaw survival and regrowth. By examining cryopreservation in five diatom species with varying ecological and morphophysiological features, I explored the preservation potential of both vegetative cells and spores. My results underscore the importance of optimized cryopreservation protocols based on species-specific characteristics, including equilibration times, freezing methods, and cell stage. My results showed that the spores of *C. socialis* and *C. costatus* exhibited higher tolerance to cryopreservation stress than vegetative cells, highlighting the unique resilience of these spore stages and their potential to facilitate broader application in biotechnological and ecological contexts. This work also identified key morphological and metabolic traits that contribute to diatom resilience, such as smaller cell size and high chlorophyll fluorescence intensity, which were correlated with improved cryopreservation outcomes. Through the iFCM, I quantified the effects of cryopreservation on cell organization, colony formation, and intensity of chlorophyll related to surface, revealing that single-cell forms are more adapted to cryopreservation stress than colony-forming cells. These observations provide valuable insights into the mechanisms governing cryopreservation success, suggesting that smaller diatoms and spore stages possess inherent characteristics that promote metabolic activity and resilience post-thaw. Lastly, further studies need to clarify the role of the bacteria associated with the culture which could play a role in the recovery.

Globally, the obtained results of this part of PhD project, contribute to the bioprospecting of the cryopreservation technique for some diatom species. The development of cryopreservation strategies would be useful both in biotechnological applications as well as in ecological fields such as germplasm conservation also in light of climate changes.

3.6 References

Ali, P., Fucich, D., Shah, A., Hasan, F., & Chen, F. 2021. Cryopreservation of cyanobacteria and eukaryotic microalgae using exopolysaccharide extracted from a glacier bacterium. Microorganisms, 9(2), 395. https://doi.org/10.3390/microorganisms9020395;

Alipanah, L., Winge, P., Rohloff, J., Najafi, J., & Bones, A. M. 2015. Molecular and cellular responses to nitrogen and phosphorus deficiency in diatoms. Plant Physiology, 167(2), 367–385. https://doi.org/10.1371/journal.pone.0193335;

Anchordoguy, T. J., Carpenter, J. F., Crowe, J. H., and Crowe, L. M. 1992. Temperature-dependent perturbation of phospholipid bilayers by dimethylsulfoxide. Biochim. Biophys. https://doi.org/10.1016/0005-2736(92)90139-d;

Annunziata, R., Mele, B., Marotta, P., Volpe, M., Entrambasaguas, L., Mager, S., … & Ferrante, M. 2022. Trade-off between sex and growth in diatoms: molecular mechanisms and demographic implications. Science Advances, 8(3). https://doi.org/10.1126/sciadv.abj9466;

Avrahami, Y., Koplovitz, G., Frada M. J. 2024. Diatom community shifts across oligotrophic-eutrophic seasonal gradients and bloom variability as a function of mixing depth in the subtropical Northern Red Sea. bioRxiv 2024.04.17.589857; doi: https://doi.org/10.1101/2024.04.17.589857;

Ben-Amotz, A. Gilboa. 1980. Cryopreservation of marine unicellular algae. I. A survey of algae with regard to size, culture age, photosynthetic activity and chlorophyll-to-cell ratio, Mar. Ecol. Prog. Ser. 2 157–161;

Bender, S., Durkin, C., Berthiaume, C., Morales, R., & Armbrust, E. 2014. Transcriptional responses of three model diatoms to nitrate limitation of growth. Frontiers in Marine Science, 1. https://doi.org/10.3389/fmars.2014.00003;

Berges, J. A., & Falkowski, P. G. 1998. Physiological stress and cell death in marine phytoplankton: Induction of proteases in response to nitrogen or light limitation. Limnology and Oceanography, 43(1), 129–135. https://doi.org/10.4319/lo.1998.43.1.0129;

Bilcke, G., Berge, K., Decker, S., Bonneure, E., Poulsen, N., Bulánková, P., … & Vyverman, W. 2020. Mating type specific transcriptomic response to sex inducing pheromone in the pennate diatom *Seminavis robusta*. ISME J 15, 562–576 https://doi.org/10.1101/2020.03.16.987719;

Bodas K, Brennig C, Diller KR, Brand JJ. 1995. Cryopreservation of blue-green and eukaryotic algae in the culture collection at the University of Texas at Austin. Cryo-Letters 16: 267-274;

Booth BC, Larouche P, Bélanger S, Klein B, Amiel D, Mei ZP. 2002. Dynamics of *Chaetoceros socialis* blooms in the North Water. Deep Sea Res. Part II Top. Stud. Oceanogr. 49: 5003–5025. https://doi.org/10.1016/S0967-0645(02)00175-3;

Boroda, A. V., Aizdaicher, N. A. & Odintsova, N. A. 2014. The influence of ultra-low temperatures on marine microalgal cells. J. Appl. Phycol. 26, 387–397. https://doi.org/10.1007/s10811-013-0093-5;

Bowler, C., Vardi, A., & Allen, A. E. 2010. Oceanographic and biogeochemical insights from diatom genomes. Annual Review of Marine Science, 2(1), 333-365. https://doi.org/10.1146/annurev-marine-120308-081051;

Buhmann, M., Day, J., & Kroth, P. 2013. Post-cryopreservation viability of the benthic freshwater diatom *Planothidium frequentissimum* depends on light levels. Cryobiology, 67(1), 23-29. https://doi.org/10.1016/j.cryobiol.2013.04.005;

Bui, T., Ross, I., Jakob, G., & Hankamer, B. 2013. Impact of procedural steps and cryopreservation agents in the cryopreservation of chlorophyte microalgae. Plos One, 8(11), e78668. https://doi.org/10.1371/journal.pone.0078668;

Bulankova P, Sekulić M, Jallet D, Nef C, van Oosterhout C, Delmont TO, Vercauteren I, Osuna-Cruz CM, Vancaester E, Mock T, Sabbe K, Daboussi F, Bowler C, Vyverman W, Vandepoele K, De Veylder L. 2021. Mitotic recombination between homologous chromosomes drives genomic diversity in diatoms. Curr Biol. 9;31(15):3221-3232.e9. https://doi.org/10.1016/j.cub.2021.05.013;

Canavate JP, Lubian LM. 1995. Relationship between cooling rates, cryoprotectant concentrations and salinities in the cryopreservation of marine microalgae. Mar Biol;124: 325–334;

Chekanov, K., Vasilieva, S., Solovchenko, A., & Лобакова, Е. 2018. Reduction of photosynthetic apparatus plays a key role in survival of the microalga *Haematococcus pluvialis* (*Chlorophyceae*) at freezing temperatures. Photosynthetica, 56(4), 1268-1277. https://doi.org/10.1007/s11099-018-0841-5;

Chong, G., Tsai, S., Wang, L., Huang, C., & Lin, C. 2016. Cryopreservation of the gorgonian endosymbiont symbiodinium. Scientific Reports, 6(1). https://doi.org/10.1038/srep18816;

Cirri, E., Vyverman, W., & Pohnert, G. 2018. Biofilm interactions—bacteria modulate sexual reproduction success of the diatom *Seminavis robusta*. Fems Microbiology Ecology, 94(11). https://doi.org/10.1093/femsec/fiy161;

Cutignano, A., Conte, M., Tirino, V., Del Vecchio, V., De Angelis, R., Nebbioso, A., ... & Romano, G. 2022. Cytotoxic Potential of the Marine Diatom *Thalassiosira rotula*: Insights into Bioactivity of 24-Methylene Cholesterol. Marine Drugs, 20(10), 595. https://doi.org/10.3390/md20100595;

Day, JG, McClellan MR. 1995. Cryopreservation and freeze-drying protocols. Methods in Molecular Biology vol 38. Humana Press, Totowa, New Jersey, 245 pp;

Day, JG, DeVille M. 1995. Cryopreservation of algae. In: Day JG, McLellan MR (eds) Cryopreservation and freeze-drying protocols. Methods in Molecular Biology, 38. Humana, Totowa, USA, pp 81–89;

Day, JG. 1998. Cryoconservation of microalgae and cyanobacteria. CryoLetters 1:7–14;

Day, J. G. 2007. Cryopreservation of microalgae and cyanobacteria. Cryopreservation and freeze-drying protocols;

Day, John G., e Roland A. Fleck. 2015. Cryo-Injury in Algae and the Implications This Has to the Conservation of Micro-Algae. Microalgae Biotechnology 1. https://doi.org/10.1515/micbi-2015-0001;

Day, J. G., Tytor, S., Egardt, J., Applegren, M., Rad-Menéndez, C., Chepurnova, O., ... & Godhe, A. 2017. Challenges for the maintenance and cryopreservation of multiple isolates of model microorganisms: An example using the marine diatom *Skeletonema marinoi*. Biopreservation and Biobanking, 15(3), 191-202. https://doi.org/10.1089/bio.2016.0026;

Degerlund M, Eilertsen HC. 2010. Main species characteristics of phytoplankton spring blooms in NE Atlantic and Arctic waters (68–80°N). Estuaries Coast; 33: 242–269. https://doi.org/10.1007/s12237-009-9167-7;

Demirel, Z., İmamoğlu, E., Deniz, İ., & Dalay, M. 2018. Optimization of cryopreservation process using response surface methodology for *Chlorella saccharophila* and *Chlorella zofingiensis*. Celal Bayar Üniversitesi Fen Bilimleri Dergisi, 14(4), 405-412. https://doi.org/10.18466/cbayarfbe.426444;

Deniz, I., Demirel, Z., Imamoglu, E., & Dalay, M. 2022. Long-term storage of microalgae: determination of optimum cryopreservation conditions. Journal of the Marine Biological Association of the United Kingdom, 102(3-4), 276-284. https://doi.org/10.1017/s0025315422000479;

Di Dato, V., Di Costanzo, F., Barbarinaldi, R., Perna, A., Ianora, A., & Romano, G. 2019. Unveiling the presence of biosynthetic pathways for bioactive compounds in the *Thalassiosira rotula* transcriptome. Scientific Reports, 9(1), 9893. https://doi.org/10.1038/s41598-019-46276-8;

Díaz-Tena, E., Barona, A., Gurtubay, L., Rodríguez-Ezquerro, A., Lacalle, L., Oyanguren, I., … & Ηλίας, A. 2016. Biomachining: preservation of *Acidithiobacillus ferrooxidans* and treatment of the liquid residue. Engineering in Life Sciences, 17(4), 382-391. https://doi.org/10.1002/elsc.201600124;

Ellegaard, M., & Ribeiro, S. 2018. The long-term persistence of phytoplankton resting stages in aquatic 'seed banks'. Biological reviews of the Cambridge Philosophical Society, 93(1), 166–183. https://doi.org/10.1111/brv.12338;

Elliott, G. D.; Wang, S.; Fuller, B. J. 2017. Cryoprotectants: A Review of the Actions and Applications of Cryoprotective Solutes That Modulate Cell Recovery from Ultra-Low Temperatures. Cryobiology 2017, 76,74−91. https://doi.org/10.1016/j.cryobiol.2017.04.004;

Falciatore, A., Jaubert, M., Bouly, J. P., Bailleul, B., & Mock, T. 2020. Diatom molecular research comes of age: model species for studying phytoplankton biology and diversity. The Plant Cell, 32(3), 547-572. https://doi.org/10.1105/tpc.19.00158;

Falkowski PG, Barber RT, Smetacek V. 1998. Biogeochemical controls and feedback on ocean primary production. Science 281(5374):200–207. https://doi.org/10.1126/science.281.5374.200;

Falkowski PG. 2002. The ocean's invisible forest. Sci Am 287(2):54–61. https://doi.org/10.1038/scientificamerican0802-54;

Falkowski, P. G. & Oliver, M. J. 2007. Mix and match: how climate selects phytoplankton. Nature Reviews Microbiology 5: 813–819. https://doi.org/10.1038/nrmicro1751;

Field, CB, Behrenfeld, MJ, Randerson, JT, Falkowski, P. 1998. Primary production of the biosphere: Integrating terrestrial and oceanic components. Science 281(5374): 237–240. https://doi.org/10.1126/science.281.5374.237;

Fleck, RA, Pickup, RW, Day, JG, Benson, EE. 2006. Characterisation of cryoinjury in *Euglena gracilis* using flow-cytometry and cryomicroscopy. Cryobiology 52: 261-268.https://doi.org/10.1016/j.cryobiol.2005.12.003;

Fleck, R. A., Benson, E. E., Bremner, D. H., & Day, J. G. 2000. Studies of free radical-mediated cryoinjury in the unicellular green alga *Euglena gracilis* using a non-destructive hydroxyl radical assay: a novel approach for developing protistan cryopreservation strategies. Free Radical Research, 32(2), 157-170. https://doi.org/10.1080/10715760000300161;

Foo, S. C., Mok, C. Y., Ho, S. Y., & Khong, N. M. 2023. Microalgal culture preservation: Progress, trends and future developments. Algal Research, 71, 103007. https://doi.org/10.1016/j.algal.2023.103007;

French, F. W., & Hargraves, P. E. 1980. Physiological characteristics of plankton diatom resting spores. Marine Biology Letters, 1, 185–195;

Frleta Matas, R., Radman, S., Čagalj, M., & Šimat, V. 2024. Influence of Nutrient Deprivation on the Antioxidant Capacity and Chemical Profile of Two Diatoms from Genus *Chaetoceros*. Marine Drugs, 22(2), 96. https://doi.org/10.3390/md22020096;

Gaonkar, C., Kooistra, W., Lange, C., Montresor, M., & Sarno, D. 2017. Two new species in the *Chaetoceros socialis* complex (Bacillariophyta): *C. sporotruncatus* and *C. dichatoensis*, and characterization of its relatives, *C. radicans* and *C. cinctus*. Journal of Phycology, 53(4), 889-907. https://doi.org/10.1111/jpy.12554;

Godhe, A., & Rynearson, T. 2017. The role of intraspecific variation in the ecological and evolutionary success of diatoms in changing environments. Philosophical transactions of the Royal Society of London. Series B, Biological sciences, 372(1728), 20160399. https://doi.org/10.1098/rstb.2016.0399;

Gwo, J., Twan, W., & Lin, S. 2023. Cryopreservation of six marine microalgae used in taiwanese aquaculture. Journal of the World Aquaculture Society, 54(5), 1235-1246. https://doi.org/10.1111/jwas.12957;

Hargraves, P. E., & French, F. W. 1983. Diatom resting spores: significance and strategies for survival. Limnology and Oceanography, 28(6), 1103–1115;

Hejduková, Eva, e Linda Nedbalová. 2021. Experimental Freezing of Freshwater Pennate Diatoms from Polar Habitats. Protoplasma 258: 1213–29. https://doi.org/10.1007/s00709-021-01648-8;

Hildebrand, M., Davis, A., Abbriano, R., Pugsley, H. R., Traller, J. C., Smith, S. R., ... & Alderete, B. 2016. Applications of imaging flow cytometry for microalgae. Imaging Flow Cytometry: Methods and Protocols, 47-67. https://doi.org/10.1016/j.cryobiol.2013.04.005;

J. Elster, J. Lukavsky, K. Harding, E.E. Benson, J.G. Day. 2008. Deployment of the encapsulation/dehydration protocol to cryopreserve polar microalgae held at the Czech Republic Academy of Sciences Institute of Botany. CryoLetters 29, 27–28;

Jewson, D., Granin, N., Zhdanov, A., Gorbunova, L., Бондаренко, Н., & Gnatovsky, R. 2008. Resting stages and ecology of the planktonic diatom *Aulacoseira skvortzowii* in

lake baikal. Limnology and Oceanography, 53(3), 1125-1136. https://doi.org/10.4319/lo.2008.53.3.1125;

Kapoore, R., Huete-Ortega, M., Day, J., Okurowska, K., Slocombe, S., Stanley, M., … & Vaidyanathan, S. 2019. Effects of cryopreservation on viability and functional stability of an industrially relevant alga. Scientific Reports, 9(1). https://doi.org/10.1038/s41598-019-38588-6;

Kim, S., Lee, J., Hur, Y., Lee, C., Park, S., & Koo, B. 2017. Marine antifreeze proteins: structure, function, and application to cryopreservation as a potential cryoprotectant. Marine Drugs, 15(2), 27. https://doi.org/10.3390/md15020027;

Koh, H., Lee, J., Han, S., Park, H., & Lee, S. 2014. Effect of the antifreeze protein from the arctic yeast *Leucosporidium* sp. AY30 on cryopreservation of the marine diatom *Phaeodactylum tricornutum*. Applied Biochemistry and Biotechnology, 175(2), 677-686. https://doi.org/10.1007/s12010-014-1337-9;

Kouzuma, A. & Watanabe, K. 2015. Exploring the potential of algae/bacteria interactions. Curr. Opin. Biotechnol. 33, 125–129. https://doi.org/10.1016/j.copbio.2015.02.007

Krause, J., Schulz, I., Rowe, K., Dobbins, W., Winding, M., Sejr, M., … & Agustí, S. 2019. Silicic acid limitation drives bloom termination and potential carbon sequestration in an Arctic bloom. Scientific Reports, 9(1). https://doi.org/10.1038/s41598-019-44587-4;

Kudo, I., Yoshimura, T., Yanada, M., & Matsunaga, K. 2000. Exhaustion of nitrate terminates a phytoplankton bloom in Funka Bay, Japan: change in SiO4:NO3consumption rate during the bloom. Marine Ecology Progress Series, 193, 45-51. https://doi.org/10.3354/meps193045;

Kusumaningtyas, P., Nurbaiti, S., Suantika, G., Amran, M. B., & Nurachman, Z. 2017. Enhanced oil production by the tropical marine diatom *Thalassiosira* sp. cultivated in outdoor photobioreactors. Applied Biochemistry and Biotechnology, 182, 1605-1618.;

Kuwano K, Saga N. 2000. Cryopreservation of marine algae: Applications in Biotechnology. In: Fingerman M, Nagabhushaman R(eds) Recent advances in marine biotechnology, Volume 4: Aquaculture. Science, New Hampshire, pp 23–40;

Kuwata, A., & Takahashi, M. 1999. Survival and recovery of resting spores and resting cells of *Chaetoceros pseudocurvisetus* (Bacillariophyceae) in sediments of Otsuchi Bay, Northeastern Japan. Journal of Phycology, 35(5), 919–923;

Kuwata, A., Takahashi, M., & Hara, Y. 1993. Comparison of the effects of nitrogen or silicon limitation on the growth and morphology of the marine planktonic diatom *Thalassiosira nordenskioeldii* Cleve. Marine Biology, 115(4), 629–634;

Leiva, J. and Dupré, E. 2011. Cryopreservation of the microalgae *Chaetoceros calcitrans* (Paulsen): analysis of the effect of DMSO temperature and light regime during different equilibrium periods. Latin American Journal of Aquatic Research, 39(2), 271-279. https://doi.org/10.3856/vol39-issue2-fulltext-8;

Litchman, E. 2022. Trait-based diatom ecology. In The molecular life of diatoms (pp. 3-27). Cham: Springer International Publishing;

Liu, M., Zhang, X., Guo, H., Zhu, Y., Wen, C., Sui, X., … & Zhang, L. 2019. DMSO-free cryopreservation of chondrocytes based on zwitterionic molecule and polymers. Biomacromolecules. https://doi.org/10.1021/acs.biomac.9b01024;

Lukesova A., Hrouzek P., Harding K., Benson E.E., Day J.G. 2008. Deployment of the encapsulation/dehydration protocol to cryopreserve diverse microalgae held at the Institute of Soil Biology, Academy of Sciences of the Czech Republic, CryoLetters 29,

21–26;

Marañón, E. 2015. Cell size as a key determinant of phytoplankton metabolism and community structure. Annual Review of Marine Science, 7(1), 241-264. https://doi.org/10.1146/annurev-marine-010814-015955;

Marella, T. K., & Tiwari, A. 2020. Marine diatom *Thalassiosira weissflogii* based biorefinery for co-production of eicosapentaenoic acid and fucoxanthin. Bioresource technology, 307, 123245. https://doi.org/10.1016/j.biortech.2020.123245;

Matas, R. F., Popović, M., Čagalj, M., & Šimat, V. 2023. The marine diatom *Thalassiosira rotula*: chemical profile and antioxidant activity of hydroalcoholic extracts. Frontiers in Marine Science. https://doi.org/10.3389/fmars.2023.1221417;

Matsumura, K.; Hayashi, F.; Nagashima, T.; Hyon, S. H. Long-Term Cryopreservation of Human Mesenchymal Stem Cells Using Carboxylated Poly-l-Lysine without the Addition of Proteins or Dimethyl Sulfoxide. J. Biomater. Sci., Polym. Ed. 2013, 24 (12), 1484− 1497;

McLellan MR. 1989. Cryopreservation of diatoms. Diatom Res., 4:301–318;

McQuoid, M. R., & Hobson, L. A. 1996. Diatom resting stages. Journal of Phycology, 32(6), 889–902;

Mehmood, M. 2023. Stress factors affecting the cryopreservation of biological components of seed virus for avian influenza vaccine production. International Journal of Biology, 15(1), 58. https://doi.org/10.5539/ijb.v15n1p58;

Michel, C., Gosselin, M., & Nozais, C. 2002. Preferential sinking export of biogenic silica during the spring and summer in the north water polynya (Northern Baffin Bay): temperature or biological control?. Journal of Geophysical Research Atmospheres, 107(C7). https://doi.org/10.1029/2000jc000408;

Mishra, B., Saxena, A., & Tiwari, A. 2020. Biosynthesis of silver nanoparticles from marine diatoms *Chaetoceros* sp., *Skeletonema* sp., *Thalassiosira* sp., and their antibacterial study. Biotechnology Reports, 28, e00571. https://doi.org/10.1016/j.btre.2020.e00571;

Mitbavkar, S., & Anil, A. C. 2006. Cell damage and recovery in cryopreserved microphytobenthic diatoms. Cryobiology, 53(1), 143-147. https://doi.org/10.1016/j.cryobiol.2006.05.002;

Montresor, M., Di Prisco, C., Sarno, D., Margiotta, F., & Zingone, A. 2013. Diversity and germination patterns of diatom resting stages at a coastal Mediterranean site. Marine Ecology Progress Series, 484, 79-95. https://doi.org/10.3354/meps10236;

Mock, T., Otillar, R., Strauss, J. *et al.* 2017. Evolutionary genomics of the cold-adapted diatom *Fragilariopsis cylindrus*. Nature 541, 536–540. https://doi.org/10.1038/nature20803;

Moreno, M., Ma, K., Schoenung, J., & Dávila, L. 2015. An integrated approach for probing the structure and mechanical properties of diatoms: toward engineered nanotemplates. Acta Biomaterialia, 25, 313-324. https://doi.org/10.1016/j.actbio.2015.07.028;

Morris, G.J., 1978. Cryopreservation of 250 strains of *Chlorococcales* by the method of two-step cooling. Brit. Phycol. J. 13, 15–24. https://doi.org/10.1080/00071617800650031;

Morschett, H., Reich, S., Wiechert, W., & Oldiges, M. 2016. Simplified cryopreservation of the microalga *Chlorella vulgaris* integrating a novel concept for cell viability estimation. Engineering in Life Sciences, 16(1), 36-44. https://doi.org/10.1002/elsc.201500056;

Mouget, J., Gastineau, R., Давидович, O., Gaudin, P., & Давидович, H. 2009. Light is a key factor in triggering sexual reproduction in the pennate diatom *Haslea ostrearia*. Fems Microbiology Ecology, 69(2), 194-201. https://doi.org/10.1111/j.1574-6941.2009.00700.x;

Nakanishi, K., Deuchi, K. & Kuwano, K. 2012. Cryopreservation of four valuable strains of microalgae, including viability and characteristics during 15 years of cryostorage. J Appl Phycol 24, 1381–1385. https://doi.org/10.1007/s10811-012-9790-8;

Oku, O., & Kamatani, A. 1995. Resting spore formation and phosphorus composition of marine diatom *Thalassiosira nordenskioeldii* in culture. Marine Biology, 123(3), 393–399;

Paredes, E., A. Ward, I. Probert, L. Gouhier, and C. N. Campbell. 2021. Cryopreservation of Algae. Cryopreservation and Freeze-Drying Protocols. Ed. by W. F. Wolkers and H. Oldenhof. Methods in Molecular Biology. New York, NY: Springer US, 607–621. doi: 10.1007/978-1-0716-0783-1_32;

Passy, S. I. 2007. Diatom ecological guilds display distinct and predictable behavior along nutrient and disturbance gradients in running waters. Aquatic botany, 86(2), 171-178. https://doi.org/10.1016/j.aquabot.2006.09.018;

Paul, C., & Pohnert, G. 2011. Interactions of the algicidal bacterium *Kordia algicida* with diatoms: regulated protease excretion for specific algal lysis. PloS one, 6(6), e21032. https://doi.org/10.1371/journal.pone.0021032;

Pelusi, A., Santelia, M. E., Benvenuto, G., Godhe, A., & Montresor, M. 2020. The diatom *Chaetoceros socialis*: spore formation and preservation. European Journal of Phycology, 55(1), 1-10. https://doi.org/10.1080/09670262.2019.1632935;

Pelusi, A., Margiotta, F., Passarelli, A., Ferrante, M., d'Alcalà, M., & Montresor, M. 2020. Density-dependent mechanisms regulate spore formation in the diatom

Chaetoceros socialis. Limnology and Oceanography Letters, 5(5), 371-378. https://doi.org/10.1002/lol2.10159;

Piasecki, B. P., Diller, K. R., & Brand, J. J. 2009. Cryopreservation of *Chlamydomonas reinhardtii*: a cause of low viability at high cell density. Cryobiology, 58(1), 103-109. https://doi.org/10.1016/j.cryobiol.2008.11.001;

Piredda, R., Tomasino, M. P., D'erchia, A. M., Manzari, C., Pesole, G., Montresor, M., ... & Zingone, A. 2017. Diversity and temporal patterns of planktonic protist assemblages at a Mediterranean Long Term Ecological Research site. FEMS Microbiology Ecology, 93(1), fiw200. https://doi.org/10.1093/femsec/fiw200;

Rembauville, M., Blain, S., Armand, L., Quéguiner, B., & Salter, I. 2015. Export fluxes in a naturally iron-fertilized area of the Southern Ocean – part 2: importance of diatom resting spores and faecal pellets for export. Biogeosciences, 12(11), 3171-3195. https://doi.org/10.5194/bg-12-3171-2015;

Rembauville, M., Manno, C., Tarling, G., Blain, S., & Salter, I. 2016. Strong contribution of diatom resting spores to deep-sea carbon transfer in naturally iron-fertilized waters downstream of South Georgia. Deep Sea Research Part I Oceanographic Research Papers, 115, 22-35. https://doi.org/10.1016/j.dsr.2016.05.002;

Rhodes, L., Smith, J., Tervit, R., Roberts, R., Adamson, J., Adams, S., & Decker, M. 2006. Cryopreservation of economically valuable marine micro-algae in the classes Bacillariophyceae, Chlorophyceae, Cyanophyceae, Dinophyceae, Haptophyceae, Prasinophyceae, and Rhodophyceae. Cryobiology, 52(1), 152-156. https://doi.org/10.1016/j.cryobiol.2005.10.003;

Rimac, V. 2023. The impact of cryoprotectant exposure time on post-thaw viability of autologous and allogeneic hematopoietic stem cells and leukocyte subpopulations. Acta Pharmaceutica, 73(4), 655-672. https://doi.org/10.2478/acph-2023-0037;

Romero, O., Kim, J., Bárcena, M., Hall, I., & Schneider, R. 2015. High-latitude forcing of diatom productivity in the southern agulhas plateau during the past 350 kyr. Paleoceanography, 30(2), 118-132. https://doi.org/10.1002/2014pa002636;

Saadaoui, I., Emadi, M., Bounnit, T., Schipper, K., & Jabri, H. 2015. Cryopreservation of microalgae from desert environments of Qatar. Journal of Applied Phycology, 28(4), 2233-2240. https://doi.org/10.1007/s10811-015-0743-x;

Sabbe, K., Chepurnov, V., Vyverman, W., & Mann, D. 2004. *Apomixis inachnanthes* (Bacillariophyceae); development of a model system for diatom reproductive biology. European Journal of Phycology, 39(3), 327-341. https://doi.org/10.1080/0967026042000236445;

Sanyal, A., Larsson, J., Andrén, T., Moros, M., Lönn, M., & Andrén, E. 2021. Not dead yet: Diatom resting spores can survive in nature for several millennia. American Journal of Botany, 109(1), 67-82;

Sharma N, Simon DP, Diaz-Garza AM, Fantino E, Messaabi A, Meddeb-Mouelhi F, Germain H and Desgagné-Penix I. 2021. Diatoms Biotechnology: Various Industrial Applications for a Greener Tomorrow. Front. Mar. Sci. 8:636613;

Sicko-Goad, L., Schelske, C. L., & Stoermer, E. F. 1986. Estimation of intracellular carbon and silica content of diatoms from natural assemblages using morphometric techniques. Limnology and Oceanography, 31(5), 882–895;

Silva, H., Silva, F., Prete, C., Hoshino, R., Faria, R., Mantovani, M., … & Guedes, C. 2020. Cryopreservation of *Chlorella vulgaris* using different cryoprotectant agents. Journal of Agricultural Science, 12(7), 75. https://doi.org/10.5539/jas.v12n7p75;

Souffreau, C., Vanormelingen, P., Sabbe, K. & Vyverman, W. 2013. Tolerance of resting cells of freshwater and terrestrial benthic diatoms to experimental desiccation and freezing is habitat-dependent. Phycologia 52, 246–255. https://doi.org/10.2216/12-087.1.

Souffreau, C., Vanormelingen, P., Verleyen, E., Sabbe, K. & Vyverman, W. 2010. Tolerance of benthic diatoms from temperate aquatic and terrestrial habitats to experimental desiccation and temperature stress. Phycologia 49, 309–324. https://doi.org/10.2216/09-30.1;

Sournia A. 1974. Circadian periodicities in natural populations of marine phytoplankton. Adv Mar Biol 12:325–389;

Stanish, L., Nemergut, D., & McKnight, D. 2011. Hydrologic processes influence diatom community composition in dry valley streams. Journal of the North American Benthological Society, 30(4), 1057-1073. https://doi.org/10.1899/11-008.1;

Stock, W., Pinseel, E., Decker, S., Sefbom, J., Blommaert, L., Chepurnova, O., … & Vyverman, W. 2018. Expanding the toolbox for cryopreservation of marine and freshwater diatoms. Scientific Reports, 8(1). https://doi.org/10.1038/s41598-018-22460-0;

Sugie, K., & Kuma, K. 2008. Resting spore formation of nutrient-depleted coastal diatoms during the spring bloom in the Oyashio region of the Western Subarctic Pacific. Marine Ecology Progress Series, 354, 43–55;

Svensson, F., Norberg, J., & Snoeijs, P. 2014. Diatom cell size, coloniality and motility: trade-offs between temperature, salinity and nutrient supply with climate change. PloS one, 9(10), e109993. https://doi.org/10.1371/journal.pone.0109993;

Tanniou, A., Turpin, V., & Lebeau, T. 2012. Comparison of cryopreservation methods for the long term storage of the marine diatom *Haslea ostrearia* (Simonsen). Cryobiology, 65(1), 45-50. https://doi.org/10.1016/j.cryobiol.2012.03.011;

Taylor R, Fletcher RL. 1998. Cryopreservation of eukaryotic algae—a review of methodologies. J Appl Phycol 10:481–501;

Whaley, D., Damyar, K., Witek, R., Mendoza, A., Alexander, M., & Lakey, J. 2021. Cryopreservation: an overview of principles and cell-specific considerations. Cell Transplantation, 30. https://doi.org/10.1177/0963689721999617;

Xu, H., Shi, Z., Zhang, X., Pang, M., Pan, K., & Liu, H. 2021. Diatom frustules with different silica contents affect copepod grazing due to differences in the nanoscale mechanical properties. Limnology and Oceanography, 66(9), 3408-3420. https://doi.org/10.1002/lno.11887;

Yee, J. C., & Yang, H. 2023. Cryopreservation of *Tetraselmis striata* through systematic evaluation of multiple parameters in the cooling process. Aquaculture, 566, 739172. https://doi.org/10.1016/j.aquaculture.2022.739172;

Yi, X., Min-xia, L., Luo, Q., Zhuo, H., Cao, H., Wang, J., … & Han, Y. 2017. Toxic effects of dimethyl sulfoxide on red blood cells, platelets, and vascular endothelial cells in vitro. Febs Open Bio, 7(4), 485-494. https://doi.org/10.1002/2211-5463.12193;

Zhang, Q., Cong, Y., Qu, S., Luo, S., Li, X., & Tang, X. 2007. A simple and highly efficient method for the cryopreservation *Oflaminaria japonica* (Phaeophyceae) germplasm. European Journal of Phycology, 42(2), 209-213. https://doi.org/10.1080/09670260701261778;

Zhou, D., Shen, X., Gu, Y., Zhang, N., Li, T., Wu, X., … & Lei, L. 2014. Effects of dimethyl sulfoxide on asymmetric division and cytokinesis in mouse oocytes. BMC Developmental Biology, 14(1). https://doi.org/10.1186/1471-213x-14-28;

Zhukova, N. and Aizdaicher, N. 2001. Lipid and fatty acid composition during vegetative and resting stages of the marine diatom *Chaetoceros salsugineus*. Botanica Marina, 44(3). https://doi.org/10.1515/bot.2001.037;

Zingone, A., Montresor, M., & Marino, D. 1990. Summer phytoplankton physiognomy in coastal waters of the Gulf of Naples. Marine Ecology, 11(2), 157-172;

Zingone, A., Casotti, R., d'Alcala, M. R., Scardi, M., & Marino, D. 1995. ‘St Martin's Summer’: the case of an autumn phytoplankton bloom in the Gulf of Naples (Mediterranean Sea). Journal of Plankton Research, 17(3), 575-593;

Zingone, A., Phlips, E. J., & Harrison, P. J. 2010. Multiscale variability of twenty-two coastal phytoplankton time series: a global scale comparison. Estuaries and Coasts, 33, 224-229. https://doi.org/10.1007/s12237-009-9261-x.

La borsa di dottorato è stata cofinanziata con risorse del
Programma Operativo Nazionale Ricerca e Innovazione 2014-202 (CCI 2014IT16M2OP005)
Fondo Sociale Europeo, Azione I.1 “Dottorati Innovativi con caratterizzazione Industriale”

CHAPTER IV

Conclusions and future perspectives

This Ph.D. thesis underscores the multifaceted potential of diatoms as a biotechnological resource and provides critical insights into their utilization for high-value compound production and long-term preservation. The research investigated two interlinked objectives: enhancing fucoxanthin production in *Thalassiosira rotula* and optimizing cryopreservation methods for diverse diatom species.

Notably, *Thalassiosira rotula* as a candidate for industrial-scale applications and bioreactor production, was related to the significant ability in the fucoxanthin (Fx) production. Compared to other species such as *Skeletonema costatum*, *Odontella sinensis*, *Nitzschia laevis*, *Chaetoceros gracilis* and *calcitrans*, the *T. rotula* strain investigated in this work, exhibited the highest fucoxanthin content, indicating its strong potential for commercial applications.
This results further show that high nitrogen (HN) treatments significantly enhanced both the biomass and morphophysiological traits of *T. rotula*, with the key advantage being the stabilization of fucoxanthin content throughout the growth cycle, crucial for industrial processes in product quality view.
Moreover, Low light (LL) conditions also played a significant role, leading to a notable increase in fucoxanthin production. However, this was associated with a decrease in cell density and biomass, highlighting the need to balance pigment yield optimization with biomass productivity. These findings underscore the importance of carefully managing cultivation parameters to maximize pigment output without compromising overall biomass.

Additionally, this research investigated on the critical role of specific genes involved in the biosynthetic pathway of fucoxanthin. Identifying and analysing these genes provides knowledge for potential genetic engineering strategies aimed at improving *T. rotula*'s efficiency as a biofactory for fucoxanthin production.

Future studies targeting these genes could elucidate their precise functions and adaptability to environmental changes, paving the way for advanced methods to enhance pigment yields.

The results obtained in this study underscore the promise of *T. rotula* in biotechnological applications, but also highlights the critical role of standard cultivation methods in maximizing its value.

In light of this, this research advances understanding of diatom cryopreservation, highlighting the influence of structural, physiological, and environmental factors on post-thaw survival and regrowth. In collaborations with Ghent University and the BCCM Diatom Culture Collection, the exploration of innovative techniques extended the scope of this research.

By examining five diatom species with diverse ecological and morphophysiological traits, the study emphasizes the importance of species-specific cryopreservation protocols, including equilibration times, freezing methods, and cell stages. Spores of *Chaetoceros socialis* and *C. costatus* revealed greater tolerance to cryopreservation stress compared to vegetative cells, showcasing their resilience and potential for broader biotechnological and ecological applications. Key findings identified traits such as smaller cell size and high chlorophyll fluorescence intensity as contributors to improved cryopreservation outcomes. Using imaging flow cytometry (iFCM), this study revealed that single-cell diatoms adapt better to cryopreservation stress than colony-forming cells. These observations underline the inherent metabolic activity and resilience of smaller diatoms and spore stages post-thaw.

The research also notes the potential role of bacteria associated with diatom cultures in recovery, warranting further investigation. Overall, the findings contribute to advancing cryopreservation techniques for diatom species, with implications for biotechnological applications and ecological germplasm conservation in the context of climate change.

La borsa di dottorato è stata cofinanziata con risorse del
Programma Operativo Nazionale Ricerca e Innovazione 2014-202 (CCI 2014IT16M2OP005)
Fondo Sociale Europeo, Azione I.1 "Dottorati Innovativi con caratterizzazione Industriale"

APPENDIX

In these three years of my research, I had the opportunity to contribute in several ongoing projects within my laboratory, resulting in the publications on various topics. One major focus in my research group was investigating the effects of the different compounds, particularly the heavy metal cadmium (Cd), on the Root Apical Meristem (RAM) and Root System (RS) (Manuscripts 1, 2).

1. Araniti, F.*, Talarico, E.*, **Madeo, M. L.,** Greco, E., Minervino, M., Álvarez-Rodríguez, S., Muto, A., Ferrari, M., Chiappetta, A., Bruno, L. 2023. Short-term exposition to acute cadmium toxicity induces the loss of root gravitropic stimuli perception through PIN2-mediated auxin redistribution in *Arabidopsis thaliana* (L.) Heynh. Plant Science, 332, 111726.
    a. *Equally contributed

2. López-González, D., Bruno, L., Díaz-Tielas, C., Lupini, A., Aci, M.M., Talarico, E., **Madeo, M.L.,** Muto, A., Sánchez-Moreiras, A.M., Araniti, F. 2023. Short-term effects of *trans*-cinnamic acid on the metabolism of *Zea mays* L. Roots. Plants, 12, 189.

In Manuscript 1 (Araniti *et al.*, 2023) I evaluated the impact of a short-term acute cadmium exposure on *Arabidopsis thaliana* seedlings, using medium supplemented with 100 µM and 150 µM Cd and in different time points. Various analyses, including morpho-histological, molecular, pharmacological, and metabolomics studies, were conducted. Using marker lines with GFP-tagged constructs, it was observed that Cd exposure induced early cell differentiation, marked by a reduction in the transition zone and increased Reactive Oxygen Species (ROS) production, such as hydrogen peroxide (H_2O_2). Cd affected microtubule orientation, cell expansion in the transition zone, and altered auxin distribution by impacting the PINFORMED (PIN) family, particularly PIN2. In this paper, I contributed to the *in vitro* culture, morpho-histological and confocal microscopy experiments.

In Manuscript 2 (López-González *et al.*, 2023), *trans*-cinnamic acid, a phenolic compound, was added to the hydroponic culture of maize to evaluate its impact on the vascular bundle elements and metabolic processes in the roots. Following a brief exposure (6 to 24 hours) at a high concentration (103 μM), a decrease in several amino acids' levels was noted, likely resulting from modified nitrogen absorption. Following 48 hours of exposure, trans-cinnamic acid appeared to trigger an alteration in lignin and galactose metabolism. My contribution is related to the *in vitro* culture and confocal microscopy analysis.

Additionally, research carried on in my group is related to the fruit quality (FRUITY) project aims to enhance the understanding of post-harvest storage conditions of fruit, to improve sensorial and internal quality of fruit throughout the supply chain.

3. Franzoni, G.*, Muto, A.*, Bruno, L., **Madeo, M. L.**, Sirangelo, T. M., Ceverista Chiappetta, A. A., Bitonti, M. B., Müller, C. T., Ferrante, A., Rogers, H. J., & Spadafora, N. D. (2024). Identification of potential molecular markers for detection of lengthy chilled storage of Prunus persica L. Fruit. Heliyon, 10(24), e40992.

    a. *Equally contributed

In Manuscript 3 (Franzoni *et al.*, 2024), I aimed to identify candidate genes for developing an antibody-based marker system to monitor chilled storage in peach fruit. In our work, I examined two cultivars: 'Sagittaria', an early-ripening peach, and 'Big Top', a mid-season nectarine known for delayed softening and resistance to supply-chain conditions. Both were subjected to storage at 1 °C and 5 °C for varying durations to simulate typical supply-chain conditions. Gene expression analysis on fruit from a subsequent year assessed the expression of five candidate genes during storage at both temperatures. My contribution to this paper was molecular and statistical analysis.

Lastly, I had the opportunity to have oral communications at three congresses, as reported below:

- **Madeo M. L.,** Ferrari M., Greca T., Bruno L., Chaerle P., Chepurnova O., Vyverman W., Montresor M., Romano G., Cozza R. "Preliminary study of Mediterranean diatoms species to improve the production of fucoxanthin and the challenge to their long-term preservation". Riunione Scientifica Annuale dei gruppi di lavoro SBI, Biologia Cellulare e Molecolare – Biotecnologie e differenziamento, Università Politecnica delle Marche (AN), 21-23 Giugno 2023 (**oral presentation as speaker**);
- **Madeo M. L**., Chaerle P., Chepurnova O., Vyverman W., Montresor M., Ferrari M., Greca T., Bruno L., Romano G., Cozza R. "Exploring cryopreservation techniques for the long-term storage of Chaetoceros socialis at different life cycle stages". Riunione Scientifica Annuale del Gruppo di Algologia, Stazione Zoologica Anton Dohrn di Napoli, 27-28 ottobre 2023 (**oral presentation as speaker**);
- **Madeo M. L**., Orefice I., Ferrari M., Greca T., Bruno L., Romano G., Cozza R. "Exploring fucoxanthin biosynthesis in *Thalassiosira rotula*: stress responses and regulatory genes". Riunione Scientifica Annuale dei gruppi di lavoro SBI, Biologia Cellulare e Molecolare – Biotecnologie e differenziamento, Università di Verona (VN), 12-14 Giugno 2024 (**oral presentation as speaker**).